POLITECNICO DI MILANO

Department of Energy

Doctoral Program in Energy and Nuclear Science and Technology

XXV Cycle - March 2013

The Molten Salt Fast Reactor as a Fast-Spectrum Candidate for Thorium Implementation

Doctoral Dissertation of:
CARLO FIORINA
Matr. n. 754131

Tutor:
Prof. Marco Enrico Ricotti

Supervisors:
Dr. Antonio Cammi
Dr. Fausto Franceschini
Dr. Lelio Luzzi

The Chair of the Doctoral Program:
Prof. Carlo Enrico Bottani

To my parents Ada and Giovanni

CONTENTS

INTRODUCTION

Background and motivation

Fast Reactors (FR) have been developed in the early stages of nuclear technology for the purpose of breeding fissile isotopes from fertile materials, thus greatly extending the fuel resources available to sustain the rapid growth of nuclear energy forecasted in the past. The U-Pu cycle has been preferred over the Th-U cycle because of the better breeding potential in a fast-spectrum and the sounder technical basis for fuel fabrication, irradiation, and reprocessing. On the other hand, Th use has been historically investigated for its capability to breed fissile material (namely, U-233) in a thermal neutron spectrum, thus possibly avoiding specific technological challenges associated to the development of FRs.

Over the course of the years, interest in fissile breeding has faded, especially in western countries, due to the slow deployment rate of new nuclear power plants and thanks to the availability of natural U resources, including the recent development of techniques for a reasonably economical extraction of U from sea water (ORNL, 2012). Conversely, waste management has emerged as one of the main problems for public acceptance of nuclear energy (Artioli et al., 2010; Salvatores and Palmiotti, 2011). Following these trends, both Th-based thermal reactors and U-based FRs started to be considered in view of their capability to operate with continuous recycle of all actinides, while potentially burning legacy TRU (TRansUranic isotope) wastes, thus drastically limiting the actinide wastes to be disposed.

Under this scenario, Th-based FRs can offer some specific advantages. The lower mass number of Th fosters a very low endogenous generation of TRUs, which could benefit public acceptance and the repository thermal performance. In addition, the low breeding capability of Th cycle may enhance the consumption of an external supply of TRUs. Past studies have also pointed out the Th potential capability to improve safety parameters (Till et al., 1980). Following these considerations, studies about Th use in FRs have started gaining momentum (Rubbia et al., 1995; IAEA, 2002; IAEA, 2005; Gruppelaar and Schapira, 2006). A new impetus to this option has been recently given by the cancellation of the Yucca Mountain nuclear waste repository project in the US, as well as by the Fukushima accident. The latter focused once again the attention of the public opinion on safety-related aspects of the nuclear energy production and on spent fuel accumulation at the reactor pools. For countries that have decided to phase out the nuclear energy option, management of the TRU legacy from Light Water Reactors has become a priority and Th may be the carrier to expedite TRU burning.

Despite the potential advantages, the implementation at an industrial scale of the Th closed cycle needs to overcome formidable challenges, including difficulties in dissolution and reprocessing of used fuel (Ramanujam, 2008), and fabrication of highly radioactive recycled fuel (Wenner et al., 2012). In particular, ThOx fuel is a particularly stable compound, which may benefit fuel disposal in once-through fuel cycle options, but necessitates dedicated dissolution processes for reprocessing. Similarly to PUREX, a nitric acid solution is used to

dissolve ThOx fuel, but addition of HF is required to reduce the dissolution time, leading to exacerbated corrosion of the equipment. As concerns fuel fabrication, problems originate from the build-up during Th-232 irradiation of U-232, mainly via (n,2n) reaction and subsequent neutron capture from Pa-231. The intensity and high energy of the gamma radiation emitted by Bi-212 (0.7-1.8 MeV) and Tl-208 (2.6 MeV), both daughters of U-232, imposes fuel handling and manufacturing behind thick shielding. In this sense, it is worth noting that the first and longest-lived isotope in the U-232's progeny is the 1.9-years half-life Th-228. By sending Th to the waste stream during reprocessing, the fuel would be momentarily free from the U-232 progeny. Drawbacks would be the necessity of a quick fabrication after reprocessing, and the accumulation of intensely radioactive Th waste. In addition, during the TRU transmutation stage spontaneous neutron emitters (primarily Cm and Cf isotopes) would require remote fuel handling independent of the of the gamma field from U-232's progeny.

The use of liquid fuel with online reprocessing would avoid most of the issues related to reprocessing, manufacturing and transporting highly radioactive recycled fuel in a closed cycle. The logical technology for the adoption of liquid fuel is the Molten Salt Reactor (MSR). In MSRs, a liquid fuel salt circulates through the core and transfers the heat to external heat exchangers via convection, thus playing the role of both fuel and coolant. The first MSRs developed used fluoride salts and Th fuel. They were conceived during the fifties for military purposes at the Oak Ridge National Laboratory (ORNL) in the US, and subsequently developed for two decades as graphite-moderated reactors for U-233 breeding and power production (MacPherson, 1985). In 2001, the Generation IV International Forum (GIF-IV) selected the MSR as one of the six innovative nuclear reactors with the potential to meet the compelling need for an increasingly sustainable, economical, safe and proliferation resistant nuclear energy production (GIF-IV, 2002). Few years after the selection of the MSR among the Generation-IV reactors, the concept evolved in the direction of fast-spectrum Th-based MSRs (Mathieu et al., 2006; 2009), identified as Molten Salt Fast Reactor (MSFR) (Merle-Lucotte et al., 2011) and mainly developed in the frame of the EURATOM EVOL (Evaluation and Viability Of Liquid fuel fast reactor system) Project (EVOL, 2012). The subject of the thesis work is the assessment of the novel MSFR technology as a promising route for combining the potential advantages of Th use in FRs with the unique fuel cycle flexibility fostered by a liquid fuel.

Objectives and outline of the work

Use of Th in fast-spectrum MSRs is a relatively recent proposal and only few studies are available in the open literature. Past works on fast-spectrum MSRs were mainly focused on chloride-based reactors for Pu breeding (Mourogov and Bokov, 2006), fertile-free TRU burning, or U-supported TRU burning (Ignatiev et al., 2007). The 30-year research experience developed at ORNL has a limited applicability to the MSFR case. Specifically, use of fluoride molten salts is still envisioned for the MSFR, which has allowed to rely, at least in a first development stage, on the ORNL experiences in terms of structural materials and reprocessing system. Limited studies have been instead carried out on the MSFR fuel cycle performances, waste management issues, thermal-hydraulics and safety aspects. Primary objective of the present thesis work is to offer an evaluation of the MSFR performances in

this sense, including an assessment of the MSFR potential to operate as a flexible conversion-ratio reactor (Chapter 1). A first-of-a-kind comparative analysis with traditional solid-fuelled FRs is performed (Chapters 2, 3, 4) in terms of main performance parameters, namely: breeding capabilities, decay heat and radiotoxicity of wastes, fuel management, TRU burning, safety aspects. For the comparison, two promising FR systems are selected (Appendix B), namely the sodium-cooled Toshiba-Westinghouse Advanced Recycling Reactor (ARR) (Dobson et al., 2008), and the European Lead SYstem (ELSY) (Alemberti et al., 2011). Both U- and Th-based versions of the two selected FRs are investigated in the thesis work. Although this is not a primary objective of the work, a comparison between Th and U use in traditional FRs is a necessary step for a better assessment of the MSFR performances vs traditional FRs, especially in view of the limited information available in literature in this sense (Till et al., 1980; Gruppelaar and Schapira, 2006; Touran et al., 2010). For both the MSFR and the traditional FRs, fuel cycle strategies are investigated envisioning the recycling of all the actinides in the core.

To ease the investigation while excluding major sources of biasing, a common tool is employed to evaluate the performances of the MSFR and of the traditional FRs (Appendix A). Specifically, an existing ERANOS-based (Rimpault et al., 2002) procedure, developed at the Paul Scherrer Institut (Switzerland) for the analysis of solid-fuelled FRs (Krepel et al., 2009), is employed and extended to allow the simulation of Th-containing cores, the possible use of fertile blankets and the online reprocessing system of the MSRs. In addition, dedicated sub-procedures are set up for the calculation of radiotoxicity and decay heat of wastes. The extended procedure is assessed against a tool recently developed at the Politecnico di Milano (Aufiero et al., submitted) and based on the Monte Carlo code SERPENT (Leppänen, 2007). The ORIGEN-S code (SCALE, 2006) is also used to assess decay heat and radiotoxicity calculations.

After characterizing the MSFR through a top-level comparison with the well-developed solid-fuelled counterparts, the work concentrates on two specific aspects of the MSFR that differentiate this technology from the others. The first one is the thermal-hydraulics (Chapter 5) that combines in MSRs a relatively high Prandtl number with the unique feature (in nuclear reactors) of the internal heat generation. This determines specific heat transfer characteristic and requires investigation to single out, or exclude, major impacts on the heat transfer phenomena in the reactor components. In particular, a theoretical investigation is carried out, leading to the derivation of a general form for correlations to be used to predict the Nusselt number for the forced convection of internally heated fluids flowing in turbulent regime in a straight circular channel. A generalized analytic approach previously developed at the Politecnico di Milano (Appendix C) is adopted to derive a specific correlation for the case of molten fluoride salts, and results are used to evaluate the impact of decay heat on the MSFR out-of-core components.

The second distinctive aspect of the MSFR technology is the reactor dynamics (Chapter 6). A liquid and circulating fuel impacts the reactor behavior due to 1) the direct deposition of fission heat inside the coolant, and 2) the movement of the delayed neutron precursors, causing their accumulation in low-flux regions and their partial decay out of the core. In addition, compared to graphite-moderated MSRs investigated in the past, the MSFR fuel is not restrained into graphite channels but flows freely in a wide core, with consequent flow

patterns that requires CFD (Computational Fluid Dynamics) codes for a proper characterization. These unique features of the MSFR exclude the use of tools developed in the past for solid-fuelled FRs, or for graphite-moderated MSRs. For this reason, a new dedicated model has been developed at the Politecnico di Milano in the frame of this and other 2 PhD theses. It consists of a set of non-linear and time-dependent coupled partial differential equations, which are simultaneously solved in the same simulation environment (namely, the simulation platform COMSOL Multiphysics) and describe the different "physics" (neutron transport, precursor diffusion and convection, thermo-fluid dynamics) occurring in the nuclear reactor. In the present thesis work, this model is presented and assessed against a similar model developed at the Technical University of Delft. The latter relies on a traditional coupling of dedicated neutron transport and thermo-fluid dynamic codes, in which the time-dependent solution is reached using the output from one code (e.g., the neutron kinetics code) as input to another code (e.g., the thermo-fluid dynamic code) at each time step. The results provided by the two codes are first used to investigate the steady-state core behavior. The effect of fuel movement on the precursor distribution is discussed and the core temperature field is investigated, thus extending to the reactor core the analysis of the MSFR heat transfer phenomena presented in Chapter 5. The MSFR transient behavior is then analyzed, pointing out general dynamic features and the most critical issues to be taken into account during core design and optimization.

REFERENCES

Alemberti, A., Carlsson, J., Malambu, E., Orden, A., Struwe, D., Agostini, P., Monti, S., 2011. European lead fast reactor – ELSY. Nuclear Engineering and Design 241, 3470-3480.

Artioli, C., Grasso, G., Petrovich, C., 2010. A new paradigm for core design aimed at the sustainability of nuclear energy: the solution of the extended equilibrium state. Annals of Nuclear Energy 37, 915-922.

Aufiero, M., Cammi, A., Fiorina, C., Leppänen, J., Luzzi, L., submitted. An extended version of the SERPENT-2 code to investigate fuel burn-up and core material evolution of the Molten Salt Fast Reactor. Submitted to Journal of Nuclear Materials. Presentation at NuMat 2012 conference, October 22-25, Osaka, Japan.

Dobson, A., 2008. GNEP Deployment Studies Preliminary Conceptual Design Studies. Technical Report. Volume IV - Advanced Recycling Reactor.

EVOL Project 2012 - Evaluation and Viability of Liquid Fuel Fast Reactor Systems. Available at: http://www.li2c.upmc.fr/.

GIF-IV, Generation IV International Forum, 2002. A Technology Road Map for Generation IV Nuclear Energy Systems. GIF-002–00, US DOE Nuclear Energy Research Advisory Committee and The Generation IV International Forum.

Gruppelaar H., Schapira, J.P., 2006. Thorium as a waste management option. Technical Report. EU 19142 EN.

IAEA, International Atomic Energy Agency, 2002. Thorium fuel utilization: options and trends. Technical Report. IAEA-TECDOC-1319.

IAEA, International Atomic Energy Agency, 2005. Thorium fuel cycle – potential benefits and challenges. Technical Report. IAEA-TECDOC-1450.

Ignatiev, V., Feynberg, O., Gnidoi, I., Merzlyakov, A., Smirnov, V., Surenkov, A., Tretiakov, I., Zakirov, R., 2007. Progress in Development of Li,Be,Na/F Molten SaltActinide Recycler & Transmuter Concept. Proc. ICAPP 2007, May 13-18, Nice, France.

Krepel, J., Pelloni, S., Mikityuk, K., Coddington, P., 2009. EQL3D: ERANOS based equilibrium fuel cycle procedure for fast reactors. Annals of Nuclear Energy 36, 550–561.

Leppänen, J., 2007. Development of a new Monte Carlo reactor physics code. PhD Thesis. Helsinki University of Technology.

MacPherson, H.G., 1985. The Molten Salt Reactor Adventure. Nuclear Science and Engineering 90, 374-380.

Mathieu, L., Heuer, D., Brissot, R., Garzenne, C., Le Brun, C., Lecarpentier, D., Liatard, E., Loiseaux, J.M., Méplan, O., Merle-Lucotte, E., Nuttin, A., Walle, E., Wilson, J., 2006. The Thorium Molten Salt Reactor: Moving on from the MSBR. Progress in Nuclear Energy 48, 664-679.

Mathieu, L., Heuer, D., Merle-Lucotte, E., Brissot, R., Le Brun, C., Liatard, E., Loiseaux, J.-M., Méplan, O., Nuttin, A., Lecarpentier, D., 2009. Possible Configurations for the Thorium Molten Salt Reactor and Advantages of the Fast Nonmoderated Version. Nuclear Science and Engineering 161, 78–89.

Merle-Lucotte, E., Heuer, D., Allibert, M., Brovchenko, M., Capellan, N., Ghetta, V., 2011. Launching the Thorium Fuel Cycle with the Molten Salt Fast Reactor. Proc. ICAPP 2011, May 2-5, Nice, France.

Mourogov, A., Bokov, P.M., 2006. Potentialities of the fast spectrum molten salt reactor concept: REBUS-3700. Energy Conversion and Management 47, 2761–2771.

ORNL, Oak Ridge National Laboratory, 2012. ORNL technology moves scientists closer to extracting uranium from seawater. Press release - August 21, 2012. Oak Ridge National Laboratory, US.

Ramanujam, A., 2008. Purex and Thorex Processes (Aqueous Reprocessing). Encyclopedia of Materials: Science and Technology, 7918-7924.

Rimpault, G., Plisson, D., Tommasi, J., Jacqmin, R., Rieunier, J., Verrier, D., Biron, D., 2002. The ERANOS code and data system for fast reactor neutronic analyses. Proc. PHYSOR 2002, October 7-10, Seoul, Korea.

Rubbia, C., Rubio, J.A.., Buono, S., Carminati, F., Fiétier, N., Galvez, J., Gelès, C., Kadi, Y., Klapisch, R., Mandrillon, P., Revol, J.P., Roche, Ch., 1995. Conceptual design of a fast neutron operated high power Energy Amplifier. Technical Report. CERN/AT/95-44 ET.

Salvatores, M., Palmiotti, G., 2011. Radioactive waste partitioning and transmutation within advanced fuel cycles: achievements and challenges. Progress in Particle and Nuclear Physics 66, 144-166.

SCALE: A Modular Code System for Performing Standardized Computer Analyses for Licensing Evaluations, ORNL/TM-2005/39, Version 5.1, Vols. I–III, November 2006. Available from Radiation Safety Information Computational Center at Oak Ridge National Laboratory as CCC-732.

Till, C. E., Chang, Y.I., Kittel, J.H., Fauske, H.K., Lineberry, M.J., Stevenson, M.G., Amundson, P.I., Dance, K.D., 1980. Fast breeder reactor studies. Technical Report. Argonne National Laboratory, ANL-80-40.

Touran, N.W., Hoffman, A.J., Lee, J.C., 2011. Performance of Thorium-Based Fuel for TRU Transmutation in Sodium-Cooled Fast Reactors. Proc. ANS Winter Meeting 2010, November 7-11, Las Vegas, US.

Wenner, M., Franceschini, F., Kulesza, J., 2012. Preliminary Comparative Shielding Analysis for Refabricating Different Fuel Vectors. Proc. ANS Winter Meeting 2012. November 11-15, San Diego, US.

CHAPTER 1: MSFR design, core physics and fuel cycle aspects - a flexible conversion ratio reactor

ABSTRACT

The present Chapter provides a discussion of the MSFR main features. At first the conceptual design routinely employed for calculations in the MSFR scientific community is presented. Due to the lack of a definite design of the heat exchangers between primary and intermediate circuits, a brief parametric study is performed to assess their overall feasibility and characteristics, which will be needed in Chapters 4 and 6 to assess the MSFR safety features. General core physics aspects are then discussed, singling out a softer spectrum compared to the MSFR, with consequent important impacts e.g. on the fission-to-capture cross-section ratio of the main actinides. Finally, the MSFR is characterized from the viewpoint of fuel cycle. It is demonstrated that it can be operated as a flexible conversion ratio reactor in a closed Th cycle by tuning the reprocessing rate and thus the content of fission products in the core. Four different fuel cycle strategies are proposed where the MSFR is used as U-233 breeder, iso-breeder, burner of transuranic isotopes, or burner of minor actinides. Related performances will be investigated in Chapters 2, 3 and 4. Some of the main results have been presented in (Fiorina et al., 2012a, 2012b, 2012c, submitted; Aufiero et al., submitted).

1.1 INTRODUCTION

Molten Salt Reactors (MSR) were conceived during the fifties for military purposes in the US, and subsequently developed for two decades as graphite-moderated U-233 breeder reactors for power production (MacPherson, 1985). MSRs are unique reactors and make use of a salt mixture that acts simultaneously as fuel and coolant, transferring the heat via convection from the core to external heat exchangers. The rationale behind the MSR technology can be identified in the high power density, design flexibility, intrinsic safety, and simplified fuel handling allowed by adoption of a liquid fuel. Studies on MSRs were mainly performed in the US at the Oak Ridge National Laboratory (ORNL) during the Molten Salt Reactor Project (Robertson et al., 1971; documentation freely available at (Energy from Thorium)). Research activities have included the realization of two MSR prototypes, namely, the Aircraft Reactor Experiment and the Molten Salt Reactor Experiment (MSRE), and the design of the 1000 MWe Molten Salt Breeder Reactor (MSBR). However, during the seventies, interest in the MSR technology has faded in favor of the liquid-metal Fast Reactor (FR) technology, considered a more promising option for fissile breeding. A renewed impetus has

been given to the MSR R&D by the Generation IV International Forum (GIF-IV) that, in 2001, selected the MSR as one of the six innovative nuclear reactors with the potential to meet the compelling need for an increasingly sustainable, economical, safe and proliferation resistant nuclear energy production (GIF-IV, 2002). Few years after the selection of the MSR among the Generation-IV reactors, and in view of the main GIF-IV goals of increased sustainability and safety, the concept evolved in the direction of fast-spectrum MSRs (Mathieu et al., 2006, 2009) and the MSFR became in 2008 a reference circulating-fuel MSR in the GIF-IV. It is presently developed in frame of the EURATOM EVOL project (EVOL, 2012).

This Chapter first describes the MSFR conceptual design presently considered (Section 1.2), including a preliminary investigation of possible designs for the heat exchangers, which will be needed for investigating the MSFR safety features in Chapters 4 and 6. In Section 1.3, the MSFR core physics is briefly investigated while Section 1.4 discusses the possibility of using the MSFR as a flexible Conversion Ratio (CR) reactor (Todreas et al., 2009) in a fully close Th cycle. Concluding remarks are provided in Section 1.5.

1.2 PRIMARY CIRCUIT DESIGN

The MSFR shows design specificities that deeply distinguish it from traditional solid-fuelled reactors. The following subsections describe the conceptual reactor design routinely used for calculations in the frame of the EVOL project. The available design includes a fairly detailed description of the core, few specifications about the out-of-core part of the primary circuit and a description of the fuel salt properties. Design of the primary heat exchangers is ongoing, but main constraints are already available, which allows to obtain important information on the expected range of performances. The MSFR envisions the use of an intermediate circuit (using FLiNaK molten salt as coolant (Benes and Konings, 2009)) to separate the radioactive primary coolant from the energy conversion system, but no details are available to date either for the intermediate circuit or for energy conversion system designs.

1.2.1 Core and primary circuit

The core of the MSFR is a cylinder with the diameter equal to the height, surrounded axially by 1-m thick steel reflectors, and radially by a fertile blanket, a boron carbide layer, and a reflector. The core is filled with the fuel salt and no core internals are envisioned to date. The fuel circulates out of the core through 16 external loops, each one including a pump and a heat exchanger. An overflow tank accommodates salt expansion in case of overheating. A salt draining system is connected to the bottom of the core to allow emptying the core for maintenance or in case of emergency. The system is expected to drain the salt in passively-cooled criticality-safe tanks, whose design has not yet been defined. A passive system is envisioned for core draining, including freezing valves that should melt as soon as electric power is lost, or in case of salt overheating.

The primary circuit is connected to 2 other circuits for salt processing. The first one is a gas system envisioning He bubbling into the fuel salt to extract gaseous and non-soluble fission products. A 30 seconds extraction time is assumed for both kind of fission products. As a matter of fact, extraction of non-gaseous fission products will be slower, but time constants for the extraction extended to a few days would have a limited impact on the

obtained results (Merle-Lucotte, 2008). The second circuit connected to the primary circuit is the salt reprocessing system necessary to separate soluble fission products from the fuel salt. Extraction is assumed as continuous, or batch on a daily basis. Few liters or few tens of liters of salt need to be extracted every day (see subsection 1.4).

The entire primary circuit, including the gas reprocessing unit, is contained in a secondary reactor vessel. A schematic view of the primary loop layout is reported in Fig. 1.1 while the main core parameters are summarized in Table 1.1.

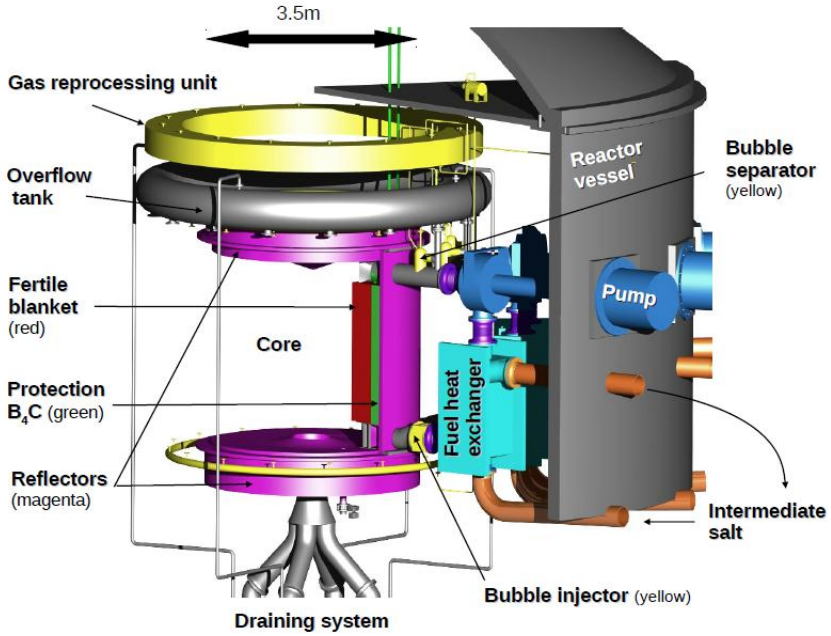

Figure 1.1: Schematic view of the MSFR primary circuit (Brovchenko et al., 2012)[1]

Table 1.1: MSFR core parameters (Merle-Lucotte, 2011)

Thermal/electric power	3000 MW/1500 MW
Core inlet/outlet temperatures	923/1023 K
Fuel salt volume	18 m^3
Fraction of salt inside the core	50%
Number of loops for heat exchange	16
Flow rate	4.5 m^3/s
Salt velocity in pipes assuming 0.3 m diameter	~4 m/s
Blanket thickness	50 cm
Blanket salt volume	7.3 m^3
Boron carbide layer thickness	20 cm

Fig. 1 shows a nearly axial-symmetric core geometry, which is often exploited to represent and model the MSFR core in a r-z 2-D fashion. The axial-symmetric representation can be extended to the entire primary circuit by approximating the 16 external loops with a single annular loop. Fig. 1.2 shows the resulting geometry and dimensions.

[1] *Note that heat exchangers are placed in the lower part of the primary circuit in Fig. 1.1, while they will be considered to be in the upper part in this thesis to allow for the set-up of a natural circulation regime in case of pump failure.*

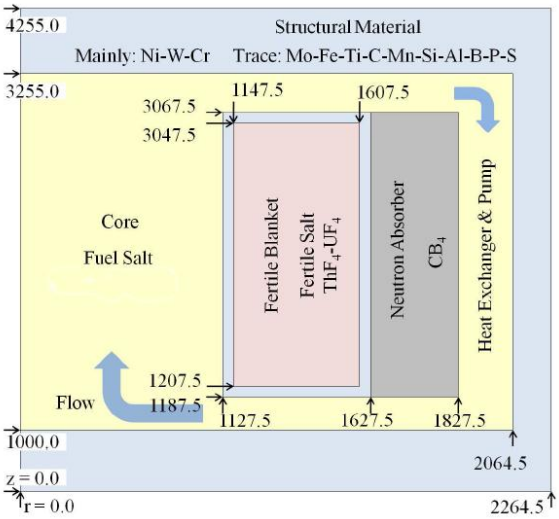

Figure 1.2: Axial-symmetric representation of the MSFR primary circuit (van der Linden, 2012)

1.2.2 Fuel salt

The fuel salt is composed by LiF for 77.5 mole%, and by a mixture of $(HN)F_3$ and $(HN)F_4$ for 22.5% (HN indicates Heavy Nuclides). A detailed investigation of this salt mixture is being carried out in the frame of the EVOL project. Table 1.2 summarizes the salt properties mainly of interest for this thesis work. Solubility of trivalent elements shows important variations with temperature. At the lowest temperature in the MSFR (923 K) it reaches a ~5% value, corresponding to ~20% the total amount of $(HN)F_3$+$(HN)F_4$. The melting point is 85 K lower compared to the lowest operating temperature in the reactor. It is worth noticing that the melting point is expected to vary mildly with the fraction of $(HN)F_3$ and in case Th is partly substituted with U, which could be necessary to control the redox potential of the mixture. For simplicity and due to the lack of detailed data in this sense, these variations will be here neglected.

Table 1.2: MSFR fuel salt properties (Merle-Lucotte et al., 2011)

Salt density [kg/m³]	$4094-8.82\cdot10^{-1}\cdot(T[K]-1008)$
Salt specific heat [J/kg-K]	$-1111+2.78\cdot T[K]$
Salt thermal conductivity [W/m-K]	$0.928+8.397\cdot10^{-5}T[K]$
Salt kinematic viscosity [m²/s]	$5.54\cdot10^{-8}\cdot\exp(3689/T[K])$
Prandtl number at 973 K [-]	16
Solubility of trivalent elements at 823-923-1023 K [%]	2.70-4.86-7.51
Melting point [K]	838

1.2.3 Start-up core loadings

Four start-up fuel compositions are considered in the present thesis for the MSFR as reported in Table 1.3: Th-U3, Th-Pu, Th-TRU and Th-U5-TRU. The Th-U3 core, i.e., a start-up core composed by Th and U-233, would minimize the transition time to the equilibrium cycle. An alternative and more realistic route to overcome the current unavailability of U-233 would consist of initially loading the core with a different fissile material. The Th-Pu core is composed by Th and Pu, conceivably from Light Water Reactor (LWR) used fuel reprocessing.

The Pu composition has been taken from Artioli et al. (2007). This start-up fuel appears more practical today as it would employ the current PUREX reprocessing technique and facilities to recover an already available fissile resource; the MSFR would then initially operate as a Pu burner. The MSFR could also be used to burn the entire TRU (TRansUranic isotope) vector produced by the LWR fleet, while initiating a new Th cycle (Merle-Lucotte et al., 2009). In this case, Th-TRU with 5-year cooled TRU from LWR used fuel would be the pursued option. Finally, the use of U enriched in U-235 is to be considered since in both Th-TRU and Th-Pu options the concentration of trivalent actinides (mainly Pu, Am, Cm) is close to, or greater than, the solubility limit at the nominal temperature and for the carrier salt considered. Use of enriched U (12.72 wt% U-235 in U, taken by Merle-Lucotte et al. (2011)) alleviates the solubility problems since no solubility issue is associated to using tetravalent elements. The blanket is composed of a 77.5 mole% LiF and 22.5 mole% ThF_4 for all cases considered.

Table 1.3: HN inventory [kg] for the different MSFR start-up options (Merle-Lucotte et al., 2011)

	Th-U3	**Th-Pu**	**Th-TRU**	**Th-U5-TRU**
Th-232	$3.798 \cdot 10^4$	$3.219 \cdot 10^4$	$3.016 \cdot 10^4$	$1.488 \cdot 10^4$
U-233	$5.039 \cdot 10^3$	-	-	-
U-235	-	-	-	$2.579 \cdot 10^3$
U-238	-	-	-	$1.770 \cdot 10^4$
Np-237	-	-	$8.038 \cdot 10^2$	$5.002 \cdot 10^2$
Pu-238	-	$2.547 \cdot 10^2$	$3.466 \cdot 10^2$	$2.184 \cdot 10^2$
Pu-239	-	$6.235 \cdot 10^3$	$5.943 \cdot 10^3$	$3.724 \cdot 10^3$
Pu-240	-	$2.958 \cdot 10^3$	$2.809 \cdot 10^3$	$1.762 \cdot 10^3$
Pu-241	-	$6.714 \cdot 10^2$	$1.408 \cdot 10^3$	$8.846 \cdot 10^2$
Pu-242	-	$8.439 \cdot 10^2$	$8.921 \cdot 10^2$	$5.552 \cdot 10^2$
Am-241	-	-	$4.487 \cdot 10^2$	$2.787 \cdot 10^2$
Am-243	-	-	$2.553 \cdot 10^2$	$1.606 \cdot 10^2$
Cm-244	-	-	$1.079 \cdot 10^2$	$6.717 \cdot 10^1$
Cm-245	-	-	9.032	4.497
Total	$4.301 \cdot 10^4$	$4.315 \cdot 10^4$	$4.318 \cdot 10^4$	$4.331 \cdot 10^4$

1.2.4 Heat exchangers

The exact design of the 16 heat exchangers between primary and intermediate circuits has not yet been defined. In this thesis work, a shell-and-tube configuration will be considered, with the primary salt in the tubes and the secondary salt in the shell. This is consistent with the MSRE and MSBR designs developed at the ORNL during the Molten Salt Reactor Project (Robertson et al., 1971). The shell has been configured to achieve the same heat transfer coefficient as for the primary salt. At the secondary side, a constant temperature of 823 K has been assumed, according to preliminary indications from the EVOL project. The following main constraints specified for the MSFR, and mainly characterizing the core transient behavior, have been taken into account: 1) inlet/outlet temperatures equal to 1023 K / 923 K, respectively; and 2) a total volume in the primary side equal to 36% of the salt in the external part of the primary circuits (i.e., in pipes, pumps and heat exchangers). Table 1.4 shows the results of a preliminary design process carried out using the Gnielinski (Gnielinski, 1976) and the Petukhov (Petukhov, 1970) correlations for the Nusselt number and the Darcy friction factor, respectively. Four possible designs are shown, differing from each other for the

diameter of the tubes. A tube diameter of the order of 5 mm appears necessary to avoid excessive velocities and ensuing erosion/corrosion problems, which are typically assumed to occur for velocities higher than 5 m/s. The advantage of employing tubes with the smallest possible diameter is clear in terms of pressure losses, though smaller tubes complicate both the design and the tube fabrication, inevitably resulting in incremental costs. In this sense, it is worth noting that diameters lower than 4 mm do not foster significant improvements in the pressure losses, thus suggesting a 4 mm tube as a possible compromise between pressure loss minimization and cost of the heat exchanger.

A specific issue of the MSFR heat exchangers relates their position, since no specification has been given in the frame of the EVOL project. To allow the set-up of a natural circulation regime in case of a loss of flow, the heat exchangers would have to be placed in the upper part of the primary circuit. A reference case has been assumed in this thesis work where the centers of the heat exchangers are placed 38.1 cm above the core center. This value results from placing the heat exchanger in the upper part of the out-of-core portion of the circuit in the axial-symmetric configuration shown in Fig. 1.2.

Table 1.4: MSFR heat exchanger parameters

Type	Tube (primary circuit) and shell (secondary circuit)			
Power exchange [MW]	187.5			
Inlet/outlet temperatures (primary side) [K]	1023/923			
Temperature of the secondary side [K]	823			
Fuel salt volume (primary side) [m³]	0.203			
Heat transfer coefficient on each side of the heat exchanger [W/K]	$2.60 \cdot 10^6$			
Tube inner diameter [mm]	10	6	4	3
Tube length [m]	7	3	2	1.75
Number of tubes [-]	369	2389	8061	16379
Salt velocity [m/s]	9.72	4.17	2.78	2.43
Reynolds number [-]	$3.9 \cdot 10^4$	$1.0 \cdot 10^4$	$4.6 \cdot 10^3$	$3.0 \cdot 10^3$
Pressure loss [Pa]	$3.1 \cdot 10^6$	$5.6 \cdot 10^5$	$3.1 \cdot 10^5$	$3.0 \cdot 10^5$

1.3 CORE PHYISCS ASPECTS

A first fundamental aspect that distinguishes the MSFR from solid-fuelled FRs is the neutron spectrum. In fact, the MSFR fuel salt contains a large amount of light elements like Li and F, causing a considerable neutron thermalization. Fig. 1.3 compares the spectrum of the MSFR with that of the lead-cooled ELSY (Section B.2) and of the sodium-cooled ARR (Section B.3). In particular, a U-based version of the ELSY (column 5 in Table 2.1) and a U-based burner version of the ARR (column 1 in Table 3.4) are selected[2]. Fig. 1.3 reveals a distinctive energy structure of the MSFR spectrum between 20 keV and 200 keV, with four marked dips. These dips are caused by the elastic scattering resonances in F (~20, 50, 100 keV) and Li (200 keV) isotopes. The harder spectrum of the ARR compared to the ELSY is mainly related to the lower CR and higher fissile-to-fertile ratio (see Appendix B and Tables 2.1 and 3.4).

[2] *Analogous results are obtained for the Th-based options.*

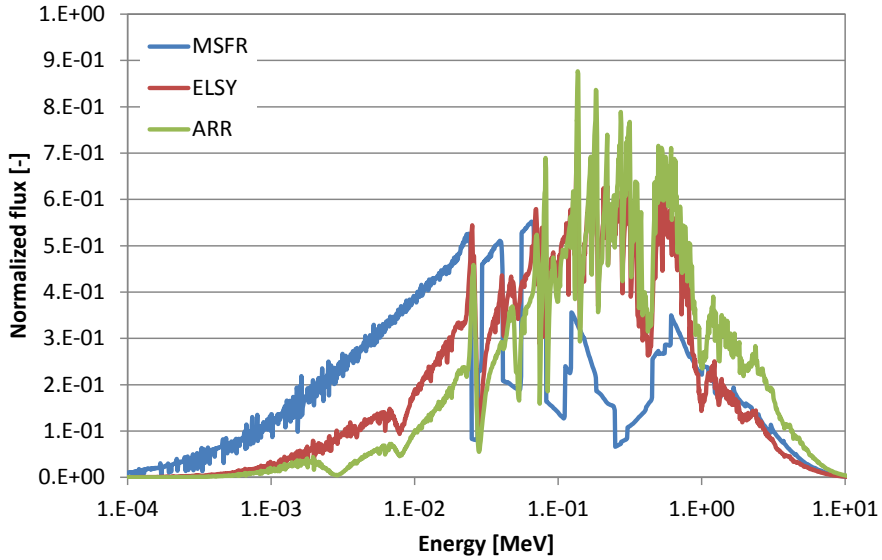

Figure 1.3: MSFR spectrum and comparison with the ELSY (U-based) and the ARR (U-based burner version)

As shown in Fig. 1.4, the softer spectrum of the MSFR compared to a solid-fuelled FR leads to smaller fission-to-capture cross-section ratios, which will cause an increased build-up of hazardous isotopes, with ensuing negative effects on radiotoxicity and decay heat of the actinide inventory (Sections 2.4 and 2.5).

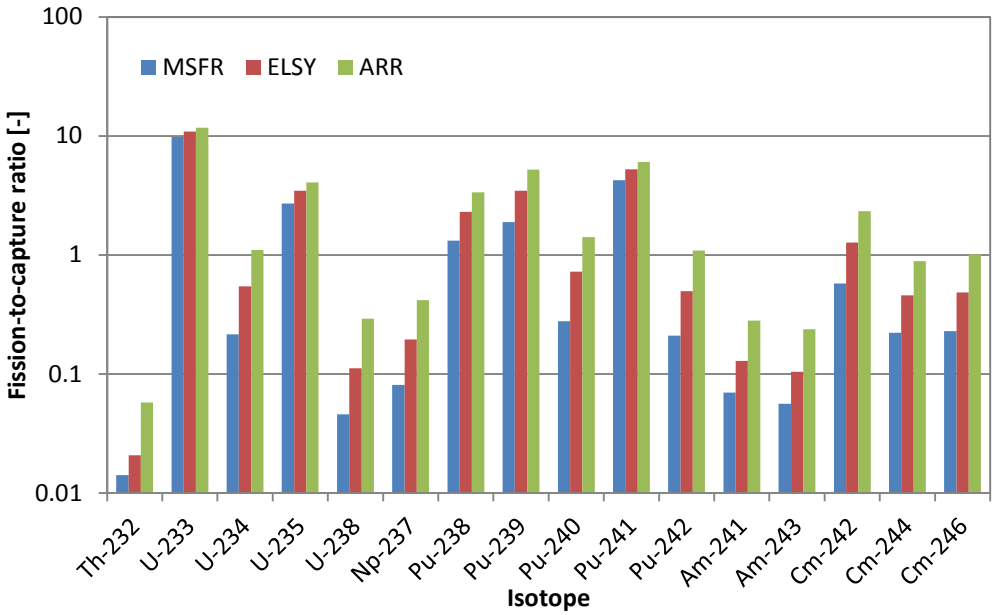

Figure 1.4: Fission-to-capture cross-section ratio for the MSFR and comparison with the ELSY (U-based) and the ARR (U-based burner version)

Fig. 1.5 quantifies the effect of the different spectra for each reaction type and energy group in the 3 reactors. Results have been obtained using ERANOS (Appendix A) and the reactivity decomposition technique discussed in Section A.5. The Watt-shaped positive reactivity contribution from neutron production is visible in all cases and is unaffected by the core design. The negative contributions from captures and fissions are instead visibly influenced by the spectrum and concentrates at particularly low energies for the MSFR. Fissions take place in the MSFR in the same energy domain as captures while concentrates at

a)

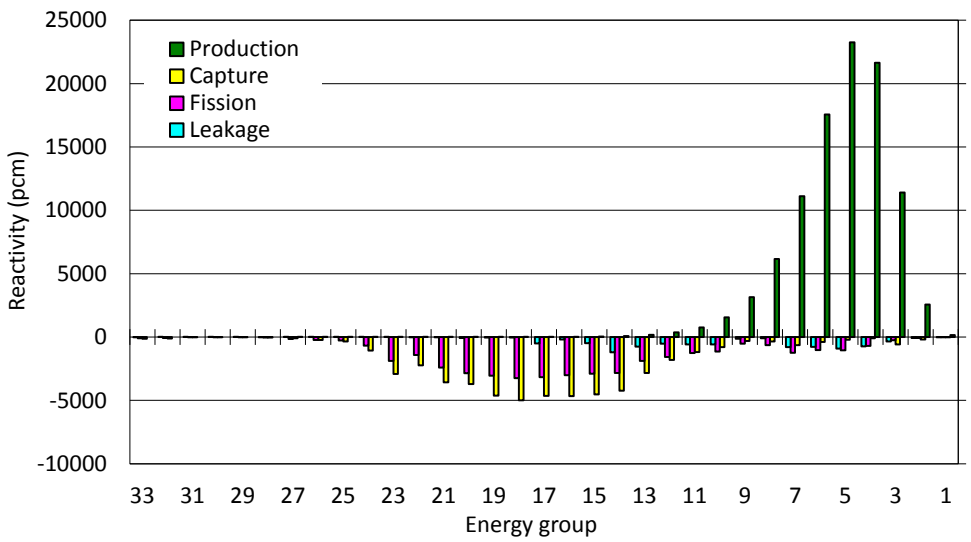

b)

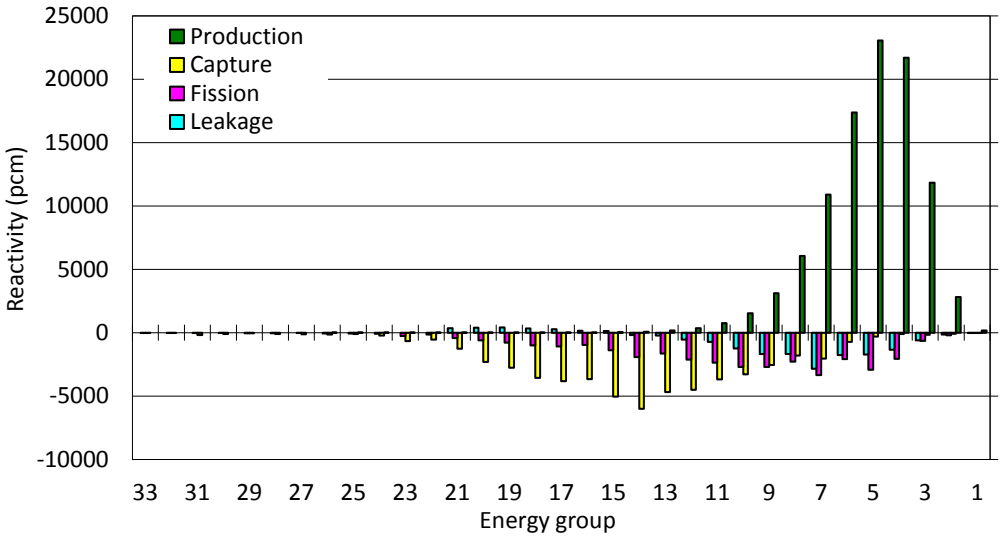

c)

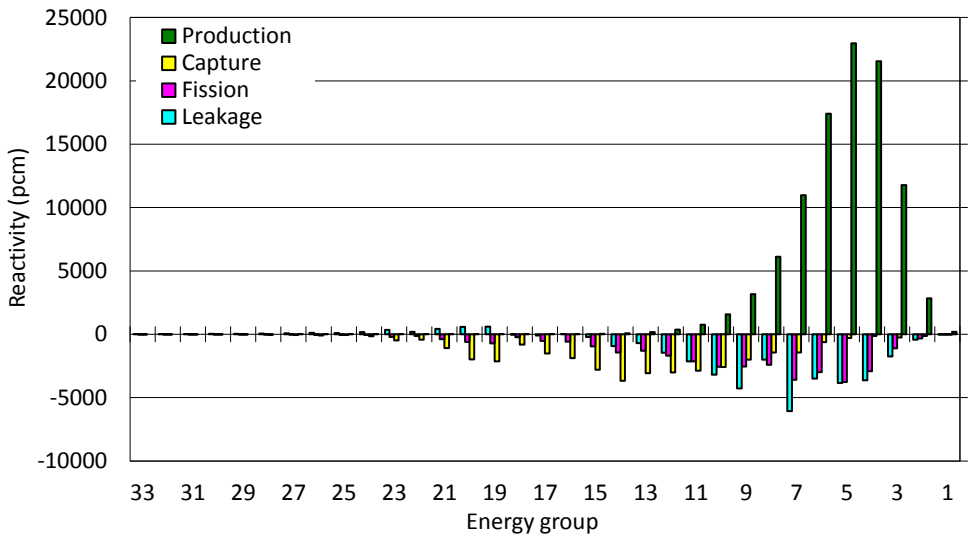

Figure 1.5: Group-wise reactivity decomposition of the MSFR nominal reactivity (a) and comparison with the U-based ELSY (b) and the U-based burner ARR (c)

higher energies in the ELSY and, particularly, in the ARR. The stronger shift toward higher neutron energy of fissions compared to captures is related to the different trend of the respective cross-sections. Specifically, the capture cross-section decreases monotonically with energy while the fission cross-section first decreases and then increases thanks to the contribution of the threshold fission reactions in the even-mass-number isotopes (see Fig. 1.6 for the specific case of the MSFR). The fractions of captures/fissions occurring in the resolved-resonance region (approximately below 4 keV according to the JEFF3.1 nuclear data library (Koning et al., 2006)) are equal to ~53%/47%, ~27%/13% and ~24%/9%, for the MSFR, ELSY and ARR, respectively. The high flux below the ~4 keV resonance region is expected to improve the MSFR Doppler feedback (Section 4.3).

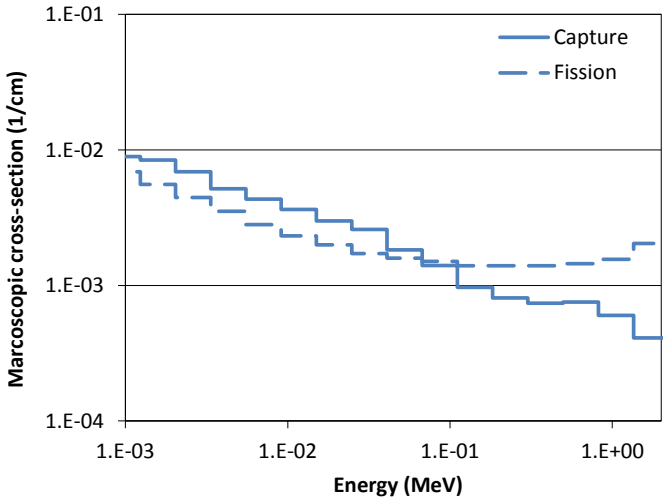

Figure 1.6: Macroscopic cross-sections for the MSFR

Table 1.5 shows the fraction of neutrons that are lost via leakages or absorptions in the MSFR, and compares it to the ELSY (U-based - column 5 in Table 2.1), the ARR (U-based burner - column 1 in Table 3.4), and to the typical values obtained for an LWR (Yang, 2012). In particular, the values reported for the MSFR refer to its use as iso-breeder reactor[3] (see next Section and column 2 in Table 2.1). The fraction of neutrons leaking from the MSFR core is in line with that of the ELSY, which in turn is in-between a LWR and the ARR. Approximately half of the leaking neutrons in the MSFR are absorbed by the blankets. The remaining fraction of fission neutrons is lost via absorption in the fuel or via parasitic absorption in coolant, fission products or control rods. The fraction of neutrons that is absorbed by fertile isotopes reflects the reactor CR: it is comparable for the MSFR and the ELSY (both iso-breeder, CR=1) and lower for a LWR (CR~0.7) and, particularly, for the burner ARR (CR~0.5). Absorption in actinides other than U-238 or Th-232 is comparable in all cases. Parasitic absorptions for the MSFR are comparable to the other FRs and much lower compared to a LWR. In particular, it is worth noting that the MSFR does not have core structures and, thanks to the online reprocessing, does not need control rods to balance the burnup reactivity swing.

[3] *Iso-breeder refers to a reactor with CR equal to 1, thus self-sustaining with natural Th or U as only feed.*

Table 1.5: Neutron losses [%] for different reactor concepts

	MSFR*	ELSY**	ARR***	LWR
Leakages	8.8	10.8	30.6	3.5
Absorptions	91.3	89.4	66.6	96.5
Fertile isotopes (U-238 or Th-232)	35.3	32.2	15.6	23.9
Other actinides	50.4	46.8	45.6	52.8
Parasitic absorptions	5.6	4.6	7.3	19.8
Coolant	1.4	1.9	0.1	3.4
Core structures	-	2.7	2.0	0.6
Fission products	4.3	2.8	2.3	6.8
Control rods	-	~0	2.9	9

**Iso-breeder (column 2 in Table 2.1) **U-based (column 5 in Table 2.1) ***U-based burner (column 1 in Table 3.4)*

1.4 FUEL CYCLE ASPECTS

The MSFR has been conceived to operate in a closed Th cycle envisioning a full recycle of all the actinides in the core, i.e., only fission products are removed from the salt during reprocessing and replaced with a fresh actinide feed. In the reference fuel cycle strategy envisioned for the MSFR (Merle-Lucotte et al., 2008, 2011), after an initial loading of fissile isotopes and Th, only Th needs to be added as feed and the reprocessing rate is maximized to increase breeding. The limiting condition is assumed to be the capability of the reprocessing system.

The present thesis work investigates the performances of the MSFR in closed Th fuel cycle from a different viewpoint. In fact, the liquid fuel and the online reprocessing system pave the way toward the use of the MSFR as a flexible CR reactor (Todreas et al., 2009). In principle, the CR can be adjusted by varying the reprocessing rate for soluble fission products. The reprocessing rate determines the quantity of fission products in the core, which in turn affects breeding through both increased captures and an increased fissile-to-fertile ratio necessary to achieve criticality. In addition, in the present thesis it is assumed that the total concentration of actinides and fission products is maintained during the fuel isotopic evolution (Section A.3), so that accumulation of fission products determines a lower actinide inventory in the core. A reduced reprocessing rate can thus be employed to negatively affect the neutron economy till the achievement of an iso-breeder reactor or, even further, to the achievement of a CR<1, requiring an external feed of fissile isotopes (e.g., TRUs) to maintain the reactor criticality.

Iso-breeder reactors are considered nowadays an attractive option (Todreas et al., 2009; Artioli et al., 2010) as they would preserve the advantages of a closed self-sustaining cycle in terms of resource utilization and waste minimization while reducing proliferation risks compared to breeder reactors. In addition, the lack of fissile material is a minor concern nowadays, especially in western countries, and makes breeding operation less attractive than in the past. In the MSFR, these advantages combine with the reduced reprocessing rate compared to the use of the MSFR as breeder reactor to make iso-breeding a particularly attractive option.

Fast-spectrum low-CR reactors can be used to efficiently burn the legacy TRUs from LWR operation (Salvatores and Palmiotti, 2011). Achievement of a CR<1 with the MSFR

would allow to operate this reactor as a Th-supported fast-spectrum burner reactor. This is a particularly interesting option as TRU burning in solid-fuelled reactors is considered of paramount importance nowadays, but is made difficult by radiation field and decay heat at the fuel fabrication step (see subsection 3.3.1). Although advantageous in terms of safety (Section 4.2), Th use in solid-fuelled reactors makes this problem even worse due to the highly penetrating gamma rays emitted by the progeny of U-232 (Section 2.6 and subsection 3.3.1), which always accompanies in-bred U-233 in a Th-based reactor. The liquid fuel of the MSFR would allow avoiding fuel fabrication while the online reprocessing system would eliminate most transportation issues.

However, for all these possible benefits to materialize, the capture cross-sections of the fission products must be proved high enough to affect breeding and reactivity without incurring in the solubility limits of some isotopes in the salt. In particular, most of the soluble fission products are lanthanides, which combines with the possible presence of Pu and heavier actinides to make the solubility of trivalent isotopes in the salt a primary concern.

1.4.1 Selected fuel cycle strategies

To assess the actual possibility, and ensuing potential advantages, of using the MSFR as a flexible CR reactor in a fully closed fuel cycle (i.e., with recycling of all the actinides), four options have been investigated, namely[4]:

- Th-feed: A fuel cycle option where breeding is the goal and the entire U-233 amount produced in the blankets is extracted, with only Th fed to the core.
- ThU3-feed: A fuel cycle option where the U-233 produced in the blankets is reinserted into the core (mixed with Th) to minimize the reprocessing rate (iso-breeding). This would simplify the reprocessing system, as well as the overall fuel cycle: only Th would be used at the front-end and only fission products and actinide reprocessing losses would have to be managed at the back-end.
- ThU3TRU-feed: A fuel cycle option where TRU burning is the goal. Since TRUs are mainly trivalent isotopes[5], the maximum achievable burning rate is set by the solubility limit of trivalent isotopes in the feed. A 20 wt% TRUs on the total actinide content is assumed, corresponding to ~4.5 mole% of trivalent isotopes in the salt, i.e., slightly below the solubility limit at the lower temperature in the reactor (see subsection 1.2.2). TRUs are assumed to derive from once-through LWR operation and have the same composition as the one used for the Th-TRU start-up core (Table 1.3). The feed is tailored to consume the U-233 generated in the blanket.
- ThU3MA-feed: A second fuel cycle option where burning of wastes is the goal, but where the advantages of a liquid fuel in terms of fuel handling are exploited to maximize the burning rate of Minor Actinides (MA)[6]. A Th-MA feed is then used, considering again a

[4] *Note that the name associated to each option refers to the feed inserted into the core, including the fissile material bred in the blankets.*

[5] *Except Np that, depending on the redox potential of the salt mixture, may become tetravalent.*

[6] *The expression Minor Actinides is generally employed to indicate isotopes different than Pu and U-238 that build-up with irradiation in a U-Pu cycle. When Th is used, this terminology may be misleading, since other actinides build-up like Pa. However in this thesis, the expression Minor Actinides will be used according to its traditional meaning, thus referring to Np, Am, Cm and Cf isotopes. Disambiguation will be done when needed.*

20% MA on the total actinide (i.e., Th + MA) inventory. Also in this case, U-233 from the blankets is entirely inserted in the core. Use of such a feed is generally not possible in FRs due to excessive radiation field and decay heat of fabricated assemblies (see subsection 3.3.1). In this case the MA feed is assumed to derive from a multi-tier fuel cycle where Pu is recycled in dedicated PWRs (Taiwo et al., 2006) and the MA are the only wastes. The isotopic composition is reported in Table 1.6.

Table 1.6: MA isotopic composition [wt%] (Yang, 2008)

Np-237	Am-241	Am-243	Cm-244	Cm-245
14.6	37.7	31.9	14	1.8

1.4.2 Preliminary viability assessment

For each fuel cycle option, reprocessing rate has been obtained by iteratively performing equilibrium calculations (see Appendix A) with different reprocessing rates, until the achievement of equilibrium reactivity equal to zero. This guarantees the reactor operability in the long term. The maximum concentration of trivalent isotopes is reached at equilibrium, i.e., after tens of years of irradiation. In fact, fission products accumulate with time and reach their equilibrium after an irradiation time equal to 6-7 times the time constant associated to reprocessing. For the ThU3TRU-feed, 3.29 liters of salt are reprocessed each day, corresponding to a time constant of 5476 days (~15 yr). Equilibrium for fission products is then reached in approximately 100 years. The same time scale is required to achieve an approximate equilibrium condition for the actinide concentrations. Results of the investigation are summarized in Table 1.7. To calculate the fraction of trivalent isotopes in the salt, all isotopes who may present a trivalent state have been included, namely: all lanthanides, TRUs and Y. Uranium is known to be tetravalent in the MSFR salt.

Table 1.7: Feed options for the MSFR and ensuing fraction of trivalent isotopes at equilibrium

Option name	General strategy	Feed composition	Reprocessing rate [1/d]	Fraction of trivalent isotopes in the salt at equilibrium [%]
Th-feed	*Breeding*: Th feed, ^{233}U from blanket to be used for other reactors	- 100 wt% Th	86.5	0.35
ThU3-feed	*Iso-breeding*: Th feed, ^{233}U from blanket reinserted in the core	- 89.3 wt% Th - 10.7 wt% ^{233}U (from blanket)	6.49*	2.24
ThU3TRU-feed	*TRU burning:* Th-TRU feed, ^{233}U from blanket reinserted in the core	- 69.3 wt% Th - 20.0 wt% TRU - 10.7 wt% ^{233}U (from blanket)	3.29*	5.57
ThU3MA-feed	*MA burning:* Th-MA feed, ^{233}U from blanket reinserted in the core	- 69.3 wt% Th - 20.0 wt% MA - 10.7 wt% ^{233}U (from blanket)	4.35*	5.35

**A ~10% margin on the U-233 production rate has been assumed. Approximately 10 kg excess U-233 is produced each year.*

Use of the MSFR as iso-breeder (ThU3-feed) or burner reactor (ThU3MA-feed and ThU3MA-feed) allows to drastically reducing the reprocessing rate compared to its use as U-233 breeder (Th-feed), which will benefit the design and operation of the reprocessing system. Solubility limits (~5%) are met by the iso-breeder case while they are slightly exceeded for the burner options. However, concentrations in Table 1.7 include all isotopes that might have a trivalent state, thus probably overestimating the actual quantity of trivalent isotopes in the salt. In addition, the solubility limit can be increased to 5.5% by increasing the lower temperature in the system by ~25 K.

It is a fortunate coincidence that the adoption of a Th-TRU or Th-MA feed with a TRU/Th or MA/Th fraction close to the solubility limits leads to an equilibrium concentration of trivalent isotopes in the fuel salt also close to the solubility limits, so that neither one of the solubility constraints (i.e., on the feed or on the fuel) compromises by itself the viability of the fuel cycle option. The ThU3TRU-feed and ThU3MA-feed cases can thus be considered as upper limits for the TRU and MA burning rates achievable with the MSFR.

It is worth noting that neutron economy can be artificially reduced e.g. through neutron poisons or elimination of blankets; this would ask for a quicker reprocessing rate and would reduce the inventory of trivalent isotopes in case their solubility at equilibrium becomes the main constraint to the achievable burning rate. However, elimination of the Th blankets would not benefit TRU burning since this would not alter the limit on solubility of TRUs in the feed salt. This limit can hypothetically be increased by inserting the feed e.g. at the highest temperature in the core, but this would imply e.g. notably higher temperatures in the reprocessing system, as well as the necessity to guarantee a proper mixing of the feed with the rest of the salt after injection and before reaching the heat exchangers.

1.4.3 Reactivity effect of fission products

The possibility to use the MSFR as a flexible CR reactor is related to the fact that fission products are poisonous enough to affect the CR without incurring in their solubility limits in the fuel salt. Fig. 1.7 shows the element-wise decomposition of the negative reactivity insertion due to fission products in the equilibrium core of the ThU3-feed case.

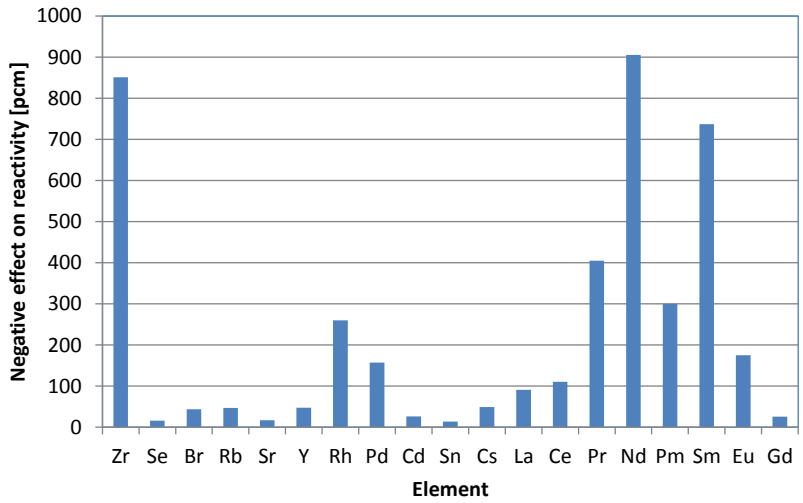

Figure 1.7: Effect on reactivity of the main fission products in the MSFR equilibrium core of the ThU3-feed case

It is interesting to note that trivalent lanthanides play by far the major role. Their negative contribution to the equilibrium reactivity amounts to 2750 pcm. The other main contributor is Zr. This may represent a problem because the possibility to efficiently extract Zr from the fuel salt is controversial (Doligez, 2011). In case Zr remained in the core, its negative contribution to reactivity would reach in 25 years that of lanthanides at equilibrium.

As mentioned, accumulation of fission products affects the CR also indirectly through a reduction of the overall actinide content. This is related to a specific modeling choice adopted in this thesis work, where it is assumed that the overall concentration of actinides and fission products is maintained during the fuel isotopic evolution. Accumulation of fission products thus implies a reduction of the actinide inventory, as shown in Table 1.8. Differences in the total actinide inventory can be notable, showing a 38% reduction when switching from breeding (Th-feed) to TRU burning (ThU3TRU-feed) operation. Effects on the reactor CR of the hypothesis of constant concentration of actinides and fission products will be briefly discussed in Section 2.2.

Table 1.8: Equilibrium actinide inventory for the MSFR feed options in Table 1.7

	Th-feed	**ThU3-feed**	**ThU3TRU-feed**	**ThU3MA-feed**
Actinide inventory [t]	42.3	33.8	26.4	30.2

1.4.4 Use of the MSFR in a U-Pu fuel cycle

For completeness, use of the MSFR in a U-Pu fuel cycle has been investigated, though this would clearly change the salt properties and thus cast doubts on the viability of this option. Only one case has been investigated, namely the use of the MSFR as iso-breeder reactor, with all Pu produced in the blankets (now containing natural U instead of Th) used as feed for the core. Iteration on the equilibrium reactivity has allowed estimating a necessary reprocessing rate of 12 l/d to guarantee the long-term operation as iso-breeder. This is to be compared to the 6.5 liters computed in the Th-U case, meaning that the spectrum of the MSFR is soft enough to make the Th cycle a better breeding option compared to the U one. Actually, looking at Fig. 1.8, it can be noted that the neutron spectrum is high at energies where the number of emitted neutrons per absorbed neutron ($\upsilon\Sigma f/\Sigma c$) is higher for U-233 than for Pu-239. The average ($\upsilon\Sigma f/\Sigma c$) is equal to 2.27 and 1.86 for U-233 and Pu-239, respectively.

In addition to the worse neutron economy, a U-Pu cycle in the MSFR has been demonstrated to cause worse performances also in terms of safety and waste management (Fiorina et al., 2012b, submitted). This combines with the weaker technical basis available to make this fuel cycle option unattractive. For this reason, use of U as main fertile material in the MSFR will not be considered in the remainder of the thesis.

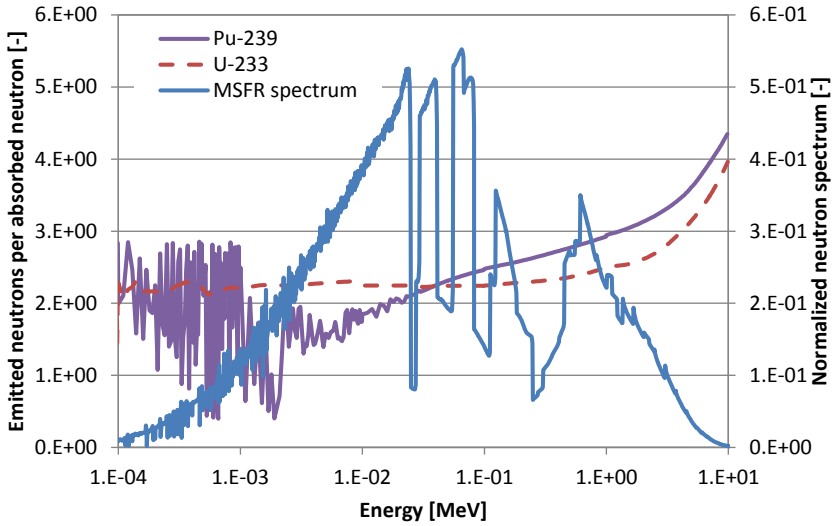

Figure 1.8: Emitted neutrons per absorbed neutron for Pu-239 and U-233, and comparison with the MSFR spectrum

1.5 CONCLUDING REMARKS

In this Chapter, the design of the MSFR has first been presented. A parametric study has been performed on the possible design for the heat exchangers between primary and intermediate circuit. A shell-and-tube configuration has been considered, showing that notably small tubes must be used to meet the constraints on the design while achieving acceptable velocities and pressure losses. However, reduction of the diameter below 4 mm is not recommended as pressure losses for lower diameters do not decrease significantly. Obtained information will be used in Chapters 4 and 6 to assess the MSFR safety features.

General core physics aspects have then been discussed. Due to the presence in the fuel of low-mass-number isotopes like Li and F, the neutron spectrum is more thermalized compared to traditional FRs. As a consequence, the fission-to-capture cross-section ratio of the actinides is greatly reduced, which is expected to have negative impacts on the build-up of heavy actinides and ultimately on the radiotoxicity and decay heat of actinide wastes (Chapters 2 and 3). On the other hand a soft spectrum concentrates neutrons in the resonance region, with ensuing positive effects expected on the Doppler reactivity feedback (Chapter 4).

Finally, fuel cycle aspects have been investigated. The possibility has been demonstrated of using the MSFR as a flexible CR reactor without design modification. By tuning the reprocessing rate it is possible to determine the content of fission products in the core, which in turn can significantly affect the neutron economy without incurring in solubility problems. Among fission products, lanthanides and Zr have been singled out as main responsible for the CR variation. Potential benefits fostered by use of the MSFR as breeder, iso-breeder or burner reactor will be discussed in details in Chapters 2, 3 and 4, also through a comparative analysis with traditional FRs (namely, the ELSY and the ARR). Use of the MSFR in a U-Pu cycle has been shown to reduce the neutron economy, since the spectrum is soft enough to make Th a better option for breeding. Following this result and the worse performances in terms of safety and waste management, the U option for the MSFR will not be considered in the remainder of the thesis.

REFERENCES

Artioli, C., Sarotto, M., Malambu, E., Sobolev, V., Massara, S., Ricotti, M.E., 2007. ELSY: neutronic design approach. Proc. ENC 2007, September 16-20, Brussels, Belgium.

Artioli, C., Grasso, G., Petrovich, C., 2010. A new paradigm for core design aimed at the sustainability of nuclear energy: the solution of the extended equilibrium state. Annals of Nuclear Energy 37, 915-922.

Aufiero, M., Cammi, A., Fiorina, C., Leppänen, J., Luzzi, L., submitted. An extended version of the SERPENT-2 code to investigate fuel burn-up and core material evolution of the Molten Salt Fast Reactor. Submitted to Journal of Nuclear Materials. Presentation at NuMat 2012 conference, October 22-25, Osaka, Japan.

Benes, O., Konings, R.J.M., 2009. Thermodynamic properties and phase diagrams of fluoride salts for nuclear applications. Journal of Fluorine Chemistry 130, 22-29.

Brovchenko, M., Heuer, D., Merle-Lucotte, E., Allibert, M., Capellan, N., Ghetta, V., Laureau, A., 2012. Preliminary safety calculations to improve the design of Molten Salt Fast Reactor. Proc. PHYSOR 2012, April 15-20, Knoxville, US.

Doligez, X., 2011. Influence du retraitement physico-chimique du sel combustible sur le comportement du MSFR et sur le dimensionnement de son unité de retraitement. PhD Thesis. Universite de Grenoble.

Energy from Thorium. Documents Related to Liquid-halide (Fluoride and Chloride) Reactor Research and Development. Available at http://www.energyfromthorium.com/pdf/.

EVOL Project 2012 - Evaluation and Viability of Liquid Fuel Fast Reactor Systems. Available at: http://www.li2c.upmc.fr/.

Fiorina, C., Aufiero, M., Cammi, A., Guerrieri, C., Krepel, J., Luzzi, L., Mikityuk, K., Ricotti, M. E., 2012a. Analysis of the MSFR Core Neutronics Adopting Different Neutron-Transport Models. Proc. ICONE 2012, July 30 – August 3, Anaheim, US.

Fiorina, C., Cammi, A., Krepel, J., Mikityuk, K., Ricotti, M. E., 2012b. Preliminary Analysis of the MSFR Fuel Cycle Using Modified-EQL3D Procedure. Proc. ICONE 2012, July 30 – August 3, Anaheim, US.

Fiorina, C., Cammi, A., Franceschini, F., Krepel, J., Luzzi, L., Ricotti, M. E., 2012c. Thorium fuel cycle in Fast Reactors: potential benefits and challenges. Proc. NENE 2012, September 5-7, Ljubljana, Slovenia.

Fiorina, C., Aufiero, A., Cammi, A., Franceschini, F., Krepel, J., Luzzi, L., Mikityuk, K., Ricotti, M. E., submitted. Investigation of the MSFR core physics and fuel cycle characteristics. Submitted to Progress in Nuclear Energy.

GIF-IV, Generation IV International Forum, 2002. A Technology Road Map for Generation IV Nuclear Energy Systems. GIF-002–00, US DOE Nuclear Energy Research Advisory Committee and The Generation IV International Forum.

Gnielinski, V., 1976. New equations for heat and mass transfer in turbulent pipe and channel flow. International Chemical Engineering 16, 359-367.

Koning, A., Forrest, R., Kellett, M., Mills, R., Henriksson, H., Rugama, Y., 2006. The JEFF-3.1 Nuclear Data Library. Nuclear Energy Agency. JEFF Report 21.

MacPherson, H.G., 1985. The Molten Salt Reactor Adventure. Nuclear Science and Engineering 90, 374-380.

Mathieu, L., Heuer, D., Brissot, R., Garzenne, C., Le Brun, C., Lecarpentier, D., Liatard, E., Loiseaux, J.M., Méplan, O., Merle-Lucotte, E., Nuttin, A., Walle, E., Wilson, J., 2006. The Thorium Molten Salt Reactor: Moving on from the MSBR. Progress in Nuclear Energy 48, 664-679.

Mathieu, L., Heuer, D., Merle-Lucotte, E., Brissot, R., Le Brun, C., Liatard, E., Loiseaux, J.-M., Méplan, O., Nuttin, A., Lecarpentier, D., 2009. Possible Configurations for the Thorium Molten Salt Reactor and Advantages of the Fast Nonmoderated Version. Nuclear Science and Engineering 161, 78–89.

Merle-Lucotte, E., Heuer, D., Allibert, M., Ghetta, V., Le Brun, C., 2008. Introduction to the Physics of Molten Salt Reactors. Materials Issues for Generation IV Systems. NATO Science for Peace and Security Series B: Physics and Biophysics 2008, 501-521.

Merle-Lucotte, E., Heuer, D., Allibert, M., Doligez, X., Ghetta, V., 2009. Optimizing the Burning Efficiency and the Deployment Capacities of the Molten Salt Fast Reactor. Proc. GLOBAL 2009, September 6-11, 2009, Paris, France.

Merle-Lucotte, E., Heuer, D., Allibert, M., Brovchenko, M., Capellan, N., Ghetta, V., 2011. Launching the Thorium Fuel Cycle with the Molten Salt Fast Reactor. Proc. ICAPP 2011, May 2-5, Nice, France.

Petukhov, B.S., 1970. In Irvine, T.F., and Hartnett, J.B., Eds., Advances in Heat Transfer 6. Academic Press. New York.

Robertson, R.C., 1971. Conceptual design study of a single-fluid molten-salt breeder reactor. Technical report, ORNL-4541.

Taiwo, T. A., Kim, T. K., Stillman, J. A., Hill, R. N., Salvatores, M., Finck, P. J., 2006. Assessment of a Heterogeneous PWR Assembly for Plutonium and Minor Actinide Recycle. Nuclear Technology 155, 34-54.

Todreas, N.E., Hejzlar, P., Nikiforova, A., Petroski, R., Shwageraus, E., Fong, C.J., Driscoll, M.J., Elliott, M.A., Apostolakis, G., 2009. Flexible conversion ratio fast reactors: Overview. Nuclear Engineering and Design 239, 2582–2595.

Salvatores, M., Palmiotti, G., 2011. Radioactive waste partitioning and transmutation within advanced fuel cycles: achievements and challenges. Progress in Particle and Nuclear Physics 66, 144-166.

van der Linden, E., 2012. Coupled neutronics and computational fluid dynamics for the molten salt fast reactor. MSc Thesis. Technical University of Delft, Netherlands.

Yang, W. S., 2008. Trends in transmutation performance and safety parameters versus TRU conversion ratio of sodium-cooled fast reactors. Proc. IEMPT-10, October 8, 2008, Mito, Japan.

Yang, W. S., 2012. Fast Reactor Physics and Computational Methods. Nuclear Engineering and Technology 44, 177-198.

CHAPTER 2: Fuel cycle performances as a breakeven reactor

ABSTRACT

The present Chapter assesses the main fuel cycle performances of the MSFR when used as a breakeven (breeder or iso-breeder) reactor in a closed fuel cycle. It includes a general assessment of claims and limitations associated to Th use in Fast Reactors (namely, the ELSY and the ARR) and it investigates the specific features of the MSFR technology. Breeding capabilities of the MSFR are confirmed, showing an achievable doubling time in the range 40-100 years, depending on the nuclear data library and on the modeling assumptions. Advantages of Th vs U in terms of radiotoxicity generation are limited, since a drastic reduction in the first few thousands of years is counterbalanced by a higher value in the very long term. Clear advantage of the Th cycle are instead observed in terms of decay heat of actinide reprocessing losses, with the caveats of a higher Sr-90 production and ensuing impacts on short-term decay heat. Among the Th-based fast-spectrum systems, the MSFR shows potential benefits in terms of waste management thanks to the high average burnup allowed by a liquid fuel, which in turn may reduce actinide reprocessing losses and ultimately radiotoxicity and decay heat of wastes. The MSFR also allows to avoid fuel fabrication and transportation, eliminating by design problems of fuel handling associated to the U-232 build-up, which is instead confirmed as a major problem for the traditional Th-based Fast Reactors. Some of the main results have been presented in (Fiorina et al., 2011, 2012a, 2012b, 2013, submitted; Franceschini et al., 2011, 2012a, 2012b, submitted; Aufiero et al., 2012, submitted).

2.1 INTRODUCTION

Operation of fast-spectrum systems in a closed U or Th cycle is considered nowadays in view of the low utilization of natural resources and of the potentially drastic reduction of nuclear wastes compared to Light Water Reactors (LWR). In a closed cycle with recycle of all the actinides, waste would originate from activated materials, fission products and actinide losses during reprocessing and fabrication. Reprocessing losses and few long-lived fission products would be the only responsible for the radiotoxicity in the very long term. From this viewpoint, Th-based Fast Reactors (FR) can offer some specific advantages as the lower mass number of Th fosters a very low endogenous generation of TRansUranic isotopes (TRU). In addition, use of U-233 instead of Pu-239 as main fissile material is often claimed to discourage

proliferation of nuclear weapons thanks to the intense and penetrating gamma field generated by the progeny of U-232 that accompanies the in-bred U-233.

Despite the potential advantages, the implementation at an industrial scale of a closed cycle needs to overcome several challenges. In particular, Th use in traditional FRs introduces difficulties in dissolution and reprocessing of used fuel, and fabrication of highly radioactive recycled fuel requiring remote manufacturing under heavy shielding. The MSFR use of liquid fuel with online reprocessing would avoid most of the issues related to reprocessing, manufacturing and transporting recycled fuel.

Objective of this Chapter is to ascertain claims and limitations related to Th use in traditional FRs, and to investigate pros and cons of the MSFR technology. The attention is focused on fuel cycle aspects of breakeven core configurations (breeder or iso-breeder) operating with full recycling of the actinide inventory. After a brief assessment of the MSFR breeding performances (Section 2.2), Sections 2.3 and 2.4 investigate radiotoxicity and decay heat generation from closed fuel cycle operation of Th vs U fast-spectrum systems, and of the MSFR vs the traditional FRs. In Section 2.5, fuel management issues are briefly investigated while concluding remarks are drawn in Section 2.6.

2.2 BREEDING PERFORMANCES

U-233 breeding is considered in the framework of the EVOL project (EVOL, 2012) as a main goal of the MSFR and a number of studies have been performed to date in this direction (see e.g., (Merle-Lucotte et al., 2009, 2011; Aufiero et al., 2012, submitted)). The present Section briefly re-assesses the MSFR equilibrium breeding performances making use of the extended-EQL3D procedure (Appendix A). As mentioned in Section 1.4, only two cases have been investigated in details, namely: iso-breeding with a 6.5 l/d reprocessing, and U-233 breeding where all U-233 produced in the blankets is extracted and 86.5 liters of fuel salt are reprocessed each day. Results for other reprocessing rates can roughly be predicted according to the following reasoning. At equilibrium, core reactivity must be zero[7]:

$$\rho = 1 - \frac{C+L+F}{P} = 1 - \frac{L+F}{P} - \frac{P(U-233)}{P}\left(\frac{C(Th-232)+C(FP)+C(U-233)+C(other)}{P(U-233)}\right) = 0 \qquad (2.1)$$

The term L/P can be considered as constant as a first approximation. F/P (approximately equal to $1/\nu$(U-233)), $C(U\text{-}233)/P(U\text{-}233)$ and $P(U\text{-}233)/P$ are mainly determined by the spectrum, thus nearly independent of the reprocessing rate. $C(other)/P(U\text{-}233)$ is a minor effect, and it is practically unaffected by reprocessing rate. Eq. 2.1 can then be written as:

$$\frac{C(Th-232)}{P(U-233)} = \frac{P}{P(U-233)}\left(1 - \frac{L+F}{P}\right) - \frac{C(U-233)+C(other)}{P(U-233)} - \frac{C(FP)}{P(U-233)} = X_1 - \frac{C(FP)}{P(U-233)} \qquad (2.2)$$

By considering U-233 as the only fissile isotope, the Conversion Ratio (CR) of the active core can be defined as:

[7] *FP indicates Fission Products.*

$$CR_{AC} = \frac{C(Th-232)-C(Pa-233)}{F(U-233)+C(U-233)} = \frac{C(Th-232)}{P(U-233)} \frac{P(U-233)}{F(U-233)+C(U-233)} - \frac{C(Pa-233)}{F(U-233)+C(U-233)} \quad (2.3)$$

$\frac{P(U-233)}{F(U-233)+C(U-233)}$ and $\frac{C(Pa-233)}{F(U-233)+C(U-233)}$ mainly depend on the neutron spectrum and on the power, which in turn are nearly independent of the reprocessing rate, so that Eq. 2.3 can then be rewritten as:

$$CR_{AC} = \frac{C(Th-232)-C(Pa-233)}{F(U-233)+C(U-233)} = \frac{C(Th-232)}{P(U-233)} X_2 - X_3 \quad (2.4)$$

By making use of Eq. 2.2, Eq. 2.4 can then be rewritten as:

$$CR_{AC} = \left(X_1 - \frac{C(FP)}{P(U-233)}\right) X_2 - X_3 \quad (2.5)$$

and the overall CR can finally be obtained as:

$$CR = CR_{AC} + \frac{(C(Th-232))_{blankets}}{F(U-233)+C(U-233)} \quad (2.6)$$

$\frac{(C(Th-232))_{blankets}}{F(U-233)+C(U-233)}$ is approximately independent of the reprocessing rate, so that Eqs. 2.5 and 2.6 can be combined to yield:

$$CR = \left(X_1 - \frac{C(FP)}{P(U-233)}\right) X_2 - X_3 + X_4 \quad (2.7)$$

where X_1, X_2, X_3 and X_4 are approximately independent of the reprocessing rate and can be computed using the reaction rates obtained e.g. for the Th-feed or the ThU3-feed MSFR.

By noting that *C(FP)/P(U-233)* at equilibrium is approximately proportional to the time constant for reprocessing, and by evaluating the reaction rates using the results for the iso-breeder MSFR, it is possible to predict the equilibrium CR, and the corresponding doubling time, as a function of the reprocessing rate. Fig. 2.1 plots the obtained results, showing also the two points directly calculated with the extended-EQL3D and the curve achieved by assuming a 10% margin on the U-233 production in the blankets (see Table 1.7).

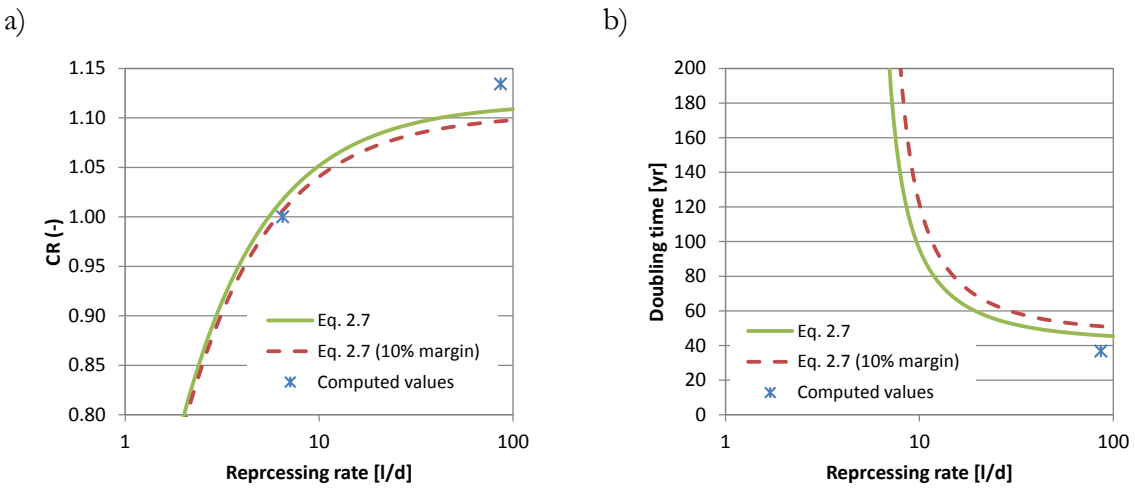

Figure 2.1: Equilibrium MSFR CR (a) and doubling time (b) as a function of reprocessing rate

The maximum achievable CR is on the order of 1.1, resulting in a ~40-50 years doubling time. Reprocessing rate strongly affects the neutron economy in the range between 1 l/d and 10 l/d, while reprocessing rates higher than ~50 l/d do not lead to significant improvements of the CR.

A fairly good agreement is observed in Fig. 2.1 between Eq. 2.7 and the computational results. The obtained curve is also consistent with that presented in Aufiero et al. (2012, submitted) and achieved with a dedicated SERPENT (Leppänen, 2007) procedure. Significant discrepancies with Aufiero et al. exist at low reprocessing rates. For instance, the mentioned work shows that only 3 liters of fuel need to be reprocessed each day to achieve iso-breeding, to be compared to the ~6 l/d computed here. This is to be ascribed to a different assumption made in the two codes. In particular, extended-EQL3D assumes that fission products substitute the actinides. This implies that the overall actinide inventory diminishes with accumulation of fission products (see Table 1.8), with detrimental effect on the CR. On the other hand, the SERPENT procedure presented by Aufiero et al. assumes that Li atoms are replaced by fission products, the actinide inventory remaining constant.

Important discrepancies have been observed in the prediction of the doubling time when changing from JEFF3.1 (Koning et al., 2006) to ENDF/B-VII.0 (Chadwick et al., 2006) nuclear data library (Aufiero et al., 2012, submitted). For a given reprocessing rate, the corresponding CR is reduced by 0.5-0.7 when evaluated using ENDF/B-VII.0 instead of JEFF3.1. As a consequence, the minimum achievable doubling time (at equilibrium) increases from 40-50 years to approximately 100 years. In addition, the minimum reprocessing rate to achieve iso-breeding is nearly doubled. These discrepancies are related to the evaluated capture cross-section of U-233, which is noticeably higher in the ENDF/B-VII.0 library. Another consequence of the higher U-233 capture cross-section is that the build-up of isotopes heavier than U-233 is increased by approximately 50%. Notably, a ~50% discrepancy is found for all isotopes heavier than U-233, indicating that no other major discrepancies exist in their cross-sections between the two nuclear data libraries. As a matter of fact, only few experimental data are available for U-233 capture in the energy domain of interest for the MSFR (Fig. 2.2), which will require new experimentation if the MSFR is to be deployed as a commercial technology.

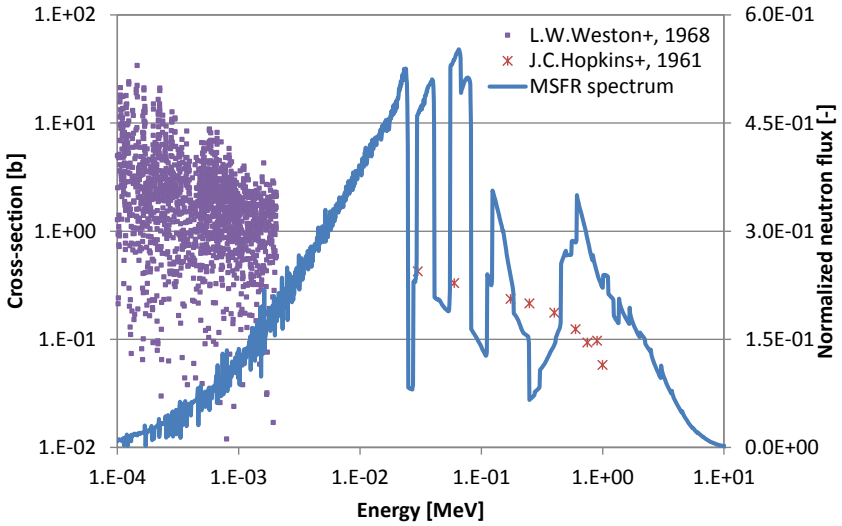

Figure 2.2: Main available experimental data for the U-233 capture cross-section

An interesting aspect to consider is that the MSFR relies on the use of radial fertile blankets, while no axial blankets are envisioned. As a matter of fact, half of the neutron leaking from the core is absorbed in the axial reflector (Section 1.3). Considering that most of the extra fissile material produced in the MSFR at high reprocessing rates is produced in the blankets (all of it in the Th-feed case – Table 1.7), this suggests that doubling times approximately reduced by half would be attainable including axial blankets in the design. In addition, it has been shown by Aufiero et al. (2012) that doubling time drastically reduced (nearly by half) compared to the equilibrium ones can initially be achieved if TRUs or Pu are employed as initial fuel. This is due to the higher fission neutron yield of Pu-239 vs U-233 (2.91 vs 2.51).

Regarding the presence of liquid blankets, proliferation issues arise from the possibility to easily retrieve U-233 through a fluorination process. The blankets also feature high quality U thanks to the small content of U-234 (1%) and, more importantly, U-232 (of the order of few hundreds of ppm in U). Nonetheless, the online reprocessing system limits transportation issues and reduces the risk of diversion of fissile material. The addition of U-238F_4 can also be considered as a security measure to directly denature the U in the molten salt phase (LeBlanc, 2010).

2.3 ACTINIDE INVENTORY

As the fuel is being irradiated, reprocessed and recycled, the actinides evolve toward their characteristic equilibrium concentrations. The equilibrium concentration for a given isotope is achieved when a net zero balance is established between its consumption, from neutron absorption and decay, and its generation from its precursors through two main pathways, neutron capture and decay. Without dwelling into the details, it is noted that as a general rule the further the isotope from the main fertile in the transmutation chain, the longer it will take to be generated, and, accordingly, to reach its equilibrium concentration. Due to the low position of Th in the actinide chain, the Th-U cycle is expected to foster low amounts of endogenously generated TRUs, increasingly smaller for Np, Pu, Am, Cm and Cf.

Table 2.1 summarizes the actinide content after 100 years of irradiation for the breakeven MSFR (Th-feed and ThU3-feed in Table 1.7). The actinide content at discharge obtained for the iso-breeder ELSY (lead-cooled, homogenous core configuration - Section B.2) and ARR (sodium-cooled, seed-and-blanket configuration - Section B.3) cores are also shown. Results have been obtained using the extended-EQL3D procedure (Appendix A) and considering a full recycle of all the actinides. In particular, the concentrations after the same cumulative fuel burnup (~9 GWth-yr/t_{HN} - GWth-yr per t of Heavy Nuclides) as for the MSFR are shown. The obtained results well approximate the equilibrium concentrations.

The low TRU content of the Th-U vs the U-Pu closed cycle can be appreciated in Fig. 2.3 displaying the content of TRUs as percent of HN. The equilibrium cycles with Th feed (Th-feed and ThU3-feed MSFR, Th-U ELSY and Th-U ARR) feature a much lower content of Pu, Am, Cm and Cf. The build-up of U-236 is the pathway to the generation of TRUs, through neutron capture to U-237 and decay to Np-237. Given that the main pathway to the generation of Pu in Th-U is through neutron capture in Np-237, the small amount of Pu generated in Th-U consists primarily of Pu-238. On the other hand the Pu vector in the U-Pu traditional FRs reflects the main breeding pathway in the U-Pu cycle, i.e. Pu-239 production from neutron captures in U-238 and decay from Np-239. As a result, the Pu isotopic makeup e.g. of the U-Pu ELSY fuel is ~57% Pu-239 and 36% Pu-240, with ~3% Pu-238, 3% Pu-241 and 4% Pu-242.

Table 2.1: HN content for the breakeven MSFR (Th-feed and ThU3-feed in Table 1.7), the ELSY and the iso-breeder ARR after 9 GWth-yr/t_{HN} of cumulative burnup

		MSFR Th-feed	MSFR ThU3-feed	Th-U ELSY	Th-U ARR	U-Pu ELSY	U-Pu ARR
HN inventory in the active core [t]		42.3	33.8	72.2	12.1	51.1	13.2
Core composition* [wt%]	**^{232}Th**	81.8	79.2	85.5	77.7	~0	~0
	^{231}Pa	$1.91\cdot10^{-2}$	$1.68\cdot10^{-2}$	$2.31\cdot10^{-2}$	$5.69\cdot10^{-2}$	~0	~0
	^{232}U	$2.40\cdot10^{-2}$	$2.12\cdot10^{-2}$	$1.96\cdot10^{-2}$	$4.94\cdot10^{-2}$	~0	~0
	^{233}U	11.1	12.6	9.56	16.0	~0	~0
	^{234}U	3.84	4.29	3.13	4.39	$3.15\cdot10^{-1}$	$6.09\cdot10^{-2}$
	^{235}U	1.02	1.17	$6.82\cdot10^{-1}$	$8.28\cdot10^{-1}$	$1.75\cdot10^{-1}$	$4.05\cdot10^{-2}$
	^{236}U	1.14	1.32	$7.27\cdot10^{-1}$	$7.49\cdot10^{-1}$	$2.32\cdot10^{-1}$	$6.09\cdot10^{-2}$
	^{238}U	$2.32\cdot10^{-3}$	$3.19\cdot10^{-3}$	~0	~0	79.7	80.6
	^{237}Np	$2.86\cdot10^{-1}$	$3.38\cdot10^{-1}$	$1.60\cdot10^{-1}$	$1.45\cdot10^{-1}$	$1.30\cdot10^{-1}$	$1.14\cdot10^{-1}$
	^{238}Pu	$3.25\cdot10^{-1}$	$3.95\cdot10^{-1}$	$1.02\cdot10^{-1}$	$8.38\cdot10^{-2}$	$5.05\cdot10^{-1}$	$2.31\cdot10^{-1}$
	^{239}Pu	$9.92\cdot10^{-2}$	$1.24\cdot10^{-1}$	$2.44\cdot10^{-2}$	$1.64\cdot10^{-2}$	9.83	12.5
	^{240}Pu	$8.39\cdot10^{-2}$	$1.10\cdot10^{-1}$	$1.48\cdot10^{-2}$	$6.75\cdot10^{-3}$	6.72	5.02
	^{241}Pu	$1.63\cdot10^{-2}$	$2.25\cdot10^{-2}$	$9.64\cdot10^{-4}$	$6.09\cdot10^{-4}$	$5.11\cdot10^{-1}$	$4.31\cdot10^{-1}$
	^{242}Pu	$1.17\cdot10^{-2}$	$1.70\cdot10^{-2}$	$1.41\cdot10^{-3}$	$4.28\cdot10^{-4}$	$6.73\cdot10^{-1}$	$3.59\cdot10^{-1}$
	Am	$7.59\cdot10^{-3}$	$1.04\cdot10^{-2}$	$2.61\cdot10^{-3}$	$5.81\cdot10^{-4}$	1.07	$4.51\cdot10^{-1}$
	Cm	$5.75\cdot10^{-3}$	$9.48\cdot10^{-3}$	$2.25\cdot10^{-4}$	$7.36\cdot10^{-5}$	$1.58\cdot10^{-1}$	$7.19\cdot10^{-2}$
	Cf	$9.83\cdot10^{-6}$	$2.28\cdot10^{-5}$	$3.61\cdot10^{-7}$	$3.03\cdot10^{-8}$	$4.33\cdot10^{-4}$	$5.86\cdot10^{-5}$

**At discharge for the ELSY and the ARR.*

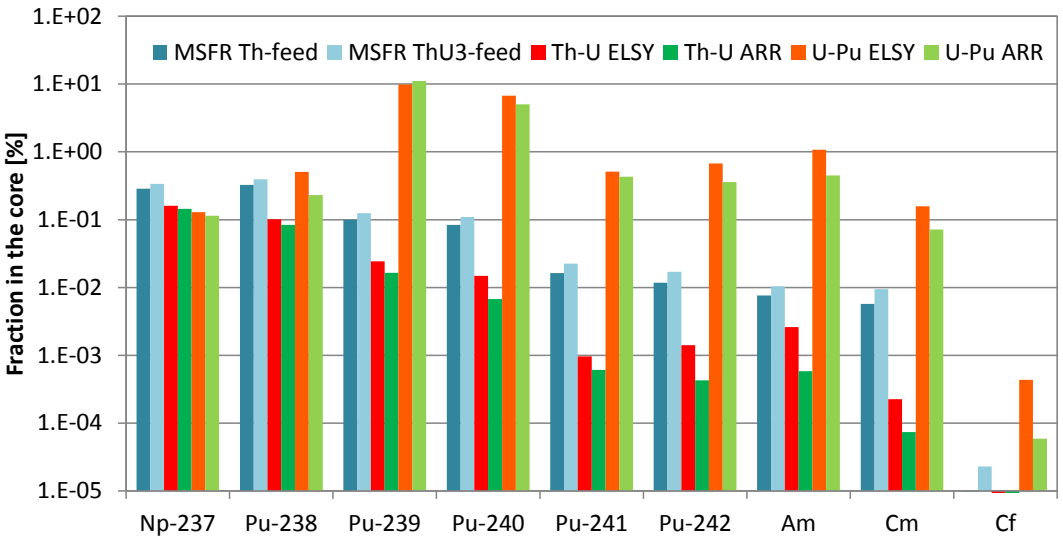

Figure 2.3: Fraction of TRUs in HN in the core after 9 GWth-yr/t_{HN} of cumulative burnup

In spite of the low TRU generation, irradiation of Th-232 causes the build-up of other actinides, especially U-234 and U-232. U-234 will be shown in the next Section to play a primary role in the long-term radiotoxicity of the fuel. Its fraction in the core is comparable in all cases, but slightly higher in the MSFR due to the softer spectrum, and in the ARR due to the high U-233 content necessary for criticality in a seed-and-blanket core configuration. U-232 is responsible of an intense gamma emission from its progeny, which greatly complicates fuel handling and fabrication in traditional solid-fuelled FRs (see Section 2.6). Its content in U amounts to 1091 ppm, 1390 ppm and 2246 ppm in the MSFR, ELSY and ARR respectively.

Fig. 2.3 shows that the softer spectrum of the MSFR relatively to the Th-U traditional FRs leads to a higher TRU content, as expected from the lower fission-to-capture cross-section ratios observed in Fig. 1.4. In particular, the relative content of Am and Cm is one or two orders of magnitude higher in the MSFR. However, the amount of TRUs is one or two orders of magnitude lower than the traditional U-Pu counterparts. In this sense, it is interesting to note that the hard spectrum of the ARR (see Fig. 1.3) fosters a lower Minor Actinide (MA) content compared to the ELSY in spite of the higher Pu enrichment needed in a seed-and-blanket configuration.

A second aspect to be considered in terms of mass evolution is the time required for each reactor to reach its equilibrium composition. Fig. 2.4 plots the evolution of the actinide inventory during the first 100 years of irradiation, starting from a U-Pu (with the Pu vector taken from Artioli et al. (2007), see Table 1.3) or a Th-U-233 core configuration. For the MSFR, only the ThU3-feed case is shown, since results for the Th-feed case are almost superimposed. Convergence is quicker for the U vs Th cycle, and for the MSFR and the ARR vs the ELSY. The slow convergence of the heaviest actinides in the Th cycle is clearly related to the number of neutron captures necessary to generate them starting from U-233 isotopes. The quicker convergence of the MSFR and the ARR compared to the ELSY is instead related the higher specific power, which is equal to 70-80 MW/t_{HN} for the former two reactors, while it is only 30 MW/t_{HN} and 20 MW/t_{HN} in the U-Pu and Th-U ELSY, respectively.

a) ThU3-feed MSFR

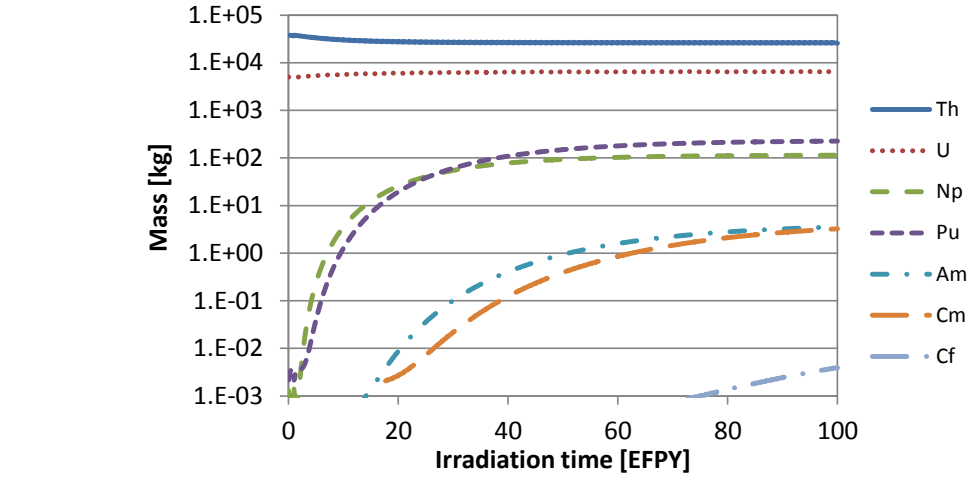

b) Th-U ELSY

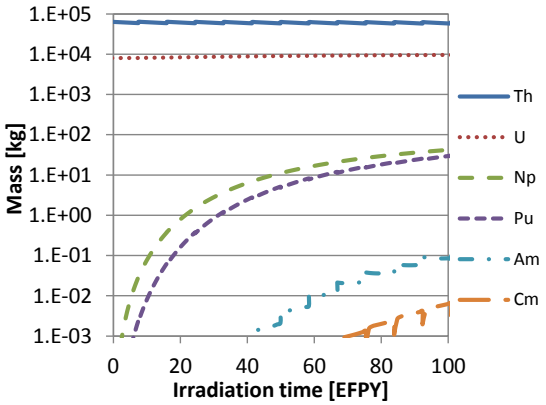

c) U-Pu ELSY

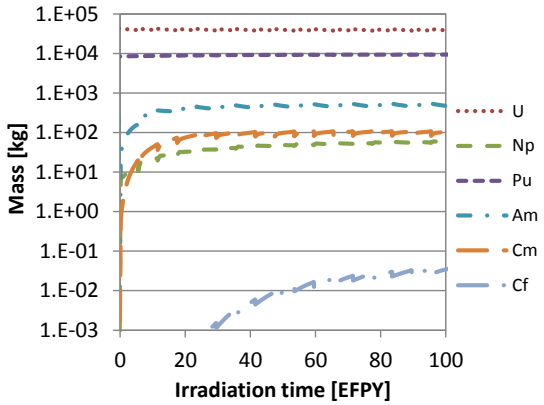

d) Th-U ARR

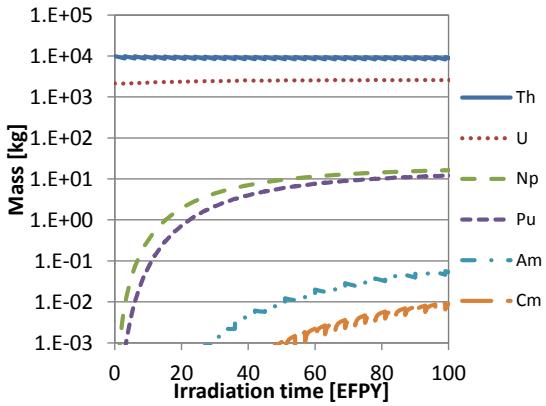

e) U-Pu ARR

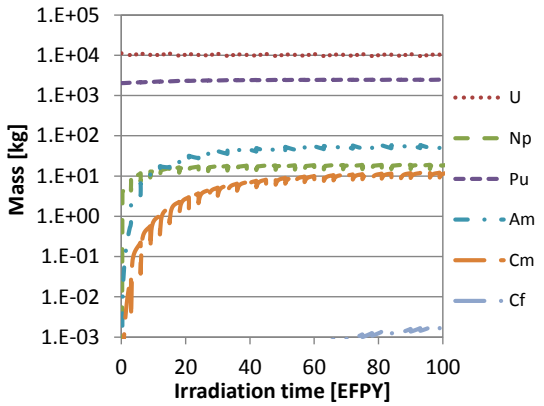

Figure 2.4: Evolution of the actinide inventory during the first 100 Equivalent Full Power Years (EFPY) or irradiation and starting from a U-Pu of Th-U-233 initial core loading for a) the iso-breeder (ThU3-feed) MSFR, b) the Th-U ELSY, c) the U-Pu ELSY, d) the Th-U ARR, and e) the U-Pu ARR

For the U-Pu traditional FRs, equilibrium compositions are representative of the reactor behavior after 40 years except for Cf, whose content is of interest mainly for fuel fabrication issues (see subsection 3.3.1). When Th is employed as fertile material, convergence is quickly reached for Th and U, but at least 60 years are needed for a nearly-complete build-up of Np and Pu (mainly Pu-238). A longer time is required for the build-up of Am, Cm and Cf.

However it will be shown that their impact on waste management and fuel handling is minimal in the Th case.

It is worth noting that the online reprocessing system in the MSFR minimizes the time required to reach the equilibrium. In fact, few years are generally envisioned in traditional FRs for the fuel to be unloaded, cooled, reprocessed and refabricated. This will approximately double the time necessary for the fuel to reach the equilibrium, even though specific technologies like use of metallic fuel and pyro-reprocessing could be used to eliminate the out-of-core cooling time also in traditional FRs.

2.4 RADIOTOXICITY OF WASTES

The actinide fuel inventory of a reactor working in a closed cycle with recycling of all the actinides needs to be disposed only at reactor decommissioning, if not further transmuted and recycled in another reactor. The radiotoxicity generated during the reactor operation is attributable to fission products and actinide losses, excluding the contribution of activated materials. Actinide losses come primarily from fuel reprocessing and manufacturing and will likely differ for the various actinides, fuel types and processes. For instance, aqueous reprocessing is the likely choice for the solid-fuelled FRs since it is more mature for implementation at industrial scale while for the MSFR the fuel is in a form more suitable for pyro-reprocessing techniques. In both cases, a detailed characterization of the reprocessing losses can only be speculative at the current stage of development. In addition fabrication losses are eliminated in the MSFR while they are difficult to quantify in solid-fuelled FRs, since the fabrication process is likely to be different compared to LWRs. For simplicity, 0.1% reprocessing and fabrication losses have been assumed in all cases as customary in the FR scientific community (NEA, 2006; Salvatores et al., 2009; Artioli et al., 2010).

It is common practice (see e.g. (NEA, 2002)) to adopt a Reference radiotoxicity Level (RL) equal to the radiotoxicity of the natural U required to fuel a typical LWR once-through core of same electrical energy output. The natural U is considered to be in secular equilibrium with the progeny. The resulting RL has been here calculated using data reported in (Rose et al., 2011) for the French EPR core, and radiotoxicity coefficients for ingestion from ICRP72 (1996). In particular, 1824 tonnes of natural U are necessary to fuel the EPR, which in turn will produce 1.65 GWe for 6 years. The radiotoxicity of natural U in equilibrium with its progeny results equal to 32 Sv/kg, which leads to a RL of $5.9 \cdot 10^6$ Sv/GWe-yr. It is worth noting that 20 Sv/kg are often used to compute the radiotoxicity of natural U. This is the case e.g. of (NEA, 2002) and is due to the lower dose coefficient for Po-210 reported by ICRP publications before ICRP72. In particular, dose coefficient of Po-210 was given for workers in previous publications, while it is given for the public starting from ICRP72. The difference is that the public is supposed to ingest radionuclides through food, i.e., in organic form, while workers generally deal with inorganic compounds.

Differences existing between ICRP publications give a clear idea of the uncertainty existing in the RL, and in radiotoxicity computations in general. In addition, the use of radiotoxicity as a discriminator to judge advanced fuel cycles is questionable (Kessler et al., 2012), since the dose coefficient would have to be combined with the actual probability of each element to reach the biosphere and eventually to enter the food cycle. Evaluations of this

kind are beyond the scope of this work, which continues to rely on traditional radiotoxicity evaluations (NEA, 2002; IAEA, 2005; Salvatores et al., 2009). However, attention should be paid when drawing conclusions from the obtained results, which must be intended only as a preliminary evaluation of the radiation exposure risk for the public associated to each fuel cycle option.

2.4.1 Impact on radiotoxicity generation of Th vs U closed fuel cycle

Before confronting the details of the MSFR radiotoxicity generation, it is worth focusing on the consequences of using Th instead of U in a closed cycle based on fast-spectrum systems. Fig. 2.5 shows the evolution over time of the ingestion radiotoxicity from actinide reprocessing losses for the ELSY equilibrium cycle. Both reprocessing losses and RL radiotoxicities are normalized per GWe-yr of energy production.

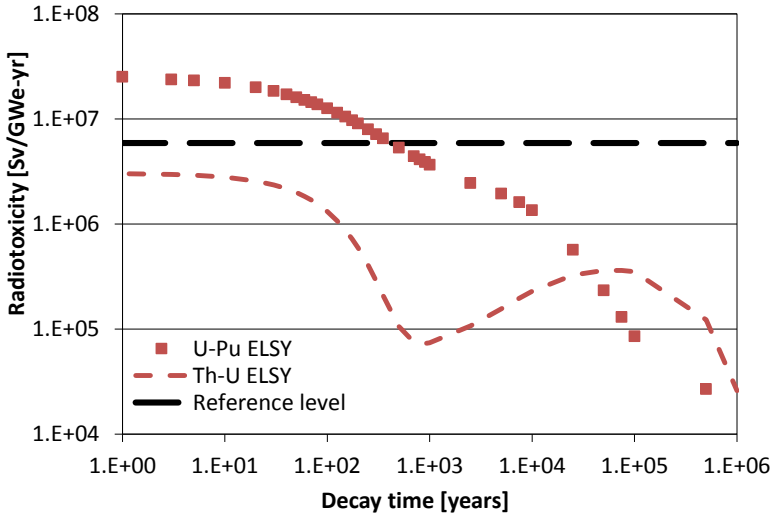

Figure 2.5: Evolution of ingestion radiotoxicity from actinide reprocessing losses for the ELSY

Fig. 2.5 shows that the Th-U cycle fosters a decreasing radiotoxicity during the first 10^3 years, one to two orders of magnitude below that of the U-Pu cycle. Subsequently, the radiotoxicity of the Th-U case starts increasing and the advantages over the U-Pu counterpart vanish at around $3.5 \cdot 10^4$ years. The radiotoxicity of Th-U continues to increase until $\sim 6 \cdot 10^4$ years, reaching a value close to that obtained after 250 years. The radiotoxicity from actinides losses in Th-U fuel cycle is below the RL already at the beginning of the simulation while, in case of the traditional U-Pu cycle, approximately 400 years are required for the radiotoxicity to become lower than the RL.

These results suggest that a closed Th cycle may represent a factual option for reducing the radiotoxic burden to the final waste repository. However, the radiotoxicity increases after 10^3 years and will conduce to a long-term peak higher than in the U closed cycle, and to a higher integral value over e.g. 10^6 years. In addition, there are intrinsic limitations in correlating radiotoxicity with actual risk of exposure that should not be forgotten. The RL itself, while it may represent a convenient term of comparison, is in essence an arbitrary number and doubts may be casted on its meaningfulness. The assumed RL, $\sim 6 \times 10^6$ Sv for GWe-yr of energy produced, is arguably a reassuring level when compared to a lethal dose of 10 Sv.

A better insight into the behaviors observed in Fig. 2.5 can be achieved by separating the effects of the different isotopes. Fig. 2.6 illustrates the main contributors to the 0.1% actinide wastes radiotoxicity of U-Pu cycle (Fig. 2.6a) and Th-U cycle (Fig. 2.6b)[8]. The major contribution for the first few decades comes from Pu-238 for both cores. Pu-238 is in fact the only TRU which is present in the Th-U cycle in a quantity roughly comparable to the U-Pu case (Table 2.1). U-232 and Th-228 (and its progeny) represent the other important contributors to radiotoxicity in the first few centuries for the Th-U cycle. Th-228 is the daughter of U-232 and after discharge they both have nearly identical activity, showing that they are in secular equilibrium. Pu-241, Am-241, Am-242m, Cm-242 and Cm-244, which also contribute to radiotoxicity in the first few decades or centuries, play a role only in the U-Pu case. This confirms that the very limited build-up of TRUs in the Th-U equilibrium cycle (see Table 2.1) is important for reducing fuel radiotoxicity. After few centuries, radiotoxicity is dominated by Pu-239 and Pu-240, in the U-Pu case, and by Th-229 and Ra-226 (and their progenies) in Th-U case. Th-229 and Ra-226 are daughters of U-233 and U-234, respectively, and the latters can actually be claimed as the isotopes responsible for the long-term radiotoxicity growth in Th case.

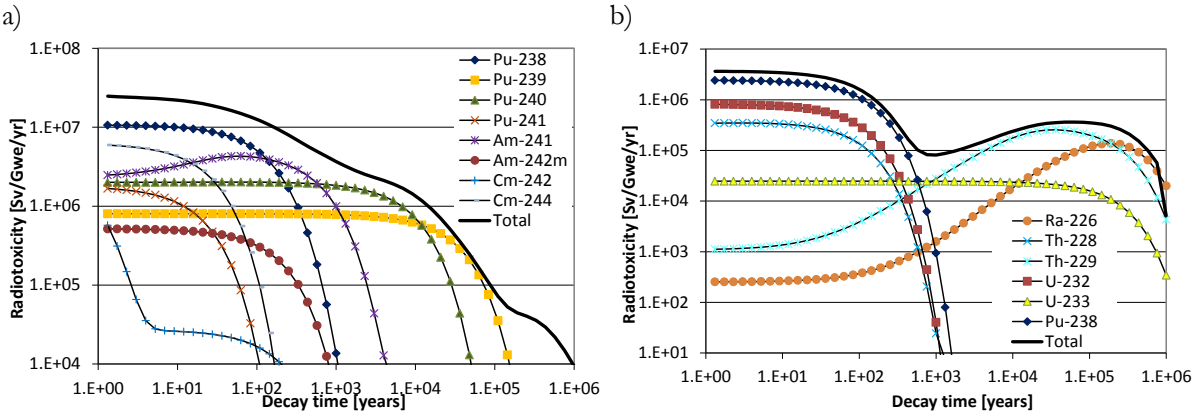

Figure 2.6: Isotopic contribution to radiotoxicity from actinide losses in a) U-Pu fuel cycle and b) Th-U fuel cycle in ELSY. Th-228, Th-229 and Ra-226 include the radiotoxicity contribution of their progenies

The equilibrium cycle radiotoxicity computed can be considered as a limiting upper boundary calculation when the reactor operates in a fully closed fuel cycle starting from an initial core of U/Pu and Th/U main fertile/fissile materials. Figs. 2.6a and 2.6b confirm this assumption. In both U-Pu and Th-U cases, a major role is played by actinides which are virtually absent in a fresh core, and which require many cycles for their complete build-up (see Fig. 2.4). In particular, Pu-238 notably contributes to the radiotoxicity of Th-U cycle. If a core is started with only Th and U-233, after 60 years of continuous operations in the ELSY only 16.5 kg of Pu-238 are present in the core, compared to the 85 kg at equilibrium. Over time scales of interest for engineering applications, the actual radiotoxicity of the U-233-started Th cycle will then be considerably lower than the equilibrium one.

[8] *Th-228, Th-229 and Ra-226 include the effect of their progenies (see Section A.4).*

2.4.2 The case of the MSFR

In Chapter 1, the MSFR has been shown to feature a softer spectrum compared to the traditional solid-fuelled FRs (Fig. 1.3), which translates into lower fission-to-capture cross-section ratios (Fig. 1.4) and ultimately in a higher build-up of hazardous isotopes (Table 2.1). The ensuing impact on radiotoxicity can be evaluated through the specific ingestion radiotoxicities (in Sv/kg_{HN}) associated to the actinide compositions of Table 2.1. Results are shown in Fig. 2.7. For the MSFR, only the ThU3-feed is reported as the Th-feed case is practically overlapping.

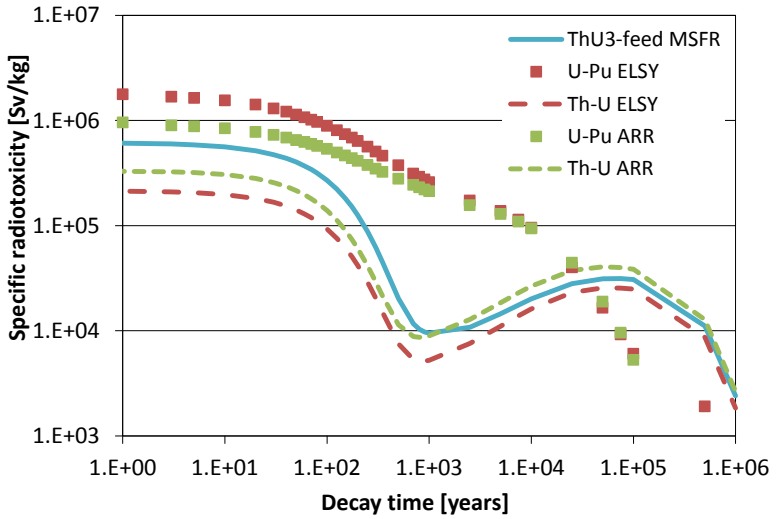

Figure 2.7: Actinide contribution to the specific ingestion radiotoxicity in the active core at equilibrium for the different reactor concepts

The effect of a softer spectrum in the MSFR is clearly visible in the initially higher radiotoxicity compared to the Th-U ELSY and ARR. The isotope mainly responsible for the initial radiotoxicity is the 88-years half-life Pu-238. Its fraction in the fuel is approximately four times higher in the MSFR than in the two traditional FRs, and contributes for ~80% to the total decay heat in the first few tens of years. The radiotoxicity evolution in the long term is instead dominated by U-233 and the MSFR shows a specific radiotoxicity between the Th-U ELSY and the Th-U ARR. Notably, the harder spectrum of the ARR vs the ELSY has no impact in the Th cycle, where its possibly positive effect is widely offset by the higher U-233 amount necessary for criticality in a seed-and-blanket configuration. On the other hand, a visible reduction of radiotoxicity is observed in the U-Pu case thanks to the lower build-up of MA and Pu-238.

The fuel specific radiotoxicity, the reprocessing and fabrication efficiency, and the average fuel burnup determine the actinide radiotoxicity generation of an operating reactor. In practice, the specific radiotoxicity (Fig. 2.7) is to be divided by the fuel average discharge burnup (unconventionally expressed in $GWe\text{-}yr/kg_{HN}$), and multiplied by the fraction of actinides that is lost during reprocessing[9]. As mentioned, reprocessing and fabrication losses have been assumed equal to 0.1% in all cases. According to this assumption, the fuel discharge burnup becomes the main discriminator when translating the specific radiotoxicity reported in

[9] *The contribution of blanket reprocessing also needs to be included.*

Fig. 2.7 from Sv/kg to Sv/GWe-yr. Namely, the fuel discharge burnup is approximately equal to: $2{\cdot}10^{-5}$and $31{\cdot}10^{-5}$ GWe-yr/kg_{HN}, for respectively Th-feed and ThU3-feed MSFR; $7{\cdot}10^{-5}$ GWe-yr/kg_{HN} for the two ELSY cases; and $10{\cdot}10^{-5}$ GWe-yr/kg_{HN} for the ARR. The resulting radiotoxicity generation for an equilibrium cycle is reported in Fig. 2.8.

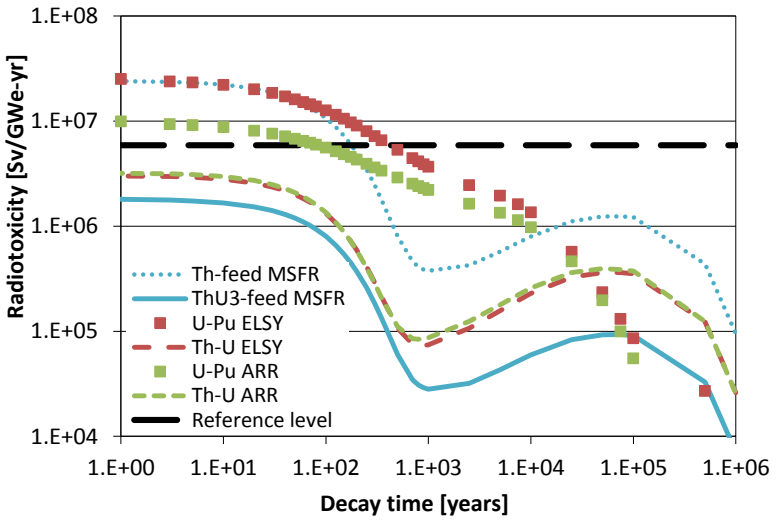

Figure 2.8: Radiotoxicity generation at equilibrium from actinide reprocessing losses for the different reactor concepts

In spite of the higher specific radiotoxicity, the low reprocessing rate and high average burnup make the ThU3-feed MSFR preferable compared to the Th-U ELSY and ARR. In Section 2.2 it has been shown that the reprocessing rate for iso-breeding is strongly dependent on possible assumptions about the fuel salt composition (namely, if fission products should replace Li or the actinides) and on the adopted nuclear data library. In addition, a ~50% higher generation of Pu-238 is predicted when employing e.g. the ENDF/B-VII.0 nuclear data library (instead of the JEFF3.1 library routinely employed in this work) as a consequence of the higher capture cross-section of U-233. However, even if a 100% margin is assumed, the iso-breeder MSFR maintains a comparable radiotoxicity profile with respect to the Th-based traditional FRs. As a consequence of the high reprocessing rate required for U-233 breeding, the Th-feed MSFR fosters instead a radiotoxicity generation similar to that of the U-Pu traditional FRs: comparable in the short-term, smaller in the intermediate to long term and higher at very large times after discharge.

In the discussion above, fission products have been neglected since their radioactive contribution is high but mainly limited to the first few hundreds of years. In particular, in Aufiero et al. (submitted) it is shown that fission products dominate radiotoxicity for 300 years, while actinides play the main role afterwards. Among the fission products however, it is possible to single out 7 long-lived isotopes, namely Se-79, Tc-99, Zr-93, Pd-107, Sn-126, I-129 and Cs-135. Fig. 2.9 shows their contribution to the radiotoxicity generation for few representative fuel cycle options. The lower radiotoxicity generation for the MSFR compared to the ELSY is related to the higher balance-of-plant efficiency, assumed to be equal to 50%, for the MSFR and 40% for ELSY. Slight differences between Th and U cycle are related to a higher generation of Sn-126 in the Th cycle. In all cases, the overall contribution to radiotoxicity from long-lived fission products is relatively small compared to that of the actinide reprocessing losses (Fig. 2.8).

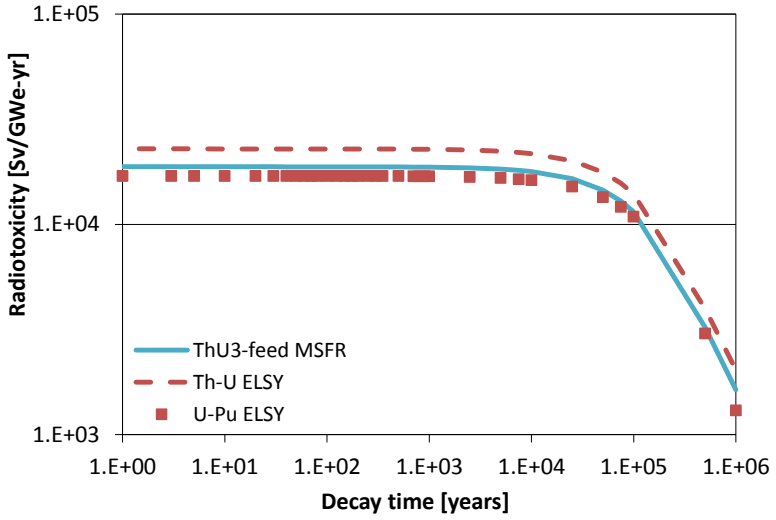

Figure 2.9: Radiotoxicity generation from long-lived fission products for the different reactor concepts

2.5 DECAY HEAT OF WASTES

Fig. 2.10 plots the decay heat from the actinide reprocessing losses. Decay heat of wastes is a concern because of the impact on reprocessing, manufacturing, and, particularly, on the final repository. Main constraints while designing a geological repository derive from the maximum temperatures inside the repository and in the surrounding geological formation. A proper comparison among the various options in Fig. 2.10 would require the use of dedicated numerical tools (Wigeland et al., 2006), which is beyond the scope of this work. On the other hand, some conclusions can be preliminarily drawn by noticing that the longest time constants related to the heat transfer phenomena in a repository are typically on the order of few hundreds of years (Wigeland et al., 2006). On this basis, the Th-based options will likely cause an initial temperature peak in the repository, and a second peak following the increase in decay heat in the 10^3-10^6 year range. Both peaks are expected to be lower compared to the initial single peak for the U-Pu counterparts. In fact, the temperature peak in the U-Pu options will be determined by the decay heat generation in the first few thousands of years, which is notably higher than the decay heat generation of the Th-U counterparts during both the initial decay and the subsequent peak. The iso-breeder MSFR is the most advantageous option while the high reprocessing rate of the Th-feed MSFR leads to a decay heat generation comparable to that of the U-Pu traditional FRs. From an isotopic point of view, a dominant role is played by the same isotopes as in the case of radiotoxicity (see (Fiorina et al., 2013) for details). Main differences comes from contributions of Cm-242 and U-232 (including Th-228 and progeny), which are in this case increased. In particular, U-232 and its progeny are responsible for 30%, 60% and 80% of the initial decay heat from actinides in MSFR, Th-U ELSY and Th-U ARR, respectively.

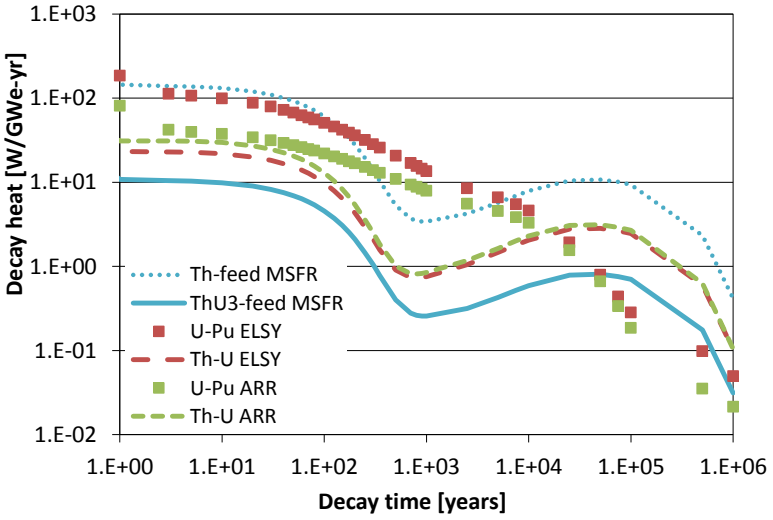

Figure 2.10: Decay heat generation from actinide reprocessing losses for the different reactor concepts

Fission products determine most of the heat generation immediately after reactor shutdown and have important implications in terms of reactor safety (see Chapter 6). Regarding the impact of fission products on fuel storage, two of them are generally assumed as particularly important, namely the ~30-year half-life Cs-137 and Sr-90 (Wigeland et al., 2006). The amount of Cs-137 generated has been found to be similar in all cases, while Sr-90 production is three times higher for the Th-based options. This will likely increase the cost of the short-middle term fuel storage, which would partially offset the longer-term improvements fostered by the Th cycle in terms of actinide wastes.

2.6 FUEL MANAGEMENT ISSUES

The liquid fuel profoundly differentiates fuel management issues of the MSFR compared to traditional solid-fuelled FRs. Table 2.2 summarizes few parameters that can be used to preliminary characterize the fuel management scheme related to a reactor system.

Table 2.2: Performance parameters of the MSFR in terms of fuel management, compared to the traditional iso-breeder FRs

	MSFR Th-feed	MSFR ThU3-feed	Th-U ELSY	Th-U ARR	U-Pu ELSY	U-Pu ARR
Fissile inventory in the core (U for Th-U and Pu for U-Pu) [t/GWe]	4.6	5.2	16.9	6.3	15.5	5.8
Fissile inventory outside the core* [t/GWe]	<1	<0.1	~16.9	~6.3	~15.5	~5.8
Reprocessing requirements [kg/GWe-d]	128.1	9.6	38.8	26.3	38.8	28.7
Reprocessing requirements for blankets [kg/GWe-d]**	52.0	3.9	-	43.7	-	20.9

**Excluding the extra fissile produced to feed or start other reactors. Considering a maximum out-of-core cooling time approximately equal to 1 month for the MSFR, and equal to the fuel irradiation time for the ELSY and the ARR.*
***Upper limit assuming the same average irradiation time as for the driver fuel.*

Thanks to a softer spectrum, a good neutron economy and a high specific power, the MSFR presents advantages in terms of fissile inventory inside the core, especially compared to

the ELSY. The out-of-core inventory is also drastically reduced thanks to the online reprocessing system. In fact, if standard reprocessing and fabrication techniques are assumed for the solid-fuelled FRs, a cooling time of few years is necessary before reprocessing the spent fuel and fabricating the new one, so that the out-of-core actinide (and fissile) inventory can be assumed of the same order of magnitude as the in-core one. On the other hand, an online reprocessing system virtually eliminates the out-of-core actinide inventory in the MSFR, though it is not clear to date if it will be possible or economically advantageous to extract, reprocess and reinsert the fuel on a daily basis. For reasons related to the decay heat and radiation emission of actinides and fission products, it may be useful to extract the fuel and cool it for some days before reprocessing. However, even considering a one-month cooling time, the out-of-core fissile inventory would be negligible compared to the traditional FRs.

For the iso-breeder MSFR, reprocessing requirements for the driver fuel are also drastically reduced compared to the solid-fuelled counterparts. This is due to the high burnup achievable using a liquid fuel. The average fuel burnup in the iso-breeder MSFR is equal to ~200 GWth-d/t_{HN}, to be compared to the ~65 GWth-d/t_{HN} and ~80-90 GWth-d/t_{HN} for the ELSY and the ARR, respectively. The same advantage is observed for the blankets if the same average irradiation time as for the driver fuel is assumed. Reprocessing requirements inevitably becomes high in the MSFR if breeding is a goal.

In addition to the lower fissile inventories and reduced reprocessing requirements, the most interesting advantage of the MSFR comes from the possibility of avoiding fuel transportation and fabrication, which represent formidable challenges for Th use in traditional FRs. In fact, the intensity and high energy of the gamma radiation emitted by two U-232 daughters, namely Bi-212 (0.7-1.8 MeV) and Tl-208 (2.6 MeV), imposes remote fuel handling and manufacturing behind thick shielding. The gamma dose rate at 0.5 meters (a typical working distance for glove-box operations) from a 5-kg sphere of U-233 containing 1500 ppm of U-232 is ~0.2 Sv/hr (Kang and von Hippel, 2001). Exposed workers would reach the annual dose limit in few minutes, and a few hours of exposure would be life-threatening.

As a matter of fact, the first and longest-lived daughter of U-232 is the 1.9-years half-life Th-228. If Th is separated from the other actinides during reprocessing the fuel would be momentarily free from the gamma-emitting U-232 progeny. However, this will require a dedicated heavily shielded storage facility with a storing capacity of several hundreds of tonnes of highly radioactive Th. In addition, fuel fabrication and transportation would have to be performed soon after reprocessing to avoid the build-up of the U-232 progeny. Fig. 2.11 plots the gamma sources from U-based and Th-based ARR assemblies after reprocessing, and compares them to that of a U-based burner version of the ARR (column 1 in Table 3.4). Results have been achieved with the ORIGEN-S code (SCALE, 2006). The gamma emission from a Th-based assembly would reach that of the burner ARR assembly in only one year. In addition, Fig. 2.12 shows that most of the gammas are emitted at high energies. A clear idea of the problem of U-232 gamma emission has been given by Wenner et al. (2012), who used the equilibrium actinide concentrations obtained in this thesis work for the ARR to demonstrate that, for a given shielded facility for fuel fabrication, the dose to workers in case of Th-based fuel assemblies would be tens of times higher compared to a U-based fuel assembly, even considering the reduced neutron emission fostered by the lower TRU build-up in the Th case.

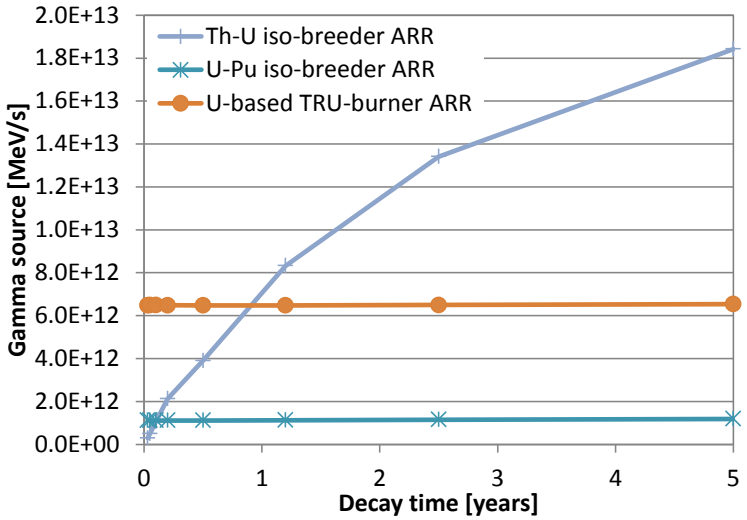

Figure 2.11: Gamma source from an assembly in different ARR versions

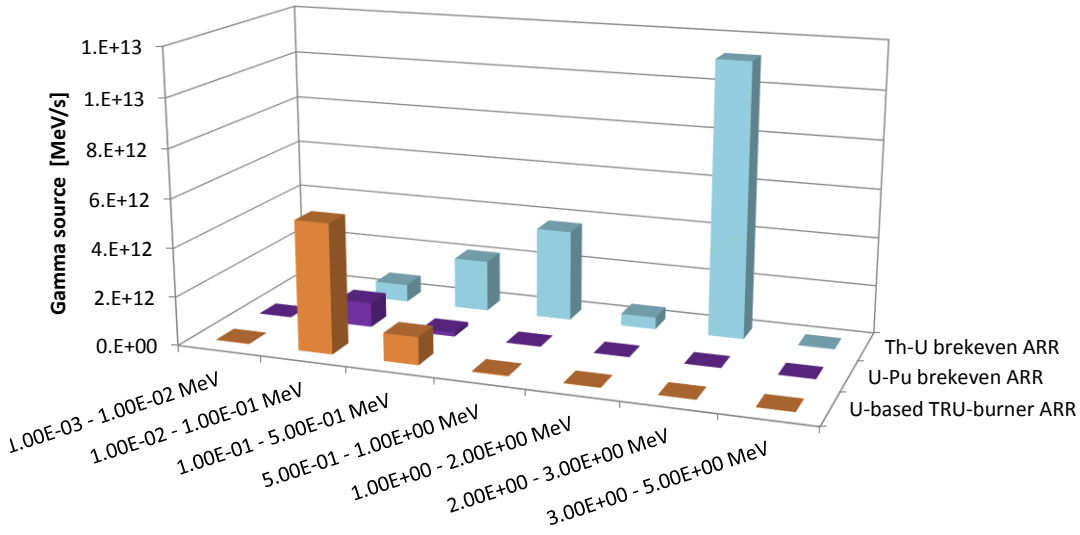

Figure 2.12: Gamma source from an assembly after 5 years of cooling for different energies and ARR versions

As a final comment, it is worth noting that the Th-U cycle is often claimed as proliferation resistant thanks to the U-232 gamma emission. This claim is however controversial. It is a fact that U handling is made difficult by the presence of U-232 progeny. In addition, shielding high energy (2.6 MeV) gammas is difficult and the characteristic energetic peak would make the U easily detectable. According to Till et al. (1980), "… ten days after purification, a one-gram sample of U-233 containing 100 ppm U-232 should be detectable through a 2 inch of lead shielding by a standard type of doorway monitor equipped with NaI detectors". On the other hand, the intense gamma field could interfere with other types of instruments, like the passive gamma-ray non-destructive assembly measurement techniques. In addition, even though separation of Th from U requires special techniques (e.g. the THOREX process), separation of the first Th-228 daughter, namely Ra-224, is expected to be much easier thanks to the markedly different chemical behavior. Ra-224 has a half-life of

3.66 days, which would allow a reasonable margin for fuel handling. As a matter of fact, 24000 ppm of U-232 in U would be necessary to meet IAEA's standard for reduced physical protection requirements (>1 Sv/hr at 1 meter (IAEA, 1999)). It is also worth noting that Pa-232 and Pa-233 have half-lives of 1.3 days and 27 days, respectively. Approximately 10 days after discharge, the Pa in the fuel would be almost free from Pa-232 and would lead to the generation of nearly pure U-233 if separated from in-bred U. Since, Pa separation is relatively easy, this possible route for the generation of U-233 represents a major concern related to the deployment of Th-based reactors (Ashley et al., 2012).

2.7 CONCLUDING REMARKS

In this Chapter the fuel cycle performances of the MSFR have been investigated and compared to those of traditional FRs. The attention has been focused on breakeven (breeder or iso-breeder) concepts, while TRU burning will be investigated in the next Chapter.

The breeding capabilities of the MSFR have first been assessed. The CR increases rapidly with increasing reprocessing rate till few tens of liters per day, while nearly saturating when approaching 100 l/d. The resulting equilibrium doubling time is in the range 40-100 years, uncertainties being related to the lack of experimental data for U-233 capture in the energy range of interest for this reactor. Room for improvements exists in the adoption of axial blankets, or in the use of Pu for the reactor start-up.

A very limited build-up of TRUs was observed in the closed Th cycle, for both the traditional FRs and the MSFR. As a consequence, the core actinide specific radiotoxicity was found to be noticeably reduced compared to the traditional U-Pu FRs in the first few thousands of years. On the other hand, Th use causes a higher specific radiotoxicity in the long term due to the progenies of U-233 and U-234. Similar pros and cons have been observed for the decay heat, but in this case the long-term peaking is of limited concern, showing that the Th cycle is a factual option to potentially reduce the number of required geological repositories. As a drawback, U-233 has a higher fission yield for Sr-90 compared to Pu-239, causing a high decay heat level in the first several tens of years, with possible incremental costs for interim fuel storage or initial forced cooling in a geological repository.

The MSFR features higher specific radiotoxicity and decay heat compared to the solid-fuelled counterparts. This is due to the softer spectrum and ensuing build-up of heavy actinides (especially Pu-238). However, for given reprocessing efficiencies, waste generation also depends on the average fuel burnup. In fact, higher burnups limit the reprocessing requirements and ultimately the actinide reprocessing losses. For the iso-breeder MSFR, the high average burnup allowed by the liquid fuel offsets the higher TRU content and makes this reactor preferable (or comparable) to the traditional FRs in terms of waste generation.

The liquid fuel of the MSFR also fosters important advantages in terms of fuel management, since fuel transportation and assembly fabrication would be avoided. This eliminates by design most of the difficulties associated to the U-232 gamma emission in a Th cycle. In addition, the high specific power, the relatively soft spectrum and the good neutron economy of the MSFR guarantee a small fissile inventory in the core, which combines with the virtually absent out-of-core actinide inventories to greatly reduce problems of fuel management.

As regards proliferation issues, the low fissile inventories and the online reprocessing system limits the U-233 amount outside the power plant and minimize the potential risk of its diversion. Thanks to the liquid fuel, the possibility also exists of denaturing the U-233 with addition of U-238. On the other hand, the relatively easy extraction of U-233 through fluorination and the very high quality of U produced in the blankets increase proliferation risks related to the use of the MSFR technology. More generally, proliferation resistance of the Th cycle is controversial. The intense gamma emission from U-232 complicates the handling of U-233, but the problem could be circumvented through U purification from Ra-224, or through Pa-233 extraction from the core.

REFERENCES

Artioli, C., Sarotto, M., Malambu, E., Sobolev, V., Massara, S., Ricotti, M.E., 2007. ELSY: neutronic design approach. Proc. ENC 2007, September 16-20, Brussels, Belgium.

Artioli, C., Grasso, G., Petrovich, C., 2010. A new paradigm for core design aimed at the sustainability of nuclear energy: the solution of the extended equilibrium state. Annals of Nuclear Energy 37, 915-922.

Ashley, S.F., Parks, G.T., Nuttal, W.J., Boxal, C., Grimes, R.W., 2012. Thorium fuel has risks. Nature 492, 31-33.

Aufiero, M., Cammi, A., Fiorina, C., Luzzi, L. 2012. Modification of the SERPENT code to study the fuel isotopic evolution of molten salt reactors with online (continuous) reprocessing. Presentation for "2012 SERPENT International Users Group Meeting". September 19-21, Madrid, Spain.

Aufiero, M., Cammi, A., Fiorina, C., Leppänen, J., Luzzi, L., submitted. An extended version of the SERPENT-2 code to investigate fuel burn-up and core material evolution of the Molten Salt Fast Reactor. Submitted to Journal of Nuclear Materials. Presentation at NuMat 2012 conference, October 22-25, Osaka, Japan.

Chadwick, M.B. et al., 2006. ENDF/B-VII.0: Next Generation Evaluated Nuclear Data Library for Nuclear Science and Technology. Nuclear Data Sheets 107, 2931–3060.

EVOL Project 2012 - Evaluation and Viability of Liquid Fuel Fast Reactor Systems. Available at: http://www.li2c.upmc.fr/.

Fiorina, C., Franceschini, F., Krepel, J., Mikityuk, K., 2011. Comparative Analysis of Uranium and Thorium Fuel Cycles in a Lead-Cooled Fast Reactor from the Perspective of Safety and Waste Management. Proc. GLOBAL 2011, December 11-16, Chiba, Japan.

Fiorina, C., Cammi, A., Krepel, J., Mikityuk, K., Ricotti, M. E., 2012a. Preliminary Analysis of the MSFR Fuel Cycle Using Modified-EQL3D Procedure. Proc. ICONE 2012, July 30 – August 3, Anaheim, US.

Fiorina, C., Cammi, A., Franceschini, F., Krepel, J., Luzzi, L., Ricotti, M. E., 2012b. Thorium fuel cycle in Fast Reactors: potential benefits and challenges. Proc. NENE 2012, September 5-7, Ljubljana, Slovenia.

Fiorina, C., Cammi, A., Franceschini, F., Krepel, J., Mikityuk, K., Ricotti, M. E., 2013. Analysis of thorium and uranium fuel cycles in an iso-breeder Lead Fast Reactor using extended-EQL3D procedure. Annals of Nuclear Energy 53, 492-506.

Fiorina, C., Aufiero, A., Cammi, A., Franceschini, F., Krepel, J., Luzzi, L., Mikityuk, K., Ricotti, M. E., submitted. Investigation of the MSFR core physics and fuel cycle characteristics. Submitted to Progress in Nuclear Energy.

Franceschini, F., Lahoda, E., Carelli, M., Wenner, M., Ferroni, P., Fiorina, C., Sartori, A., Ricotti M.E., Petrovic, B., 2011. A Comprehensive Approach to Waste Management with Thorium. Invited keynote paper from IAEA. Technical Meeting on World Thorium Resources, October 17 - 21, Thiruvananthapuram, India.

Franceschini, F., Fiorina, C., Huang, M., Petrovic, B., Wenner, M., Krepel, J., 2012a. Radiotoxicity Characterization of Multi-Recycled Thorium Fuel. Proc. WM Symposia 2012, February 26 - March 1, Phoenix, US.

Franceschini, F., Lindley, B., Fiorina, C., Lahoda, E., Wenner, M., 2012b. Analysis of a fuel cycle strategy to achieve low-radiotoxicity waste. Proc. IEMPT-12, September 24-27, 2012, Prague, Czech Republic.

Franceschini, F., Lindley, B., Fiorina, C., Phillips, C., Lahoda, E., Wenner, M., submitted. Promises and Challenges of Thorium Implementation for Transuranic Transmutation. Submitted to WM Symposia 2013, February 24 - 28, Phoenix, US.

IAEA, International Atomic Energy Agency, 1999. The Physical Protection of Nuclear Material and Nuclear Facilities. Technical Report. INFCIRC/225/Rev.4.

IAEA, International Atomic Energy Agency, 2005. Thorium fuel cycle – potential benefits and challenges. Technical Report. IAEA-TECDOC-1450.

ICRP, International Commission on Radiological Protection, 1996. ICRP Publication 72: Age-dependent Doses to the Members of the Public from Intake of Radionuclides Part 5, Compilation of Ingestion and Inhalation Coefficients. Annals of the ICRP 26/1.

Kang, J., von Hippel, F.N., 2001. U-232 and the proliferation resistance of U-233 in spent fuel. Science and Global Security 9, 1-32.

Kessler, J., Apted, M., Kozak, M., Nutt, W., Sowder, A., Swift, P., 2012. Radiotoxicity Index: An Inappropriate Discriminator for Advanced Fuel Cycle Technology Selection. Proc. WM 2012 Symposia, Feb 26- March 1, Phoenix, US.

Koning, A., Forrest, R., Kellett, M., Mills, R., Henriksson, H., Rugama, Y., 2006. The JEFF-3.1 Nuclear Data Library. Nuclear Energy Agency. JEFF Report 21.

LeBlanc, D., 2010. Molten salt reactors: A new beginning for an old idea. Nuclear Engineering and Design 240, 1644–1656.

Leppänen, J., 2007. Development of a new Monte Carlo reactor physics code. PhD Thesis. Helsinki University of Technology.

Merle-Lucotte, E., Heuer, D., Allibert, M., Doligez, X., Ghetta, V., 2009. Optimizing the Burning Efficiency and the Deployment Capacities of the Molten Salt Fast Reactor. Proc. GLOBAL 2009, September 6-11, 2009, Paris, France.

Merle-Lucotte, E., Heuer, D., Allibert, M., Brovchenko, M., Capellan, N., Ghetta, V., 2011. Launching the Thorium Fuel Cycle with the Molten Salt Fast Reactor. Proc. ICAPP 2011, May 2-5, Nice, France.

NEA, Nuclear Energy Agency, 2002. Accelerator-Driven Systems (ADS) and Fast Reactors (FR) in advanced nuclear fuel cycles. Technical Report. NEA-3109.

NEA, Nuclear Energy Agency, 2006. Physics and safety of transmutation systems: a status report. Technical Report. NEA-6090.

Rose, S.J., Wilson, J.N., Capellan, N., David, S., Guillemin, P., Ivanov, E., Meplan, O., Nuttin, A., Siem, S., 2011. Minimization of actinide waste by multi-recycling of thoriated fuels in the EPR reactor. Annals of Nuclear Energy 38, 2619–2624.

Salvatores, M., Chabert, C., Fazio, C., Hill, R., Peneliau, Y., Slessarev, I., Yang, W.S., 2009. Fuel cycle analysis of TRU or MA burner fast reactors with variable conversion ratio using a new algorithm at equilibrium. Nuclear Engineering and Design 239, 2160-2168.

SCALE: A Modular Code System for Performing Standardized Computer Analyses for Licensing Evaluations, ORNL/TM-2005/39, Version 5.1, Vols. I–III, November 2006. Available from Radiation Safety Information Computational Center at Oak Ridge National Laboratory as CCC-732.

Till, C. E., Chang, Y.I., Kittel, J.H., Fauske, H.K., Lineberry, M.J., Stevenson, M.G., Amundson, P.I., Dance, K.D., 1980. Fast breeder reactor studies. Technical Report. Argonne National Laboratory, ANL-80-40.

Wenner, M., Franceschini, F., Kulesza, J., 2012. Preliminary Comparative Shielding Analysis for Refabricating Different Fuel Vectors. Proc. ANS Winter Meeting 2012. November 11-15, San Diego, US.

Wigeland, R. A., Bauer, T. H., Fanning, T. H., Morris, E.E., 2006. Separations and transmutation criteria to improve utilization of a geologic repository. Nuclear Technology 154, 95-106.

CHAPTER 3: Fuel cycle performances as a burner reactor

ABSTRACT

The present Chapter focuses on the MSFR performances as a burner reactor in a closed fuel cycle. The investigation is carried out through a comparative analysis with traditional Fast Reactors, including both U- and Th-based versions. The MSFR emerges as a promising option for quickly transmuting an initial transuranic loading into typical Th-U equilibrium compositions, with potential advantages in terms of waste management. A significant transuranic burning rate can also be achieved via a transuranic feed in a low-conversion-ratio version of the MSFR: with a 60% share in electricity production, the MSFRs could recycle and burn the transuranics produced by the remaining 40% once-through Light Water Reactors. Comparison with traditional burner Fast Reactors shows that the MSFR features a lower burning rate for transuranics (including Pu), but a potentially higher transmutation rate for minor actinides (Np, Am, Cm, Cf) thanks to the liquid fuel and the ensuing possibility of using a feed composed only of Th and minor actinides (without Pu). Thorium use in traditional Fast Reactors has a limited impact on burning performances. On one hand it slightly increases burning rates thanks to the inherently worse neutron economy of Th-232 vs U-238. On the other hand, Th use exacerbates problems of fuel handling typical of transmutation reactors due to the intense gamma field form U-232's progeny. Some of the main results have been presented in (Fiorina et al., 2011, 2012a, 2012b, 2013, submitted; Franceschini et al., 2011, 2012a, 2012b, submitted; Aufiero et al., 2012, submitted).

3.1 INTRODUCTION

Following increasing concerns from the public opinion, and technical reasons associated to number and costs of geological repositories for nuclear waste disposal, transmutation of the TRansUranic isotopes (TRU) legacy from Light Water Reactor (LWR) operation has become a main objective for the development of innovative reactors (GIF-IV, 2002; Artioli et al., 2010; Salvatores and Palmiotti, 2011). By recovering and recycling actinides from used fuel, implementation of a transmutation strategy can also enhance use of nuclear resources, which can be of strategic importance if nuclear energy production is continued in the future. In this scenario, Fast Reactors (FR) play a dominant role since highly effective transmutation of TRUs requires multi-recycling the fuel and a fast-spectrum facilitates the closure of the fuel cycle thanks to a lower build-up of hazardous isotopes. Use of Th may offer specific

advantages. The inherently low neutron economy in a fast-spectrum favors the consumption of an external supply of TRUs while the low mass number limits their endogenous generation. On the other hand, transmutation adds significant costs, risks and technical challenges to the nuclear fuel cycle; it requires large investments and long-term commitment; it poses proliferation concerns related to the necessity of reprocessing the fuel. A major challenge comes from the need to remotely fabricating the fuel due to the intense neutron and gamma radiation field from recycled fuel.

The present Chapter aims at investigating the TRU burning capabilities of the MSFR through a comparative analysis with traditional FRs. Both U and Th version of the ELSY and the ARR (Appendix B) are considered to shed light on the pros and cons of using Th as support fertile material in a fast-spectrum transmutation reactor with recycle of all the actinides.

Two possibilities exist for TRU burning in FRs. The first one is discussed in Section 3.2 and consists in loading initially the reactor with TRUs and operating the reactor in a closed cycle till the initial loading has been transmuted into the equilibrium core compositions. The second, more effective, option is to use low-CR (Conversion Ratio) reactors and use a feed composed by Th or U (natural or depleted) and by a TRU fissile top-up (Section 3.3). Section 3.4 investigates in some details a fuel cycle strategy for the MSFR that combines the use of TRUs in the initial core loading and in the feed, plus a final transmutation stage in which the in-core TRU inventory is consumed using the MSFR in iso-breeding mode (i.e., using Th and U-233 from the blankets as only feed). Final remarks are provided in Section 3.5.

3.2 CONSUMPTION OF AN INITIAL TRU LOADING

A first possibility of using a reactor to burn radioactive wastes is to use the TRU legacy from LWR operation as start-up core loading. In particular, in FRs the fuel can be multi-recycled till the initial U-TRU or Th-TRU loading is replaced with equilibrium concentrations. For the TRU burning to be effective, the equilibrium actinide inventory must have lower radiotoxicity and decay heat compared to the initial TRU loading. From this perspective, a fast-spectrum is essential to increase the actinide fission-to-capture cross-section ratios (Fig. 1.4), thus limiting the endogenous generation of TRUs. If Th is used as feed, the equilibrium core will feature the characteristic radiotoxicity and decay heat profiles discussed in Sections 2.4 and 2.5, with ensuing potential improvements over the initial TRU loading.

3.2.1 Effectiveness of transmutation

Various fuel cycle options exist for burning an initial TRU-loading, depending on the initial TRU composition, and on the subsequent use of the reactor as breeder, iso-breeder or burner, which in turn will determine the equilibrium composition. For brevity, only the case of iso-breeder reactors (that use only U or Th as feed) employing an initial loading of TRUs from once-through LWR operation will be considered. This is expected to give general indications of the burning potential of Th-based vs U-based fuel cycles in fast-spectrum systems, and of the MSFR vs the traditional FRs.

As discussed in subsection 1.2.3, the use of an initial Th-TRU loading in the MSFR is not possible due to the solubility limits of trivalent actinides in the carrier salt. Even though the

possibility exists to increase the solubility limits through a higher core temperature (see subsection 1.2.2), a more realistic choice would be to mix the TRUs with (tetravalent) U enriched in U-235. Both options, identified as Th-TRU and Th-U5-TRU in Table 1.3, will be here considered.

For the ESLY and the ARR, initial addition of enriched U is not required. On the other hand, fabrication issues suggest that use of 10-years cooled TRUs would be preferable instead of the 5-years cooled TRUs employed for the MSFR. The isotopic composition is reported in Table 3.1

Table 3.1: Isotopic composition [wt%] of the 10-years cooled LWR TRU vector employed for the ELSY and the ARR

Np-237	Pu-238	Pu-239	Pu-240	Pu-241	Pu-242	Am-241	Am-243	Cm-244	Cm-245
4.72	2.17	47.39	22.8	8.41	6.83	5.61	1.55	0.45	0.04

The fraction of TRUs in the core necessary to achieve criticality for the ELSY and the ARR has been iteratively determined and results are shown in Table 3.2. The Table also lists the resulting fraction of Minor Actinides (MA) in the core, showing that the traditional limit of 5% MA (Salvatores, 2002) is met in all cases.

Table 3.2: TRU and MA fractions [wt%] in the start-up core for the ELSY and the ARR

	TRU fraction in the core	MA fraction in the core
Th-U ELSY	20	2.5
U-Pu ELSY	19	2.4
Th-U ARR	28	3.5
U-Pu ARR	22	2.7

To evaluate the TRU burning capabilities of each reactor system and fuel cycle options, radiotoxicity and decay heat of the initial core actinide inventory will be compared with the equilibrium one, achieved through the use of the extended-EQL3D procedure (Appendix A). As mentioned, only iso-breeder versions of the investigated reactors have been considered. In particular, the same core configurations considered in Chapter 2 are investigated. For the ELSY, this includes the Th and U versions described in Section B.2. For the ARR, only the two Th-based and U-based iso-breeder designs (Table B.2) will be considered, while excluding the low-CR burner design. For the MSFR, iso-breeding translates into the ThU3-feed option of Table 1.7. The equilibrium compositions of these 5 options are those reported in Table 2.1.

Radiotoxicity

Fig. 3.1 shows the results achieved in terms of initial and equilibrium radiotoxicity for the three different reactors, considering both the U and Th options in the traditional FRs. A first result is that transition from a TRU-started core to equilibrium composition does not reduce radiotoxicity in the U-Pu ELSY. A small reduction is observed for the U-Pu ARR, whose harder spectrum limits the build-up of MA. In particular, the reduced radiotoxicity in the first 10^3 years can be ascribed to the lower fraction of Pu-238 and Am-241 in the ARR vs the ELSY equilibrium core (see Table 2.1 and Fig. 2.6a).

When Th is used, the transition of the core composition from the initial TRU loading to the equilibrium changes the radiotoxicity profiles from those typical of a U-Pu cycle to those typical of the Th-U cycle (see subsection 2.4.1), with ensuing advantages and disadvantages. In

particular, radiotoxicity is drastically reduced for the first few tens of thousands of years, while it is increased afterwards. As discussed in subsection 2.4.1, whether or not the transition is to be considered beneficial is controversial, since the radiotoxicity peak would be decreased by nearly one order of magnitude, while the integral radiotoxicity over 10^6 years would be higher (e.g. by 4 times in the Th-U5-TRU started MSFR).

Fig. 3.1 clearly singles out the negative effect of a softer spectrum on the reactor capability to reduce the radiotoxicity of an initial TRU loading. In a Th-U equilibrium, a softer spectrum induces a higher content of Pu-238, which is the main responsible for the radiotoxicity in the first few hundreds of years (Fig. 2.6b). The MSFR is in this sense the worst option. The possible necessity of mixing TRUs with enriched U at start-up would further reduce the radiotoxicity reduction (if any).

a) MSFR

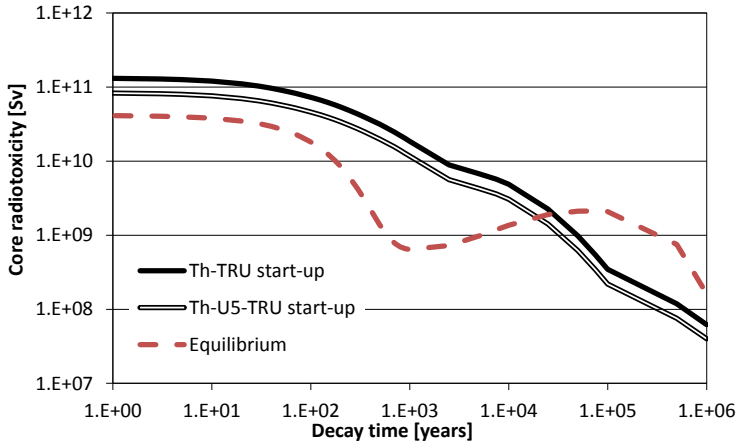

b) Th-U ELSY

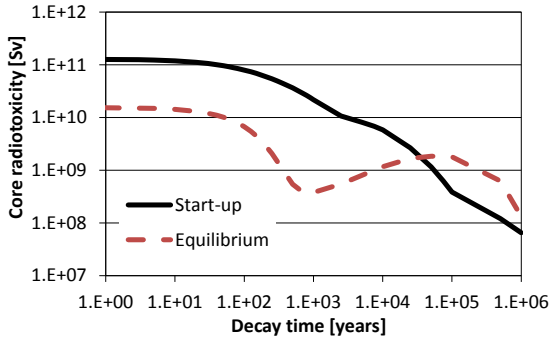

c) U-Pu ELSY

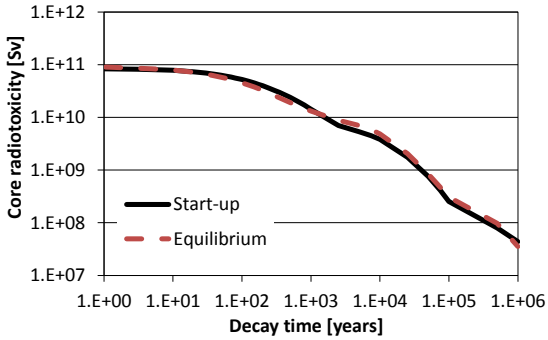

d) Th-U ARR

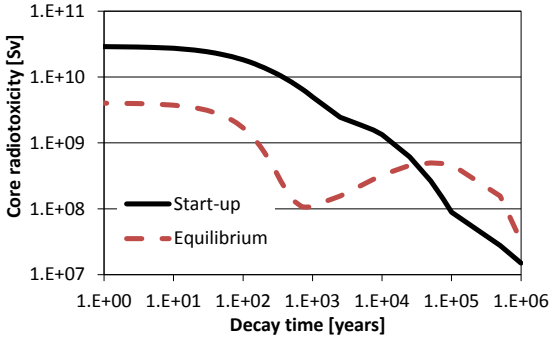

e) U-Pu ARR

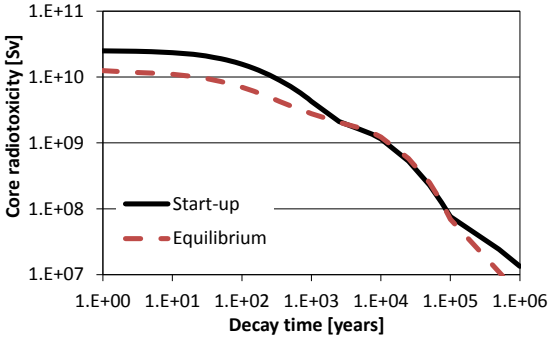

Figure 3.1: Radiotoxicity profiles of TRU start-up core and equilibrium actinide inventory for a) the iso-breeder MSFR, b) the Th-U ELSY, c) the U-Pu ELSY, d) the Th-U ARR, and e) the U-Pu ARR

Decay heat

Results similar to those achieved for radiotoxicity have been obtained for the actinide decay heat, as shown in Fig. 3.2. A slightly worse behavior is observed due to: 1) the relatively higher contribution of U-232 (and progeny) to the decay heat compared to radiotoxicity (see Section 2.5), which increases the decay heat of the Th-U equilibrium core for the first few centuries; and 2) the higher contribution of Cm-242, which is responsible for the initial peak in the U-Pu cases.

a) MSFR

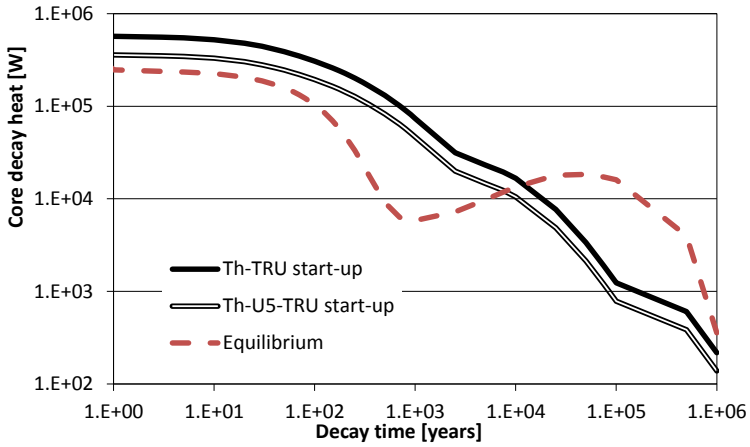

b) Th-U ELSY

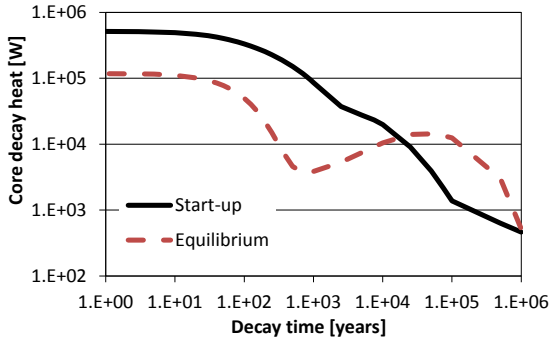

c) U-Pu ELSY

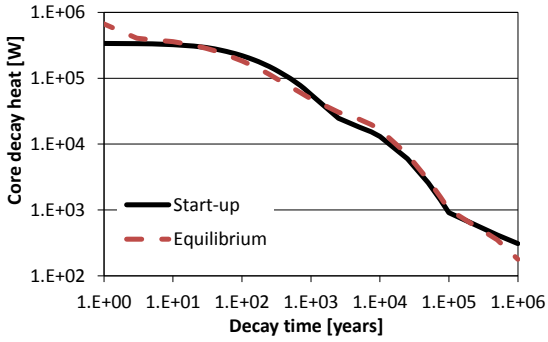

d) Th-U ARR

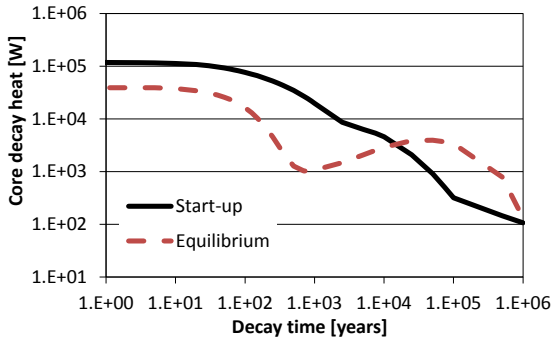

e) U-Pu ARR

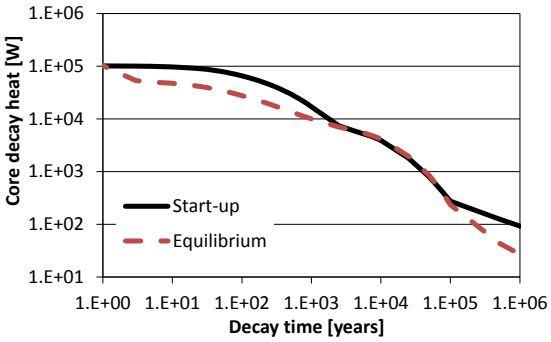

Figure 3.2: Decay heat profiles of TRU start-up core and equilibrium actinide inventory for a) the iso-breeder MSFR, b) the Th-U ELSY, c) the U-Pu ELSY, d) the Th-U ARR, and e) the U-Pu ARR

Decay heat is mainly of interest as it determines the temperature peak in a possible geological repository. Similarly to the case of radiotoxicity, transmutation of an initial TRU loading is mostly ineffective in a U-Pu cycle, since the equilibrium core decay heat is

comparable to that of the initial TRU loading. On the other hand, the transition from the initial TRU loading to the Th equilibrium is expected to improve the repository thermal performances, possibly reducing the required number of repositories. In fact, heat transfer phenomena in a geological repository feature maximum time constants of few hundreds of years (Wigeland et al., 2006), which allows to benefit from the low initial decay heat while excluding possible negative impacts from its long-term increment.

Also in this case, the softer spectrum of the MSFR has negative effects and an even more negative impact would come from the use of enriched U for the core start-up. Notably, the advantage of TRU transmutation is lower in this case for the ARR compared to the ELSY, which is due to the high U-232 fraction in the equilibrium core (Table 2.1).

3.2.2 Transmutation time

In spite of the potential advantages achievable in the transition from an initial TRU loading to an equilibrium Th-U core, the time required for this transition plays a fundamental role as very long transitional periods would de facto frustrate the effectiveness of transmutation. Fig. 3.3 shows the evolution of the main actinides for 100 Equivalent Full Power Years (EFPY). Two reactor features mainly determines such evolution: the core specific power (in Watt per kilogram of Heavy Nuclides - W/kg_{HN}) and the neutron spectrum.

a) Th-TRU started MSFR

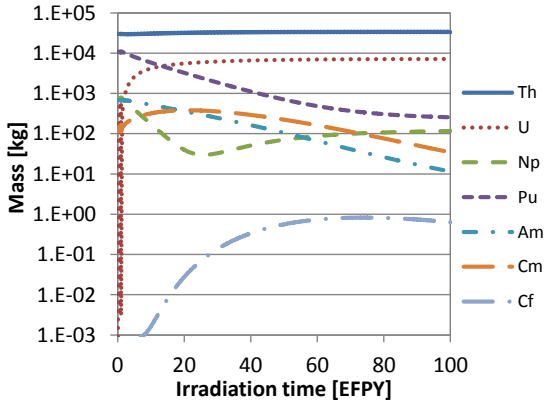

b) Th-U5-TRU started MSFR

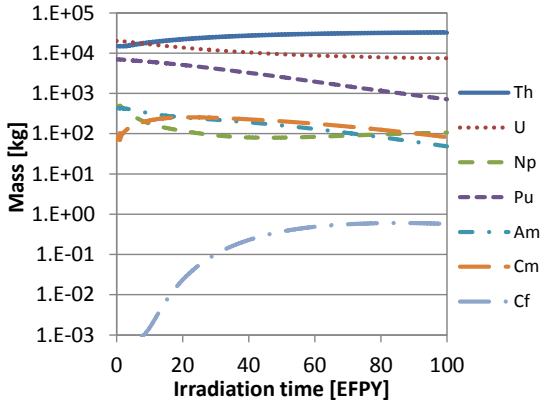

c) Th-TRU started Th-U ELSY

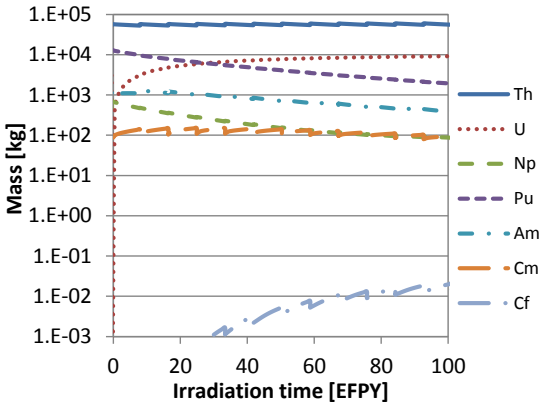

d) Th-TRU started Th-U ARR

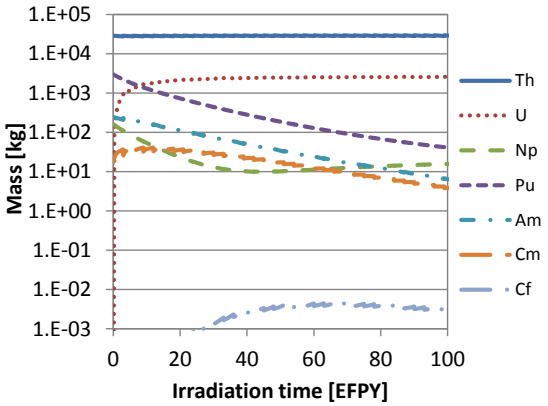

Figure 3.3: Isotopic evolution with irradiation for a) the iso-breeder Th-TRU started MSFR, b) the iso-breeder Th-U5-TRU started MSFR, c) the TRU-started Th-U ELSY, d) the TRU-started Th-U ARR

The core specific power is ~4 times lower in the ELSY compared to the other two reactors, causing a very slow burn-down of Pu, Am and Cm. After 100 EFPY, more than 2 tonnes of Pu are still in the core, while the amount of Cm is the same as the initial one. On the other hand, 100 EFPY are sufficient for an almost complete burn-down (to the equilibrium level) of Pu, Am and Np in the Th-TRU started MSFR and in the ARR. Burning of Cm is a slower process, and its amount is reduced by only 3 times after 100 EFPY in the MSFR and in the ARR. Transmutation time in the MSFR is greatly extended if the initial inventory includes enriched U. This is due to the persistency in the fuel of U-238, which in turn generates Pu-239 and heavier isotopes.

For a better evaluation of the capability of the three reactors to approach the equilibrium state in terms of radiotoxicity[10], Fig. 3.4 shows the radiotoxicity after 300 years of cooling of the actinide inventory as a function of the cumulative irradiation time, expressed in EFPY. To ease the comparison between different reactors, the radiotoxicity has been normalized to its initial value. Notably, the MSFR behaves like the ARR if initially loaded with TRUs, while it is only slightly better than the ELSY if U-238 is used at start-up.

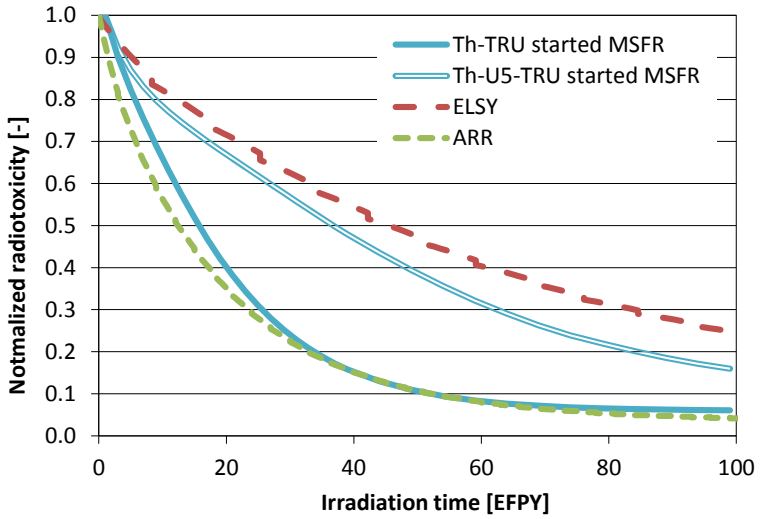

Figure 3.4: Radiotoxicity associated to the evolving actinide inventory, after 300 years of cooling

The main effect of a softer spectrum in the MSFR is the notable build-up of Cf, whose amount reaches 1 kg in 60 EFPY and is slowly reduced afterwards. A higher initial build-up of Cm can also be observed. As a matter of fact, build-up of Cm and Cf is a lower concern for the MSFR, since their impact on the overall radiotoxicity and decay heat is small, especially in the long term, and no significant consequences are expected in terms of fuel handling thanks to the liquid fuel. On the other hand, the build-up of Cm and Cf isotopes is a concern in the traditional solid-fuelled FRs as they represent the main responsible for neutron emission. This combines with the build-up of U-232 (that is completed in 2-3 cycles) to require remote fuel handling and manufacturing.

A second specific advantage of molten fuel and online reprocessing is to accelerate the transition toward equilibrium compared to solid-fuelled reactors, where the fuel has to be periodically removed, cooled, reprocessed and remanufactured. The out-of-core cooling time,

[10] *Similar results have been obtained for decay heat and are not reported here for brevity.*

especially for aqueous reprocessing, is comparable to the irradiation time which doubles the time required to reach the equilibrium.

In view of the problems for fuel handling and considering the extension of the transmutation time due to out-of-core cooling, transmutation of an initial TRU loading in the ELSY can arguably be considered a viable option and doubts can be casted on the overall advantages in case of the ARR. On the other hand, the capability to reach equilibrium in a time scale compatible with the reactor lifetime, without incurring in problems of fuel handling, is a considerable potential advantage of the MSFR, which makes it a promising option to expedite the transition from the current U-based cycle to a Th-based cycle.

3.3 TRU BURNING DURING REACTOR OPERATION

A sizeable TRU burning can be achieved employing low-CR reactors with the TRU legacy from LWR operation used as fissile top-up in the feed, and operating with full recycle of the actinides. FRs are advantageous for this fuel cycle strategy, since highly effective TRU burning requires multi-recycle of the fuel and a fast spectrum can limit the ensuing build-up of hazardous isotopes. However, fuel handling remains challenging as the achievement of high TRU burning rates requires fuels with high fractions of TRUs (and MA), causing intense radiation field and heat load. The MSFR emerges as a natural choice for TRU burning as it would combine the advantages of a fast-spectrum and a fully closed cycle with the unique possibility of avoiding fuel fabrication.

3.3.1 U- or Th-supported TRU burning in the ARR

Before confronting the issue of TRU burning in the MSFR, it is worth focusing on traditional low-CR FRs (namely, the ARR – see Section B.3). This will provide reference performances to better evaluate the MSFR burning capabilities. Use of both U and Th as support fertile materials is here considered. In fact, little information is available in the open literature regarding Th-supported TRU burning in FRs (Touran et al., 2010), but the inherently lower CR of Th is advantageous when the main objective is to enhance the burning rate, thus minimizing the deployment of transmutation reactors. Thorium is also claimed to reduce decay heat and neutron source as a consequence of the lower endogenous generation of TRUs.

Transmutation reactors can be used to directly burn TRUs from current LWR operations. However, studies in the past have pointed out possible advantages of recycling Pu in LWRs, while burning only MA in FRs (Salvatores, 2005; Taiwo et al., 2006). As a matter of fact, use of a U-MA or Th-MA feed is impractical for fuel handling, safety and fuel performance issues, so that blending of MA with recycled Pu is generally considered (Yang, 2008). To test the TRU burning capabilities of the ARR, two possible TRU feed has then been considered, namely: 10-years cooled TRUs from once-through LWR operation (MA/Pu~0.1), and MA blended with multi-recycled Pu in LWRs in one-to-one ratio (MA/Pu~1). The isotopic composition of the two vectors is reported in Table 3.3.

Table 3.3: Isotopic composition [wt%] of the TRU vectors used as feed for the ARR

	Np-237	Pu-238	Pu-239	Pu-240	Pu-241	Pu-242	Am-241	Am-243	Cm-244	Cm-245
Once-through MA/Pu~0.1	4.72	2.17	47.39	22.8	8.41	6.83	5.61	1.55	0.45	0.04
Multi-recycled MA/Pu~1*	7.3	2	18.2	13.4	5.9	10.6	18.8	15.9	7	0.9

**(Yang, 2008).*

Combination of the two TRU feeds in Table 3.3 with a U or Th fertile support yields four possible strategies for TRU burning in the ARR. The equilibrium methodologies presented in Appendix A have been applied to the ARR burner design (Section B.3) with the mentioned four fuel cycle options and results have been summarized in Table 3.4.

Table 3.4: Equilibrium cycle performance for the investigated ARR feed/fertile isotope options

Fertile isotope		U	Th	U	Th
MA/Pu ratio in the feed		~0.1	~0.1	~1	~1
CR [-]*		0.47	0.36	0.40	0.29
TRU burning rate [kg/GWe-yr]		494	593	563	665
MA burning rate [kg/GWe-yr]**		61	70	296	332
Fissions in U-238 or Th-232 [% of total]		9.03	1.97	7.96	1.64
Core HN inventory [t]		10.2	9.6	10.2	9.6
Equilibrium core composition at discharge [wt%]	**Th-232**	~0	58.34	~0	47.50
	Pa-231	~0	0.05	~0	0.05
	U-232	~0	0.05	~0	0.05
	U-233	~0	6.40	~0	5.15
	U-234	0.36	2.42	0.69	2.45
	U-235	0.10	0.49	0.16	0.49
	U-236	0.16	0.52	0.22	0.51
	U-238	63.16	~0	55.21	~0
	Np-237	0.93	1.02	0.97	1.07
	Pu-238	1.65	2.06	3.03	3.86
	Pu-239	11.62	5.60	8.91	3.11
	Pu-240	12.65	11.89	11.69	11.38
	Pu-241	1.84	1.85	1.62	1.65
	Pu-242	3.61	4.51	5.64	7.25
	Am-241	1.42	1.77	2.88	3.83
	Am-242m	0.11	0.13	0.24	0.29
	Am-243	1.15	1.45	3.65	4.96
	Cm-244	0.90	1.06	3.59	4.57
	Cm-245	0.22	0.25	0.94	1.16
	Cm-246	0.13	0.14	0.57	0.68
	Cf-250	$4.55 \cdot 10^{-4}$	$3.89 \cdot 10^{-4}$	$1.75 \cdot 10^{-3}$	$1.65 \cdot 10^{-3}$
	Cf-252	$5.95 \cdot 10^{-6}$	$5.12 \cdot 10^{-6}$	$2.05 \cdot 10^{-5}$	$1.92 \cdot 10^{-5}$
MA fraction [wt%]**		4.72	5.82	13.3	17.3

**CR defined considering Th-232 and U-238 as the only fertile materials and all other isotopes as fissile. It corresponds to the TRU regeneration rate (Wade and Hill, 1997) in the U-based cores, while TRUs must be substituted by trans-Th isotopes to employ the same definition of CR to Th-based cores. In all cases, it is computed as the ratio of the rate of non-fission capture rate in U-238 or Th-232 to the rate of TRU or trans-Th destruction by fission.*

***MA indicates traditional minor actinides, i.e., Np, Am, Cm, Cf.*

As expected, replacing U with Th without changing fuel design and fuel management scheme lowers the CR, from 0.47 to 0.36 for the ~0.1 MA/Pu feed and from 0.40 to 0.29 for the ~1 MA/Pu feed. The inferior neutron economy is fostered by: reduced fission contribution from Th-232 compared to U-238 (~2% of total fissions from Th-232 compared to 8-9% from U-238); lower neutron yield of in-bred U compared to Pu (on average, ~2.35 neutrons emitted per neutron absorbed in U-233 vs. ~2.5 for Pu-239); lower fuel density for Th (~10% for the cases in Table 3.3) and higher fraction of neutron leakage. As a result of the lower CR, the Th cases display a higher TRU and MA burning rate compared to the counterpart U configurations with same fuel design and fuel management scheme. The lower CR, and higher TRU burning rate, observed for the cases with the ~1 MA/Pu feed derives from the low fissile quality of the feed, which entails a higher TRU content in the core and a consequent lower amount of fertile isotopes.

The different breeding pathway, U-238->Pu-239 in U vs. Th-232->U-233 in Th, entails a much lower endogenous production of Pu in the Th cores, reflected in the lower Pu inventory at equilibrium, e.g., respectively 2.8 vs 2.2 t in the U vs Th burner options with ~0.1 MA/Pu feed. On the other hand, the MA content is mainly determined by the fed TRUs and is higher in the Th cases due to the higher transmutation rate. Therefore, for low CR reactors with similar TRU burning rates, the choice of Th over U as the TRU carrier does not per se conduce to a lower TRU content at equilibrium[11] and the possible claimed advantages of Th vs U in terms of fuel handling in low-CR burner reactors are to be excluded. To quantify the differences between U and Th use in this sense, the decay heat at manufacturing and the radioactive field for a fuel assembly are given in the Figs. 3.5 and 3.6[12], where they are compared to the standard case of a U-Pu iso-breeder FR (the U-Pu iso-breeder ARR described in Section B.3, with composition in Table 2.1). Results have been achieved with the ORIGEN-S code (SCALE, 2006).

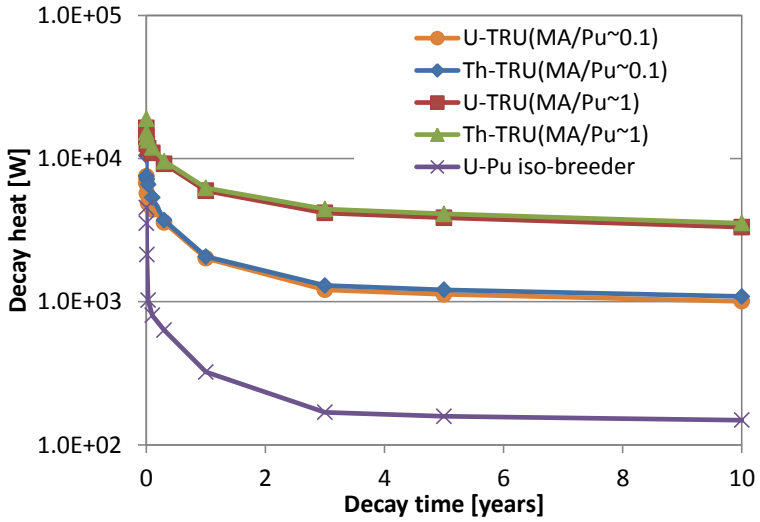

Figure 3.5: Decay heat of a discharged ARR fuel assembly

[11] *Only for reactor designs with higher CR, the low endogenous generation of TRUs from Th becomes the predominant effect, culminating in the much lower content of TRUs in the Th breakeven design (62 kg) compared to the U counterpart (2.3 t), as shown in Table 2.1.*

[12] *It is supposed that the fuel is reprocessed after 3 years, and that irradiated Th is replaced with fresh Th (see Section 2.6).*

a) Neutron source

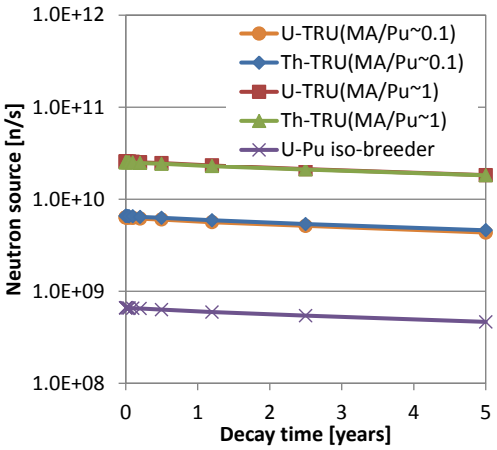

b) Gamma source

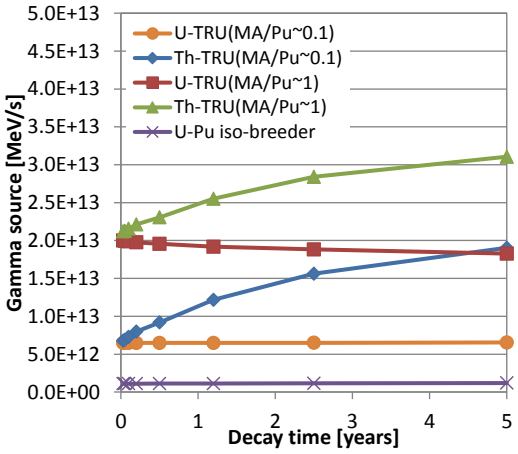

Figure 3.6: Radiation field from an ARR fuel assembly after reprocessing (with Th removal during reprocessing): a) neutron source; b) gamma source

For the burner options, the decay heat generation is initially ~10 kW per assembly, with a relatively sharp decrease during the first few years mainly as a consequence of the rapid decay of the ~180-day half-life Cm-242. After approximately three years, the decay heat stabilizes at a value of 1-3 kW per assembly, 5 to 15 times higher compared to a U-Pu iso-breeder core at equilibrium. The decay of 18-year half-life Cm-244 and of 88-year half-life Pu-238, the main contributors to the decay heat after 3 years of cooling, will then drive further reductions in decay heat until other longer-lived actinides become relevant. Since the inventory of Cm and Pu-238 in the burner concepts considered is not significantly affected by the adopted fertile isotope (Table 3.4), the actinide decay heat in the time range of relevance for fuel handing is virtually the same for Th or U-based burners.

Cm-244 and Cf-252 are the main responsible for neutron emission, which result for a burner core one or two orders of magnitude higher compared to a traditional U-Pu iso-breeder core. Due to the higher content of Cm and Cf, the neutron source for the ~1 MA/Pu feed is considerably higher than for the ~0.1 MA/Pu feed. Also in this case, there are limited differences between Th and U use.

The gamma source immediately after reprocessing for the U and Th burners is nearly identical as still driven by the content of TRUs. In particular, Am-241, Cm-244 and Pu-238 accounts for respectively ~45%, ~30% and ~15% of the total gamma emission, with the emitted radiation in the energy range from 10 to 100 keV. However, for the Th cores, the gamma emission increases after reprocessing due to the build-up of the daughters of U-232, Bi-212 and Tl-208 in particular. The intensity and high energy of the gamma radiation emitted by Bi-212 (0.7-1.8 MeV) and Tl-208 (2.6 MeV) greatly exacerbate problems of fuel handling and manufacturing. Using the equilibrium concentration in Table 3.4, Wenner et al. (2012) have demonstrated that the Th options causes a dose to workers tens of times higher compared to the TRU counterpart for a given shielded facility.

Summarizing, Th use fosters an increased TRU burning rate due to the lower breeding capabilities, but advantages are not observed in terms of decay heat and neutron source. This is due to the fact that in a low-CR FR the inventory of Pu-238 and MA is mainly determined by the feed, while their endogenous generation from the fertile isotopes plays a secondary role. In addition, Th use greatly increases the gamma emission due to the U-232's progeny.

In both U and Th cases, this intense radiation field combines with the very high heat load to create a major obstacle to the commercial deployment of burner FRs, especially if relying on homogeneous fuel recycle schemes, unless a technological breakthrough in remote fuel manufacturing occurs. Taking into account these problems, and due to safety (see subsection 4.2.1) and fuel performance considerations, it is customary in the FR scientific community to set an upper limit to the MA content in U-supported burner cores to ~5% (Salvatores, 2002). This limit is essentially an arbitrary number, but its significance emerges also from the results here obtained, showing that a 5% limit corresponds to having fuel assemblies with a decay heat of the order of 1 kW, thus asking for specific precaution during fabrication (Itoh et al., 2008; Takata et al., 2008; Ikeda et al., 2011). In addition, it will be shown in subsection 4.2.1 that the core safety experiences a drastic deterioration for higher MA contents. Thorium use does not reduce decay heat while it will be shown in subsection 4.2.1 to improve safety, but with limited effects for high MA contents. As a consequence, it is reasonable to assume the traditional 5% limit for both the U- and Th-based ARR. This constraint is met only when using TRUs from once-through LWR operation as fuel, which set the upper limit for TRU- and MA-burning in the ARR to 500-600 kg/GWe-yr and 60-70 kg/GWe-yr, respectively.

3.3.2 TRU burning with the MSFR

In Chapter 1, it has been shown that the MSFR can be operated as a burner reactor by affecting the neutron economy through a lower reprocessing rate and higher content of fission products in the core. A Th-TRU or Th-MA feed can be used with a maximum ~20 wt% TRUs or MA (due to the solubility of trivalent isotopes in the salt at the lowest temperature in the core), which sets the maximum achievable burning rates. In fact, the total mass of Th and TRUs fed to the core is ultimately determined by the energy output. The MSFR generates ~1100 GWth-d per year, which requires fissioning of ~1150 kg of actinides. At equilibrium, masses in the core do not change, which implies that fed Th and TRUs/MA are entirely burnt. This translates into a maximum achievable TRU burning rate of $0.2 \cdot 1150 = 230$ kg per years, corresponding to 153 kg/GWe-yr. As mentioned in Chapter 1, elimination of the U-233 blankets would not benefit the burning rate since this would not alter the solubility limit of TRUs or MA in the feed salt. This limit could be increased through insertion of the feed at temperatures higher than the minimum one in the core. However, feasibility or economic competitiveness of this option are questionable and should have to be demonstrated, so that the stricter ~20 wt% limit is considered in this thesis work.

If TRUs from once-through LWR were used as feed, the resulting transmutation rate of 153 kg/GWe-yr would be approximately 1/3 – 1/4 that achievable in the ARR. However, it should be emphasized that TRU burning rate is usually normalized to the energy output under the assumptions that energy production with transmutation reactors will be more expensive than that from LWRs: a higher TRU burning rate per energy produced implies a lower share of the electricity production from transmutation reactors if the goal is to burn all the wastes from LWR operation. Normalization with the energy output when comparing two transmutation reactors has instead intrinsic limitations. For instance, the MSFR TRU burning rate is penalized by the higher expected efficiency of its energy system (50% vs 42%). For the comparison to be meaningful, the burning rate should be further normalized using the extra-cost associated to the use of the advanced reactor considered vs standard LWRs, but detailed

cost estimate are not available in the open literature for both reactors here considered and are beyond the scope of the work.

An interesting aspect of the use of the MSFR for TRU burning is related to the possibility of selecting the TRU feed without incurring in problems of fuel manufacturing and transportation. Under the assumption that TRU burning is limited by solubility of trivalent isotopes in the feed, and noting that TRUs are all trivalent (except for Np that can be partly tetravalent), virtually the same burning rate could be achieved for any TRU vector. The only constraint on the TRU composition would be set by solubility of trivalent isotopes and fission products inside the core at equilibrium. In fact, it has been shown in Chapter 1 that use of a Th-TRU feed with TRUs from once-through LWR operation determines an equilibrium concentration of trivalent actinides and fission products comparable to, or slightly higher than, the solubility limits. A better feed from the viewpoint of neutron economy would ask for a reduction of the reprocessing rate, which in turn would cause the concentration of trivalent isotopes to exceed the solubility limits. This is not the case of a feed only composed of MA. As mentioned, this would be extremely difficult in low-CR FRs, while in the MSFR it would combine a very high MA-burning rate (equal to 153 kg/GWe-yr, two times higher compared to the ARR) with a reduced concentration of trivalent isotopes at equilibrium (thanks to the higher reprocessing rate induced by the use of a worse feed - Table 1.7). As mentioned in Chapter 1, neutron economy can be artificially reduced through neutron poisons to allow for a quicker reprocessing rate in case solubility of trivalent isotopes at equilibrium becomes the main constraint to the achievable burning rate.

It is worth noticing that the 20wt% limit of TRUs in the feed sets a lower limit for the equilibrium CR[13]. In fact, the CR is defined as:

$$CR = \frac{fissile\ produced}{fissile\ burned} = \frac{fissile\ burned - fissile\ in\ the\ feed}{fissile\ burned} = 1 - \frac{fissile\ in\ the\ feed}{fissile\ burned} \tag{3.1}$$

At equilibrium, concentrations of all isotopes do not vary, so that the entire feed must be consumed. Consumption of the 20wt% TRU feed occurs through fission or capture followed by fission. Consumption of Th occurs through direct fission, or through neutron captures in Th-232 followed by fission. All these consumption processes must be accounted as fissile burning except for direct fission of Th-232. Eq. 3.1 can then be rewritten as:

$$CR = 1 - \frac{fissile\ in\ the\ feed}{total\ feed \cdot (1 - ff \cdot 0.8)} \tag{3.2}$$

where *ff* is the fraction of fissions in the fertile isotopes and is approximately equal to 1% in the MSFR. Assuming the fissile (i.e., TRU or MA) fraction in the feed as limited to 20%, it follows a lower limit for the CR equal to ~0.8.

The equilibrium concentrations resulting from continuous operation of the MSFR as TRU- and MA-burner reactor are reported in Table 3.5, where the case of the Th-based ARR

[13] *CR defined considering Th-232 as the only fertile materials and all other isotopes as fissile. It corresponds to the TRU regeneration rate (Wade and Hill, 1997), but TRUs must be substituted by trans-Th isotopes to employ the same definition of CR to Th-based cores. It is computed as the ratio of the rate of non-fission capture rate in U-238 or Th-232 to the rate of TRU or trans-Th destruction by fission.*

using TRUs from once-through LWR as feed is also shown. The higher CR and lower TRU burning rate of the MSFR vs the ARR are reflected in the higher content of U-233 and lower content of TRUs. The content of Am and Cm is higher in the ARR compared to the ThU3TRU-feed MSFR, meaning that the effect of a harder spectrum is offset by the higher amount of Am and Cm fed to the core. The effect of the spectrum is instead clearly visible in the higher content of Cf in the MSFR. In spite of the lower content of Cm, the fraction of Cf in the core is 5 times higher compared to the ARR. The ThU3MA-feed MSFR features peculiar equilibrium concentrations, with an amount of Am comparable to the ARR, but a much higher Cm and Cf content due to the softer spectrum. The high content of Cm also causes a sizeable build-up of Pu-238 and Pu-240 as a consequence of the decay of Cm-242 and Cm-244, respectively.

Table 3.5: Equilibrium concentrations [wt%] for the burner MSFR and comparison with the ARR

		ThU3TRU-feed MSFR	ThU3MA-feed MSFR	Th-TRU (MA/Pu~0.1) ARR
Core HN inventory [t]		26.4	30.2	9.6
Core composition [wt%]	**Th-232**	68.0	65.0	58.2
	Pa-231	$1.47\cdot10^{-2}$	$1.65\cdot10^{-2}$	$5.37\cdot10^{-2}$
	U-232	$1.87\cdot10^{-2}$	$2.11\cdot10^{-2}$	$4.84\cdot10^{-2}$
	U-233	11.9	11.3	6.39
	U-234	4.06	3.83	2.41
	U-235	1.12	1.01	$4.90\cdot10^{-1}$
	U-236	1.29	1.09	$5.21\cdot10^{-1}$
	U-237	$1.73\cdot10^{-3}$	$1.23\cdot10^{-3}$	$4.70\cdot10^{-4}$
	U-238	$3.62\cdot10^{-3}$	1.41	$1.06\cdot10^{-3}$
	Np-237	$5.92\cdot10^{-1}$	$8.72\cdot10^{-1}$	$8.51\cdot10^{-1}$
	Pu-238	1.06	2.09	2.06
	Pu-239	2.17	$9.68\cdot10^{-1}$	5.59
	Pu-240	4.33	2.46	11.9
	Pu-241	1.11	$4.63\cdot10^{-1}$	1.85
	Pu-242	1.69	1.00	4.50
	Am	$9.93\cdot10^{-1}$	3.52	3.35
	Cm	1.31	4.67	1.61
	Cf	$7.28\cdot10^{-3}$	$2.75\cdot10^{-2}$	$1.48\cdot10^{-3}$

A notable amount of Cm (specifically Cm-242 and Cm-244) determines a high decay heat from actinides in the short term, as plotted in Fig. 3.7, showing a comparison between the decay heat from actinides of the burner (ThU3TRU-feed and ThU3MA-feed) and the iso-breeder (ThU3-feed) MSFR. In the MSFR, the total decay heat from fission products is approximately 100-150 MW few seconds after reactor shut-down, and quickly drops to ~5 MW after 1 week (Aufiero et al., 2012, submitted). The contribution from actinides is thus non-negligible and use of the MSFR as burner reactor requires improved heat removal capabilities of the reprocessing system and of the drain tanks for long-term fuel cooling. For instance, after one-week cooling ~10 MW and ~4 MW would be produced by actinides in the

ThU3MA-feed and the ThU3-feed equilibrium core, respectively. Assuming ~5 MW produced by fission products, this would imply a ~60% higher decay heat for the former.

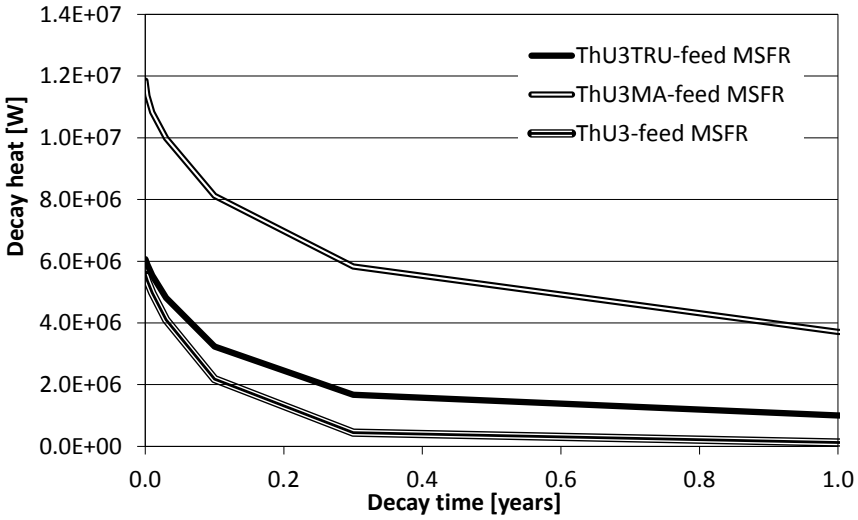

Figure 3.7: Decay heat from actinides after reactor shutdown for different MSFR feed options at equilibrium

The high TRU content of the burner MSFR also impacts radiotoxicity and decay heat in the longer term. Fig. 3.8 compares the equilibrium radiotoxicity and decay heat profiles in the two burner options with that of the iso-breeder MSFR and of the Th-U5-TRU start-up core (Table 1.3). Radiotoxicity and decay heat in the ThU3TRU-feed and ThU3MA-feed cases are drastically increased for tens of thousands of years compared to the iso-breeder case. A clear worsening is also observed vs the Th-U5-TRU start-up core, which implies that burning of an external TRU supply will be achieved at the expense of an increasing in-core radiotoxicity and decay heat. The possibility exists to operate the reactor in iso-breeder mode in the last years of operation. This would change the highly radiotoxic TRU content of the equilibrium ThU3TRU-feed and ThU3MA-feed cores into the more benign ThU3-feed equilibrium compositions.

a) Radiotoxicity

b) Decay heat

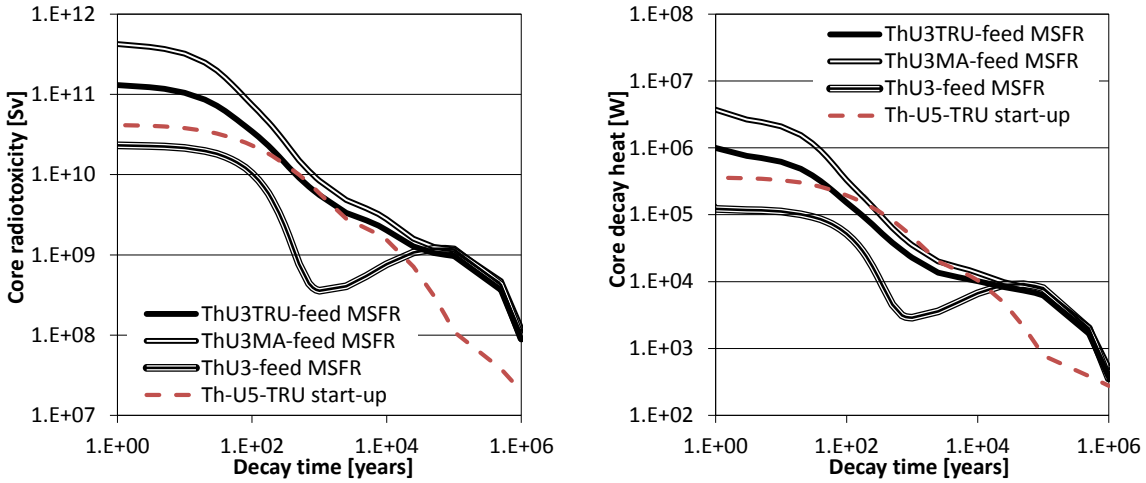

Figure 3.8: Radiotoxicity (a) and decay heat (b) of the actinide inventory for different MSFR feed options at equilibrium, and for the initial Th-U5-TRU fissile loading

3.4 EXAMPLE OF A POSSIBLE STRATEGY

Sections 3.3 and 3.4 have discussed the MSFR potential capabilities to burn the TRU legacy from LWRs using it as initial core loading or as feed. This Section investigates in some details a fuel cycle strategy combining the two burning modes. In particular, the Th-U5-TRU start-up core (Table 1.3) is considered following the possible solubility problems of the Th-TRU and Th-Pu start-up options. TRUs from once-through LWR operation are considered for the feed (ThU3TRU-feed MSFR – Table 1.7), since they represent a significant fraction of the nuclear wastes presently generated. The amount of TRUs transmuted with this fuel cycle strategy in a 100 years period, on average ~180 Kg/GWe-yr including the TRUs in the start-up fuel, match those generated by once-through LWRs with a 3:2 support ratio of MSFRs to LWRs in terms of electricity production (Shwageraus, 2003; Rose et al., 2011). As mentioned, to minimize the radiotoxicity contribution from the disposal of the MSFR fuel inventory when not further recycled, it is desirable to switch from ThU3TRU-feed to ThU3-feed (iso-breeding) in the last years of the MSFR operation. This would allow to maintain a low reprocessing rate while lowering the core radiotoxic content to that of a pure Th-U equilibrium cycle.

Fig. 3.9 shows the actinide radiotoxicity contributions for the proposed MSFR fuel cycle strategy, namely: a Th-U5-TRU start-up core with a 100 year operation with ThU3TRU-feed and a final 50 year operational period with ThU3-feed. The consumption terms are represented by the total radiotoxicity of the TRU feed burnt during the 100-year transmutation period and of the start-up fuel inventory. The production terms account for the radiotoxicity of the actinide reprocessing losses accumulated during the 150-year operational period and of the final actinide inventory.

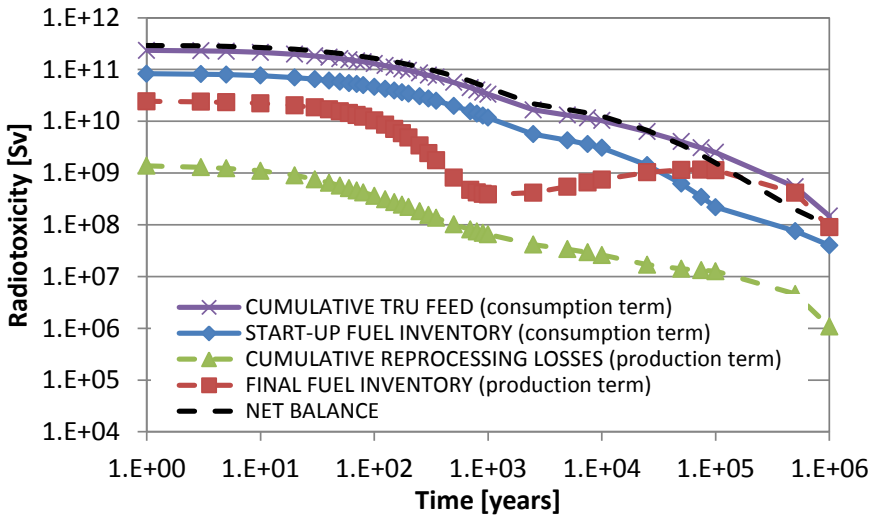

Figure 3.9: Actinide radiotoxicity contributions for the 150-year MSFR fuel cycle strategy analyzed

Consumption terms are dominant over the production terms. The radiotoxicity from the reprocessing losses is negligible thanks to the extremely low reprocessing rate for ThU3-feed and ThU3TRU-feed options and the small actinide process losses assumed, i.e. 0.1% of the reprocessed actinides. Switching to a "pure" Th cycle in the last decades of the operational period, which implies the exhaustion of the TRU supply from LWR fuel reprocessing, minimizes the radiotoxicity contribution from the final actinide inventory. The long-term

spike in the radiotoxicity production term from the accumulation of U-233 and U-234 decay products is of limited magnitude and appears an acceptable compromise in light of the radiotoxicity consumption achievable with the fuel cycle strategy proposed.

The decay heat impacts the heat load on the repository and thereby is related, with some approximation, to the cost and number of repositories for nuclear waste disposal. A detailed evaluation of the benefits on waste disposal deriving from the fuel cycle strategy proposed is beyond the scope of this study and would require evaluating the impact on decay heat of the relevant fission products, such as Cs and Sr. However some top-level conclusions can still be drawn analyzing the actinide decay heat contributions shown in Fig. 3.10. The fuel cycle strategy selected involves a 100-year transmutation phase of an LWR TRU feed in the MSFR which results in actinide reprocessing losses with clearly much lower decay heat. As regards initial and final actinide inventories, the 150-year MSFR operation assumed allows a corresponding delay in the actinide permanent disposal while transitioning to a fuel inventory with lower decay heat profile. It should be noted that the introduction of the MSFRs would also offset a portion of once-through LWRs (a 3:2 MSFR: LWR support ratio during the transmutation phase, as previously discussed) thus amplifying the waste management benefits shown in Figs. 3.9 and 3.10.

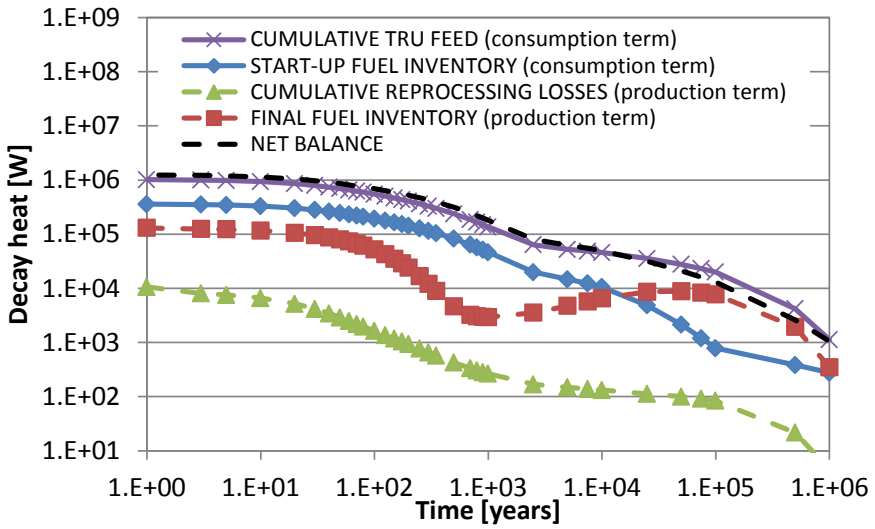

Figure 3.10: Actinide decay heat contributions for the 150-year MSFR fuel cycle strategy analyzed

3.5 CONCLUDING REMARKS

In this Chapter, the TRU burning capabilities of the MSFR have been analyzed and compared to traditional FRs. Both Th- and U-based FRs have been considered for the comparison, which has allowed to draw some conclusions also on the pros and cons of the Th option in a TRU-transmutation scenario.

At first, the possibility to transmute an initial TRU loading through a subsequent prolonged operation in a closed cycle has been investigated. This strategy turned out to be ineffective if U-based traditional FRs are used, since radiotoxicity and decay heat of the equilibrium core are comparable to those of the initial TRU loading. If Th is used as feed, radiotoxicity and decay heat profiles are instead significantly affected. The equilibrium core will have a lower radiotoxicity and decay heat for several thousands of years compared to the

initial TRU loading. On the other hand, these fuel cycle metrics will be worse in the very long term. Benefits of transmutation are then questionable in terms of radiotoxicity, whose peak value is reduced at the cost of a higher integral value e.g. over 10^6 years. The lower decay heat in the short-middle term is instead a factual advantage of the equilibrium Th-U composition vs the initial TRU loading as it would reduce number and/or costs of the geological repositories for final waste disposal.

In this scenario, the MSFR presents both pros and cons. A disadvantage comes from the softer spectrum, causing a higher build-up of Pu-238, and ultimately a higher radiotoxicity and decay heat of the equilibrium core. A major advantage is instead given by the high specific power, which combines with the lack of out-of-core cooling time for the fuel to yield a short transmutation time (comparable to a reactor lifetime), thus making the MSFR a promising option for a quick transition from the current U-based fuel cycle to a closed Th-U cycle. However, if U enriched in U-235 is mixed with TRUs in the start-up core, transmutation time becomes much longer due to the persistence in the fuel of U-238, which in turn keeps generating Pu-239 and heavier actinides.

Waste transmutation via a TRU feed in low-CR reactors has then been analyzed. TRU burning in traditional FRs is limited by the deterioration of safety with increasing TRU content (see Chapter 4), and by fuel fabrication issues associated to the intense heat load and radiation field in a TRU-rich multi-recycled fuel. By assuming a traditional 5% limit on the content of MA (Np, Am, Cm and Cf), it turns out that only TRUs from once through LWR can be used as feed in a low-CR reactor like the ARR (CR~0.4). This constraint is independent of the adopted fertile material, since endogenous generation of TRUs is small and the MA inventory is mainly determined by the quantity of TRUs fed to the core. This determines a maximum achievable TRU burning rate equal to ~500 and ~600 kg/GWe-yr for the U- and Th-based cores, respectively, corresponding to a MA burning rate equal to 60-70 kg/GWe-yr. As expected, TRU burning rate is slightly increased by Th use thanks to the inherently lower neutron economy. On the other hand, Th use exacerbates problems of fuel handling due to the intense and penetrating gamma rays emitted by the progeny of U-232.

As explained in Chapter 1, a low CR is achievable in the MSFR through a low reprocessing rate and ensuing high content of fission products in the core. The solubility of TRUs in the fed salt sets the upper limit for the TRU transmutation rate to ~150 kg/GWe-yr, which translates into a lower limit for the CR equal to ~0.8. An interesting aspect of the MSFR that differentiates it from traditional FRs is that the composition of the TRU feed is not strictly limited by issues of fuel fabrication and transportation. This paves the way toward the use of the MSFR as a MA-burner reactor, with Pu recycled in other reactors. The resulting MA burning rate of ~150 kg/GWe-yr would be 2 times higher compared to that achievable in the ARR (according to the 5% limit of MA in the core). A main drawback of the MSFR is once again the softer spectrum, causing a substantial increment of radiotoxicity and decay heat of the equilibrium fuel.

Finally, a possible fuel cycle strategy has been investigated in some details, envisioning the use of the MSFR to transmute TRUs from once-through LWR operation. The analysis revealed that with a 60% share in electricity production, the MSFRs could recycle and burn the TRUs produced by the remaining 40% once-through LWRs. Actinide reprocessing losses would be negligible while the radiotoxicity and decay heat of the final fuel inventory could be

minimized by using the MSFR as iso-breeder in the last years of operation to convert the final TRU content in the core into the more benign Th-U equilibrium compositions.

REFERENCES

Artioli, C., Grasso, G., Petrovich, C., 2010. A new paradigm for core design aimed at the sustainability of nuclear energy: the solution of the extended equilibrium state. Annals of Nuclear Energy 37, 915-922.

Aufiero, M., Cammi, A., Fiorina, C., Luzzi, L. 2012. Modification of the SERPENT code to study the fuel isotopic evolution of molten salt reactors with online (continuous) reprocessing. Presentation for "2012 SERPENT International Users Group Meeting". September 19-21, Madrid, Spain.

Aufiero, M., Cammi, A., Fiorina, C., Leppänen, J., Luzzi, L., submitted. An extended version of the SERPENT-2 code to investigate fuel burn-up and core material evolution of the Molten Salt Fast Reactor. Submitted to Journal of Nuclear Materials. Presentation at NuMat 2012 conference, October 22-25, Osaka, Japan.

Fiorina, C., Franceschini, F., Krepel, J., Mikityuk, K., 2011. Comparative Analysis of Uranium and Thorium Fuel Cycles in a Lead-Cooled Fast Reactor from the Perspective of Safety and Waste Management. Proc. GLOBAL 2011, December 11-16, Chiba, Japan.

Fiorina, C., Cammi, A., Krepel, J., Mikityuk, K., Ricotti, M. E., 2012a. Preliminary Analysis of the MSFR Fuel Cycle Using Modified-EQL3D Procedure. Proc. ICONE 2012, July 30 – August 3, Anaheim, US.

Fiorina, C., Cammi, A., Franceschini, F., Krepel, J., Luzzi, L., Ricotti, M. E., 2012b. Thorium fuel cycle in Fast Reactors: potential benefits and challenges. Proc. NENE 2012, September 5-7, Ljubljana, Slovenia.

Fiorina, C., Cammi, A., Franceschini, F., Krepel, J., Mikityuk, K., Ricotti, M. E., 2013. Analysis of thorium and uranium fuel cycles in an iso-breeder Lead Fast Reactor using extended-EQL3D procedure. Annals of Nuclear Energy 53, 492-506.

Fiorina, C., Aufiero, A., Cammi, A., Franceschini, F., Krepel, J., Luzzi, L., Mikityuk, K., Ricotti, M. E., submitted. Investigation of the MSFR core physics and fuel cycle characteristics. Submitted to Progress in Nuclear Energy.

Franceschini, F., Lahoda, E., Carelli, M., Wenner, M., Ferroni, P., Fiorina, C., Sartori, A., Ricotti M.E., Petrovic, B., 2011. A Comprehensive Approach to Waste Management with Thorium. Invited keynote paper from IAEA. Technical Meeting on World Thorium Resources, October 17 - 21, Thiruvananthapuram, India.

Franceschini, F., Fiorina, C., Huang, M., Petrovic, B., Wenner, M., Krepel, J., 2012a. Radiotoxicity Characterization of Multi-Recycled Thorium Fuel. Proc. WM Symposia 2012, February 26 - March 1, Phoenix, US.

Franceschini, F., Lindley, B., Fiorina, C., Lahoda, E., Wenner, M., 2012b. Analysis of a fuel cycle strategy to achieve low-radiotoxicity waste. Proc. IEMPT-12, September 24-27, 2012, Prague, Czech Republic.

Franceschini, F., Lindley, B., Fiorina, C., Phillips, C., Lahoda, E., Wenner, M., submitted. Promises and Challenges of Thorium Implementation for Transuranic Transmutation. Submitted to WM Symposia 2013, February 24 - 28, Phoenix, US.

GIF-IV, Generation IV International Forum, 2002. A Technology Road Map for Generation IV Nuclear Energy Systems. GIF-002–00, US DOE Nuclear Energy Research Advisory Committee and The Generation IV International Forum.

Ikeda, K., Kochendarfer, R.A., Moriwaki, H., Kunishima, S., 2011. Enhancing TRU burning and Am transmutation in Advanced Recycling Reactor. Nuclear Engineering and Design 241, 1438–1453.

Itoh, K., Ikeda, K., Hishida, K., Kuroda, T., Yamaguchi, A., Takata, T., 2008. Development of the Cooling Technology on TRU Fuel Pin Bundle during Fuel Fabrication Process (1) Whole Study Plan and Fabrication of Test Apparatus. Proc. ICAPP 2008, June 8-12, US.

Rose, S.J., Wilson, J.N., Capellan, N., David, S., Guillemin, P., Ivanov, E., Meplan, O., Nuttin, A., Siem, S., 2011. Minimization of actinide waste by multi-recycling of thoriated fuels in the EPR reactor. Annals of Nuclear Energy 38, 2619–2624.

Salvatores, M., 2002. The physics of transmutation in critical or subcritical reactors. Comptes Rendus Physique 3, 999–1012.

Salvatores, M., 2005. Nuclear fuel cycle strategies including Partitioning and Transmutation. Nuclear Engineering and Design 235, 805–816.

Salvatores, M., Palmiotti, G., 2011. Radioactive waste partitioning and transmutation within advanced fuel cycles: achievements and challenges. Progress in Particle and Nuclear Physics 66, 144-166.

SCALE: A Modular Code System for Performing Standardized Computer Analyses for Licensing Evaluations, ORNL/TM-2005/39, Version 5.1, Vols. I–III, November 2006. Available from Radiation Safety Information Computational Center at Oak Ridge National Laboratory as CCC-732.

Shwageraus, E., 2003. Rethinking the Light Water Reactor fuel cycle. PhD Thesis. Massachussets Institute of Technology, US.

Taiwo, T. A., Kim, T. K., Stillman, J. A., Hill, R. N., Salvatores, M., Finck, P. J., 2006. Assessment of a Heterogeneous PWR Assembly for Plutonium and Minor Actinide Recycle. Nuclear Technology 155, 34-54.

Takata, T., Yamaguchi, A., Hishida, K., Kuroda, T., Itoh, K., Ikeda, K., 2008. Development of the Cooling Technology on TRU Fuel Pin Bundle during Fuel Fabrication Process (3) Development of Analytical Tool. Proc. ICAPP 2008, June 8-12, US.

Touran, N.W., Hoffman, A.J., Lee, J.C., 2011. Performance of Thorium-Based Fuel for TRU Transmutation in Sodium-Cooled Fast Reactors. Proc. ANS Winter Meeting 2010, November 7-11, Las Vegas, US.

Wenner, M., Franceschini, F., Kulesza, J., 2012. Preliminary Comparative Shielding Analysis for Refabricating Different Fuel Vectors. Proc. ANS Winter Meeting 2012. November 11-15, San Diego, US.

Wigeland, R. A., Bauer, T. H., Fanning, T. H., Morris, E.E., 2006. Separations and transmutation criteria to improve utilization of a geologic repository. Nuclear Technology 154, 95-106.

Yang, W. S., 2008. Trends in transmutation performance and safety parameters versus TRU conversion ratio of sodium-cooled fast reactors. Proc. IEMPT-10, October 8, 2008, Mito, Japan.

CHAPTER 4: Safety parameters and inherent safety features

ABSTRACT

The present Chapter preliminary investigates the MSFR safety features through a detailed analysis of its feedback coefficients, β_{eff} and generation time, for different fuel compositions. Reactivity decomposition techniques are employed for a better understanding of the phenomenology underlying each safety parameter. Inherent safety features are also investigated based on a simple prediction of the core steady-state after the main accidental transient initiators. For comparison, safety parameters and inherent safety are investigated for traditional Fast Reactors, both U and Th-based. Thorium use in fast-spectrum systems displays significant advantages over U thanks to a lower reactivity insertion in case of spectrum hardening. Among the Th-based systems, the MSFR emerges as a safe option thanks to the lack of positive feedbacks, the liquid fuel, and the promising inherent safety features. Some of the main results have been presented in (Fiorina et al., 2011, 2012a, 2012b, 2012c, 2013, submitted (a), submitted (b), submitted (c); Guerrieri et al., 2012).

4.1 INTRODUCTION

Starting from the late seventies and following some major nuclear accidents, safety aspects have gradually emerged as a main driving force for the development of evolutionary or innovative nuclear power plants. Among the innovative reactors, a dominant role is played by Fast Reactors (FR), especially sodium-cooled: they can rely on a sound technical basis compared to other innovative concepts; they improve sustainability thanks to the possibility to achieve breeder configurations; they minimize wastes by allowing the closure of the fuel cycle; and they can be used as effective burner reactors. However, their characteristics in terms of safety are controversial. On one hand, they generally operate at ambient pressure, thus eliminating the major driving force for the release of radioactive isotopes into the biosphere. In addition, they have been proved able to withstand all typical double-fault accidents without significant consequences on the environment (Wade and Hill, 1997). On the other hand, a limited operational experience exists for FRs, which makes more difficult a safety assessment and a comparison with Light Water Reactors (LWR). A specific issue is that coolant voiding in FRs generally causes a positive reactivity insertion, representing a serious safety issue and an obstacle to licensing. In this sense, few past studies (see e.g. (Till et al., 1980)) have singled out possible safety improvements fostered by Th use, though Th cycle implementation in FRs has

seldom been considered a credible option in the past due to the worse neutron economy in a fast-spectrum and to specific problems of fuel reprocessing and fabrication.

In this context, the MSFR has the unique advantage among FRs of eliminating by design the problem of coolant voiding. In addition, a liquid fuel inherently enhances safety since: 1) the possibility exists to quickly drain the fuel in criticality-safe passively-cooled tanks; 2) there are no issues of pellet-cladding interaction with possible failure of the cladding in case of power ramps; and 3) the possibility exists to extract all gaseous fission products from the core through gas bubbling, thus dramatically reducing the radioactive source in the core.

This Chapter aims at assessing pros and cons of Th vs U use and of the MSFR vs the traditional FRs in terms of safety. Investigation is based on an accurate characterization of feedback coefficients, β_{eff} and generation time. The attention is focused first on the traditional solid-fuelled FRs, both U- and Th-based (Section 4.2). This gives first indications of Th impact on safety parameters, and provides a term of comparison for the subsequent analysis of the MSFR safety parameters (Section 4.3). Reactivity decomposition techniques are employed and safety parameters investigated for different fuel compositions to offer a general overview of their specific features. Section 4.4 preliminarily investigates the MSFR performances in terms of inherent safety through a quasi-static approach. Also for inherent safety, the attention is focused at first on the impact of Th use in traditional FRs. The conclusions of the Chapter are provided in Section 4.5.

4.2 SAFETY PARAMETERS FOR Th- AND U-BASED TRADITIONAL FRs

Before confronting the issue of safety in the MSFR, it is worth taking a closer look at the safety parameters typical of the traditional FRs, focusing in particular on the effect of Th use. In fact, only few studies on the subject have been performed in the past (Till et al., 1980), but differences are expected due to a notably different trend of fission and capture cross-sections of main fissile and fertile isotopes in Th vs the U option. In particular, Fig. 4.1 shows that U-233 features a steeper fission cross-section but flatter capture cross-section. Th-232 and U-238 have a similar capture cross-section, but Th-232 has a higher threshold and lower cross-section for fission, which has already been observed to cause a reduced fission rate in fertile isotopes (~2% vs ~8%, see Table 3.4). Table 4.1 also shows that delayed neutron yields are different for isotopes typical of the Th vs the U option. In particular, yields are higher for Th-232 and U-233 compared to U-238 and Pu-239, respectively.

For the purpose of evaluating the safety features typical of Th- and U-based traditional FRs, the equilibrium safety parameters of the ARR are investigated in this Section. Both the burner and the iso-breeder ARR designs have been investigated (Section B.3, with compositions in Tables 2.1 and 3.4). For the burner case, the 4 fuel cycle options discussed in subsection 3.3.1 have been considered, namely: U or Th supported burning of TRansUranic isotopes (TRU) from once-through traditional LWRs (MA[14]/Pu~0.1) or from multi-recycled fuel in dedicated LWRs (MA/Pu~1). Table 4.2 summarizes the safety-related parameters for the investigated ARR designs and fuel cycle options at the End Of Cycle (EOC). Computed values relate the equilibrium core configuration, which in turn has been achieved employing the extended-EQL3D procedure (Appendix A).

[14] *MA indicates Minor Actinides, namely Np, Am, Cm, Cf.*

a) Fissile isotopes

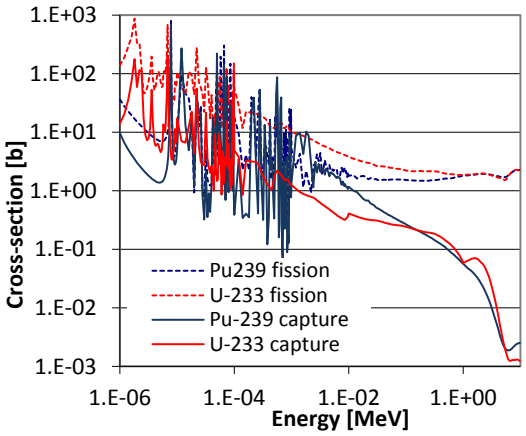

b) Fertile isotopes

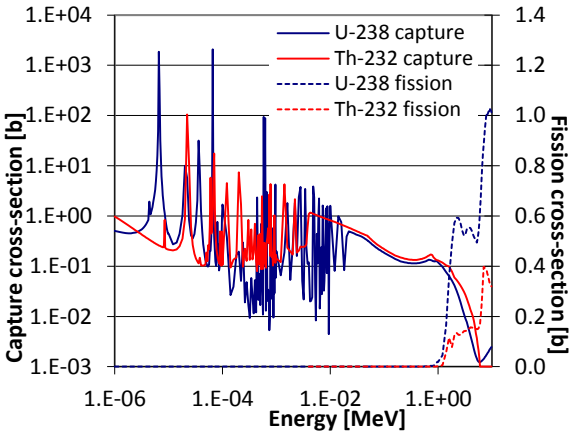

Figure 4.1: Cross-sections for the main fissile and fertile isotopes

Table 4.1: Delayed neutron yield [pcm] for various isotopes

Th-232	U-233	U-235	Pu-239	Pu-240	Pu-241	Pu-242	Am-241	Am-243	Cm-244	Cm-245
5270	751	1640	661	900	1600	1830	427	850	435	640

Table 4.2: Equilibrium safety parameters at EOC for the investigated ARR cores and feed/fertile isotope options

Core type	Standard burner				U-based iso-breeder	Th-based iso-breeder
Fertile	U	Th	U	Th	U	Th
Fissile make-up feed	TRUs	TRUs	TRUs	TRUs	-	-
MA/Pu ratio in the feed	~0.1	~0.1	~1	~1		
CR [-]*	0.47	0.36	0.40	0.29	1	1
Active core voiding [pcm]	1322	757	1829	1573	1772	-346
Coolant expansion coefficient - active core [pcm /K]	0.34	0.20	0.48	0.41	0.46	-0.09
Coolant expansion coefficient - whole core [pcm /K]	-0.55	-0.82	-0.23	-0.35	-0.18	-0.82
Doppler coefficient [pcm /K]	-0.28	-0.25	-0.18	-0.15	-0.37	-0.66
Fuel exp. coeff. [pcm /K]	-0.12	-0.09	-0.14	-0.12	-0.19	-0.06
Fuel coefficient (Doppler + expansion) [pcm /K]	-0.40	-0.34	-0.32	-0.26	-0.56	-0.72
Radial exp. coeff. [pcm /K]	-0.94	-0.92	-0.93	-0.92	-1.01	-0.77
β_{eff} [pcm]	315	285	277	244	361	342
Generation time [μs]	0.35	0.37	0.28	0.29	0.29	0.39
Burnup reactivity swing [pcm]	5138	5602	3376	3721	2905	4885
Required control rods to comply with the 0.8 $ limit [-]	21	25	16	20	11	18

**Conversion Ratio defined considering Th-232 and U-238 as the only fertile materials and all other isotopes as fissile. It corresponds to the TRU regeneration rate (Wade and Hill, 1997) in the U-based cores, while TRUs must be substituted by trans-Th isotopes to employ the same definition of CR to Th-based cores. In all cases, it is computed as the ratio of the rate of non-fission capture rate in U-238 or Th-232 to the rate of TRU or trans-Th destruction by fission.*

4.2.1 Burner design

Doppler coefficient is negligibly affected by Th use and the slight worsening can be ascribed to the lower fertile content in the core (see Table 3.4). The most relevant impact on safety is the drastic reduction of void reactivity and coolant expansion coefficient. The positive reactivity insertion in case of core voiding is a major concern in sodium-cooled FRs as double-fault accidents like an Unprotected[15] Loss Of Flow (ULOF) may lead to sodium boiling. Coolant expansion plays a major role during accidental transients, especially when driven by a coolant temperature increase (e.g., ULOHS – Unprotected Loss Of Heat Sink). It also determines the non-minimum-phase behavior of FRs with a positive value of this coefficient, which disturb the performances of the control system. Thorium is then expected to foster improved safety and controllability, which combines with the increased burning rate pointed out in subsection 3.3.1 to make Th-FRs an attractive option for waste transmutation.

The phenomenology underlying this improvement can be conveniently investigated using the reactivity decomposition technique described in Section A.5. Fig. 4.2 reports the isotope-wise decomposition of the void reactivity insertion for the U- and Th-based burner ARR using TRUs from once-through LWR (columns 1 and 2 in Table 4.2).

a)

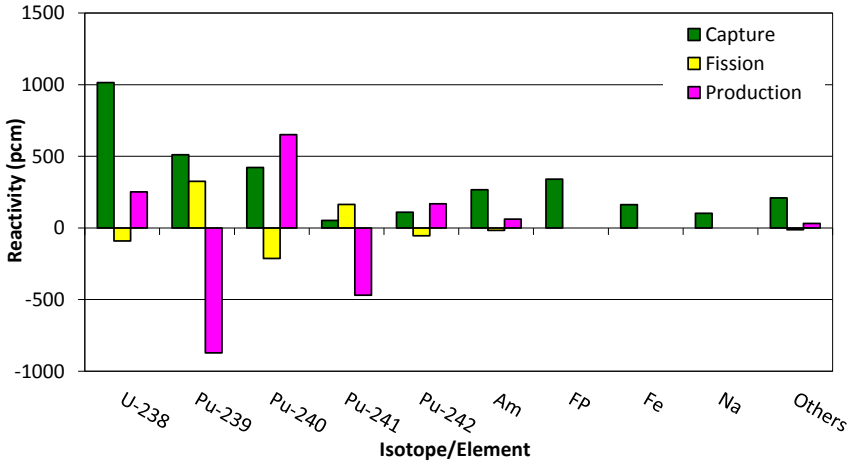

b)

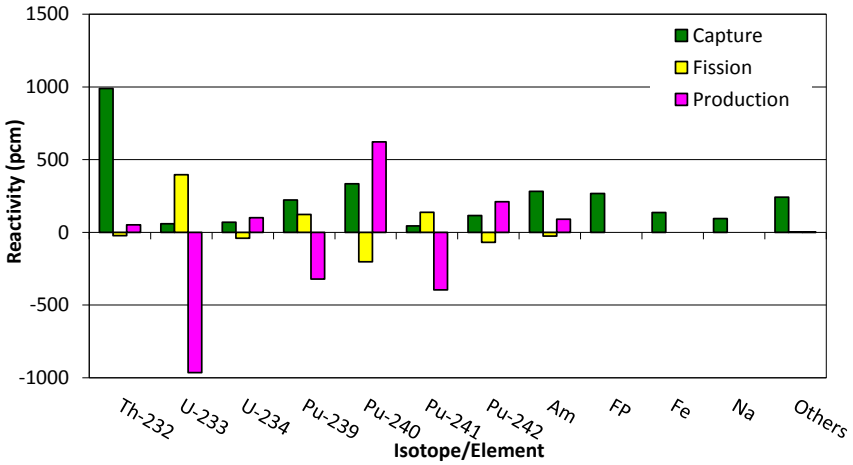

Figure 4.2: Isotope-wise decomposition of void reactivity for a) U and b) Th-based burner ARR using a TRU feed from once-through LWR (columns 1 and 2 in Table 4.2). FP indicates Fission Products

[15] *"Unprotected" refers to a transient where control rods fail to shut the reactor down.*

Core voiding directly causes a small reactivity insertion due to the reduced captures in sodium. However, the main effect is spectrum hardening. This primarily causes a reduction of captures, with ensuing increased reactivity, as a consequence of the generally decreasing trend of capture cross-section with energy. The main contributors are U-238 and Th-232, with a lower reactivity insertion for the latter. This is to be ascribed to its lower fraction in the core (see Table 3.4) while no significant differences can be observed in the trend of capture cross-sections (Fig. 4.1). Partial replacement of Pu-239 with U-233 in the Th case leads to an additional improvement following the flatter capture cross-section of the latter. A further substantial contribution to the reactivity insertion caused by capture decrement comes from Pu-240 and Am isotopes, with ensuing negligible differences between U and Th options due to the similar content of these two isotopes (subsection 3.3.1).

A second effect of spectrum hardening is a variation of fissions. In this case odd and even mass number isotopes show opposite behaviors. In particular, even-mass-number isotopes generally feature a threshold fission cross-section, so that spectrum hardening causes an increment of fissions, with consequent positive reactivity insertion due to increased productions. The lower energy threshold and lower fission cross-section of Th-232 vs. U-238 contributes to reducing the positive void reactivity. Odd-mass-number isotopes feature instead a fission cross-section that decreases with energy, thus reacting with a fission decrement in case of spectrum hardening. Thanks to a strongly decreasing fission cross-section, U-233 gives a strongly negative contribution to the overall reactivity. It is interesting to observe that Am, although mainly composed of odd-mass-number isotopes, behaves like an even-mass-number isotope. In fact, the fission cross-sections of Am-241 and Am-243 decrease till ~100 keV, but feature a steep increment at higher energies.

Finally, spectrum hardening is responsible for a higher fission neutron yield, causing an increment of neutron productions and an ensuing reactivity insertion approximately equal to ~150 pcm and ~ 300 pcm for the U and Th cases, respectively. The higher value for the Th case is to be ascribed to the steeper increment of the fission neutron yield with neutron energy of U-233 vs Pu-239.

Following the above reasoning, Th use fosters a lower reactivity increment due to spectrum hardening both directly and through U-233 breeding. Albeit advantageous in terms of void reactivity and coolant coefficient, this negatively impacts fuel and radial core expansion effects, both characterized by an increased coolant-to-fuel ratio leading to a spectrum softening. However, these coefficients maintain a comparable value in the Th cases thanks to the higher leakages associated to a lower CR.

β_{eff} and reactivity swing are negatively affected by Th use. β_{eff} is mostly determined in both cases by TRUs, leading to a low value that is partly compensated in the U case by a sizeable contribution to fissions (~8%) from U-238. Th-232 has high delayed neutron yield (Table 4.1), but very small fission rate (~2%). The higher reactivity swing in the Th cases is caused by the lower CR. Combination of a high reactivity swing and a low β_{eff} increases the number of required control rods to meet the typical 0.8 $ limit on the control rods worth (Wade et al., 1997).

The safety features of both U and Th options are significantly reduced when the ~1 MA/Pu feed is used (columns 3 and 4 in Table 4.2). The low content of fertile isotopes reduces the Doppler effect and β_{eff} while the high TRU content leads to a deterioration of

void reactivity and coolant expansion coefficients. The beneficial effect on fuel expansion coefficient does not compensate the deterioration of the other coefficients. The relative trend in feedback coefficients between U and Th observed for the ~0.1 MA/Pu feed, including the beneficial impact of Th on coolant effects, is noted also for the ~1 MA/Pu feed. However, the differences between U and Th are reduced as a consequence of the lower fertile-to-fissile ratio, and higher TRU content necessary to maintain criticality with the lower quality feed. It follows that Th can assist TRU burning in FRs, but very high TRU burning rate will cause similar safety problems as for the U-based burners.

4.2.2 Iso-breeder design

As singled out previously, U-233 has a steeper fission cross-section and a flatter capture cross-section compared to Pu-239 (Fig. 4.1), thus reacting with a strongly negative reactivity insertion in case of spectrum hardening. For the burner configurations, this has a limited impact due to the small U-233 inventory while, with increasing CR, fissions from in-bred Pu-239 and U-233 become dominant over the contribution from TRUs. In the Th-based iso-breeder ARR, the negative reactivity insertion fostered by U-233 surpasses the relatively small positive contribution of Th-232, leading to a negative void reactivity insertion. Fig. 4.3 shows the isotope-wise decomposition of the void reactivity, confirming the beneficial effect of U-233. As expected from subsection 4.2.1, also a lower fission increment in Th-232 vs U-238 plays a role, but minor in this case. Coolant expansion coefficients feature the same phenomenology as the void reactivity insertion, thus showing a similar improvement. On the other hand, fuel and radial expansions cause the coolant-to-fuel ratio to increase, and the spectrum to soften, with an ensuing advantage for the U option. However, improvements in coolant expansion coefficient and core voiding offset the worsening of fuel and radial core expansion coefficients.

a) U-based ARR

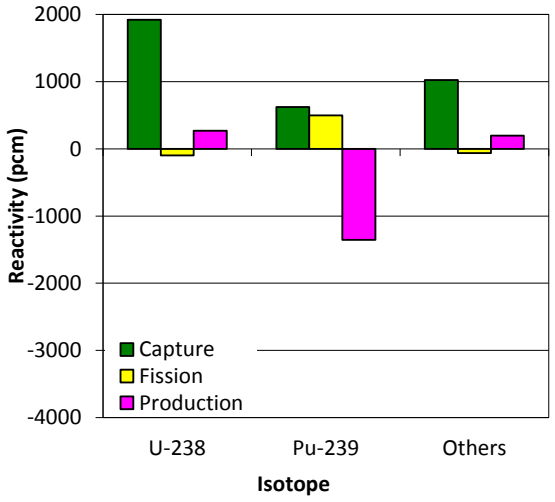

b) Th-based ARR

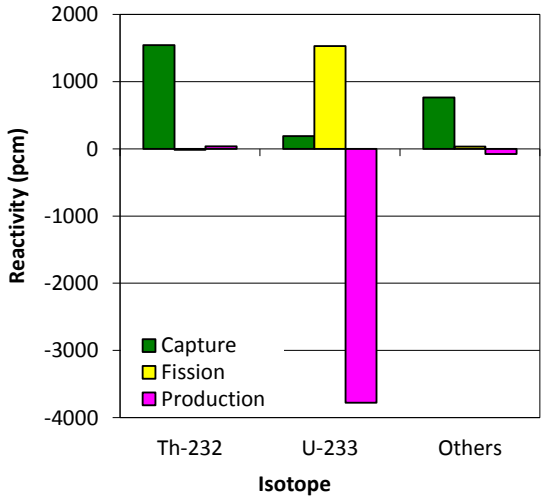

Figure 4.3: Isotope-wise decomposition of void reactivity for a) U-based iso-breeder and b) Th-based iso-breeder ARR

Remarkably, Th use notably improves also the Doppler coefficient for the iso-breeder core configuration. Fig. 4.4 indicates that the negative contribution to the Doppler coefficient is dominated by the increment of captures in the fertile isotopes, with a 0.2 pcm/K stronger

effect for the Th case. Increased captures in the resonance region cause a suppression of the flux below 10 keV, with a consequent spectrum hardening, as shown in Fig. 4.5. Spectrum hardening fosters an additional reactivity reduction due to reduced fission in the fissile isotopes, leading to a further advantage for the Th option.

a) U-based ARR b) Th-based ARR

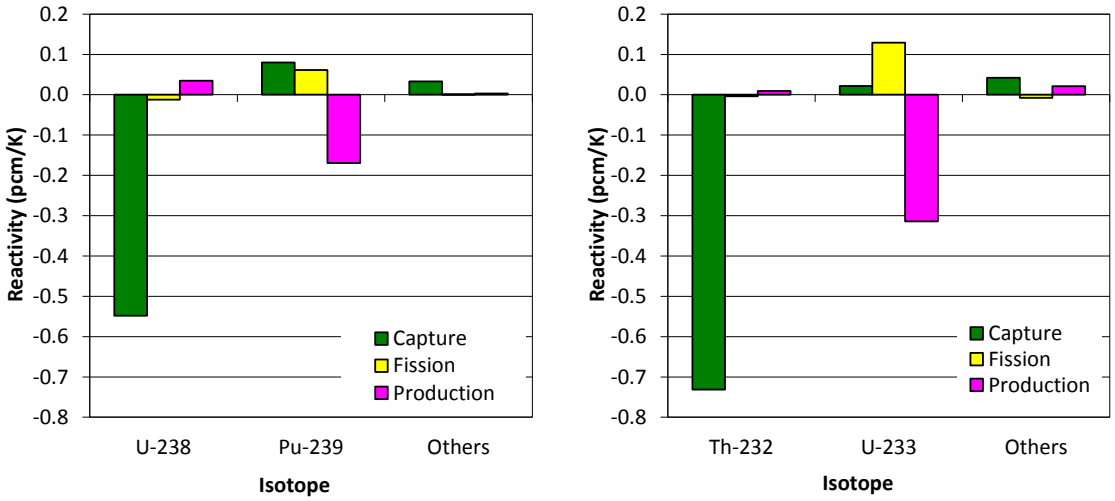

Figure 4.4: Isotope-wise decomposition of the Doppler coefficient for a) U-based iso-breeder and b) Th-based iso-breeder ARR

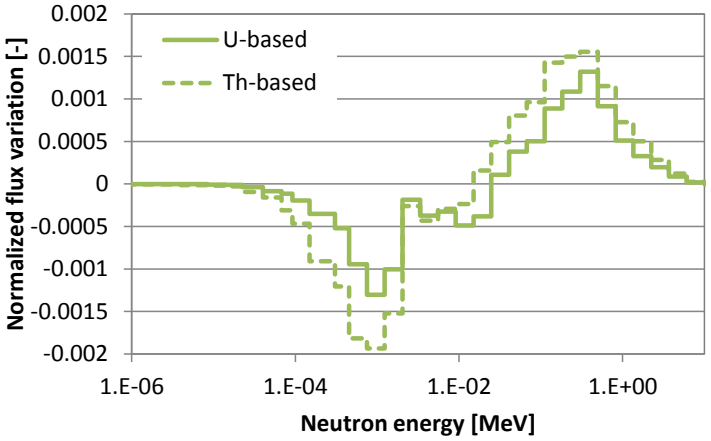

Figure 4.5: Flux variation in the iso-breeder ARR in case of Doppler resonance broadening

β_{eff} is higher in the iso-breeder vs the burner core configuration following 1) the higher U-238 content in the U case, and 2) the presence of U-233 instead of TRUs as main fissile material in the Th case. The higher β_{eff} combines with a reduced burnup reactivity swing associated to the use of a denser fuel to reduce the required number of control rods necessary to comply with the 0.8 $ limit. Thorium use causes worse performances in this sense due to the lower internal breeding and ensuing higher reactivity swing.

4.3 SAFETY PARAMETERS FOR THE MSFR

The previous Section has investigated in some details the safety parameters typical of traditional FRs, including an assessment of the pros and cons of Th use. Based on these results, this Section investigates the impacts on safety parameters of adopting a specific reactor

design like the MSFR, thus giving a first fundamental piece of information on its features in terms of safety and controllability.

4.3.1 Reactivity feedbacks in the MSFR

Following a simplified treatment, the multiplication factor of a core can be expressed as:

$$k_{eff} = \frac{k_\infty}{1+B^2L^2} \tag{4.1}$$

The value of the feedback coefficients is determined by the variation of k_∞, B or L triggered by a temperature or density variation.

Doppler effect

Like in other reactors, the Doppler effect is paramount to the safety and maneuverability of the MSFR. It acts mainly on the k_∞ and, as temperature increases, it contributes negatively to reactivity thanks to increased captures in the fertile isotopes in the resonance region. As shown in the previous Section, the effect of increased captures is generally enhanced by the ensuing local spectrum hardening. In FRs it is common practice to define a Doppler constant K_D, under the assumption that the core reactivity has the logarithmic trend:

$$\rho = \rho^* - K_D ln(\frac{T}{T^*}) \tag{4.2}$$

Such a simple dependency has been found to be valid with a very good approximation also in the MSFR, as shown in Fig. 4.6 for the case of a Th-U3 start-up core (see Table 1.3).

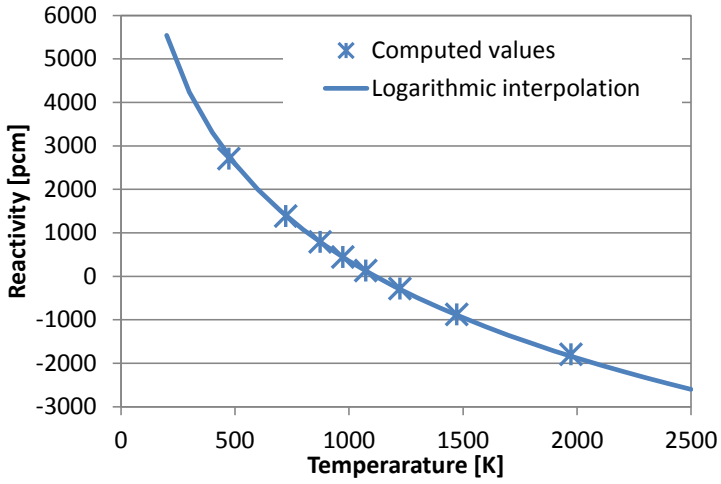

Figure 4.6: Typical reactivity variation with temperature (excluding the effect of density) for the MSFR

This implies that K_D can be computed knowing two reactivities at two generic temperatures (973 K and 1073 K in this work). Note that a logarithmic dependency of reactivity on temperature implies a feedback coefficient inversely proportional to the temperature:

$$\alpha_D(T) = \frac{K_D}{T} \tag{4.3}$$

As a matter of fact, no significant differences exist in the phenomenology underlying the Doppler feedback coefficient in the MSFR vs the traditional FRs. An isotope wise decomposition is reported in Fig. 4.7, while the change in neutron flux is shown in Fig. 4.8. Results have been obtained for the equilibrium composition resulting from the ThU3TRU-feed option (see Tables 1.7 and 3.5). The Doppler effect is still dominated by the increased captures in Th, which in turn suppresses the flux in the resonance region and causes a reduction of the fission (and production) rate in U-233. Contribution of other isotopes is mostly negligible, except for a negative reactivity insertion from reduced productions in U-235, Pu-239 and Pu-241, and a positive reactivity insertion from reduced captures in fission products. The latters are present in substantial amount in the ThU3TRU-feed MSFR and feature a capture cross-section that generally decreases with energy in the energy range of interest.

A main difference compared to the traditional FRs is the strength of the Doppler coefficient, of the order of few pcm per K, which is due to the combined effect of a softer spectrum (Fig. 1.3) and of Th use (see previous Section).

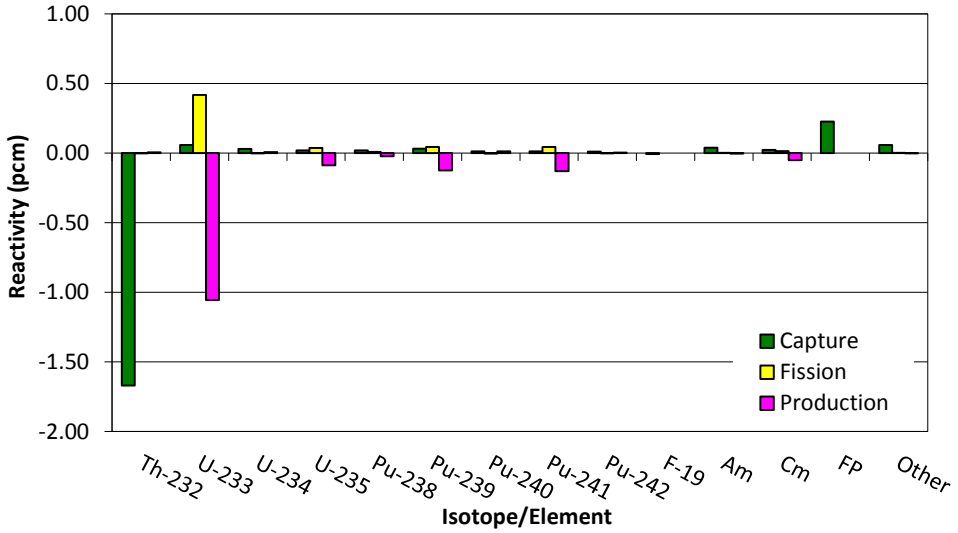

Figure 4.7: Isotope-wise decomposition of the Doppler coefficient in the ThU3TRU-feed equilibrium MSFR

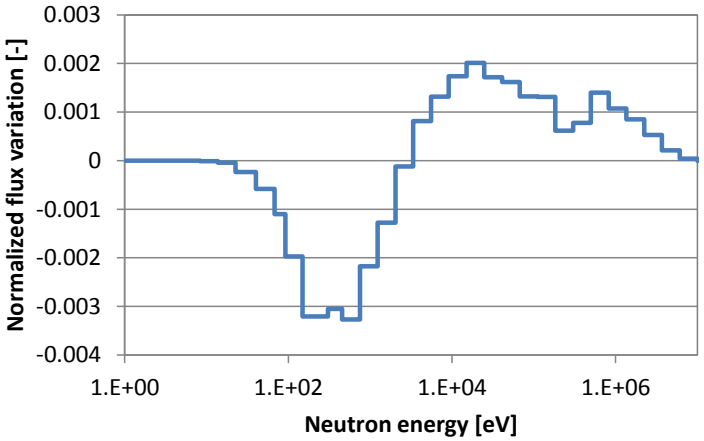

Figure 4.8: Flux variation in case of Doppler resonance broadening in the ThU3TRU-feed equilibrium MSFR

Fuel expansion

A second reactivity feedback is determined in the MSFR by fuel expansion, whose phenomenology is different than for traditional FRs. In the latters, the fuel expansion causes a reduced fuel-to-coolant ratio, leading to a spectrum softening and ultimately to a slight reactivity reduction. In the MSFR, fuel expansion mainly impacts the term L^2 in Eq. 4.1. In fact, according to a one-group diffusion theory, it is possible to write:

$$L^2 = \frac{\bar{D}}{\Sigma_a} \propto \frac{1}{d^2} \tag{4.4}$$

When temperature increases, the density d is expected to decrease, leading to a negative feedback coefficient. According to a 6-factor formula for reactivity, the density coefficient is expected to grow (in absolute terms) with increasing temperature roughly as:

$$|\alpha_d(T)| \propto \frac{1}{(1-\beta_e(T-T^*))^2} \tag{4.5}$$

Following the decreasing trend of the Doppler coefficient and the increasing trend of the fuel expansion coefficient, the overall fuel coefficient is expected to feature a minimum. Fig. 4.9 plots the overall reactivity feedback coefficient for the Th-U3 start-up core (Table 1.3), showing that the minimum is found at approximately 1300 K. This implies that at the temperatures of interest for the MSFR and for the Th-U3 start-up composition the Doppler effect is dominant or comparable to the fuel expansion effect. Fig. 4.9 also shows that the fuel coefficient is of the order of 5 pcm, i.e., one order of magnitude higher compared to the ARR. Albeit advantageous during positive power excursions, the large negative temperature feedback of the MSFR must be taken into account during possible transients leading to overcooling or during the fuel salt loading. If the molten salt is loaded with a fissile content sufficient for criticality at nominal conditions, a salt temperature ~50 K below the operating temperature will bring the reactor to a condition of prompt criticality.

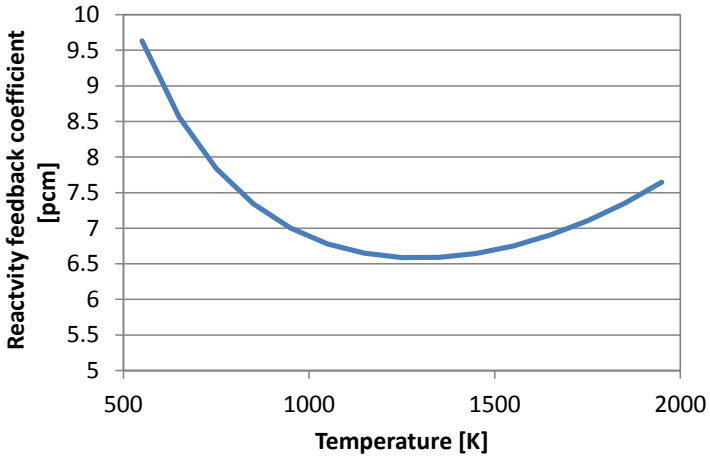

Figure 4.9: Typical behavior of the fuel reactivity feedback coefficients for the MSFR (compositions of the Th-U3 start-up core – see Table 1.3)

It is worth noting that the possibility is considered in the frame of the EVOL project (EVOL, 2012) to operate the gas bubbling for extraction of non-soluble fission products directly inside the core. However, the MSFR fuel expansion coefficient translates into a reactivity insertion of 100-200 pcm for a 1% density increase. Attention should then be paid to set a limit on the gas fraction in the core, as a problem to the gas injection system may cause a sudden density (and reactivity) increase.

Core expansion

Reactivity variations also derive from the expansion of the core structures, which increases the core dimensions. For a bare cylindrical reactor, it results:

$$B^2 = \left(\frac{\pi}{H_c}\right)^2 + \left(\frac{2.405}{R_c}\right)^2 \propto \frac{1}{l^2} \tag{4.6}$$

l indicates a generic linear dimension and increases with temperature, resulting in a positive feedback coefficient. This may represent a concern for the MSFR safety, but the effect is actually negligible. In fact, Eqs. 4.4 and 4.6 allow to write:

$$B^2 L^2 \propto \frac{1}{l^2 d^2} \tag{4.7}$$

Salt density varies according to its volumetric thermal expansion coefficient, while core dimensions vary through the linear thermal expansion coefficient of the core structures. Hence, Eq. 4.7 shows that the same temperature increase in the fuel salt and in the core structures would cause the same absolute reactivity variation - while opposite in sign - in case the linear thermal expansion coefficient of the core structures was equal to the volumetric thermal expansion coefficient of the salt. In reality, the linear thermal expansion coefficient of a typical nickel alloy (as the one used for the MSFR core structures) is of the order of $1.5 \cdot 10^{-5}$ K^{-1}, which is one order of magnitude lower than the volumetric thermal expansion coefficient of the fuel salt. In addition, during a transient, the fuel salt undergoes notable and quick temperature excursions, while a smaller and slower temperature variation is expected in the core structures. In fact, limited thermal excursions in the core structures will likely be a main requirement to preserve their integrity.

Expansion of salt in the blankets

Reactivity is also affected by the blanket density. A blanket temperature increase and density decrement lead to a reduction in reactivity due to fewer neutrons back-scattered to the core by the blankets and thereby lost due to neutron absorption in the boron carbide layer. This effect is mostly negligible as it results in a ~0.1 pcm/K negative coefficient and blanket temperature is expected to remain relatively constant during reactor operation. However, a ~500 pcm reactivity insertion is expected in case the blankets are filled starting from a voided configuration. This indicates that blankets should preferably be filled with fertile salts before the core is filled with the fuel, so to avoid possible criticality accidents.

4.3.2 Equilibrium safety parameters for different fuel cycle options

Table 4.3 summarizes the equilibrium safety parameters for the four MSFR feed options listed in Table 1.7. It includes the subdivision of β_{eff} into the 8 precursor groups used in the JEFF3.1 library (Koning et al., 2006), with decay constants equal to $1.25 \cdot 10^{-2}$ s^{-1}, $2.83 \cdot 10^{-2}$ s^{-1}, $4.25 \cdot 10^{-2}$ s^{-1}, $1.33 \cdot 10^{-1}$ s^{-1}, $2.92 \cdot 10^{-1}$ s^{-1}, $6.66 \cdot 10^{-1}$ s^{-1}, 1.63 s^{-1}, and 3.55 s^{-1}, from group 1 to 8, respectively. Table 4.4 shows the respective fractions in the core of the isotopes mainly affecting safety parameters.

Table 4.3: MSFR equilibrium safety parameters*

	MSFR Th-feed	MSFR ThU3-feed	MSFR ThU3TRU-feed	MSFR ThU3MA-feed
Doppler coeff. [pcm/K]	-3.25	-2.91	-1.89	-1.52
Fuel exp. coeff. [pcm/K]	-3.01	-3.23	-3.25	-3.01
Fuel coeff. (expansion + Doppler) [pcm/K]	-6.26	-6.14	-5.14	-4.53
Coolant exp. coeff. [pcm/K]	-	-	-	-
Core exp. coeff. [pcm/K]	~0	~0	~0	~0
Generation time [μs]	0.95	1.01	0.96	0.80
β_{eff} [pcm]	334.8	332.1	321.7	291.0
β_{eff}^1 [pcm]	22.8	22.8	18.4	17.0
β_{eff}^2 [pcm]	50.0	50.1	51.2	45.5
β_{eff}^3 [pcm]	41.6	41.5	36.1	32.8
β_{eff}^4 [pcm]	66.7	66.6	62.2	56.2
β_{eff}^5 [pcm]	106.5	105.2	101.3	92.7
β_{eff}^6 [pcm]	18.5	17.8	21.8	19.8
β_{eff}^7 [pcm]	23.4	22.9	24.9	21.4
β_{eff}^8 [pcm]	5.3	5.2	5.8	5.6

**The reported values of β_{eff} do not take into account the fuel salt circulation and out-of-core decay of the delayed neutron precursors*

Table 4.4: MSFR equilibrium masses [wt%]

	Th-feed	ThU3-feed	ThU3TRU-feed	ThU3MA-feed
Th-232	81.0	69.7	51.6	53.7
U-233	11.0	11.1	9.0	9.3
U-234	3.8	3.8	3.1	3.2
Pu-239	0.1	0.1	1.6	0.8
Pu-241	~0	~0	0.8	0.4
Am	~0	~0	0.8	2.9
Cm	~0	~0	1.0	3.9
Fission products	0.9	12.1	24.2	17.4

As anticipated in the previous subsection, the MSFR shows notable advantages in all feedback coefficients compared to a traditional FR (see Table 4.2 for the ARR). First of all, there are no positive feedback coefficients, except for the core expansion feedback coefficient that, as mentioned, is negligible. In addition, the negative coefficients have larger magnitude in the MSFR than in traditional FRs, independent of the fuel composition. Doppler and fuel expansion coefficients display similar values, with Doppler dominating only in the Th-feed equilibrium. The different proportions between these two coefficients imply that the

temperature at which the minimum value of the overall fuel coefficient (Fig. 4.9) is found strongly depends on the salt composition: it is at temperatures lower than the nominal one in the ThU3-feed, ThU3TRU-feed and ThU3MA-feed cases, and higher for the Th-feed case. Comparing Tables 4.3 and 4.4 it appears clearly the proportionality between Doppler effect and fraction of Th-232 in the core. An exception is the ThU3MA-feed MSFR that features a lower Doppler coefficient compared to the ThU3TRU-feed MSFR in spite of the higher Th fraction. This is to be ascribed to the low amount of Pu-239 and Pu-241, and high amount of Am (see Fig 4.7). The fuel expansion coefficient is mainly caused by increased leakages and is nearly independent of the fuel composition. As a consequence, the overall feedback coefficients associated to the fuel temperature presents a limited dependence on the composition, changing by only 28% when using the MSFR as breeder or MA burner. This feature well assists the fuel cycle flexibility of the MSFR.

Generation time is improved compared to the ARR, and it is comparable in all cases except for the ThU3MA-feed option. Generation time gives a measure of the time required for a fission neutron to give a new fission and is reduced by the presence of isotopes with high fission cross-section at high energy. This is the case of Am-241, Am-243 and Cm-244 that are all present in significant amount in the ThU3MA-feed equilibrium core and feature fission cross-sections with a minimum at 50-100 keV and a steep increase till 1 MeV (Fig 4.10).

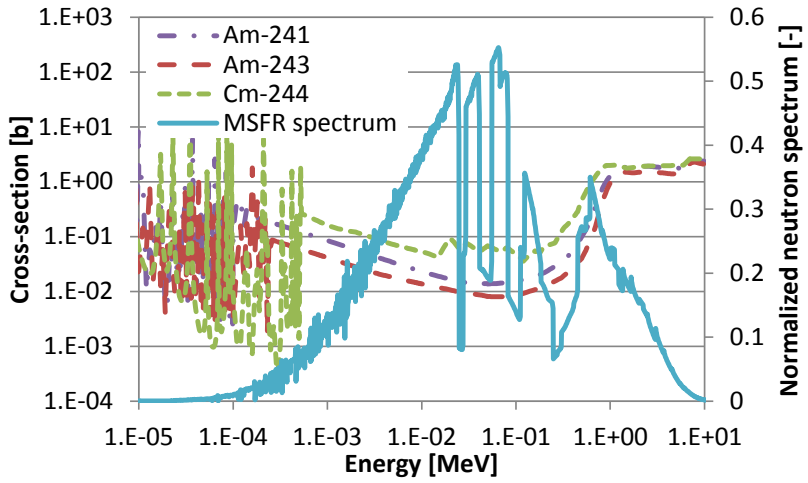

Figure 4.10: Fission cross-sections for Am-241, Am-243 and Cm-244 and comparison with the MSFR neutron spectrum

β_{eff} is comparable to that of the ARR. It displays a similar value in all equilibrium cores, except for the ThU3MA-feed equilibrium. Also in this case, the low value for such feed option can be ascribed to the notable amount of Am-241, Am-243 and Cm-244, all featuring a low delayed neutron yield (Table 4.1). As a matter of fact, the β_{eff} here calculated does not take into account that the fuel salt continuously circulates out of the core, thus causing some of the delayed neutron precursors to be lost in the out-of-core fuel path. The fraction of precursors actually available in the core is then expected to be lower. In particular, the out-of-core decay of precursors is on the order of 35% for the MSFR (see subsection 6.4.2). In addition, precursors do not necessarily accumulate in high flux regions as in solid-fuelled reactors, which causes a further reduction of the precursor effectiveness. The combination of these two effects reduces drastically (~60%, see subsection 6.4.2) the reactivity margin with respect to a

condition of prompt-criticality. However, a low value of the β_{eff} is mainly a concern in nuclear reactors since 1) it increases the required number of control rods necessary to balance the reactivity swing in a cycle while limiting the consequences of their accidental extraction, and 2) it strengthen the effect of feedback coefficients, whose impact on the reactor transient behavior is in fact better predicted by expressing them in dollars. Both consequences are of limited concern in the MSFR, since the burnup reactivity swing is virtually zero and all feedback coefficients are negative.

4.3.3 Safety parameters for the initial core loadings

The liquid fuel of the MSFR allows for a wide variety of fuel compositions, which can be employed for selecting an initial fissile loading based on resource availability and fuel cycle objectives. Four possible start-up core loadings have been presented in Table 1.3, whose safety parameters are shown in Table 4.5. The same features as for the equilibrium cores (Table 4.3) are observed, with the Doppler coefficients that reduce with decreasing fissile quality and decreasing fertile content in the core, and the fuel expansion coefficient which is instead only mildly affected by the core composition. The overall fuel coefficients always maintain a reassuringly positive value, well above 4 pcm/K. A first interesting aspect is the short generation time in Th-TRU and Th-U5-TRU start-up options, which can be ascribed to the high content of Pu-239. As shown in Fig. 4.1, Pu-239 has a nearly flat fission cross-section in the energy range of interest for the MSFR, while that of U-233 is steeply decreasing with energy. As a consequence, fissions are shifted at higher energies when U-233 is replaced by Pu-239, with a detrimental effect on generation time. Such explanation, although preliminary and qualitative, is confirmed by the fission rates reported in Fig. 4.11, showing that the cores containing Pu-239 (Th-TRU, Th-Pu and Th-U5-TRU) features notably more fissions at high energies. It also worth noting that the Th-U5-TRU case features a particularly high β_{eff}, which is fostered by the high delayed neutron yield of U-235 (Table 4.1).

Table 4.5: MSFR safety parameters for different start-up options

	Th-U3	**Th-Pu**	**Th-TRU**	**Th-U5-TRU**
Doppler coeff. [pcm/K]	-4.19	-2.58	-1.69	-1.54
Fuel exp. coeff. [pcm/K]	-3.10	-2.81	-2.56	-2.68
Fuel coeff. (expansion + Doppler) [pcm/K]	-7.29	-5.39	-4.25	-4.22
Coolant exp. coeff. [pcm/K]	-	-	-	-
Core exp. coeff. [pcm/K]	~0	~0	~0	~0
Generation time [μs]	1.13	0.8	0.64	0.67
β_{eff} [pcm]	318.1	276.5	302.1	440.8
β_{eff}^1 [pcm]	23.7	6.7	6.8	11.2
β_{eff}^2 [pcm]	47.3	53.8	57.2	72.2
β_{eff}^3 [pcm]	41.3	22.8	23.0	35.6
β_{eff}^4 [pcm]	63.9	43.0	48.0	76.7
β_{eff}^5 [pcm]	100.6	92.6	97.9	138.9
β_{eff}^6 [pcm]	15.2	22.7	30.1	47.7
β_{eff}^7 [pcm]	21.4	28.9	32.3	44.5
β_{eff}^8 [pcm]	4.6	6.0	6.9	14.0

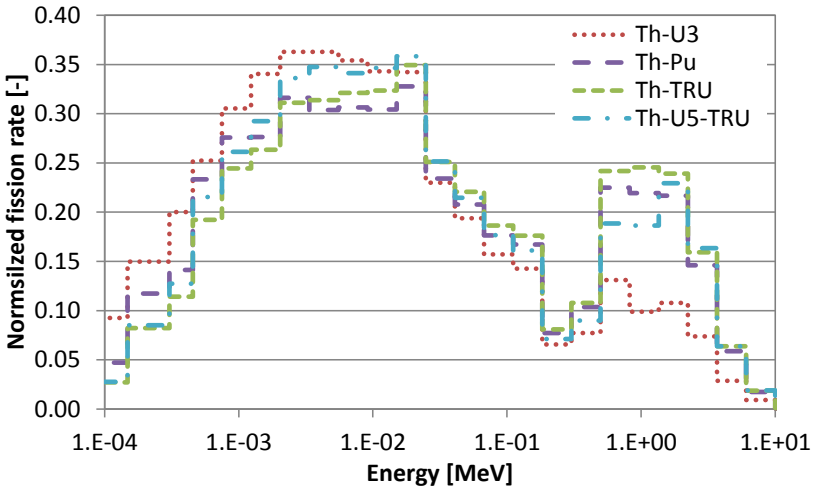

Figure 4.11: MSFR fission rate for different start-up core loadings

4.3.4 Evolution with time

A specific aspect of the MSFR safety parameters is the evolution with time. As mentioned in the previous Chapter, this reactor combines a high specific power with the lack of out-of-core cooling times to determine a quick evolution of masses in the core. This is beneficial if the goal is the transmutation of a TRU loading. On the other hand, safety parameters reflect the core compositions, especially in terms of main fertile and fissile isotopes, and experience a quick change, generally quicker than for radiotoxicity that instead depends on slowly varying isotopes like Cm. As an example, Fig. 4.12 shows the evolution of safety parameters in the fuel cycle strategy proposed in Section 3.4 and envisioning a Th-U5-TRU start-up core, 100 years of TRU burning (ThU3TRU-feed) and 50 years of iso-breeding operation (ThU3TRU-feed) to consume the TRUs in the core.

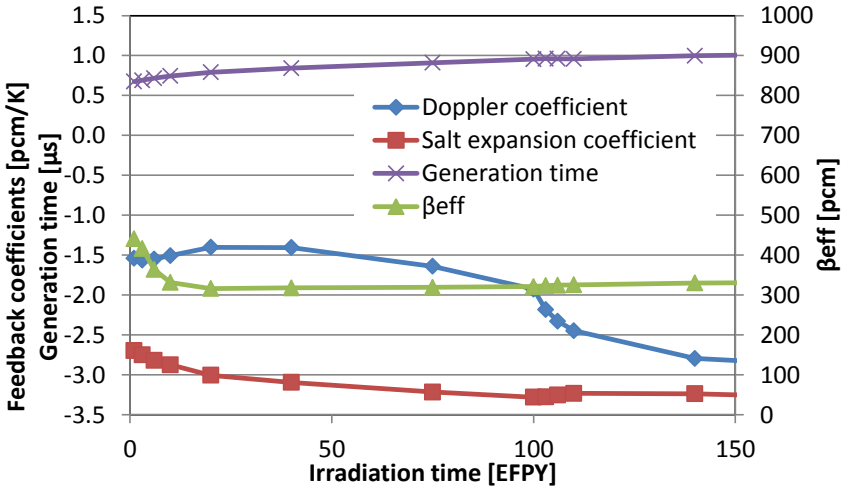

Figure 4.12: Evolution of safety parameters with irradiation time for the MSFR fuel cycle strategy proposed in Section 3.4

The initial safety parameters fostered by Th-U5-TRU are characterized as noted by low feedback coefficients and generation time but very high β_{eff}. β_{eff} then decreases to a minimum value after only 10 years as U-235 is consumed and its beneficial effect on β_{eff} is lost. The feed variation after 100 Equivalent Full Power Years (EFPY) leads to a second quick variation of safety parameters, particularly for the Doppler coefficient. These variations will require some

flexibility in the control system. However, in spite of the quick variation, anomalous variations or oscillations in the core safety parameters are not observed.

4.4 INHERENT SAFETY FEATURES

Core safety parameters discussed in the previous Sections can be used to predict the core steady-state after a transient, allowing to evaluate the capability of the core to withstand the consequences of major transient initiators (provided that severe conditions are not reached before the achievement of the steady-state). In this Section, inherent safety features of the ARR are first investigated based on a consolidated approach developed for sodium-cooled pool-type FRs. Subsequently, a similar approach is proposed for the MSFR and employed to preliminarily analyze its inherent safety performances in comparison with the ARR.

4.4.1 The case of the ARR

Inherent safety features of the ARR are investigated in this subsection using an approach proposed by Wade and Chang (1987) and Wade and Hill (1997). To this purpose, it is useful to group the feedback coefficients into three parameters generally identified as *A, B, C* (Wade and Chang, 1987). *A* represents the reactivity variation associated to the fuel temperature increase from the average coolant temperature to the average fuel temperature at nominal conditions. *B* represents the reactivity variation associated to the increase in fuel and coolant temperatures from iso-thermal zero-power conditions (at inlet temperature) to the average coolant temperature. *C* is the reactivity feedback coefficient associated to the inlet core temperature. Results for the same ARR core compositions discussed in Section 4.2 are reported in Table 4.6 (see (Wade and Fujita, 1989) for details about the calculation procedure).

Table 4.6: Equilibrium parameters at EOC for inherent safety of the investigated ARR cores and feed/fertile isotope options

Core type	Standard burner				U-based iso-breeder	Th-based iso-breeder
Fertile	U	Th	U	Th	U	Th
Fissile make-up feed	TRUs	TRUs	TRUs	TRUs	-	-
MA/Pu ratio in the feed	~0.1	~0.1	~1	~1		
CR* [-]	0.47	0.36	0.40	0.29	1	1
A [m$]**	-465	-464	-341	-315	-234	-441
B [m$]**	-479	-540	-478	-539	-456	-532
CΔTc [m$]**	-492	-578	-434	-492	-476	-715
A/B [-]	0.97	0.86	0.71	0.58	0.51	0.83
CΔTc/B [-]	1.03	1.07	0.91	0.91	1.05	1.35
$(1+(A/B))^2\|B\|$ [m$]	1861	1865	1404	1353	1044	1779
Required control rods for inherent safety [-]	18	20	15	18	12	15

**CR defined considering Th-232 and U-238 as the only fertile materials and all other isotopes as fissile. It corresponds to the TRU regeneration rate (Wade and Hill, 1997) in the U-based cores, while TRUs must be substituted by trans-Th isotopes to employ the same definition of CR to Th-based cores. In all cases, it is computed as the ratio of the rate of non-fission capture rate in U-238 or Th-232 to the rate of TRU or trans-Th destruction by fission.*

*** Evaluated without considering the control rod driveline and vessel thermal expansion (Wade and Fujita, 1989; Yang, 2008).*

Using the A, B and C parameters, it is possible to write the following reactivity and energy balances:

$$A(\bar{P}-1)+B\left(\frac{\bar{P}}{\bar{F}}-1\right)+C\delta T_{in}+\delta\rho_{ext}=0 \tag{4.8}$$

$$\delta T_{out}=\delta T_{in}+\Delta T_c\left(\frac{\bar{P}}{\bar{F}}-1\right) \tag{4.9}$$

where $\bar{P}$ and $\bar{F}$ are the reactor power and flow rate, normalized to their nominal level. ΔT_c indicates the coolant temperature rise across the core, δT_{out} and δT_{in} represent variations of outlet and inlet temperatures, and $\delta\rho_{ext}$ is the reactivity variation through control rod movements. In general, in a sodium-cooled FR the core outlet temperature can increase up to $1.5\Delta T_c$ before leading to structural damage (Wade and Chang, 1987). Assuming a 33% margin on this temperature increase, the condition to be met is a maximum core outlet temperature increase equal to ΔT_c. By imposing this condition at the end of a transient, it is possible to use reactivity and energy balances (Eqs. 4.8 and 4.9) to derive sufficient conditions for the reactor safety.

First of all, it should be recognized that a pump overspeed accident does not lead to an increased outlet temperature, at least in the short term (Wade and Chang, 1987). More interesting is the case of an ULOF. For this kind of accident $\bar{P}$ is approximately zero at the end of the transient while it is assumed that external reactivity and inlet temperature remain unchanged. The condition on δT_{out} yield:

$$\frac{A}{B}<1 \tag{4.10}$$

Table 4.6 shows that this condition is satisfied for all cases considered, with some disadvantage for the burner core configurations. This is a consequence of using oxide fuel, whose high operating temperature (~1300 K) implies a high reactivity insertion in case of reactor power reduction (as in an ULOF). In this case, a low Doppler effect is advantageous and the cores with high MA content show better performances. Thorium has some specific benefits thanks to the more negative *B* value fostered by a low coolant expansion coefficient. The condition expressed by Eq. 4.10 is met by the iso-breeder cores thanks to the low fuel temperature (~1000 K) fostered by metallic or nitride fuels. In this case, the more negative Doppler effect of Th leads to a higher value of A and to an inferior (but still acceptable) safety performance compared to the U metal iso-breeder core.

The ULOHS transient causes an increase of the inlet temperature leading to the reactor shut-down. The flow rate is supposed unaltered and the condition on the outlet temperature leads in this case to:

$$\frac{C\Delta T_c}{B}>1 \tag{4.11}$$

The condition expressed by Eq. 4.11 is met with better confidence in the iso-breeder cores, with Th showing additional margin compared to U. For the burner options, the

condition in Eq. 4.11 can be met when using TRU feed from once-through LWR, with a small advantage for the Th case. The ~1 MA/Pu feed leads to a notable deterioration of the reactor response to an ULOHS as a consequence of the high coolant coefficient.

An inverse accident compared to an ULOHS is represented by a reduction of the inlet temperature. As a reference case, it is assumed an inlet temperature reduction equal to $2\Delta T_c$, corresponding approximately to Na freezing. This is a limiting case, as Na freezing would be the initiator of an ULOF transient. Under the hypothesis of a fixed flow rate, reactivity and energy balances give:

$$\frac{C\Delta T_c}{B} < 1.5\left(1+\frac{A}{B}\right) \sim 3 \tag{4.12}$$

which is largely satisfied in all cases, showing that this accident is not a concern for the ARR safety performance.

One last accident whose consequences can be predicted using a quasi-static approach is a "slow" Unprotected Transient OverPower (UTOP), where a control rod is accidentally extracted over a time span comparable to the time constant related to heat transfer phenomena in the core. For this event it is assumed that flow rate and inlet temperature are unchanged. The usual condition on the outlet temperature yield,

$$\delta\rho_{ext} < |B|\left(1+\frac{A}{B}\right) \tag{4.13}$$

which implies that one should limit a control rod worth to the value at the right-hand side of Eq. 4.13. Table 4.6 shows the estimated number of control rods to cope with this requirement. It is generally comparable to the number of rods necessary to meet the typical limit of 0.8 $ (Table 4.2) control rod worth. Thorium is in this case penalizing due to the low internal breeding and consequent high reactivity swing.

Application of the quasi-static reactivity balance for predicting the consequences of the above transients is inadequate to characterize the first few tens of seconds of an ULOF (Wade and Chang, 1987), where the pump coast-down may be quicker than the power reduction as a consequence of the delayed neutron hold back time. In this case it is possible to demonstrate that the consequences of the increased power-to-flow ratio can be mitigated by minimizing the quantity $(1+(A/B))^2|B|$ (Wade and Chang, 1987). Thorium use has a limited impact, except for the iso-breeder case, where it has a negative effect. However, transient analysis would be required for a proper assessment.

4.4.2 The case of the MSFR

The previous subsection has confirmed for the ARR the capability of sodium-cooled FRs to withstand typical double-fault accidents, with a note of caution for the ULOHS transient for cores with a high TRU content. Thorium use in the ARR has been proved to determine similar inherent safety features as for the U-based versions. This combines with the promising safety parameters observed in subsection 4.2.1 and to the higher TRU burning rate (Table 3.4) to make Th a promising fertile support for TRU burning, especially considering that remote fuel fabrication will be needed in TRU burner cores independent of the gamma field from U-

232's progeny. The MSFR features good breeding potential, low waste generation in a closed cycle, good TRU burning capabilities, and promising safety parameters. However, for all these benefits to materialize, its response to accidental events must be proved comparable or improved compared to U- or Th-based traditional FRs. In this subsection, a preliminary approach is proposed to investigate the MSFR inherent safety features, accounting for MSFR specificities like the movement of delayed neutron precursors and the direct deposition of fission heat into the coolant.

Similarly to traditional FRs, three main transient initiators can be identified for the MSFR, resulting in 5 main accidental transients. A reactivity insertion is the first relevant initiator and results in an accidental transient if a positive reactivity is inserted (UTOP). In the MSFR, control rods may not be necessary to balance the reactivity swing thanks to the online reprocessing system, but they may be necessary to drive the reactor operational transients (start-up, shut-down, load following). In addition, malfunctioning of the reprocessing system may cause a quick injection of fissile material. The primary pumps represent a second transient initiator. They may trigger two different accidental transients as they may experience an overspeed (pump overspeed) or a coast-down (ULOF). Finally, the heat exchangers may lose (ULOHS) or increase (chilled inlet) their cooling capabilities following abnormal events in the intermediate or secondary circuits.

Energy and reactivity balances can be used also for the MSFR to predict the asymptotic reactor state after an accidental transient initiator. The only exception is the ULOHS transient, causing a quick temperature rise in the core (see subsection 6.5.5) that is ultimately driven by decay heat and requires draining of the salt in the passively-cooled tanks before the possible set-up of an asymptotic state. An asymptotic state is instead expected to set-up for an UTOP, ULOF, chilled inlet and pump overspeed. The following equations govern the variation of reactivity between the initial and final steady-states in the MSFR:

$$\delta\rho = (\alpha_d + \alpha_D)\delta T_{AV} + \delta\rho_0 + \delta\rho_{ext} = 0 \tag{4.14}$$

$(\alpha_d + \alpha_D)\delta T_{AV}$ indicates the reactivity variation due to a variation of the average core temperature while $\delta\rho_0$ is the reactivity variation due to a variation in velocity and ensuing out-of-core decay of delayed neutron precursors. According to a simplified precursor balance, $\delta\rho_0$ can be evaluated as (Cammi et al., 2011):

$$\delta\rho_0 = \delta\left(\sum_{i=1}^{8} \frac{\beta_{eff}^i \lambda_i}{\lambda_i + \frac{1-e^{-\lambda_i \tau_{EC}}}{\tau_C}}\right) \tag{4.15}$$

where τ_{EC} and τ_C are the out-of-core and in-core transit time of the fuel salt.

At steady-state the power *Pow* produced by the reactor has to match that dissipated by the heat exchangers, thus being approximately equal to:

$$Pow = U \cdot (T_{AV} - T_{sec}) \tag{4.16}$$

where T_{AV} is the average temperature in both core and heat exchangers while T_{sec} is the temperature at the secondary side of the heat exchangers, which is here considered as constant. The heat transfer coefficient U is the harmonic mean of the coefficients at the primary and secondary sides of the heat exchangers. The one at the secondary side can be considered as constant if considering transients mainly involving the primary circuit, while that at the primary side depends on the salt flow rate. A dependency according to the Gnielinski correlation (Gnielinski, 1976) has been here assumed for turbulent flow conditions. The analytic results Nu=4.36 is instead used in case of a laminar flow[16].

For a given power, inlet and outlet temperatures[17] can be computed as:

$$T_{in} = T_{AV} - \frac{Pow}{2c_p\Gamma} \tag{4.17}$$

$$T_{out} = T_{AV} + \frac{Pow}{2c_p\Gamma} \tag{4.18}$$

where Γ is the mass flow rate.

Note that Eqs. 4.16, 4.17 and 4.18 assume that the average between inlet and outlet core temperatures is equal to the core average temperature, which is not necessarily the case if recirculation zones exist in the core (see Chapter 6). In addition, this average temperature is used also in Eq. 4.14 to evaluate reactivity feedbacks. This is an approximation, since a proper evaluation would require an effective temperature computed using direct and adjoint fluxes as weights. However, impact on the results of these approximations is limited, which will be discussed in some details in Chapter 6.

Finally, an equation is needed to predict the flow rate due to natural circulation in case of a loss of flow. To this purpose, it is necessary to equate the driving force from buoyancy to the pressure losses Δp in the primary loop:

$$\Delta p = g \cdot \Delta\Theta \cdot \left(d(T_{out}) - d(T_{in})\right) \tag{4.19}$$

where $\Delta\Theta$ is the height difference between the center of the core and the center of the heat exchangers (38.1 cm[18]), g the gravitational acceleration and d the fuel salt density. The pressure losses Δp are mainly driven by the heat exchangers and have been here computed applying to the data in Table 1.2 the Petukhov correlation for turbulent flows (Petukhov, 1970), and the analytic results $f=Re/64$ for laminar flows (f is the Darcy friction factor). Concentrated pressure losses have been neglected for simplicity.

---

[16] Note that this result is valid only for constant wall heat flux and fully developed conditions. It is used here only as a first approximation. In particular, it is worth noting that the result for constant wall temperature would be Nu=3.66. It will be shown that a lower Nusselt number at the end of an accidental transient is generally advantageous, since it reduces the core power. It follows that the choice of using the result for constant wall heat flux goes in the direction of providing conservative results.

[17] Note that inlet and outlet refer to the surfaces where the fuel salt enters and exits from the cylindrical core, where power is produced. Roughly the same bulk temperatures characterize outlet and inlet of the heat exchanger, respectively.

[18] This value results from placing the heat exchanger in the upper part of the out-of-core portion of the circuit in the axial-symmetric configuration shown in Fig. 1.2.

Eqs. 4.14 to 4.19 can be used to predict the consequences of an accidental transient resulting in a new steady-state, and mainly involving the primary circuit. In fact, heat transfer capabilities at the secondary side of the heat exchangers are assumed to be maintained. The main accidental transients for the MSFR are discussed in the following, with reference to the data and nominal reactor conditions reported in Tables 1.1, 1.2 and 1.4. The discussion is based on the prediction of the core parameters at the end of a transient while simple conditions like those in Eqs. 4.10 to 4.13 cannot be derived following the lack of specific constraints on core temperatures.

UTOP

A first transient is the UTOP, which may be triggered in the MSFR by an accidental extraction of a control rod (if present) or by an accidental injection of fissile material from the reprocessing system. The reactivity insertion is expected to be small in the MSFR since 1) there is no burnup reactivity swing and ideally no control rods are needed to balance it, and 2) only few liters or few tens of liters of salt need to be extracted and reinserted in the core each day. In all cases, it is reasonable to assume that a maximum reactivity insertion of 0.8 $ can be achieved by design as in the case of traditional FRs. This corresponds to approximately 100 pcm. According to Eq. 4.14 and assuming the worst feedback coefficient in Tables 4.3 and 4.5 (4.22 pcm/K in the Th-U5-TRU start-up core), this will lead to a increment of the average core temperature equal to 23.7 K (Eq. 4.14). Such an increment will also be experienced by the average temperature at the primary side of the heat exchangers, causing an increment of the power equal to 23.7% (Eq. 4.16), and a 23.7 K (Eqs. 4.17 and 4.18) increment of the difference between core inlet and outlet temperatures. As a result, the outlet temperature will be increased by ~35.6 K. Clearly, these results can be used to predict the temporary state-steady that would be achieved after the initial power peak and ensuing oscillations (i.e., after 10 seconds – see subsection 6.5.1), and before the behavior of intermediate and secondary circuits will start playing a main role (i.e., after few minutes). In case the intermediate and secondary circuits were able to dissipate the 23.7% excess power, the core would maintain the same steady-state also in the long term. In case the power output of the secondary circuit was unchanged, temperatures would increase in the intermediate circuit, thus reducing the heat exchange with the primary circuit and ultimately the core power. In the long term, the core would produce the same power as before the transient, but all temperatures of primary and intermediate loop would be increased by 23.7 K. In all cases, the UTOP appears as a minor concern, provided that the energy released during the initial power peak caused by a reactivity insertion will be small (as will be shown in subsection 6.5.1).

Chilled inlet

A reduction of the core inlet temperature will generally happen following a reduction of temperatures at the secondary circuit, which in turn may be caused e.g. by depressurization of the steam generator. The worst-case scenario is represented by a coolant temperature in the secondary circuit that reduces to a level close to salt freezing (~727 K). Here it has been assumed that the salt at the secondary side of the heat exchanger experiences a 100 K reduction (from 823 K to 723 K average temperature).

The asymptotic system response to such perturbation can be predicted by noticing that the reactivity balance 4.14 imposes the average temperature to remain unchanged at the end of the transient. The final reactor power will be equal to the power transferred at the heat exchangers, which in turn is proportional to the difference between the average temperature in the heat exchangers (and in the core), and the temperature at the secondary side. In the simulated transient, such difference changes from ~150 K to ~250 K, so that the reactor power would change from 3 GW to ~5 GW. The core outlet temperature would approximately increase by half of the total increase of the inlet-outlet core temperature difference, which in turn is proportional to the power increment. In the case considered here, the outlet temperature would increase by ~33 K, independent of the neutronic properties of the salt composition. In the long term, the consequences of the chilled inlet will depend on the event responsible for the lower temperature at the intermediate and secondary circuits. However, the 33 K increment of the maximum temperature in the core allows to consider also the chilled inlet as lower concerns for the MSFR safety, provided that the initial power growth due to the cold salt entering the core will be limited (as will be shown in subsection 6.5.2).

It is worth noting that the inlet temperature in the heat exchangers will be reduced by ~33 K, which combines with the reduced temperatures at the secondary sides to pose some concerns related to possible freezing of the primary salt at the tube walls (the melting point of the primary salt is 838 K). In this case the accident would degenerate in a loss of flow.

Pump overspeed

A pump overspeed is a kind of accident that is possible mainly in case a variable-speed pump is used. An increased pump speed causes a higher delayed neutron loss (Eq. 4.15), and an ensuing reactivity reduction which will be compensated by a reduction of the core temperatures. A reduced average core temperature will generally results in a lower temperature at the primary side of the heat exchanger, and, consequently, in a lower power transferred to the intermediate loop. On the other hand, a higher velocity enhances the heat transfer coefficient, thus promoting a higher heat exchange. The overall results of the mentioned effects on the asymptotic power depends on: 1) the reactivity loss due to additional delayed neutron losses; 2) the reactivity feedback coefficient associated to the salt temperature, which will determine the core temperature reduction necessary to offset the reactivity loss; and 3) the velocity dependence of the heat transfer coefficient of the heat exchanger, which will determine the enhancement of its heat transfer capabilities. Eqs. 4.14 to 4.19 have been solved using MATLAB for the 4 equilibrium cores and the 4 start-up options listed in Tables 4.3 and 4.5, and results have been summarized in Table 4.7. The assumption has been made of a twofold increase of the pressure difference imposed by the pump. Among the heat exchangers proposed in Table 1.4, the case with 4 mm tube diameter and 300 kPa of pressure drop has been considered.

Table 4.7: Asymptotic variation of characterizing MSFR core parameters after a pump overspeed (heat exchanger with 0.4 mm tubes)

	δT_{AV}	δT_{out} [K]	δT_{in} [K]	P/P_0 [%]	Γ/Γ_0 [%]	$\delta\rho_0$ [pcm]
Th-feed eql.	-0.9	-10.7	8.9	119.6	148.6	-5.7
ThU3-feed eql.	-0.9	-10.7	8.9	119.5	148.6	-5.6
ThU3TRU-feed eql.	-1.1	-11.0	8.7	119.4	148.6	-5.8
ThU3MA-feed eql.	-1.2	-11.0	8.7	119.4	148.6	-5.2
Th-U3 start-up	-0.7	-10.4	9.0	119.7	148.6	-5.3
Th-Pu start-up	-1.0	-10.9	8.8	119.4	148.6	-5.6
Th-TRU start-up	-1.5	-11.4	8.4	119.1	148.6	-6.4
Th-U5-TRU start-up	-2.2	-12.4	7.9	118.5	148.6	-9.5

Reactivity variation due to increased precursor losses is negligible, which causes the average temperature in the core (and heat exchangers) to be practically unaffected. The increment in the heat transfer coefficient is instead dominant, making negligible the dependency on the fuel composition and causing the core power to increase by ~20%. However the increment of the flow rate is nearly 50%, which reduces the power-to-flow ratio and determines a lower outlet temperature at the end of the transient. As in the case of the UTOP and chilled inlet transients, the MSFR emerges as a safe reactor also in case of a pump overspeed.

Clearly, the long-term consequences of the transient will be dictated by the behavior of intermediate and secondary circuits, as well as by intervention of the operator or of the safety systems. Under the hypothesis that the power output of the secondary circuit will remain unchanged, the core power will remain unchanged and the only differences compared to the nominal steady-state would be: 1) a slightly lower core average temperature, 2) a reduced outlet-inlet temperature difference, and 3) higher temperatures (~30 K) in the intermediate circuit to offset the increment of heat transfer capabilities at the primary side of the heat exchangers.

ULOF

A loss of flow with a complete coast-down of all the available pumps may happen in a reactor following e.g. an electricity shortage. Generally, this would compromise in the long term the heat transfer capabilities of all the loops (primary, intermediate, secondary). The dynamics of intermediate and secondary circuits would depend on their heat capacity and on the set-up of a natural circulation regime. As a general rule, the heat capacity would be higher, and natural circulation improved compared to the primary circuit thanks to the relative flexibility in its design. As a first approximation, and for the first few minutes, it is then reasonable to assume temperature and heat transfer capabilities at the secondary side of the heat exchangers as constant. As in the case of the pump overspeed, Eqs. 4.14 to 4.19 have been solved using MATLAB for the 4 equilibrium cores and the 4 start-up options listed in Tables 4.3 and 4.5, and results have been summarized in Table 4.8. Also in this case, the heat exchangers with 4 mm tube diameter (Table 1.4) have been considered.

Table 4.8: Asymptotic variation of characterizing MSFR core parameters after an ULOF (heat exchanger with 0.4 mm tubes)

	δT_{AV}	δT_{out} [K]	δT_{in} [K]	P/P_0 [%]	Γ/Γ_0 [%]	$\delta\rho_0$ [pcm]
Th-feed eql.	16.6	350.0	-316.8	18.4	2.4	104.2
ThU3-feed eql.	16.8	350.4	-316.8	18.4	2.4	103.3
ThU3TRU-feed eql.	19.5	356.1	-317.2	18.7	2.4	100.0
ThU3MA-feed eql.	20.0	357.1	-317.2	18.8	2.4	90.4
Th-U3 start-up	13.6	343.4	-316.3	18.1	2.4	98.8
Th-Pu start-up	16.0	348.6	-316.7	18.3	2.4	86.1
Th-TRU start-up	22.1	361.7	-317.5	19.0	2.4	93.9
Th-U5-TRU start-up	32.6	383.9	-318.7	20.2	2.5	137.5

$\delta\rho_0$ depends on the flow variation, which is approximately the same in all cases except for the Th-U5-TRU start-up core, where the high β_{eff} determines a higher reactivity insertion. The impact on the average core temperature is however mild thanks to the high feedback coefficient of the fuel temperature. The variation of the average core temperature slightly impacts the final core power, but the major effect in this sense comes from the variation in the heat transfer coefficient at the primary side of the heat exchangers, which is the same in all cases. In fact, the flow regime at the end of the transient is laminar and the Nusselt number is independent of the flow rate. Besides, the final flow rate is similar in all cases, which is still due to the similar power since the buoyancy effect is proportional to the power through the term T_{out}-T_{in} (Eq. 4.19). As a general result, the ratio between power and flow rate is reduced by approximately 7 times, yielding an equivalent increase of the term T_{out}-T_{in}. Variation in T_{in} is similar in all cases since a higher T_{AV} is compensated in Eq. 4.17 by a higher power. On the other hand, a higher T_{AV} combines in Eq. 4.18 with a higher power to give noticeably different variations of the outlet temperature for different fuel compositions.

The ~300-400 K variation of inlet and outlet temperatures is unacceptable from a safety viewpoint. In particular, such a reduction of the lower temperature of the system would cause salt freezing, as the salt melting point is only 85 K lower than the inlet temperature (see Table 1.2). It is worth noting that use of heat exchangers with larger tubes would improve the outcome of a loss of flow thanks to the initially high Reynolds number and heat transfer coefficient, which would cause a stronger reduction of the power transferred to the intermediate circuit after the onset of a natural circulation regime. For instance use of a heat exchanger with tube diameters equal to 6 mm and 1 cm (see Table 1.4) would determine a final power-to-flow ratio equal to 6 and 3.5, respectively. However, the inlet temperature in the two cases would still be reduced by more than 200 K.

To improve the natural circulation capabilities of the MSFR, the distance $\Delta\theta$ between the centers of core and heat exchangers should be maximized (Eq. 4.19). The 85 K limit on the inlet temperature variation would be met with $\Delta\theta$ equal to 3 m and 1.5 m when using a heat exchanger with tube diameters of 0.4 mm and 0.6 mm, respectively. Results are summarized in Tables 4.9 and 4.10, showing that also the increase of the outlet temperature would be limited.

Table 4.9: Asymptotic variation of characterizing MSFR core parameters after an ULOF (heat exchanger with 0.4 mm tubes, 3 m between the centers of core and heat exchangers)

	δT_{AV}	δT_{out} [K]	δT_{in} [K]	P/P_0 [%]	Γ/Γ_0 [%]	$\delta\rho_0$[pcm]
Th-feed eql.	11.9	96.6	-72.8	17.9	6.6	74.7
ThU3-feed eql.	12.0	96.8	-72.7	17.9	6.6	73.9
ThU3TRU-feed eql.	14.0	99.6	-71.5	18.1	6.7	72.1
ThU3MA-feed eql.	14.4	100.1	-71.3	18.2	6.7	65.2
Th-U3 start-up	9.7	93.4	-74.1	17.6	6.6	70.5
Th-Pu start-up	11.8	96.4	-72.9	17.9	6.6	63.4
Th-TRU start-up	16.4	102.9	-70.2	18.4	6.7	69.5
Th-U5-TRU start-up	24.2	113.9	-65.5	19.2	6.9	102.3

Table 4.10: Asymptotic variation of characterizing MSFR core parameters after an ULOF (heat exchanger with 0.6 mm tubes, 1.5 m between the centers of core and heat exchangers)

	δT_{AV}	δT_{out} [K]	δT_{in} [K]	P/P_0 [%]	Γ/Γ_0 [%]	$\delta\rho_0$[pcm]
Th-feed eql.	15.6	109.3	-78.1	8.8	3.1	97.7
ThU3-feed eql.	15.8	109.5	-78.0	8.8	3.1	96.9
ThU3TRU-feed eql.	18.3	113.1	-76.6	8.9	3.1	93.8
ThU3MA-feed eql.	18.7	113.8	-76.3	9.0	3.1	84.9
Th-U3 start-up	12.7	105.1	-79.7	8.6	3.0	92.6
Th-Pu start-up	15.0	108.5	-78.4	8.8	3.1	81.1
Th-TRU start-up	20.8	116.8	-75.1	9.1	3.1	88.6
Th-U5-TRU start-up	30.8	130.9	-69.3	9.6	3.2	129.9

For the natural circulation regime in the primary circuit to be effective, the power produced in the core must be transferred to the secondary circuit and dissipated into the environment, which in turn requires an effective natural circulation in all circuits. However, flow rates will generally be reduced. A higher temperature or a lower heat transfer coefficient at the secondary side of the heat exchanger will reduce the power exchanged and thus the power in the core. Solving Eqs. 4.14 to 4.19, it turns out that the final power-to-flow ratio would be decreased compared to that calculated in Tables 4.8 to 4.10. This allows to consider the case with unaltered heat transfer capabilities at the secondary side of the heat exchanger as a limiting case for safety. Only in the unlikely event of a temperature drop at the secondary sides sufficient to balance the reduced heat transfer coefficient, a higher power in the core would be possible.

As a final comment, it is worth noting that a bulk temperature above the salt freezing point does not guarantee that salt freezing will not occur at the tube walls. In fact, in case of a drastic flow reduction the temperature difference between primary and secondary salts will be concentrated at the primary side. The tube walls will then assume approximately the same temperature as the secondary salt, which in turn is approximately equal to 800-850 K, comparable or lower than the melting point of the primary salt (838 K). This suggests that improving the MSFR resistance to ULOF transients will also require higher temperatures in the intermediate circuit.

4.5 CONCLUDING REMARKS

In this Chapter, the safety aspects of the MSFR have been assessed based on the individuation, evaluation and characterization of feedback coefficients, β_{eff} and generation time, including a comparison with the Th- and U-based traditional FRs. Reactivity decomposition techniques have been employed for a better understanding of the phenomenology underlying each safety parameter, thus giving an insight into the observed differences between Th and U use, and between the MSFR and the traditional FRs. A simple approach has been developed to evaluate the MSFR capabilities to withstand all typical double-fault accidents, for different fuel cycle options. For comparison, a traditional method for the inherent safety of sodium-cooled FRs has been applied to the case of U and Th versions of the ARR.

Th use in fast-spectrum systems determines a lower reactivity increment due to spectrum hardening thanks to the lower cross-section and higher threshold for fission of Th-232 vs U-238, and to the steeper fission cross-section and flatter capture cross-section of U-233 vs Pu-239. In case of the traditional FRs, this determines notable improvements of the core void reactivity, which becomes negative in the Th-based iso-breeder ARR. Spectrum hardening plays a role also in the Doppler phenomenology, determining some advantages for the Th option in case a significant amount of U-233 is present in the core. As a drawback, Th use lowers (in absolute terms) the negative feedback coefficients associated to core and fuel expansions in traditional FRs. Use of Th has consequences also on the β_{eff}. In particular, U-233 has a higher delayed neutron yield compared to Pu-239 while the possible beneficial effect of fissions in fertile isotopes is frustrated by the very low fission rate of Th-232 compared to U-238. As a result, β_{eff} for Th-based iso-breeder FRs is comparable to that of the U counterparts thanks to the sufficient amount of U-233, while the Th option presents lower values in burner core configurations. This combines with the higher burnup reactivity swing (due to the lower internal breeding) to yield a considerably higher number of required control rods in Th vs U traditional FRs. If burner FRs are considered with a very high TRU burning rate, differences between Th and U tightens due to the lower fertile-to-fissile ratio.

Investigation of the MSFR safety parameters has shown that only Doppler and fuel expansion induce significant reactivity feedbacks. The Doppler coefficient is characterized by the same phenomenology as for traditional FRs, with an increment of captures in Th-232 and an ensuing spectrum hardening causing a reduced fission rate in the fissile isotopes. However, Th use and a softer spectrum combine to give a notably stronger coefficient, nearly one order of magnitude higher compared e.g. to the ARR. Dependency of the Doppler coefficient with temperature and composition is analogous to traditional FRs, with a logarithmic trend of reactivity vs temperature and a reduction of Doppler with lower CR and higher Am content. The fuel expansion coefficient presents instead a phenomenology that deeply differentiates it from traditional FRs. It results from a change of the neutron diffusion length in the core and from the ensuing increase of leakages. Spectrum softening due to an increased coolant-to-fuel ratio is instead mainly responsible for the fuel expansion feedback in traditional FRs. The resulting negative feedback is tens of times higher in the MSFR, increases with fuel temperature, and is only mildly affected by core compositions, thus assisting the fuel cycle flexibility of the this kind of reactor. In addition to Doppler and fuel expansion, only blanket density and core expansion can affect the core reactivity. Blanket density variation causes a

negative feedback, but negligible. Core expansion is potentially a positive feedback, but it has been proved to be 10 times lower compared to the fuel salt expansion. In addition, it would act in a delayed way and it could be triggered mainly by salt heating, thus slightly reducing the fuel expansion coefficient without acting per se as a positive feedback. β_{eff} and generation time are comparable to the case of traditional FRs, if a static fuel is assumed. A notable reduction of β_{eff} is caused by salt circulation (see Chapter 6), but a low value of this parameter is a limited concern in the MSFR thanks to the lack of a burnup reactivity swing and of positive feedbacks.

Th use in traditional FRs presents both pros and cons in terms of inherent safety. The higher Doppler opposes a power decrement in the core while a reduced coolant coefficient reduces the reactivity insertion when core temperatures increase. Independent of the core configuration and fuel, the ARR generally complies with the safety requirements to withstand typical double-fault accidents. The MSFR inherent safety has also been investigated through an analysis of the steady-state reached after an accidental transient initiator, for different fuel cycle strategies. Although specific limits are not presently available for the maximum allowed temperature in the core, the steady-states reached by the MSFR in case of UTOP and pump overspeed accidents appear widely acceptable for all the fuel compositions investigated. The chilled inlet is not a concern unless it causes freezing of the primary salt in the heat exchangers. In case of an ULOF, the final steady-state shows unacceptable temperatures. However, the MSFR response to this kind of accident can be improved by a proper choice of type and position of the heat exchangers. For instance, acceptable conditions at steady-state are achieved selecting shell-and-tube heat exchangers with 0.4 mm tubes and positioned 3 m above the core center. Residual concerns remain for the possible freezing of the primary salt at the tube walls in the heat exchangers. This would suggest redesigning the MSFR with temperatures in the intermediate circuit above the freezing point of the primary salt (i.e., 838 K). The possibility also exists of draining the fuel salt in the passively-cooled tanks envisioned for the MSFR. The same safety measure will be necessary in case of an ULOHS, since the decay heat will determine a quick temperature rise in the core, preventing the achievement of a steady-state. Provided the effectiveness of the draining system is proved and its intervention fully passive, the overall safety of the MSFR appears promising.

Summarizing, Th use generally fosters advantages in traditional FRs thanks to the low reactivity insertion in case of spectrum hardening. Adoption of the liquid-fuel MSFR technology further improves safety parameters thanks to the softer spectrum and the lack of positive feedbacks. Also from the standpoint of safety, a liquid fuel is particularly attractive for Th use since the reduced reactivity insertion in case of spectrum hardening improves the Doppler effect without impacting core and fuel expansion coefficients. Inherent safety features of the MSFR are promising and allow the core to withstand typical double-fault accidents, even though core draining is necessary in case of an ULOHS or an ULOF. No significant performance deterioration is observed when using the MSFR as a burner reactor. However, the MSFR transient response has to be investigated to rule out possible unsafe situations that may be reached before the asymptotic state is achieved, which will be the subject of Chapter 6. In addition, the preliminary safety assessment performed has been based on the analysis of the primary circuit behavior, while an analysis of the overall power plant would be needed for a better prediction of a reactor transient, especially in the long term.

REFERENCES

Cammi, A., Di Marcello, V., Guerrieri, C., Luzzi, L., 2011. Transfer Function Modeling of Zero-Power Dynamics of Circulating Fuel Reactors. Journal of Engineering for Gas Turbines and Power 133, 052916-1–052916-8.

EVOL Project 2012 - Evaluation and Viability of Liquid Fuel Fast Reactor Systems. Available at: http://www.li2c.upmc.fr/.

Fiorina, C., Franceschini, F., Krepel, J., Mikityuk, K., 2011. Comparative Analysis of Uranium and Thorium Fuel Cycles in a Lead-Cooled Fast Reactor from the Perspective of Safety and Waste Management. Proc. GLOBAL 2011, December 11-16, Chiba, Japan.

Fiorina, C., Cammi, A., Krepel, J., Mikityuk, K., Ricotti, M. E., 2012a. Preliminary Analysis of the MSFR Fuel Cycle Using Modified-EQL3D Procedure. Proc. ICONE 2012, July 30 – August 3, Anaheim, US.

Fiorina, C., Aufiero, M., Cammi, A., Guerrieri, C., Krepel, J., Luzzi, L., Mikityuk, K., Ricotti, M. E. 2012b. Analysis of the MSFR Core Neutronics Adopting Different Neutron-Transport Models. ICONE 2012 July 30 – August 3, US.

Fiorina, C., Cammi, A., Franceschini, F., Krepel, J., Luzzi, L., Ricotti, M. E., 2012c. Thorium fuel cycle in Fast Reactors: potential benefits and challenges. Proc. NENE 2012, September 5-7, Ljubljana, Slovenia.

Fiorina, C., Cammi, A., Franceschini, F., Krepel, J., Mikityuk, K., Ricotti, M. E., 2013. Analysis of thorium and uranium fuel cycles in an iso-breeder Lead Fast Reactor using extended-EQL3D procedure. Annals of Nuclear Energy 53, 492-506.

Fiorina, C., Franceschini, F., Memmott, M., submitted (a). Safety aspects of Th-use in FRs. Submitted to FR 2013 March 4-7, Paris, France.

Fiorina, C., Cammi, A., Krepel, J., Mikityuk, K., Ricotti, M. E., submitted (b). Analysis of the safety-related parameters for Th- and U-fuelled Lead Fast Reactors. Submitted to ICAPP2013 April 14-18, 2013. Jeju, Korea.

Fiorina, C., Aufiero, A., Cammi, A., Franceschini, F., Krepel, J., Luzzi, L., Mikityuk, K., Ricotti, M. E., submitted (c). Investigation of the MSFR core physics and fuel cycle characteristics. Submitted to Progress in Nuclear Energy.

Gnielinski, V., 1976. New equations for heat and mass transfer in turbulent pipe and channel flow. International Chemical Engineering 16, 359-367.

Guerrieri, C., Aufiero, M., Cammi, A., Fiorina, C., Luzzi, L., 2012. A Preliminary Study of the MSFR Dynamics. ICONE 2012 July 30 – August 3, US.

Koning, A., Forrest, R., Kellett, M., Mills, R., Henriksson, H., Rugama, Y., 2006. The JEFF-3.1 Nuclear Data Library. Nuclear Energy Agency. JEFF Report 21.

Petukhov, B.S., 1970. In Irvine, T.F., and Hartnett, J.B., Eds., Advances in Heat Transfer 6. Academic Press. New York.

Till, C. E., Chang, Y.I., Kittel, J.H., Fauske, H.K., Lineberry, M.J., Stevenson, M.G., Amundson, P.I., Dance, K.D., 1980. Fast breeder reactor studies. Technical Report. Argonne National Laboratory, ANL-80-40.

Wade, D. C., Chang, Y. I., 1987. The Integral Fast Reactor (IFR) Concept: Physics of Operation and Safety. Proc. Int. Topical Meeting on Advances in Reactor Physics Mathematics and Computation, April 17-30, Paris, France.

Wade, D.C., Fujita, E.K., 1989. Trends vs. Reactor Size of Passive Reactivity Shutdown and Control Performance. Nuclear Science and Engineering 103, 182-195.

Wade, D. C., Hill, R. N., 1997. The design rationale of the IFR. Progress in Nuclear Energy 31, 13-42.

Wade, D. C., Wigeland, R.A., Hill, D.J., 1997. The safety of the IFR. Progress in Nuclear Energy 31, 63-82.

Yang, W. S., 2008. Trends in transmutation performance and safety parameters versus TRU conversion ratio of sodium-cooled fast reactors. Proc. IEMPT-10, October 8, 2008, Mito, Japan.

CHAPTER 5: Heat transfer in channels with internally heated fluids and impact of the decay heat on the MSFR out-of-core components

ABSTRACT

The present Chapter investigates the effect of the internal heat generation on the heat transfer phenomena under forced cooling conditions. Reference is made to the simple situation of a straight circular channel, which is representative of most of the MSFR out-of-core components, while the in-core thermal-hydraulics requires the adoption of CFD codes for a proper analysis and will be treated in Chapter 6. A general form of a correlation to predict the Nusselt number is derived and undefined parameters are obtained for the case of molten salts through interpolation of results provided by a dedicated analytic model previously developed at the Politecnico di Milano. The obtained correlation is used to predict the impact of decay heat on the design and operation of the MSFR out-of-core components. The obtained results suggest a generally small effect, with a note of caution for the design of components with low velocities and large diameters, especially in case of laminar flow. Finally, a preliminary design is discussed for an experimental facility that could be used to validate the proposed correlation. Some of the main results have been presented in (Fiorina et al., 2010; Luzzi et al., 2012).

5.1 INTRODUCTION

A main and characterizing feature of Molten Salt Reactors (MSR) is the dual role of the molten salts, acting as both fuel and coolant. This requires investigation in view of the little information available in the open literature regarding the thermal-hydraulics of internally heated fluids. Dedicated models and tools have been developed for specific applications like combustion processes (see e.g. (FLUENT, 2005)), but they are not directly applicable to the case of MSRs. Despite the scarcity of available data and theoretical studies, the presence of an internal heat generation perturbs the temperature field and consequences are to be expected on the thermal-hydraulics of MSRs. Among various aspects requiring investigation, the present Chapter focuses on the heat transfer phenomena occurring in molten salts flowing in forced convection in a channel. Main objective is to shed lights on the impact of decay heat on the heat transfer coefficients, and thus on the wall temperatures, in the MSFR out-of-core components. The in-core temperature field will be investigated in Chapter 6 with suitable CFD tools.

The Chapter is organized as follows. In Section 5.2, a heat transfer correlation is proposed for evaluating the Nusselt number for the turbulent flow of internally heated molten salts in straight circular channels. The proposed correlation is used in Section 5.3 to predict the effect of the internal heat generation on the MSFR out-of-core components. Section 5.4 preliminarily discusses a possible experimental set-up that could be used to validate the results presented in this Chapter. Concluding remarks are finally provided in Section 5.5.

5.2 HEAT TRANSFER CORRELATION

An accurate analytic treatment of the heat transfer for internally heated fluids has been developed in the past at the Politecnico di Milano (see Appendix C). Treatments of this kind, as well as dedicated CFD codes, can be used to investigate the details of heat transfer processes in many engineering applications. Nevertheless, when dealing with complex systems, computational requirements make often impractical the direct application of such techniques. In addition, simpler tools are needed to achieve first general information in preliminary design processes, as in the case of the MSFR out-of-core components. In these contexts, it can be useful to rely on the use of heat transfer correlations. The present Section proposes a theoretical derivation of a correlation form for the Nusselt number in channels featured by internally heated fluids. Undefined parameters are then obtained for the case of molten salts (Prandtl numbers approximately in the range $7.5<Pr<20$) through interpolation of data provided by the tool described in Appendix C.

5.2.1 Brief overview of available correlations for internal forced flow

Nusselt number correlations valid for a wide range of Reynolds and Prandtl numbers have been proposed in the past and can be used also for molten salts. For instance, the Dittus-Boelter (Dittus and Boelter, 1930), Colburn (Colburn, 1933), and Sieder-Tate (Sieder and Tate, 1936) correlations can be used for high-Reynolds turbulent flows. The Hausen (Hausen, 1959) and Gnielinski (Gnielinski, 1976) correlations are valid also for lower Reynolds numbers.

More recent studies have been carried out in order to increase the accuracy of the mentioned correlations for Reynolds and Prandtl numbers of interest in specific fields. As regards molten salts, the Hausen and Gnielinski correlations have been recently tested using a dedicated experimental facility, and a slightly modified version of a Gnielinski correlation has been proposed (Yu-ting et al., 2009). Another interesting work can be found in (Bin et al., 2009), where the Sieder-Tate and the Hausen correlations are assessed, and a modified Sieder-Tate correlation is proposed.

All the correlations mentioned above can be used with a good degree of accuracy in many applications in the field of engineering, but they are not suitable for situations where the working fluid is featured by an intense internal heat generation, as in the case of MSRs. Some preliminary studies on the subject are available in literature (Kinney & Sparrow, 1966; Poppendiek, 1954; Siegel & Sparrow, 1959), but they are in most cases partial treatments and they do not lead to the proposal of correlations to be used for turbulent flows. Recently, a research activity on internally heated molten salts has been undertaken at the Politecnico Di Milano (Cammi et al., 2009; Fiorina, 2009; Di Marcello et al., 2010; Di Marcello, 2010; Luzzi et al., 2010), focusing in particular on graphite-moderated MSR concepts. In the frame of such

research activity, a new correlation has been proposed (Di Marcello et al., 2010; Luzzi et al., 2010), giving a clear indication of the importance of internal heat generation in the heat transfer phenomena occurring in MSRs. As an example, Fig. 5.1 shows the Nusselt number in the core channels of the Molten Salt Breeder Reactor (MSBR) (Robertson et al., 1971) as predicted by the traditional correlations mentioned above, as well as by the correlation proposed by Di Marcello et al. (2010). A non-negligible difference is observed, especially for low Reynolds numbers. A drawback of the proposed correlation is that it has been obtained through simple interpolation of numerical/analytic results, without relying on a theoretical background and resulting in a complex functional form.

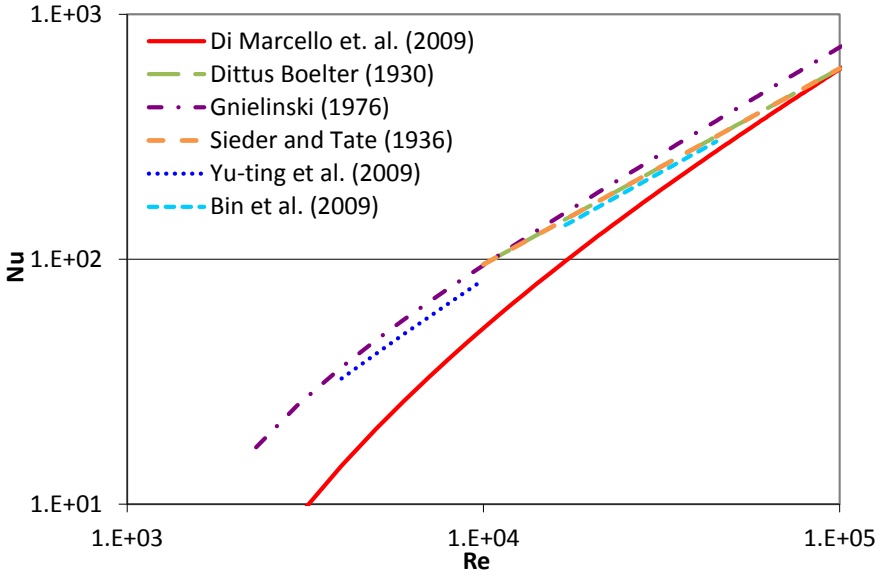

Figure 5.1: Nusselt number in the average core channel of the MSBR as predicted by Di Marcello et al. (2010) and by traditional heat transfer correlations

5.2.2 Derivation of a general correlation form

In this subsection, the problem of heat transfer in channels featured by internally heated fluids is treated theoretically, and a general form of the Nusselt number correlation is derived by means of the Π-theorem (see e.g. (Langhaar, 1962)) and thanks to some physical considerations. In order to obtain such correlation, the field of investigation is restricted to a smooth channel with circular cross-section, hydro-dynamically and thermally developed turbulent flow, uniform internal heat generation Q and constant (inward or outward) wall heat flux j_w (Fig. 5.2).

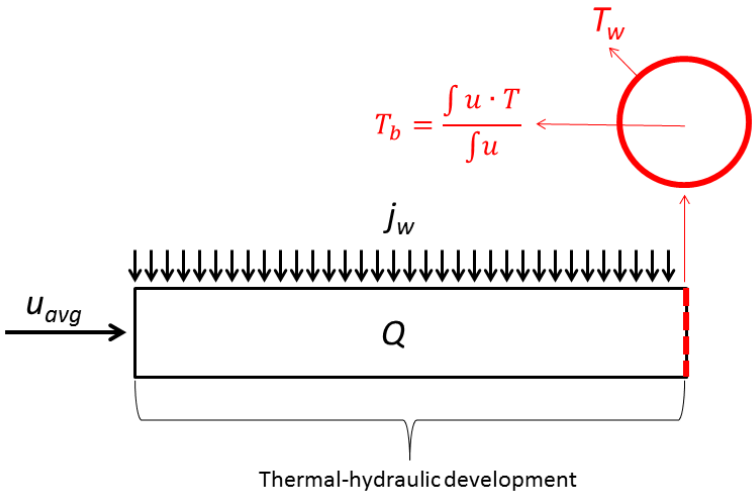

Figure 5.2: Schematic representation of the investigated heat transfer process; a condition of full thermal-hydraulic development is considered

As a first step in the derivation of the heat transfer correlation, it should be recognized that the linearity (with respect to temperature) of the energy equation (Eq. C.1a) allows to treat the physical situation here analyzed as the superimposition of two simpler situations:

situation 1. A fluid flow without internal heat generation, but featured by constant wall heat flux, which is the typical case considered by traditional heat transfer correlations;

situation 2. An internally heated fluid flowing in an adiabatic channel.

Hence, it is possible to compute the temperature difference between wall and bulk temperatures as:

$$(T_w - T_b)_{Q+j_w} = (T_w - T_b)_Q + (T_w - T_b)_{j_w} \tag{5.1}$$

where the subscript $Q+j_w$ refers to the complete situation with both internal heat generation and wall heat flux, while the subscripts Q and j_w indicate that the temperature differences are computed in the simplified situation of internal heat generation alone (situation 2) and wall heat flux alone (situation 1), respectively.

This preliminary consideration immediately allows to draw some conclusions on the heat transfer features of internally heated fluids. In fact, the presence of internal heating in situation 2 will result in a higher temperature at the channel wall, where the fluid is slower. In case of an inward wall heat flux the temperature difference $(T_w\text{-}T_b)_{Q+j_w}$ will be increased compared to the classical one $(T_w\text{-}T_b)_{j_w}$, thus suggesting a worsening of the heat transfer coefficient. In case of an outward heat flux, $(T_w\text{-}T_b)_{Q+j_w}$ will instead be decreased (in absolute terms) and the heat transfer coefficient improved.

Introduction of Eq. 5.1 in the definition of heat transfer coefficient leads to (note that j_w is assumed positive if entering the channel):

$$h_{Q+j_w} = \frac{j_w}{(T_w - T_b)_Q + (T_w - T_b)_{j_w}} = \frac{1}{\frac{(T_w - T_b)_Q}{j_w} + \frac{(T_w - T_b)_{j_w}}{j_w}} = \frac{1}{h_Q^{-1} + h_{j_w}^{-1}} \quad (5.2)$$

Attention must be paid to the term h_Q. Although similar to h_{j_w} in its definition, it does not represent a heat transfer coefficient, since it includes in the same definition the temperatures of the situation 2 (with internal heat generation and with adiabatic walls) and the heat flux of situation 1 (without internal heat generation). It is now possible to rewrite the previous equation in terms of Nusselt numbers as:

$$Nu_{Q+j_w} = \frac{1}{Nu_Q^{-1} + Nu_{j_w}^{-1}} = Nu_{j_w} \frac{1}{1 + \frac{Nu_{j_w}}{Nu_Q}} \quad (5.3)$$

Eq. 5.3 implies that the Nusselt number in case of internally heated fluids and constant wall heat flux Nu_{Q+j_w} can be computed by means of traditional correlations for the value of Nu_{j_w} (subsection 5.2.1) with the introduction of the corrective factor:

$$\zeta = \frac{1}{1 + \frac{Nu_{j_w}}{Nu_Q}} = \frac{1}{1 + \frac{h_{j_w}}{h_Q}} = \frac{1}{1+\sigma} \quad (5.4)$$

What is required to properly characterize the heat transfer of internally heated fluids is then the derivation of the term σ as a function of the parameters characterizing the system. Assuming constant the properties of the fluid, it is possible to write:

$$\sigma = \sigma(c_p, \mu, d, k, D, u_{avg}, Q, j_w) \quad (5.5)$$

Some of the dependencies which appear in Eq. 5.5 can be made explicit, thus reducing the experimental/computational efforts in the derivation of a functional form for σ. By recalling the definition of σ (Eq. 5.4), and introducing the definition of h_Q (Eq. 5.2), it is possible to write:

$$\sigma = \frac{h_{j_w}}{h_Q} = \frac{h_{j_w}(T_w - T_b)_Q}{j_w} \quad (5.6)$$

The terms h_{j_w} and $(T_w - T_b)_Q$ are independent of j_w. Moreover, the term $(T_w - T_b)_Q$ is directly proportional to Q - see for example (Poppendiek, 1954). It follows:

$$\sigma = \frac{Q}{j_w} \sigma'(c_P, \mu, \rho, k, D, u_{avg}) \quad (5.7)$$

The dependency of two variables has been made explicit and use of Π-theorem in the previous equation finally leads to:

$$\sigma = \frac{QD}{j_w} \varphi(Pr, Re) \quad (5.8)$$

Such useful result allows to characterize the heat transfer in a channel with internal heat generation using only two parameters (Prandtl and Reynolds numbers), similarly to the case of a flows without heat generation. Clearly, this is also based on the assumption of constant physical properties (particularly for viscosity). The overall correlation for the Nusselt number in case of simultaneous wall heat flux and internal heat generation should then assume the form:

$$Nu_{Q+j_w} = \zeta Nu_{j_w} = \frac{1}{1+\sigma} Nu_{j_w} = \frac{1}{1+\frac{QD}{j_w}\varphi(Pr,Re)} Nu_{j_w} \tag{5.9}$$

Assuming as positive the function $\varphi(Pr,Re)$ (see next subsection and Eq. 5.12), Eq. 5.9 confirms that the Nusselt number in case of internally heated fluids is increased/decreased in case of outward/inward wall heat flux. The correction is higher when the Q/j_w ratio is higher, and when the channel diameter is increased. In case the wall heat flux is exiting the channel (j_w<0), Nu_{j_w} may become negative for high values of the ratio QD/j_w. Physically this means that the bulk temperature is lower than the wall temperature, although the heat is flowing out of the channel. In fact, as already pointed out, in case of an adiabatic channel, lower temperatures are to be expected at the channel center as a consequence of the higher velocities. If a small (if compared to the internal heat generation) inward wall heat flux is introduced, it will change the gradient close to the wall, but it will not change the overall trend of decreasing temperature with increasing velocity in the central part of the channel, and it will be possible to have a bulk temperature lower than the wall temperature.

5.2.3 Data interpolation and application to molten salts

The results of the previous subsection can be used to derive Nusselt number correlations for internally heated fluids. In particular, if the correlations available in literature for Nu_{j_w} are adopted, what is required is the derivation of the function $\varphi(Pr,Re)$. In case of laminar flow, the function $\varphi(Pr,Re)$ can be analytically demonstrated to be constant (Poppendiek, 1954) and equal to 3/44. In case of turbulent flows, it can have a complex shape but, by restricting the field of application, it is reasonable to assume a simple dependency like:

$$\varphi(Pr,Re) = a_1 Pr^{a_2} Re^{a_3} \tag{5.10}$$

where a_1, a_2 and a_3 are constants to be determined. At this point, it is possible to employ the analytic model described in Appendix C to evaluate the function φ and derive the constants a_1, a_2 and a_3. In particular, Eq. 5.9 can be rearranged as:

$$\varphi(Pr,Re) = \frac{j_w}{QD}\left(\frac{Nu_{j_w}}{Nu_{Q+j_w}} - 1\right) \tag{5.11}$$

and the Nusselt numbers can be computed using Eq. C.3. Computing the function φ for 100 different combinations of Prandtl and Reynolds numbers in the ranges 7.5<Pr<20 and 10^4<Re<10^5, and interpolating Eq. 5.10 in the least square sense, it is possible to obtain the following correlation:

$$\varphi(Pr, Re) = 1.656 \cdot Pr^{-0.4} Re^{-0.5} \tag{5.12}$$

Eq. 5.12 interpolates the results given by the analytic model with an average error equal to 4.9% and a maximum error equal to 10.2%. Such discrepancies can be considered acceptable for preliminary calculations. Extrapolation to Reynolds numbers as low as 2300 gives discrepancies of about 20% compared to the analytic results. Adopting Eq. 5.12, the overall correlation for the Nusselt number in case of both internal heat generation and wall heat flux would be:

$$Nu_{Q+j_w} = \frac{1}{1+\frac{QD}{j_w}\varphi(Pr,Re)} Nu_{j_w} = \frac{1}{1+\frac{QD}{j_w}1.656 \cdot Pr^{-0.4} Re^{-0.5}} Nu_{j_w} \tag{5.13}$$

5.3 IMPACT OF THE INTERNAL HEAT GENERATION ON THE MSFR OUT-OF-CORE COMPONENTS

Effect of heat generation inside the MSFR core requires CFD tools for a proper characterization and will be discussed in the next Chapter. The developed correlation (Eq. 5.13) can instead be used to preliminarily investigate the impact of decay heat on the heat transfer processes in a number of MSFR out-of-core components, including pipes of the primary circuit, tubes of the heat exchanger, and channels of the salt reprocessing system. As observed in subsection 5.2.2, the effect of the internal heat generation superimposes linearly with the effect of heat transfer at the channel wall. Independent of the wall heat flux, the effect of internal heat generation translates into a wall temperature increased by the term $(T_w - T_b)_Q$ (see Eq. 5.1), which can conveniently be used to assess the impact of internal heat generation on a generic component. To this purpose, Eqs. 5.6 and 5.8 can be rearranged to yield:

$$(T_w - T_b)_Q = \frac{QD^2\varphi(Pr,Re)}{kNu_{j_w}(Pr,Re)} = \frac{QD^2\varphi(D,u_{avg})}{kNu_{j_w}(D,u_{avg})} \tag{5.14}$$

where the dependency on Re and Pr has been changed to a dependency on diameter and average velocity by using the MSFR salt properties (Table 1.2).

At this point, it is possible to evaluate the term $(T_w - T_b)_Q$ by using the correlation 5.12 for φ and suitable correlations for Nu_{j_w}. As mentioned in subsection 5.2.3, Eq. 5.12 is mainly valid for $10^4 < Re < 10^5$, but it can be extrapolated to $Re = 2300$ with acceptable discrepancies. For the Nusselt number, the Dittus-Boelter correlation can be used for $Re > 10^4$. For $2300 < Re < 10^4$, the Gnielinski correlation gives instead more accurate results. For $Re < 1000$, the flow can be considered laminar, and Eq. 5.14 becomes:

$$(T_w - T_b)_Q = \frac{QD^2\varphi(Pr,Re)}{kNu_{j_w}(Pr,Re)} = \frac{QD^2 3/44}{k48/11} = \frac{QD^2 3}{k192} \tag{5.15}$$

The internal heat generation Q in the out-of-core components of the MSFR is determined by decay heat, which is on the order of 5% the total power (see Table 6.1), i.e., ~8

MW/m^3. Fig. 5.3 shows the results of the numerical evaluation of Eq. 5.14. It only shows results for $Re<10^3$ and $2300<Re<10^5$. The scale of the colorbar has been limited to 120 K in the laminar region to allow a better visualization of results in the turbulent region. In fact, the term $(T_w-T_b)_Q$ would reach ~300 K at the right corner of the laminar region.

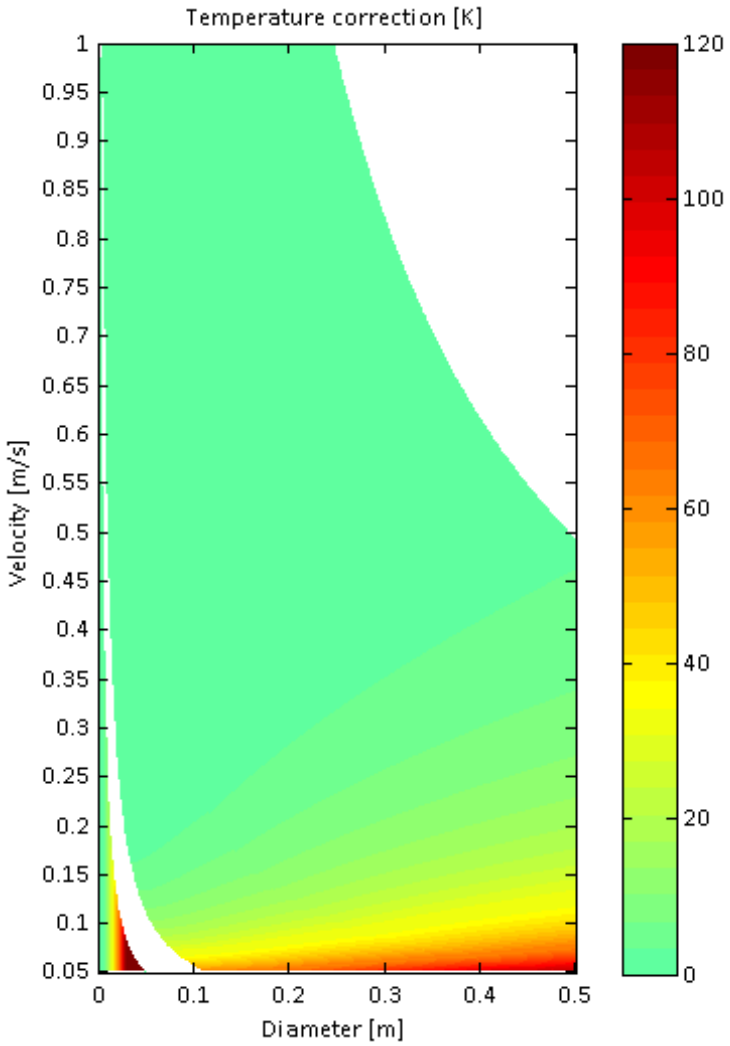

Figure 5.3: Temperature correction $(T_w-T_b)_Q$ due to the internal heat generation

Fig. 5.3 can be used as a design tool for the MSFR out-of-core components, allowing at a glance to individuate proper combinations of velocities and diameters. It clearly shows that the internal heat generation has an extremely limited impact on wall temperatures for high velocities. This excludes any significant effects on the pipes of the primary circuit and on the tubes of the heat exchangers when the core is operated at the nominal flow rate, with velocities on the order of few meters per second (see Tables 1.1 and 1.4). For the heat exchangers, the small tube diameter (<1 cm) excludes important effects also for lower velocities. The impact of internal heat generation can instead be significant for the pipe walls for flow velocities below ~0.3 m/s. This is the case of a loss of flow accident, where the flow rate can decrease from 4.5 m^3/s to ~0.2 m^3/s (i.e., by approximately 20 times). In this case, the temperature of the pipe walls would be noticeably higher than what would be expected from the bulk temperature. The difference would vary drastically based on the pipe diameter, ranging from 3.5 K to 35 K for a pipe with a diameter ranging from 20 cm to 40 cm. This is a

non-negligible effect if one considers that the possibility to adopt a cooling system for the pipes of the MSFR primary circuit is being evaluated in the frame of the EVOL project (EVOL, 2012) to reduce material corrosion. Flow velocities lower than 0.2 m/s are to be avoided. This may be the case of a protected (i.e., envisioning reactor shutdown) loss of flow. In that case, the flow rate in the primary circuit would be sustained by natural circulation, but the heat source would be small (approximately 5% the nominal one) and distributed throughout the primary circuit. In case the flow rate was reduced to ~0.1 m^3/s, the excess wall temperature caused by the internal heat generation would range from ~9 K to ~90 K for a pipe diameter ranging from 20 to 40 cm. Hence, the bulk temperature increase from outlet to inlet of the heat exchanger would be ~200 K, but pipes wall may potentially show a 100 K higher temperature.

The effect of internal heat generation must be considered for designing the channels employed in the salt reprocessing system. Reprocessing rate is in fact extremely limited in the MSFR, of the order of few liters or few tens of liters per day (Table 1.7). This would suggest employing low extraction/injection rates to limit as much as possible the effects of an accidental fissile injection. Fig. 5.3 suggests instead avoiding very low flow rates. In addition, for a given flow rate, a proper design should privilege a small diameter and a high velocity, especially in case of laminar flow. As an example, one can consider a channel used to transfer the fuel salt from the core to the reprocessing system. Adoption of a channel with 5 cm diameter and 5 cm/s of flow velocity would result in a reasonable salt extraction rate of 1 liter every 10 seconds. Considering a channel 2 m long, the internal heat generation would cause an acceptable increment of the bulk temperature of ~50 K, but the wall temperature close to the end of the channel would be approximately 300 K higher than the bulk one.

The above results rely on the hypothesis of fully developed flows, thus overestimating the wall-to-bulk temperature difference that will actually be observed in the MSFR piping. However, they give a clear indication of the importance of using pipes and channels with small diameters and high velocities, which also goes in the direction of minimizing the MSFR actinide inventory.

5.4 POSSIBLE EXPERIMENTAL SETUP

Theoretical treatments as the ones described in the previous Sections can provide reasonable results for preliminary studies, but their validity can be tested only through appropriate experimental campaigns. Some data on the subject were provided by Kinney and Sparrow in the 1966. Unfortunately, only few of them are available nowadays in the open literature (Kinney and Sparrow, 1966). In addition, the facility was used to test water, with Prandtl numbers on the order of 3-4. Prandtl numbers in the approximate range $7.5<Pr<20$ are instead required to test Eq. 5.12 and, in general, to simulate the fluoride molten salts.

With the objective of validating the correlation proposed in the previous Section (Eq. 5.12), the set-up of a proper experimental facility is thus being considered at the Politecnico di Milano. To this purpose, Eq. 5.14 can be employed:

$$\varphi(Pr, Re) = Nu_{j_w} \frac{(T_w - T_b)_Q}{\frac{QD^2}{k}} \tag{5.16}$$

Assuming Nu_{jw} as known from available correlations, what is necessary from an experimental point of view is the evaluation of the term $(T_w-T_b)_Q$. This requires a facility able to reproduce the condition of an internally heated, thermally and hydro-dynamically developed turbulent flow in a straight, circular and adiabatic channel. The experimental set-up must be suitable for measuring wall and bulk temperatures. The possibility to measure a radial temperature profile should also be considered e.g. for the additional purpose of testing CFD codes. Following the assumptions used to derive Eq. 5.12, a uniform (and precisely-known) internal heat generation Q should be guaranteed. In addition, the definition of the dependency of φ upon Prandtl and Reynolds numbers requires the possibility to vary in a known way the fluid properties, as well as the possibility to vary and measure the fluid velocity.

A suitable starting point for the required experimental analyses is the facility adopted by Kinney and Sparrow (1966). This set-up was used to test water (close to ambient temperature and at atmospheric pressure), which could also be considered for the experimental set-up here under investigation. It would avoid high temperatures (and the related problems of structural materials and instrumentation) and use of toxic molten fluoride salts, while the Prandtl number typical of molten salts could be achieved by using thickening agents. However, attention should be paid to the possible non-Newtonian effects related to the use of thickening agents. In addition, it should be taken into account that simulation of molten salts using a different fluid with the same Prandtl number is theoretically possible only for constant fluid properties. A facility using water will then be useful to assess Eq. 5.12, but it will be impossible to investigate additional correction factors allowing e.g. for the variation of viscosity with temperature.

A schematic view of the possible facility is shown in Fig. 5.4. A closed loop can be used, with a heat exchanger required for cooling the working fluid after it has been warmed in the test section. Such test section must be long enough to assure condition of full thermal and hydro-dynamic development. Kinney and Sparrow (1966) adopted a test section length equal to 85 times its diameter, 40 of which for the sole hydraulic development. As a matter of fact, by analyzing their results, it appears that the remaining 45 diameters for the thermal development can be reduced at least to 30 diameters (this reduces by 33% the total power required). Internal heating in the fluid can be obtained through Joule effect by forcing an electrical current to flow into it. This is possible by choosing an electrically insulating material (e.g., polyvinyl dichloride) for the channel wall in the test Section, and by placing electrodes at the sides of it. In this way, the current is forced to flow longitudinally in the fluid. Adopting electricity to heat up the water also solves the problem of the knowledge of the volumetric power Q, which can easily be derived by measuring the electric current in the circuit and the voltage difference at the electrodes. Alternate current might help reducing problems of electrolysis, but further evaluations would be needed to exclude major problems in this sense, especially considering the presence of salting agents in the salts and the high voltages required (see below). A cylindrical shell is posed outside the duct to reduce thermal losses towards the ambient. In this shell, a certain amount of power is dispersed through electrical resistors in order to reach the desired adiabatic boundary condition at the pipe wall. Particular attention is necessary to well insulate the test Section in critical zones such as contact points with the structure that supports the pipe, near which the temperature field might be distorted by

relatively high thermal losses. To overcome such difficulty, the arrangement illustrated in Fig. 5.4 can be adopted, where a single beam is used as supporting structure, with the test Section connected to it through a silica aerogel support.

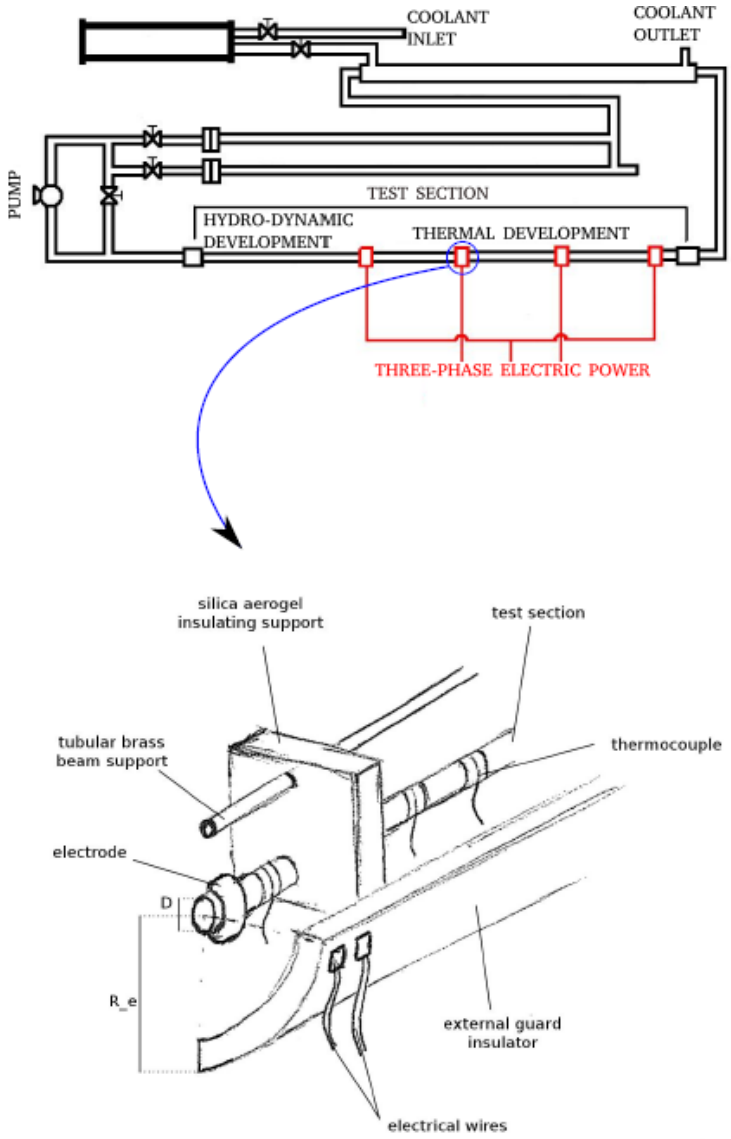

Figure 5.4: Schematic view of the possible experimental facility (section detail hand-drawn by Jacopo De Amicis)

The velocity of the fluid can be varied by using an appropriate pump or valves, and it can be measured by means of standard techniques (e.g., Coriolis flow meter). As regards temperature measurements, for validating Eq. 5.12 it is sufficient to measure wall and bulk temperatures just before the outlet of the heated Section (but sufficiently distant from the last electrode, to avoid disturbances due to the distorted electric field). Wall temperature can be achieved using a thermocouple. In view of the electric field in the fluid, and in order to avoid flow disturbances, the thermocouple can be placed outside the channel, drilled partway in a shallow hole through the pipe wall. In fact, the adiabatic condition allows to consider as approximately constant the temperature throughout the wall. The information about bulk temperatures can be gained using two mixing chambers before and after the test Section, possibly compensating the obtained information considering the heat produced after the wall

temperature measuring point. This suggests preliminary calculations to assess the electric field configuration and the resulting heating non-uniformity close to the electrodes. Voltage measurement should be taken to assess these calculations after the facility has been set up. A moving and electrically insulated thermocouple could also be placed inside the fluid and adopted to measure the entire radial temperature profile, which could be useful to validate CFD codes, as well as a redundant measurement for the bulk temperature (assuming as approximately known the velocity profile). As regards the irregular electric field close to the electrodes, the distorted heat generation is also expected to perturb the temperature profile, but according to Kinney and Sparrow, the effect of a small perturbation should propagate for a distance equal to 2-3 diameters at most. To confirm this, it is being considered the use of thermocouples throughout the length of the heated Section, at least at wall. This would also allow to draw information about the thermal development of the fluid.

A main difficulty about the experiment is related to the small magnitude of the temperature difference between wall and bulk temperatures. Eq. 5.14 and use e.g. of the Dittus-Boelter correlation for Nu_{jw} yield:

$$(T_w - T_b)_Q = \frac{QD^2\varphi(Pr,Re)}{kNu_{j_w}} = \frac{QD^2}{k}\frac{1.656}{0.023}Re^{-1.3}Pr^{-0.8} \tag{5.17}$$

Taking into account that the proportions of the tube are fixed because of the necessary thermal development of the flow, assuming a 30 diameter long heated Section, and assuming the thermal conductivity of the water approximately equal to 0.6 W/(m·K) it is possible to write:

$$(T_w - T_b)_Q = \frac{\mathrm{Q}_{tot}}{7.5\pi Dk}\frac{1.656}{0.023}Re^{-1.3}Pr^{-0.8} \cong 1.2[K \cdot m/(SV^2)]\,\sigma_e \mathrm{V}^2 Re^{-1.3}Pr^{-0.8} \tag{5.18}$$

where Q_{tot} is the total power in the heated Section, V the effective phase voltage and σ_e the electric conductivity.

The temperature difference is then directly proportional to the Q_{tot}/D ratio, and to the product of the fluid electrical conductivity and the voltage. A minimum diameter of the tube equal to 1 inch has been assumed to make the dimensions of the thermocouples reasonably small compared to it. As concerns the electrical conductivity, use of salted water is necessary to have acceptable voltages. Kinney and Sparrow (1966) used a 4 molal solution of NaCl in water. With a voltage of 400 V and a total power of 44 kW they were able to attain a $(T_w\text{-}T_b)_Q$ on the order of 1 K for Prandtl and Reynolds numbers equal to 4 and $8\cdot10^4$, respectively. In the present case, Prandtl and Reynolds numbers as high as 20 and 10^5, respectively, are to be investigated. This calls for a highly conductive fluid to keep as low as possible the necessary voltage. Use of NaCl limits the thermal conductivity to about 25 S/m, which has been considered too small for the purposes of the facility. A preliminary investigation allowed to single out a 4 molal solution of KBr in water as a suitable candidate. KBr is in fact inexpensive and allows to reach a noteworthy 50 S/m electrical conductivity (Isono, 1984). The effect of KBr addition to the Prandtl number of water is negligible and goes in the direction of slightly increasing it.

Assuming D=2.54 cm, σ_e=50 S/m, and using the properties of salted water in (Isono, 1984), Eqs. 5.17 and 5.18 allow to obtain power and voltage as a function of $(T_w\text{-}T_b)_Q$. Assuming the worst condition necessary to validate Eq. 5.12 (i.e., Pr=20, Re=10^5), the data reported in Fig. 5.5 are obtained. It is clear that high voltages are required to achieve temperature differences above 1 K. For instance, if 1.5 K is considered an acceptable temperature difference to be measured, 930 V would be required, with a notable total power equal to 260 kW. Velocities in the test Section would be high (~10 m/s), while the temperature difference between inlet and outlet is not a concern, being on the order of 10 K.

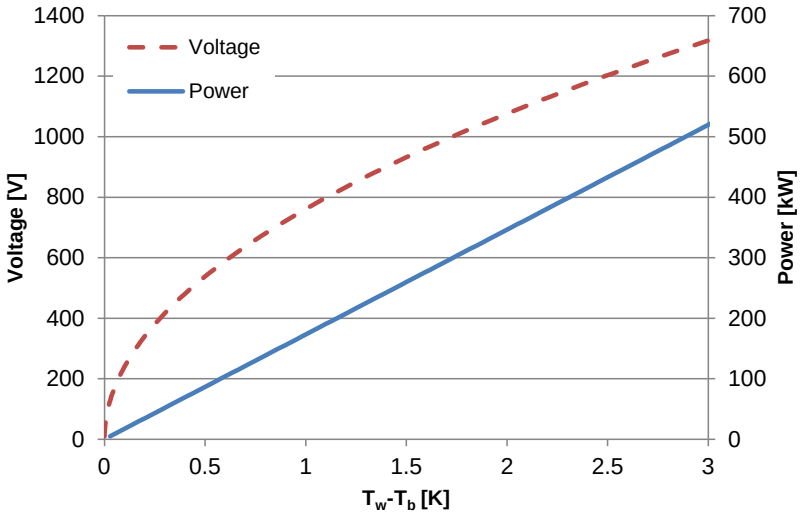

Figure 5.5: Voltage and power as a function of the desired $(T_w\text{-}T_b)_Q$ - Pr=20, Re=10^5

5.5 CONCLUDING REMARKS

The problem of heat transfer for internally heated fluids flowing in forced convection in a straight circular channel has been faced on a theoretical ground. After making the assumption of full thermal-hydraulic development of the flow, some physical considerations and application of the Π-theorem have made possible the achievement of a general form for a heat transfer correlation. It has been shown that the effect of internal heat generation can be described by means of a corrective factor to be applied to traditional correlations (e.g., the Dittus-Boelter or Gnielinski correlations) for the Nusselt number. The corrective factor has been demonstrated to be lower than one in case of inward wall heat flux, thus implying an overestimation of the heat transfer coefficient in case traditional correlations were used. In case of outward wall heat flux, the correction factor is instead generally higher than one. The possibility also exists of a negative heat transfer coefficient in case the wall heat flux is small compared to the internal heat generation. It has been shown that the corrective factor can be fully characterized by making explicit the dependency on just Reynolds and Prandtl numbers. On this basis, a preliminary correlation has been proposed for molten salts by interpolating the results provided by an analytic approach previously developed at the Politecnico di Milano.

The developed correlation has been used to carry out a parametric investigation of the effect of decay heat on the MSFR out-of-core components. The volumetric power determines higher temperatures at the channel wall, but the effect is significant only in case of large

diameters and/or low velocities. This might be the case of the primary loop piping during a loss of flow accident, or of the channels of the salt reprocessing system.

Finally, a possible experimental facility for testing the proposed correlation has been discussed. In spite of some technical difficulty related to the achievement of internal heat generation through Joule effect, the facility appears feasible. The possibility of actually constructing this facility in the next future is being evaluated at the SIET laboratories in Piacenza (Italy).

REFERENCES

Bin, L., Yu-ting, W., Chong-fang, M., Meng, Y., Hang, G., 2009. Turbulent convective heat transfer with molten salt in a circular pipe. International Communications in Heat and Mass Transfer 36, 912-916.

Cammi, A., Di Marcello, V., Fiorina, C., Luzzi, L., 2009. .Assessment of COMSOL capabilities to analyse the thermo-hydrodynamic behavior of the MSR core Proc. COMSOL Conference 2009, October 14-16, Milan, Italy.

Colburn, A.P., 1933. A method of correlating forced convection heat transfer data and a comparison with fluid friction. Transactions of the American Institute of Chemical Engineers 29, 174-210.

Di Marcello, V., Cammi, A., Luzzi, L., 2010. A Generalized Approach to Heat Transfer in Pipe Flow with Internal Heat Generation. Chemical Engineering Science 65, 1301-1310.

Di Marcello, 2010. Development of a multiphysics approach to the modelling and analysis of Molten Salt Reactors. PhD thesis. Politecnico di Milano, Milan, Italy.

Dittus, F.W., Boelter, L.M.K., 1930. Heat Transfer in Automobile Radiators of the Tubular Type. University of California publications in Engineering, 443-461.

EVOL Project 2012 - Evaluation and Viability of Liquid Fuel Fast Reactor Systems. Available at: http://www.li2c.upmc.fr/.

Fiorina, C., 2009. A generalized approach to assess the COMSOL® capabilities for the analysis of the MSR thermo-fluid dynamics. MSc thesis. Politecnico di Milano, Milan, Italy.

Fiorina, C., 2010. Thermal fluid-dynamics of fluoride molten salts in a circular channel. Technical Report, CeSNEF-IN-11-2010, Politecnico di Milano.

FLUENT 6.2 User's Guide, Fluent Inc., 2005.

Gnielinski, V., 1976. New equations for heat and mass transfer in turbulent pipe and channel flow. International Chemical Engineering 16, 359-367.

Hausen, H., 1959. Neue Gleichungen für die wärmeübertragung bei freier oder erzwungener Stromüng (new equations for heat transfer in free or forced flow). Allgemein Wärmetechnik 9, 75-79.

Isono, T., 1984. Density, Viscosity, and Electrolytic Conductivity of Concentrated Aqueous Electrolyte Solutions at Several Temperatures. Alkaline-Earth Chlorides, $LaCl_3$, Na_2SO_4, $NaNO_3$, NaBr, KNO_3, KBr, and $Cd(NO_3)_2$. Journal of Chemical & Engineering Data 29, 45-52.

Kinney, R.B., Sparrow, E.M., 1966. Turbulent pipe flow of an internally heat generating fluids. Journal of Heat Transfer, Transaction of the ASME 88C, 314-322.

Langhaar, H.L., 1962. Dimensional analysis and theory of models. John Wiley and Sons. New York, US.

Luzzi, L.; Cammi, A.; Di Marcello, V., Fiorina, C., 2010. An Approach for the Modelling and the Analysis of the MSR Thermo-Hydrodynamic Behaviour. Chemical Engineering Science 65, 4873-4883.

Luzzi, L., Aufiero, M., Cammi, A., Fiorina, C., 2012. Thermo-Hydrodynamics of Internally Heated Molten Salts for Innovative Nuclear Reactors. In: Jin-hai Zheng Editor, "Hydrodynamics - Theory and Models", chap. 6, InTech Publisher.

Poppendiek, H.F., 1954. Forced-convection heat transfer in pipes with volume-heat sources within the fluids. Chemical Engineering Progress Symposium Series 50, 93-104.

Robertson, R.C., 1971. Conceptual design study of a single-fluid molten-salt breeder reactor. Technical report, ORNL-4541.

Sieder, E.N., Tate, G.E., 1936. Heat transfer and pressure drop of liquids in tubes. Industrial and Engineering Chemistry 28, 1429-1435.

Siegel, R., Sparrow, E.M., 1959. Turbulent flow in a circular tube with arbitrary internal heat source and wall heat transfer. Journal of Heat Transfer, Transaction of the ASME 81, 280-290.

Yu-ting, W.; Bin, L.; Chong-fang, M.; Meng, Y., Hang, G., 2009. Convective heat transfer in the laminar-turbulent transition region with molten salt in a circular tube. Experimental Thermal and Fluid Science 33, 1128-1132.

CHAPTER 6: Steady-state and transient behavior

ABSTRACT

The present Chapter investigates the steady-state and transient behavior of the MSFR. To this purpose a dedicated multi-physics model of the MSFR primary circuit is developed. The model is assessed against a similar model developed at the Technical University of Delft, showing a good agreement. Discrepancies are observed in the predicted temperature field with ensuing mild impact on the transient behavior. Obtained results confirm the promising MSFR features in terms of safety and controllability predicted in Chapter 4, although recirculation zones in the core are observed and need to be eliminated to reduce core temperatures and to limit possibly negative impacts on the MSFR safety features. In addition, a quick core draining in passively-cooled tanks is necessary in case of a loss of heat sink or a loss of flow. Some of the main results have been presented in (Fiorina et al., 2012, submitted (a), submitted (b); Aufiero et al., 2012, submitted; Cammi et al., 2012).

6.1 INTRODUCTION

The most distinguishing feature of the MSFR is the presence of a liquid fuel. As shown in the previous Chapters, this has a notable impact on both the fuel cycle aspects and on the reactor thermal-hydraulics. A liquid and circulating fuel also affects the reactor dynamics due to the motion of the delayed neutron precursors and due to the direct release of fission power into the working fluid. This asks for a detailed investigation of the reactor steady-state and transient behavior to shed light on unique features or anomalous behaviors compared to the traditional solid-fuelled reactors, thus giving a better insight on the significance of the safety parameters analyzed in Chapter 4.

The unique physical environment characterizing the MSFR, and the Molten Salt Reactors (MSR) in general, precludes the use of traditional simulation tools. In particular, the analysis of such systems requires codes able to take into account the movement of delayed neutron precursors, their subsequent out-of-core decay and the presence of a heat-generating fluid. Efforts in this sense have been spent by different authors and for a variety of molten salt systems (Lapenta et al., 2001; Lecarpentier and Carpentier, 2003; Dulla et al., 2004; Yamamoto et al., 2005, 2006; Krepel et al., 2005, 2007; Suzuki and Shimazu, 2006, 2008; Wang et al., 2006; Dulla and Ravetto, 2007; Nicolino et al., 2008; Kophazi et al., 2009; Zhang et al.; 2009a, 2009b, 2009c). An approach to the MSR dynamics has also been proposed at the Politecnico di Milano (see e.g. (Cammi et al., 2011)) for graphite moderated concepts. It consists of a set of

non-linear and time-dependent coupled Partial Differential Equations (PDE), which are simultaneously solved in the same simulation environment (namely, the simulation platform COMSOL Multiphysics) and describe the different "physics" (neutron transport, precursor diffusion and convection, thermo-fluid dynamics) occurring in the nuclear reactor.

In the present Chapter, the mentioned approach developed at the Politecnico di Milano is extended to the analysis of the MSFR primary circuit, and assessed against a similar model developed at the Technical University of Delft (Netherlands). The latter model relies on a more traditional coupling of dedicated neutron transport and thermo-fluid dynamic codes, in which the time-dependent solution is achieved using the output from one code (e.g., the neutron kinetics code) as input to another code (e.g., the thermo-fluid dynamic code) at each time step.

The results provided by the two codes are used to investigate the steady-state and transient behavior of the MSFR. A primary objective is to confirm the promising MSFR safety features predicted in subsection 4.4.2. In particular, reactivity and energy balances have been used in subsection 4.4.2 to predict the new steady-state reached by the reactor at the end of an accidental transient. The present Chapter aims at 1) pointing out specific phenomena that cannot be predicted using lumped approaches, and 2) investigating possible unsafe reactor configuration reached during the first stages of a transient that may lead to a reactor damage before the achievement of a steady-state. In addition, investigation of the loss-of-heat-sink accident is carried out, for which a steady-state cannot be achieved due to the continuous temperature increase caused by decay heat.

Section 6.2 describes in some details the modeling approach for the two models employed. In Section 6.3, their capability to correctly predict the MSFR core physics is assessed through a comparison between them, and against dedicated codes. The two models are then used to investigate the steady-state and transient behavior of the MSFR in Sections 6.4 and 6.5, respectively. Conclusions of the Chapter are provided is Section 6.6.

6.2 MODELLING APPROACH

This Section presents the model developed for the transient analysis of the MSFR (from here on identified as Polimi, since developed at the Politecnico di Milano). Modeling choices are mostly consistent with the model developed at the Technical University of Delft (from here on identified as TUDelft) and here employed for assessment purposes. As mentioned, a main difference between the two models is that the Polimi model is directly implemented as a single PDE problem, while the TUDelft model is based on the coupling of dedicated codes for neutronics and thermo-fluid dynamics. Other differences between the two models will be explained when relevant.

6.2.1 Geometry and main assumptions

As mentioned in Chapter 1, the current MSFR conceptual design features a nearly axial-symmetric core geometry, which can be extended to the entire primary circuit by approximating the 16 external loops with a single annular loop (Fig. 1.2). This approximation is here employed to reduce the problem dimensionality and model the MSFR in a 2-D fashion (Fig. 6.1). Ensuing drawbacks from the standpoint of steady-state and transient simulation are:

1) approximate pressure drops and mixing effects in the out-of-core part of the circuit; 2) the impossibility to predict some local effects in the core, like the flow pattern close to inlet and outlet of each loop; 3) the impossibility to explicitly represent pumps and heat exchangers. The latter shortcoming can be partly overcome by substituting pumps and heat exchangers with suitable momentum and heat sources (or sinks).

The heat exchanger is simulated by a volume force opposite to the fluid flow and causing an overall pressure drop of 300 kPa at nominal conditions (a heat exchanger with 4 mm tubes is here considered, see Table 1.4). To take into account the velocity-dependency of the pressure losses and in view of the turbulent flow in the tubes, the volume force is multiplied by the ratio between actual and nominal flow rates, to the power of 1.75 (Incropera et al., 2006). The pump is simulated by a volume force in the direction of the flow and able to establish the nominal volumetric flow rate of 4.5 m^3/s.

The heat transfer with the intermediate circuit is simulated through a heat sink proportional to the temperature difference between primary and secondary circuits, and to the harmonic mean of the heat transfer coefficients on each side of the heat exchanger. The heat transfer coefficient related to the primary circuit is provided with a dependency on velocity in accordance with the Dittus-Boelter correlation (Dittus and Boelter, 1930). Volume and position occupied by the heat sink are in this case important for a proper transient simulation. The occupied volume is set to 36% of the out-of-core part of the primary circuit (Table 1.4) and positioned in the upper part of the out-of-core circuit (see Fig. 6.1) to enable for a natural circulation in case of a loss of flow.

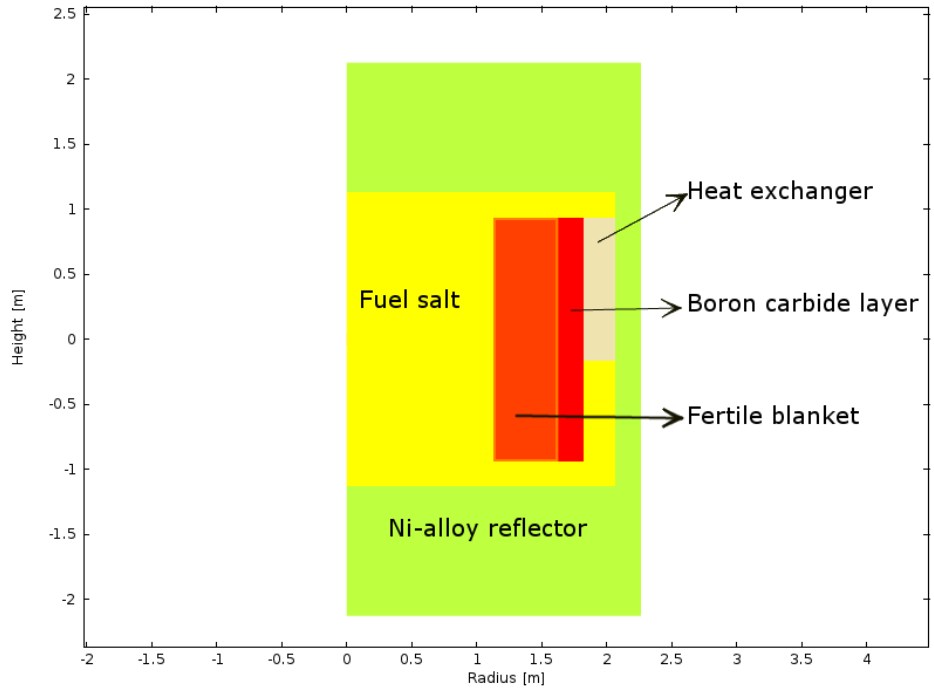

Figure 6.1: Schematic view of the investigated geometry: the primary circuit is approximated as an annular loop to allow for a 2-D representation

6.2.2 Multi-physics modeling

To simulate the MSFR steady-state and transient behavior, a multi-physics approach is adopted envisioning a node-wise coupling of the various quantities. Specifically, the models

employed in this Chapter couples thermo-fluid dynamics and neutronics, including the movement of the delayed neutron precursors. The Polimi model also includes equations for the decay heat.

Thermo-fluid dynamics

Fluid dynamics is modeled through incompressible Reynolds-Averaged Navier-Stokes (RANS) equations for mass conservation and momentum conservation:

$$\frac{\partial d}{\partial t} + d\,\nabla \cdot \boldsymbol{u} = 0 \tag{6.1}$$

$$d\frac{\partial \boldsymbol{u}}{\partial t} + d\,\boldsymbol{u} \cdot \nabla \boldsymbol{u} + \nabla p - \nabla \cdot \left((\mu + \mu_T)(\nabla \boldsymbol{u} + (\nabla \boldsymbol{u})^T)\right) = \boldsymbol{f} \tag{6.2}$$

with natural circulation effects taken into account through the Boussinesq approximation:

$$f_z = \beta_e d^* g(T - T^*) \tag{6.3}$$

The local turbulent viscosity μ_T is obtained by solving the standard k-ε model with logarithmic wall functions (see e.g. (Cebeci et al., 2005) for details).

Temperature distributions are obtained by means of a traditional equation for energy conservation, with the turbulent conductivity that is derived from the turbulent viscosity, assuming a turbulent Prandtl number equal to 0.85:

$$dc_p\frac{\partial \boldsymbol{T}}{\partial t} + dc_p\boldsymbol{u}\cdot\nabla T - \nabla \cdot ((k + k_T)\nabla T) = Q \tag{6.4}$$

$$k_T = \frac{c_p \mu_T}{Pr_T} = \frac{c_p \mu_T}{0.85} \tag{6.5}$$

The term Q is determined by the local fission and decay heat sources (see Eqs. 6.11 and 6.12).

Considering past numerical studies of the author on molten salts (Cammi et al., 2009; Fiorina, 2009), the following thermal wall function is applied in the Polimi model at the boundary between salt and core structures:

$$T^+ = Pr_T\left[\frac{1}{\kappa} ln(9.793y^+) + 9.24\left(\left(\frac{Pr}{Pr_T}\right)^{3/4} - 1\right)\left(1 + 0.28e^{-0.007\frac{Pr}{Pr_T}}\right)\right] \tag{6.6}$$

A condition of thermal insulation is applied at the external boundaries of the geometry and around the blanket, where the temperature field is not solved. In the TUDelft model instead, conditions of thermal insulation are applied to all boundaries between fuel salt and core structures, and the temperature field is solved only in the salt.

Neutronics

Neutron fluxes are predicted according to a multi-group diffusion approach. For each energy group g, the flux ϕ_g is described by the following equation:

$$\frac{1}{v_g}\frac{\partial \phi_g}{\partial t} - \nabla \cdot \left(\bar{D}_g \nabla \phi_g\right) = -\left(\Sigma_{a,g} + \sum_{g'}\left(\Sigma_{g \to g'}\right)\right)\phi_g + \sum_{g'}\left(\Sigma_{g' \to g}\phi_{g'}\right) + \chi_{p,g}\sum_{g'}\left(\upsilon_{p,g'}\Sigma_{f,g'}\phi_{g'}\right) \quad (6.7)$$

Six energy groups[19] are used for the Polimi model and the cross-sections are derived for each material using the SERPENT Monte Carlo code (Leppänen, 2007) and the JEFF-3.1 library (Koning et al., 2006). A simple logarithmic temperature dependence is employed, using the cross-sections at 900 K and 1200 K for the interpolation. Cross-sections are also assumed to be directly proportional to the local density. Nine energy groups are instead used in the TUDelft model, with the cross-sections derived from the deterministic code SCALE (SCALE, 2006) and the ENDF/B-VII.0 library (Chadwick at al., 2006). Cross-sections are computed every 100 K and a square-root interpolation is performed between these points. In this case, density dependency is included in the temperature dependency. Different cross-section sets are used based both on the material and on the position in the core (see (van der Linden, 2012) for further details). For both the Polimi and the TUDelft model, the Th-U3 start-up core (Table 1.3) is considered for the cross-section calculation.

Different from the neutron transport equations, precursor equations cannot be used in their traditional form but require diffusion and convective terms to allow for the fuel motion (see e.g. (Kophazi et al., 2009; Cammi et al., 2011; Cammi et al., 2012; van der Linden, 2012)). The turbulent diffusivity necessary to evaluate the diffusion term can be computed from the turbulent viscosity assuming a turbulent Schmidt number equal to 0.85 (Jiang and Campbell, 2008). For each precursor group *i*, the concentration c_i is described by the following equation:

$$\frac{dc_i}{dt} + \boldsymbol{u} \cdot \nabla c_i - \nabla \cdot \left(\frac{\mu_T}{d0.85}\nabla c_i\right) = \chi_{d,i}\sum_g\left(\upsilon_{d,g}\Sigma_{f,g}\phi_g\right) - \lambda_i c_i \quad (6.8)$$

Eight and six precursor groups are employed for the Polimi and TUDelft models, respectively, with the time constants inherited from the respective nuclear data libraries.

The boundary conditions for the equations describing neutron diffusion, and precursor diffusion and convection are the same for the Polimi and TUDelft codes. In particular, a zero-neutron-flux boundary condition is applied to the external boundaries of the geometry while homogeneous Neumann conditions are applied to the precursor equations at the boundaries of the fuel salt domain.

Decay heat and power sources

The Polimi model includes equations to simulate the behavior of the isotopes responsible for the decay heat, subdivided in "decay heat groups" based on their decay constant. The same equation form as for the case of precursors is employed (Eq. 6.8). In this case however, it has been chosen not to model the concentration of the isotopes responsible for the decay heat, but the decay heat itself. This corresponds to multiplying the equations governing concentrations by the respective decay constants and by the average energy released for each decay. As a result, the following equation has been used to predict the volumetric power D_i generated by the ith decay heat group:

[19] *With upper boundaries equal to 748.5 eV, 5530.8 eV, 24787.5 eV, 0.4979 MeV, 2.2313 MeV, and 19.6403 MeV.*

$$\frac{dD_i}{dt} + \boldsymbol{u} \cdot \nabla D_i - \nabla \cdot \left(\frac{\mu_T}{d0.85} \nabla D_i \right) = Q f_i \lambda_i - \lambda_i D_i \tag{6.9}$$

where f_i is the fraction of the total fission power associated to the ith group. The advantage of modeling directly the decay heat is that the parameters λ_i and f_i appearing in the equations can be achieved directly by interpolating the decay heat curve $D_T(t)$ provided by a core depletion core with the following function:

$$D_T(t) = Q(0) \sum_i f_i e^{-\lambda_i t} \tag{6.10}$$

For the calculations performed in this thesis, the SERPENT code has been used to compute the decay heat curve, taking into account the online removal of the fission products through the extended code version developed by Aufiero et al. (2012, submitted). As mentioned, the Th-U3 start-up core has been considered. However, for a proper evaluation of the decay heat a short depletion time has to be included to allow the achievement of the equilibrium condition for the short-lived fission products mainly responsible for the decay heat in the time scale of an accident.

Following the scoping nature of the calculations presented here, only 3 decay heat groups have been considered. This allows to reproduce well the profile of the decay heat for few minutes after the core shut-down, with discrepancies for the overall energy release of the order of few percents. The interpolation process allowed to obtain the values of λ_i and f_i listed in Table 6.1, showing that decay heat is equal to 4.3% the nominal one during reactor operation. At reactor shutdown, the decay heat reduces to 3.1% with a time constant of approximately 5 seconds while further power reduction requires minutes or tens of minutes. It is worth noting that similar results are generally achieved for other fuel compositions, with a decay heat of the order of 4-5% at shut-down, rapidly decreasing to ~3%, and approaching 1.5-2% after several minutes.

Table 6.1: Parameters adopted to model decay heat. λ_i and f_i are the decay constants and power fractions associated to the decay heat groups

Decay heat group	λ_i [s^{-1}]	f_i [-]
1	0.1973	0.0117
2	0.0168	0.0129
3	$3.58 \cdot 10^{-4}$	0.0186

The volumetric heat source Q in Eqs. 6.4 and 6.9 is determined by the fission source and by the decay heat. If the equations for decay heat are neglected (as in the TUDelft model), the following equation is used:

$$Q = \sum_g \left(\Sigma_{f,g} \phi_g \varepsilon \right) \tag{6.11}$$

while, when including Eqs. 6.9, the heat source is written as:

$$Q = \sum_g \left(\Sigma_{f,g} \phi_g \varepsilon (1 - f_1 - f_3 - f_3) \right) + \sum_i D_i \tag{6.12}$$

6.2.3 Discretization and numerical solution

As regards the Polimi model, the equations presented in the previous subsection are discretized and solved using the commercial software COMSOL Multiphysics. A finite element discretization scheme with Lagrangian linear elements is adopted. The mesh is triangular, with a progressive refinement close to the walls between salt and core structures. In the vicinity of the walls, rectangular elements are used. Fig. 6.2 shows the adopted mesh in the vicinity of the core inlet. The total number of cells is equal to 39896, resulting in 237490 degrees of freedom. This guarantees a satisfactory mesh-independence of the solution, i.e., doubling the number of elements in the mesh changes the solution by few parts per thousands.

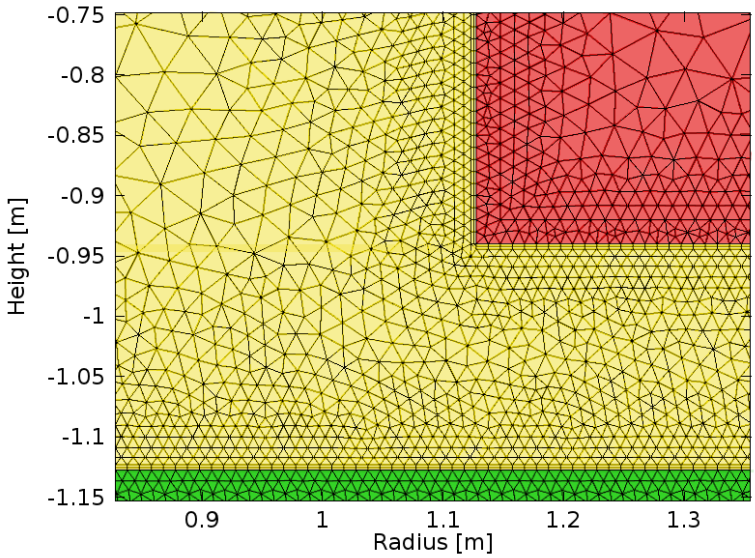

Figure 6.2: Mesh adopted for the Polimi model in the vicinity of the core inlet

The TUDelft model is based on the coupling between two in-house developed codes. Specifically, the DALTON code (see e.g. (Boer et al., 2010) for details) is used for neutron transport and precursor diffusion and convection. This code has also the capability for adjoint eigenvalue calculations. The finite-volume code HEAT (see e.g. (de Zwaan et al., 2007) for details) is used for the CFD analysis. In addition, cross-section interpolation is performed using dedicated SCALE sub-procedures. The overall coupling is achieved through a PERL script. DALTON and HEAT adopt two different rectangular meshes and a Fortran routine performs projections from one mesh to the other. A coarser mesh (Fig. 6.3) is used for DALTON, resulting in 5148 elements. The mesh adopted for HEAT has been achieved using 16 cells for each cell used in DALTON. In this case, full mesh independence was not achieved due to the excessive computational requirements. In particular, the maximum temperature in the core was found to vary by few degrees when doubling the elements in the mesh, which is considered a reasonable compromise between accuracy and computational cost. Further details about the TUDelft model can be found in (de Zwaan et al., 2007; van der Linden, 2012)[20].

[20] *Compared to the model presented in (van der Linden, 2012), few additional features have been included by the author, namely: 1) the mesh for the thermo-fluid dynamic model has been refined; 2) PI controllers have been added for the power and the flow rate; 3) the possibility has been included of varying the neutron velocity in order to make the time constants of neutronics comparable to those of thermo-fluid dynamics and*

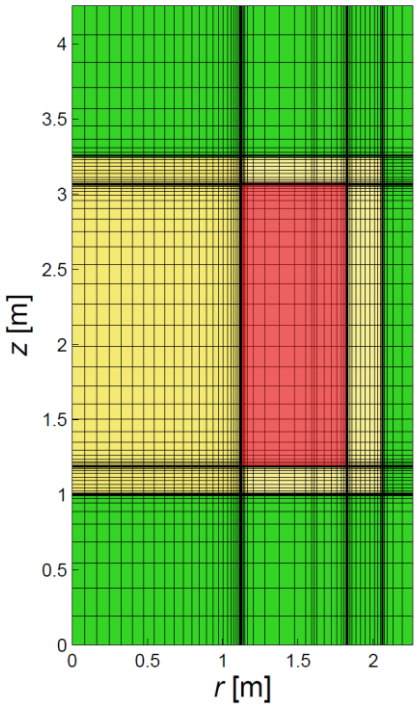

Figure 6.3: Mesh adopted for neutron fluxes and precursor distributions in the TUDelft model

6.3 NEUTRONIC ASSESSMENT

Before discussing the detailed results of the multi-physics modeling, it is worth assessing the capability of both the Polimi and the TUDelft models to correctly predict the MSFR features in terms of core physics. This Section first assesses the results provided by the Polimi model using dedicated core physics codes. Subsequently, the consistency of the results provided by the Polimi and TUDelft models is checked. The TUDelft code used for neutronics has been extensively benchmarked earlier, for example for pebble-bed reactor studies (Boer et al., 2010) and for other molten salt related investigations (Kophazi et al., 2009).

6.3.1 Assessment of the Polimi model against dedicated core physics codes

The Polimi model has been developed based on the computing platform COMSOL Multiphysics. Thermo-fluid dynamics has been simulated using an available COMSOL module, thus not requiring further assessment. On the other hand, the equations governing the MSFR neutronics have been implemented based on a general equation solver and the obtained results require testing against dedicated codes to exclude possible coding mistakes, or inaccuracies related to the approximation employed (e.g., diffusion instead of transport). Clearly, a static fuel must be considered, as traditional core physics codes are not capable of predicting the effect of fuel circulation. In this subsection, the JEFF3.1 nuclear data library is employed for

---

thus facilitate the achievement of a steady-state; 4) the possibility has been included of varying the β_{eff}, which can be used e.g. to compute the λ-eigenvalue of the core with and without delayed neutrons, so to obtain an estimate of the β_{eff}; 5) the possibility has been included to change the number of neutrons emitted per fission, thus affecting the core k_{eff}, which can be used to facilitate the achievement of a steady-state; 6) fuel properties and core design have been updated according to the data reported in Chapter 1.

all codes and results are obtained for the equilibrium composition for the ThU3-feed option (see Tables 1.7 and 2.1). Similar results to those presented in the following have been achieved also for other fuel compositions, and details can be found in (Fiorina et al., 2012, submitted (a)).

Fig. 6.4 compares the neutron spectrum provided by the Polimi model with those obtained using ERANOS and the discrete-ordinate BISTRO module (Appendix A), with 6 and 1968 energy group structure. The 6-group structure selected for the Polimi model is able to reproduce the overall shape of the spectrum, though clearly most details are lost. Comparison with the 6-group results provided by ERANOS shows a good agreement, with a slightly harder spectrum predicted by the Polimi model. As far as the spatial distribution of the flux is concerned, Fig. 6.5 reports the radial and axial traverses, at mid-plane and at the reactor centerline, respectively. Results are shown as obtained using the Polimi model and ERANOS[21], showing a very good agreement.

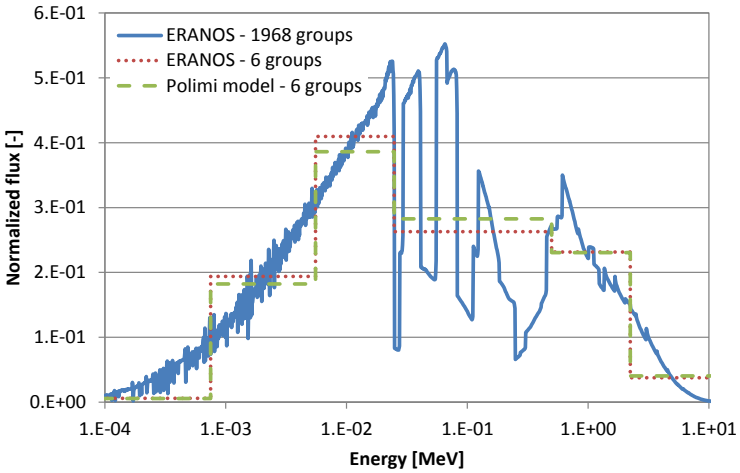

Figure 6.4: Neutron spectrum as predicted by ERANOS and by the Polimi model

a) Radial profile

b) Axial profile

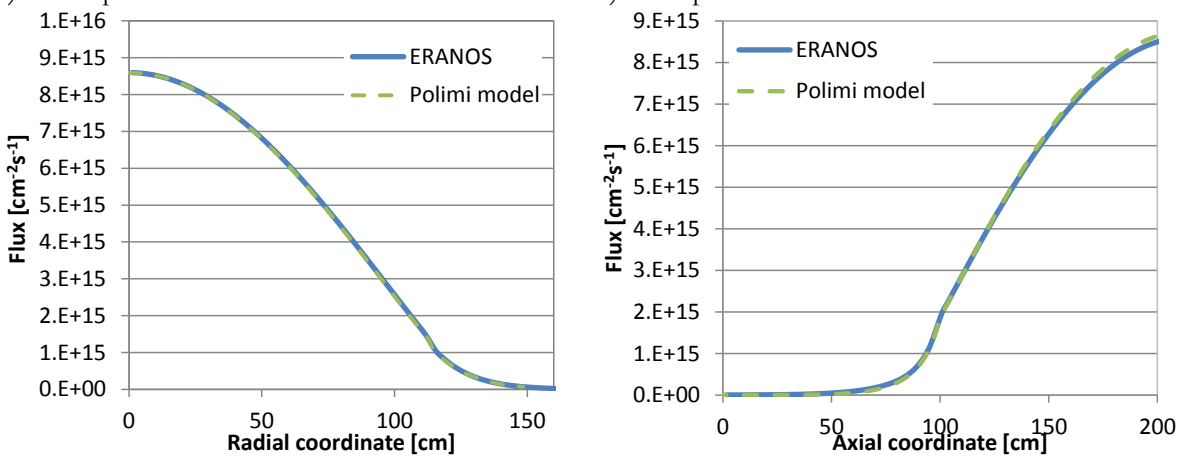

Figure 6.5: Flux profiles as predicted by ERANOS and by the Polimi model: a) radial flux at mid-plane (zero is the reactor centerline); b) axial flux at the reactor centerline (zero is the lower part of the 1 m thick steel reflector)

The equilibrium safety parameters evaluated through ERANOS and the Polimi model are listed in Table 6.2. The SERPENT results are also shown, since SERPENT has been used to

[21] *No significant differences exist between results obtained using different energy discretizations.*

prepare the cross-section set for the Polimi model. The Polimi model does not have adjoint flux calculation capabilities, so that the β_{eff} has been attained through λ-eigenvalue calculations. In particular, a reference reactivity has been obtained through a λ-eigenvalue calculation neglecting all precursor equations. The worth of each precursor group has then been derived by subtracting this reference reactivity to the reactivity resulting from another λ-eigenvalue calculation performed including the respective precursor equation. α-eigenvalue calculations have been used for the neutron generation time (Singh et al., 2009). Accordingly, the estimated value corresponds to a generation time where the weighting flux is the fundamental α-mode, instead of the standard fundamental λ-mode. Nonetheless, for a critical reactor the two modes tend to be superimposed.

Table 6.2: Equilibrium core safety parameters for the equilibrium ThU3-feed option

	Doppler coeff. [pcm/K]	**Expansion coeff. [pcm/K]**	**Generation time* [μs]**	**β_{eff} [pcm]**
Polimi model	-2.99	-3.24	0.96	322.5
ERANOS (33 groups)	-2.91	-3.23	1.01	332.3
SERPENT	-3.04±0.1	-3.49±0.1	1.30±0.001	318.2±1

**Average neutron lifetime for the SERPENT calculations.*

A good agreement on the Doppler coefficient is observed for all codes. Particularly close values are achieved for the Polimi model and SERPENT. In fact, Doppler coefficient is mainly determined by the cross-section set, and cross-sections for the Polimi model have been generated using SERPENT. On the other hand, salt expansion coefficient is only mildly affected by cross-sections (see Section 4.3) and the value predicted by the Polimi model is in this case closer to that provided by ERANOS. Since SERPENT is not capable to provide a direct estimate of the generation time, the reported value is the average neutron lifetime, which explains the observed discrepancies compared the other codes. In the Polimi model, the generation time is instead very close to that predicted by ERANOS. β_{eff} also shows good agreement for the different codes. For a better assessment, Table 6.3 shows the fraction of β_{eff} associated to each precursor group. This subdivision is of paramount importance in the MSFR, since fuel circulation will determine a reduction of the β_{eff} that is strongly dependent on it. Results for the three models confirm the good predictive capabilities of the Polimi model observed in Table 6.2.

Table 6.3: Group-wise subdivision of the β_{eff} for the equilibrium ThU3-feed option

	β_{eff}^1 [pcm]	**β_{eff}^2 [pcm]**	**β_{eff}^3 [pcm]**	**β_{eff}^4 [pcm]**	**β_{eff}^5 [pcm]**	**β_{eff}^6 [pcm]**	**β_{eff}^7 [pcm]**	**β_{eff}^8 [pcm]**
Polimi model	22.2	48.1	40.5	64.5	102.1	17.7	22.3	5.1
ERANOS (33 groups)	22.8	50.1	41.5	66.6	105.2	17.8	22.9	5.2
SERPENT	21.7	47.8	40.2	63.4	100.5	17.4	22.2	4.9

6.3.2 Comparison between Polimi and TUDelft models

This subsection describes preliminary assessment studies dedicated at a comparison between the results provided by Polimi and TUDelft models for the sole neutronics. In fact, the capability of the two models to reproduce reactivity feedbacks, generation time and effective delayed neutron fraction (β_{eff}) is essential for providing consistent results in terms of steady-state and, particularly, transient reactor behavior.

The capability of the Polimi and TUDelft models to predict the β_{eff} has been tested adopting static and iso-thermal (973 K) salt conditions, so to avoid influences on results related to different velocity and temperature fields. The β_{eff} has been estimated for both models as a difference between reactivities computed through two λ-eigenvalue computations with and without precursor sources. As a result, 299.8 pcm and 289.4 pcm are predicted by the Polimi and TUDelft models, respectively, showing an acceptable 3% discrepancy. An α-eigenvalue computation has been used to approximate the neutron generation time. The Polimi model predicts a generation time equal to 1.03 μs, to be compared to the 0.91 μs of the TUDelft model. In this case, the discrepancy between the two models is of the order of 10-15%, which has been ascribed to the different nuclear data libraries employed to compute the cross-sections, with ensuing differences on the k_{eff}.

Fig. 6.6 plots that the overall (Doppler + fuel expansion) reactivity feedback coefficient for the two models, showing an excellent agreement for the temperature range of interest for the MSFR, namely between salt freezing (838 K) and melting of the nickel alloy for the core structures (approximately 1600 K). The jigsaw behavior of the coefficient predicted by TUDelft is to be ascribed to cross-section preparation with SCALE. As usual in core physics codes, SCALE adopts cross-section libraries prepared (e.g., using NJOY) at selected temperatures (typically, 600 K, 900 K, 1200 K, …) and performs interpolation to predict cross-sections in-between. It is then expected to give "exact" solutions only at the temperatures where cross-sections are directly available. As a confirmation, it can be observed that Polimi and TUDelft models predict nearly the same coefficient at 600 K, 900 K and 1200 K. The smooth trend of the coefficient predicted by the Polimi model is related to the fact that only two cross-section sets (at 900 K and 1200 K) have been used for the interpolation. A non-negligible discrepancy can be observed between the two models above 1500 K. At these temperatures, the feedback coefficient is dominated by density effects (see subsection 4.3.1 and Fig. 4.9), and the cross-sections of the TUDelft model were computed using a slightly lower fuel expansion coefficient ($1.78 \cdot 10^{-4}$ K^{-1} instead of 2.15 10^{-4} K^{-1}, consistently with previously available data). However, impact on the results presented in this Chapter is negligible since temperatures above 1500 K are generally not reached.

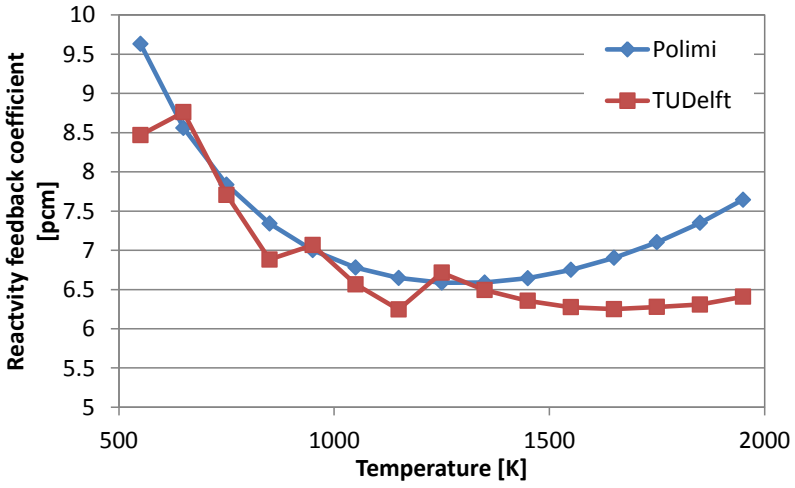

Figure 6.6: Temperature dependency of the fuel reactivity feedback coefficient

6.4 STEADY-STATE BEHAVIOR

6.4.1 Thermal-hydraulics

Fig. 6.7 shows the temperature and velocity fields in the core of the MSFR as predicted by the Polimi and TUDelft models. For a better comparison, decay heat from actinides and fission products has been turned off in the Polimi model, even though its impact is small. The velocity field is predicted consistently by the two models. In particular, a wide recirculation zone exists close to the blankets, while the fuel is nearly stagnating at the core center, close to the axial reflectors. Recirculation is due to inertial and viscous effects, while removal of the gravity force does not impact significantly the results.

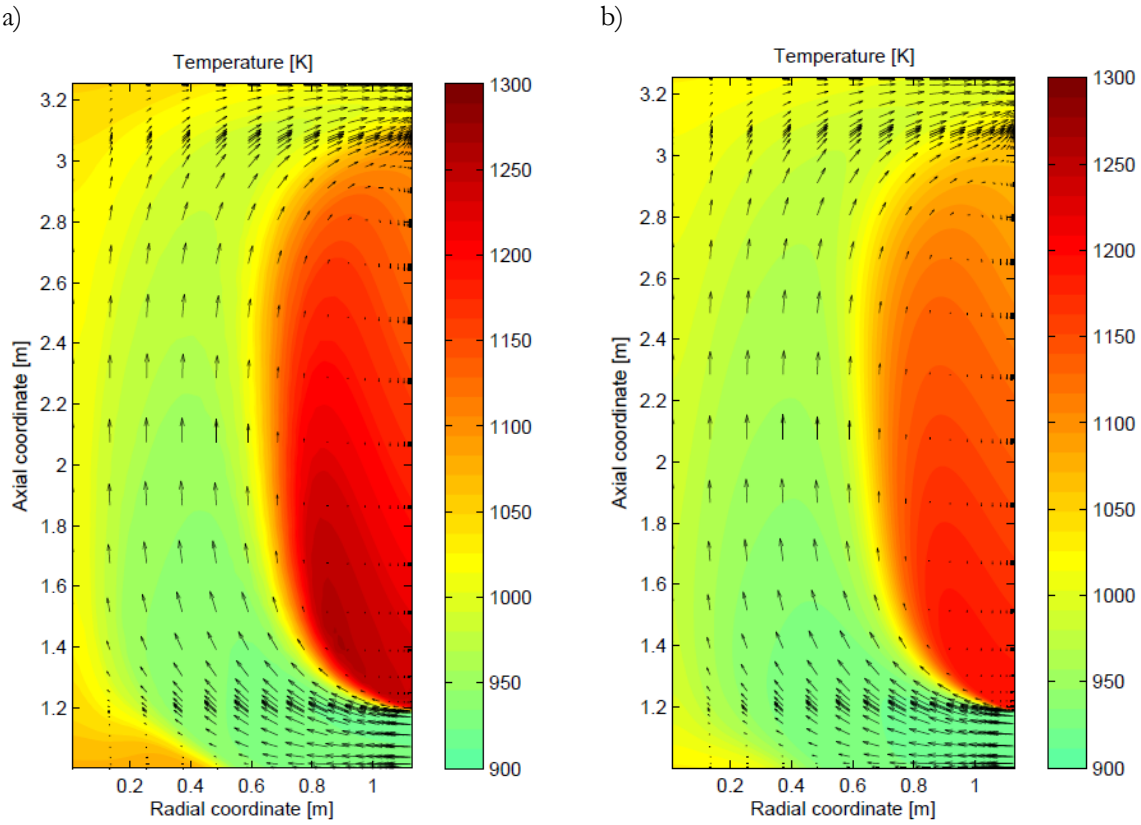

Figure 6.7: Velocity and temperature fields in the core as predicted by a) Polimi and b) TUDelft models

In the recirculation zone close to the blankets, the predicted temperature is approximately 200 K higher than at the outlet. Although acceptable in terms of melting temperature of the core structures (~1500-1600 K), this generates unnecessary thermal stress and material problems that could be avoided through an improved thermal-hydraulic design. R&D efforts in this direction are already being spent in the framework of the EVOL project (EVOL, 2012) and include investigations of: 1) suitable diffusors at the core inlet; 2) use of a distribution plate at the bottom of the core; and 3) hourglass shaping of the active core region.

The Polimi model generally predicts higher local temperatures in the recirculation zones, which is related to a lower predicted turbulent viscosity (and turbulent conductivity), as shown in Fig. 6.8. Turbulent viscosity depends on turbulent kinetic energy and dissipation, which in turn are predicted by the k-ε turbulence model. Differences can partly be ascribed to different

meshes. In particular, a full mesh independence of the solution was not obtained in the TUDelft model due to the excessive computational requirements. In addition, some coding details differ between the two models, like for instance the numerical method for the solution and the implementation of wall functions. In the attempt to exclude major coding mistakes, the fuel salt flow rate has been reduced (by approximately 20 times) till the suppression of the recirculation zones. As a result, discrepancies between the two codes have mostly disappeared.

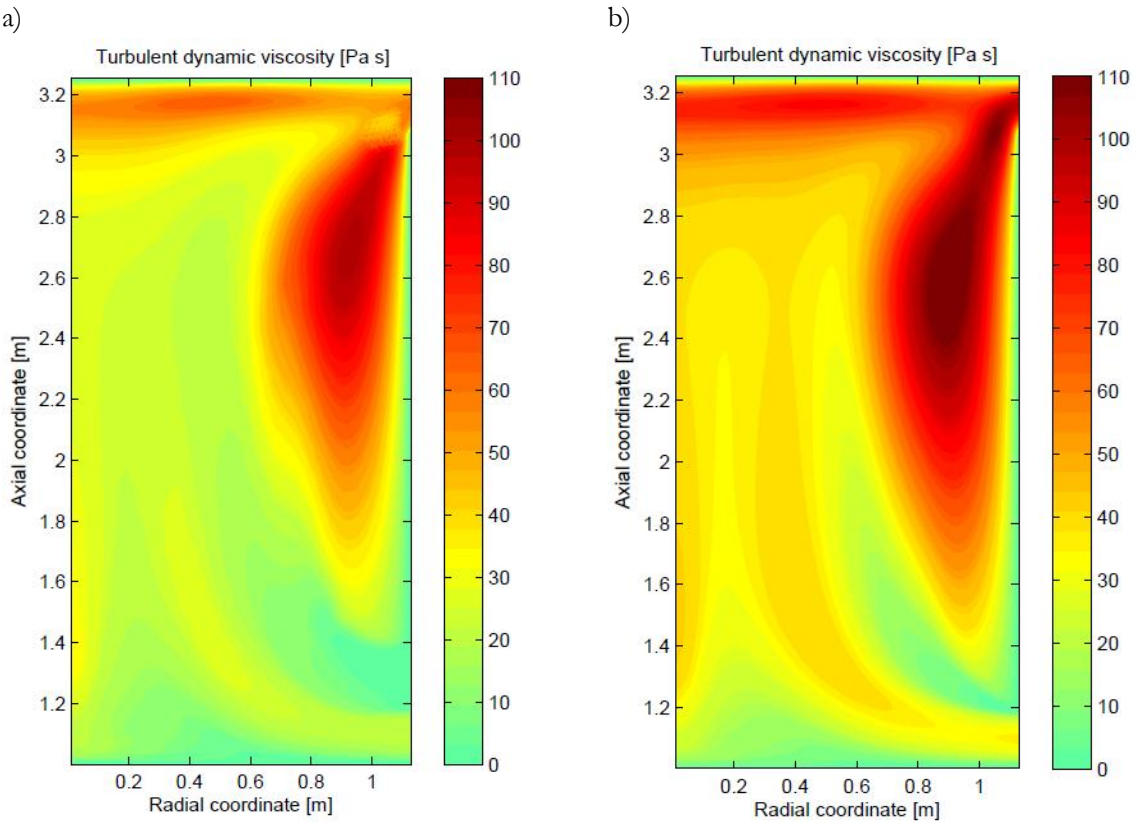

Figure 6.8: Turbulent dynamic viscosity in the core as predicted by a) Polimi and b) TUDelft models

In order to have an indication on the uncertainties related to the thermo-fluid dynamic calculation, a different turbulence modeling has also been employed. Specifically, an additional calculation has been performed with the Polimi model substituting the k-ε with the k-ω (Wilcox, 1998) turbulence model. Wider recirculation zones have been observed, including a stagnation zone at the radial axis, close to the upper reflector. Predicted temperatures in the recirculation zone close to the blanket are tens of degrees higher than those predicted by the k-ε model and they reach 1500 K in the mentioned stagnation point. This confirms for the MSFR case the well-known difficulties of the two-equation RANS turbulence models to predict recirculation and stagnation phenomena.

6.4.2 Neutronics

Neutron fluxes are not affected by fuel-salt motion and maintain the typical symmetric shape generally observed in nuclear reactors. Distribution of precursors and, consequently, of the delayed neutron source is instead of interest as it is a unique feature of the MSFR. In addition, it is strongly coupled to the fluid dynamics of the core and differences are expected between the two models following the differences in the predicted turbulent viscosity. Fig. 6.9

plots the delayed neutron source as predicted by the Polimi and TUDelft models. It appears clearly how delayed neutrons are emitted throughout the primary circuit, with a detrimental effect on β_{eff}. In particular, only ~65% of delayed neutrons are emitted inside the core, while the others are emitted in the out-of-core path of the salt and do not contribute to β_{eff}. The effectiveness of delayed neutrons is further reduced by the axial drift of the salt, which brings precursors outside of the high-flux region at the core center. The problem of precursor decay in low-flux regions is amplified in the MSFR by the existence of recirculation zones at the core boundaries. As a result, the β_{eff} at the MSFR operating conditions results equal to only 134.3 pcm and 123.8 pcm for the Polimi and TUDelft models, respectively. The ~10 pcm discrepancy in the β_{eff} is consistent with the difference in the β_{eff} for static fuel (299.8 pcm and 289.4 pcm).

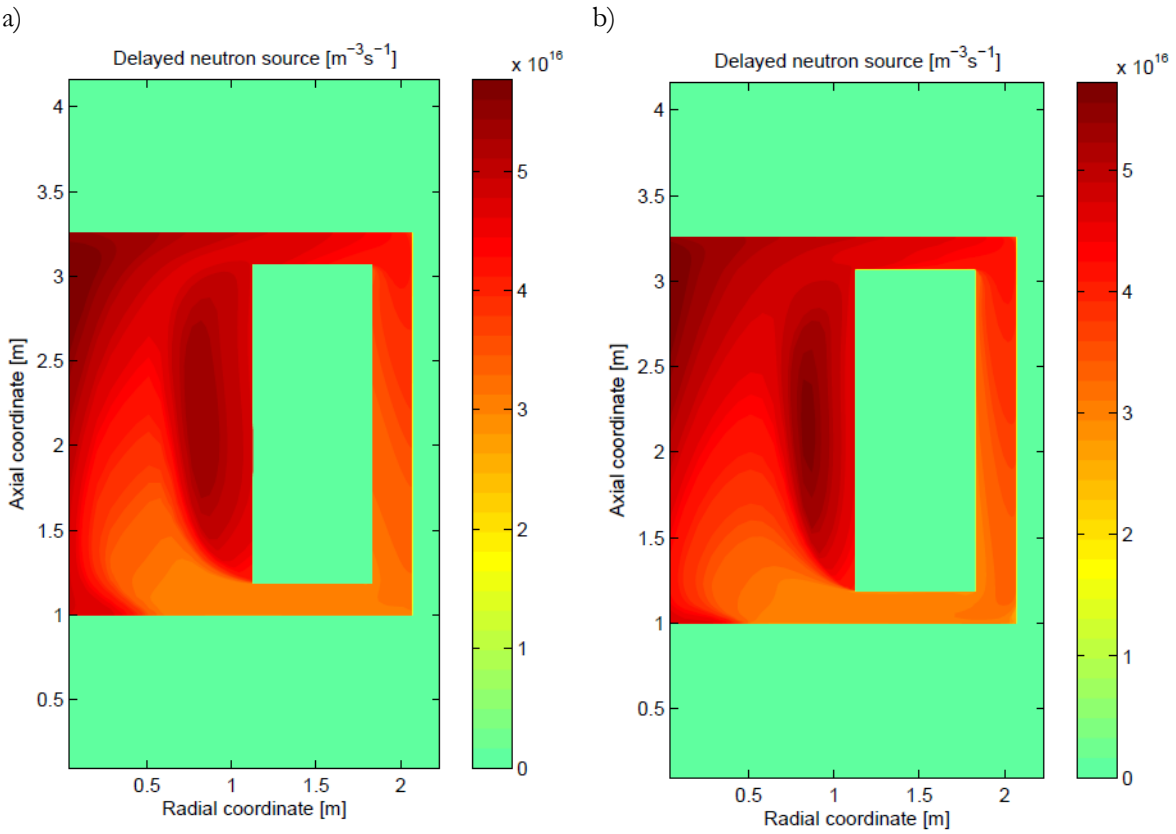

Figure 6.9: Delayed neutron source in the primary circuit predicted by a) Polimi and b) TUDelft models

Agreement between the two codes in terms of precursor distribution is good. In particular, the fraction of delayed neutrons that decay in the out-of-core part of the primary circuit amounts to 34.80% and 34.85% in the Polimi and TUDelft models, respectively. Consistently with the lower turbulent diffusivity singled out in the previous subsection, the high-delayed-neutron-source regions close to the axial reflectors are wider in the Polimi model. On the other hand, the predicted delayed neutron source in the large recirculation area close to the blanket is stronger in the TUDelft model, which can be ascribed to the different delayed neutron groups adopted for the two models. The higher delayed neutron source in a peripheral core region causes a slightly larger reduction of β_{eff} due to fuel motion in the

TUDelft model. In fact the reduction of β_{eff} is equal to 55% and 57% in the Polimi and TUDelft model, respectively.

6.5 TRANSIENT BEHAVIOR

In subsection 4.4.2, a simple approach has allowed to predict the new steady-state reached by the MSFR after possible accidental transient initiators. The 5 typical transients generally considered for the safety analysis of traditional Fast Reactors (FR) have been considered, namely: Unprotected [22] Transient OverPower (UTOP), chilled inlet, pump overspeed, Unprotected Loss Of Flow (ULOF), and Unprotected Loss Of Heat Sink (ULOHS). No other severe accidental transients have been individuated and it has been proved that the reactor will reach an acceptable asymptotic state in all cases but the ULOF and the ULOHS. In the last two cases, draining of the salt in passively-cooled tanks is foreseen and, as concerns the ULOF, the possibility exists to modify the out-of-core design of the MSFR to allow for a sufficient natural circulation and thus guarantee improved inherent safety features.

A primary objective of this Section is to single out, or exclude, the possibility of a core damage before the achievement of the steady-state, which would compromise the inherent safety features predicted in subsection 4.4.2. In addition, the developed multi-physics model allows for a detailed characterization of the various phenomena at play, thus giving indications about the degree of approximations introduced by the assumptions made in subsection 4.4.2. For instance, the average core temperature was assumed as equal to the average of inlet and outlet temperatures, but the previous Section has pointed out the existence of recirculation zones in the core that cause a much higher average core temperature. In addition, in subsection 4.4.2 the average core temperature was used to evaluate reactivity feedbacks, but salt recirculation zones cause strong temperature variations along the radial dimension and suggest possible inaccuracies related to this assumption (weighted averages should in fact be used, with direct and adjoint fluxes as weights). It is worth noting that these effects mainly derive from the existence of in-core salt recirculation zones, which should be eliminated in a future core design. However, they are worth being quantified as it will be difficult to exclude completely the possible onset of secondary flows in the core for each combination of core powers and flow rates.

As a general comment, presented results are not intended as a comprehensive safety analysis. This would require a detailed core design, probably without recirculation zones, and details about the system design that are currently unavailable. For instance, the reactor behavior during a loss of flow is strongly dependent on the pressure drop in the circuit. The pressure drop strongly depends on the heat exchanger design, which is still speculative at the current stage of development. Localized pressure drops at the heat exchanger inlet and outlet, and in the pump, should also be taken into account. In addition, the velocity dependence of pressure drop and heat transfer coefficient should be carefully evaluated, while here simple dependencies have been used assuming turbulent and fully developed hydrodynamic conditions.

[22] *"Unprotected" refers to a transient where control rods fail to shut the reactor down.*

The following subsections discuss the MSFR response to the aforementioned transient initiators. In view of the axial-symmetry of the developed models, only symmetric transients will be investigated, while it is not possible to deal e.g. with abnormal events occurring to one or few of the 16 primary loops. In addition, the equations simulating the decay heat in the Polimi model will not be used to allow for a better comparison with the TUDelft model. The effect of decay heat will be included in the analysis when significant.

6.5.1 UTOP

A definite design is not available for the MSFR control or reprocessing system, so it is not yet possible to define worst-case scenarios for transient overpowers caused by control rod ejection or fissile injection[23]. In subsection 4.4.2, it has been assumed that an accidental reactivity insertion can be limited to 100 pcm by design. Following the main objective of evaluating the MSFR transient response, it is worth considering two different and characterizing cases, namely: a relatively small 50 pcm reactivity insertion and a super-prompt-critical 200 pcm insertion. A step-wise variation is selected as it is particularly demanding from a numerical viewpoint, thus representing a good test for the models. In addition, it gives rise to the maximum power excursion for a given reactivity insertion. Fig. 6.10 shows the evolution of power and average core temperature for the two reactivity insertions.

The initial power increase triggered by the reactivity insertion is counteracted by Doppler effect and salt expansion. The power decreases and, for a few seconds, it tends to stabilize. After 2-3 seconds, the salt heated up during the initial power peak re-enters the core, causing a sudden power decrease. Power and core temperatures then stabilize at a new level without additional oscillations. The energy released during the initial power peak is limited and deposits directly into the coolant, so that no core damage is expected even in the unrealistic scenario of a step-wise reactivity insertion. This allows to employ the asymptotic reactor state as predicted in subsection 4.4.2 to evaluate the consequences of an UTOP, thus confirming the notable MSFR capabilities to withstand such kind of accidents. In this sense it is worth noting that the average asymptotic temperature variation predicted in Fig. 6.10 is 10% higher compared to that predicted using feedback coefficients (Fig. 6.6) as in subsection 4.4.2. A 10% difference can be considered as acceptable for preliminary investigations.

The limited impact of a reactivity insertion combines with the lack of a burnup reactivity swing (and of the control rods necessary to counterbalance it) and with the atmospheric operating pressure to make a control rod extraction a lower concern in the MSFR. This is not the case e.g. for traditional liquid-metal FRs, where reactivity swing can be notable (especially in burner concepts) and consequences of an UTOP pose strict constraints on the control rod worth and, consequently, on the minimum number of necessary control rods (see Section 4.2 and subsection 4.4.1). In addition, it is worth noticing that reactivity insertion from the

[23] *It is worth noting that a fissile injection from the reprocessing system would cause a significantly different response compared that predicted through a single initial reactivity insertion (which is instead representative of a rod extraction). In fact, the fissile injected in the core would continue recirculating in the primary circuit, causing an oscillatory power response (see e.g. (Aufiero et al., 2012)). However, the amplitude of the oscillations rapidly decreases and the first power excursion can be assumed as the most dangerous for the core integrity. In addition, one should consider that the reactivity insertion in the long term will be considerably lower compared to the initial one due to progressive dilution of the injected fissile material. Hence, the asymptotic state will show lower temperature variations compared to those predicted in the present subsection.*

reprocessing system is a much lower concern in the MSFR compared to other MSRs. In fact, thanks to the fast spectrum, the reprocessing requirements are generally on the order of few liters or few tens of liters per day, which allows to strongly limit the maximum fuel insertion rate by design.

a)

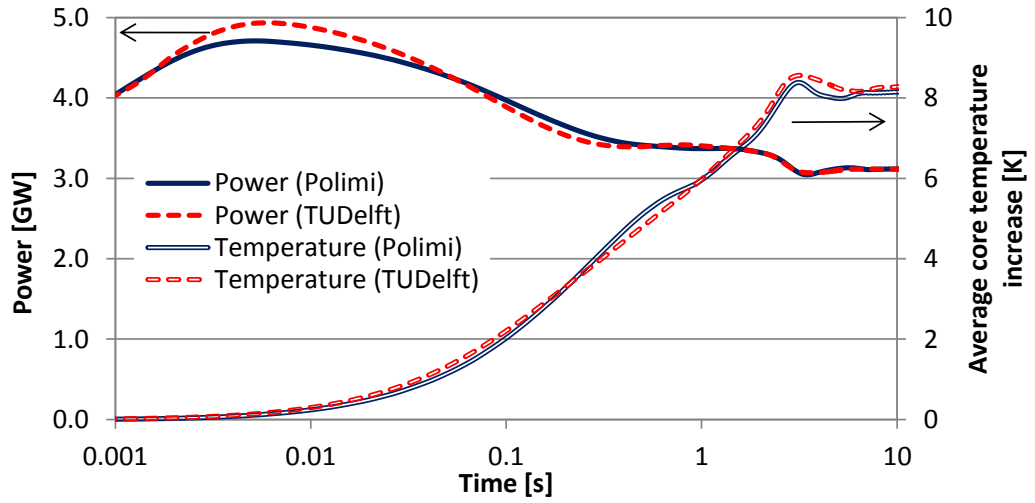

b)

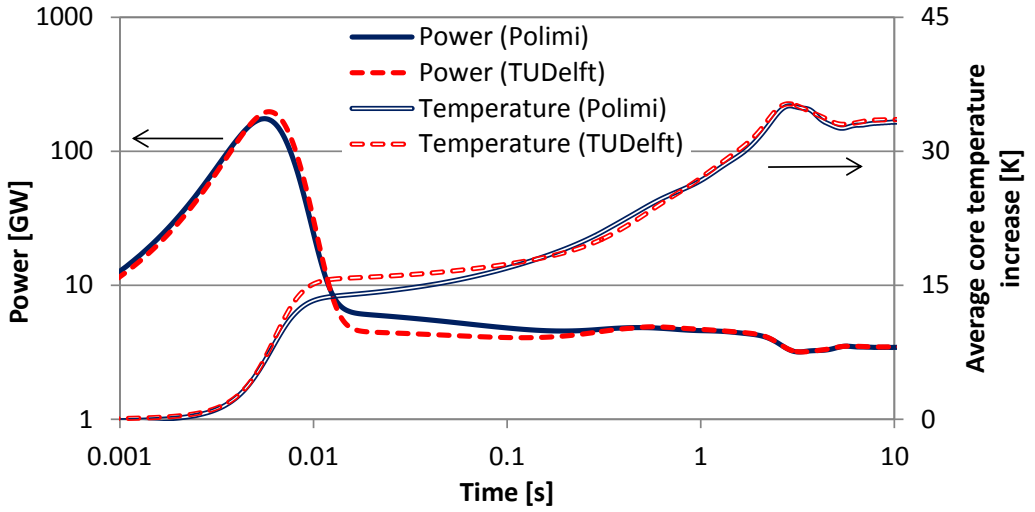

Figure 6.10: Evolution of power and average temperature in the core after a step-wise reactivity insertion equal to a) 50 pcm, and b) 200 pcm (super-prompt-critical)

Agreement between the Polimi and TUDelft models is excellent. The only visible discrepancy is in the higher power peak in the latter model, which is related to the lower feedback coefficient (Fig. 6.6) and β_{eff} (subsection 6.4.2). The higher power peak momentarily determines a higher temperature increase that, in turn, causes a steeper (and stronger) temperature decrease afterwards. However, these differences concentrate on a time-scale of 0.1 seconds, with negligible consequences on the overall energy released and thus on the temperature increase.

6.5.2 Chilled inlet

As mentioned in subsection 4.4.2, the worst-case scenario for a chilled inlet transient is caused by a coolant temperature in the intermediate circuit that reduces to a level close to salt freezing (~727 K), i.e., approximately 100 K lower than the nominal conditions. This would increase the power transferred to the intermediate circuit, and that produced in the core, from 3 GW to ~5 GW. Since the core average temperature would be unchanged to preserve the reactivity balance, the core outlet/inlet temperatures would approximately increase/decrease by half of the total increase of the inlet-outlet core temperature difference (~30 K). Fig. 6.11 plots the system response computed considering that the temperature at the secondary side of the heat exchangers varies with a time constant of 1 second. Fig. 6.12 shows the asymptotic temperature variation in the core.

The initial power peak due to the quick reduction of the inlet temperature has limited amplitude and negligible effects on temperatures, thus showing that the asymptotic reactor state is sufficient for predicting the consequences of a chilled inlet accident. On the other hand, the existence of recirculation zones determines a different asymptotic state compared to that predicted in subsection 4.4.2. In fact, following the power increment, recirculation zones tend to heat up and cause the core average temperature to increase. To preserve the reactivity balance, the effective core temperature must be unchanged, which requires a lower temperature at the core center. This asks for a reduction of the average of inlet and outlet temperatures, equal to -25 K and -21 K for Polimi and TUDelft models, respectively. The stronger variation in the Polimi model is related to the wider and hotter recirculation zones. A lower average of inlet and outlet temperatures implies a reduced transferred power at the heat exchanger. An asymptotic core power equal to 4.45 MW and 4.60 MW is predicted by the Polimi and TUDelft models, respectively. This is to be compared to the 5 GW predicted by assuming that average and effective core temperatures are both equal to the average between inlet and outlet core temperatures. As a consequence of the lower asymptotic power and of the lower average of inlet and outlet temperatures, the core outlet temperature increases by only 6 K in the TUDelft model while it remains unchanged in the Polimi model. On the other hand, when recirculation zones exist, they become the hottest regions in the core and their temperature increase can be on the order of 100 K. In addition, inlet temperatures decrease by approximately 40 K instead of the 30 K predicted above, which exacerbates the problems related to the possibility of salt freezing in the tube walls of the heat exchanger (see subsection 4.4.2). Salt freezing would cause the chilled inlet accident to degenerate in a loss of flow.

Summarizing, a chilled inlet accident has a generally small impact on the core temperatures, provided that salt freezing is avoided in the tubes of the heat exchangers. The reactor steady-state after the transient is the most challenging state and can be used to characterize the consequences of this class of accidents. Simple balances like the ones used in subsection 4.4.2 are capable of predicting the final reactor state with reasonable accuracy, but it should be kept in mind that possible core recirculation regions will experience a notable temperature increment, and will cause a higher decrement of the inlet temperature.

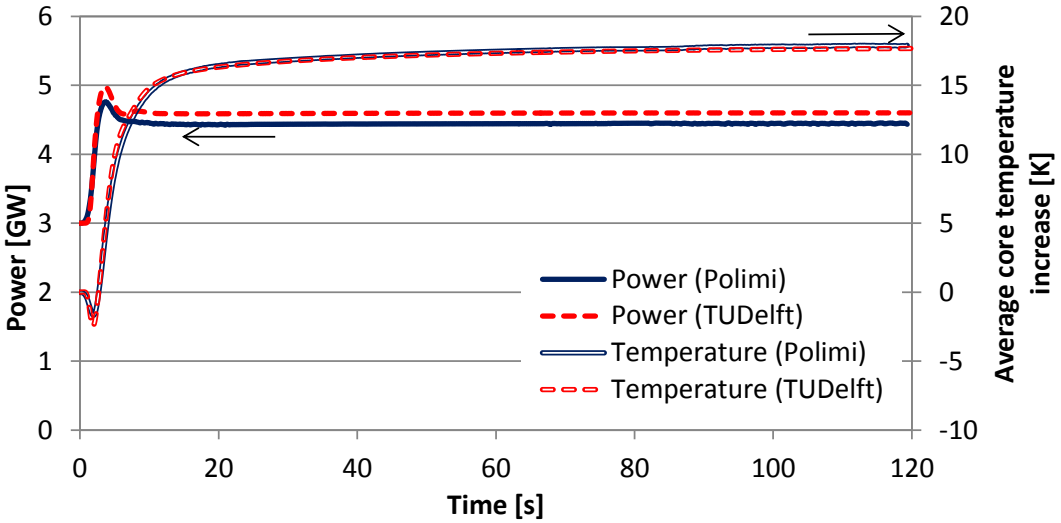

Figure 6.11: Evolution of power and average temperature in the core during a chilled inlet accident

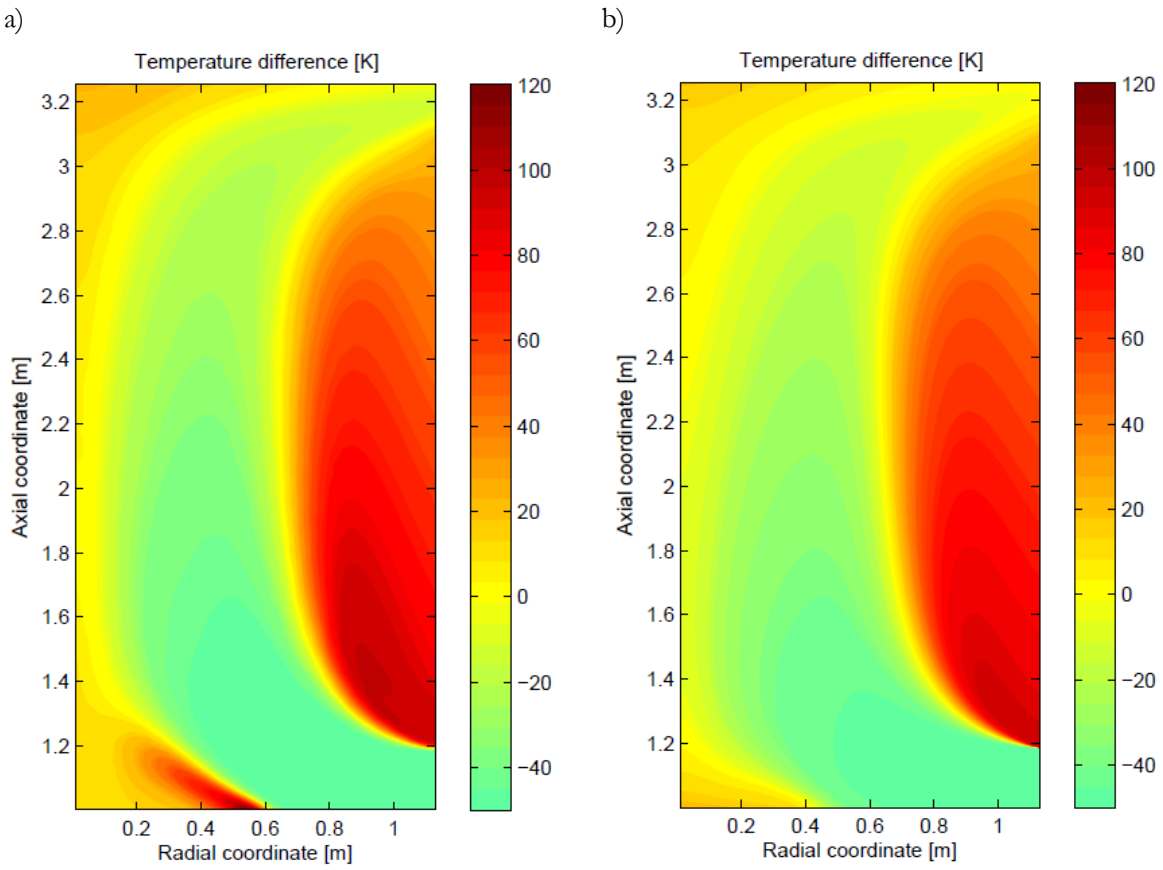

Figure 6.12: Asymptotic temperature variation (positive numbers mean increase) in case of a chilled inlet transient as predicted by a) Polimi and b) TUDelft models

6.5.3 Pump overspeed

According to the prediction of the simplified model employed in subsection 4.4.2, a pump overspeed negligibly affects reactivity and core average temperature, but causes higher velocities in the heat exchanger and enhances the heat transfer coefficient at the primary side. This results in a ~600 MW power increase in case the pressure difference imposed by the

pumps is doubled. However, the power-to-flow ratio also increases and maximum temperatures in the core reduce.

An additional effect plays a role in case recirculation zones exist in the core. In fact, the increased velocity increases the turbulent viscosity (and conductivity), as shown in Fig. 6.13. This causes the temperatures in the recirculation zones to decrease (Fig. 6.14), which in turn leads to higher temperatures in the flowing salt at the core center to preserve the reactivity balance (that requires a slight reduction of the effective core temperature due to the higher precursor losses). Higher temperatures in the flowing salt results in higher temperatures in the heat exchanger, which combine with the improved heat transfer coefficient to cause a ~750 MW power increase, as shown in Fig. 6.15 (a 5 second time constant is assumed for the increase of the pressure difference imposed by the pumps). The power increase predicted by the Polimi model is stronger as a consequence of the higher increment of turbulent viscosity.

In general, the overall asymptotic effect of a pump overspeed is a reduction of the highest temperatures in the system, both for core configurations with or without recirculation zones. In addition, the core remains in a safe configuration throughout the transition between initial and final state, thus confirming that the pump overspeed accident is a minor concern for the MSFR.

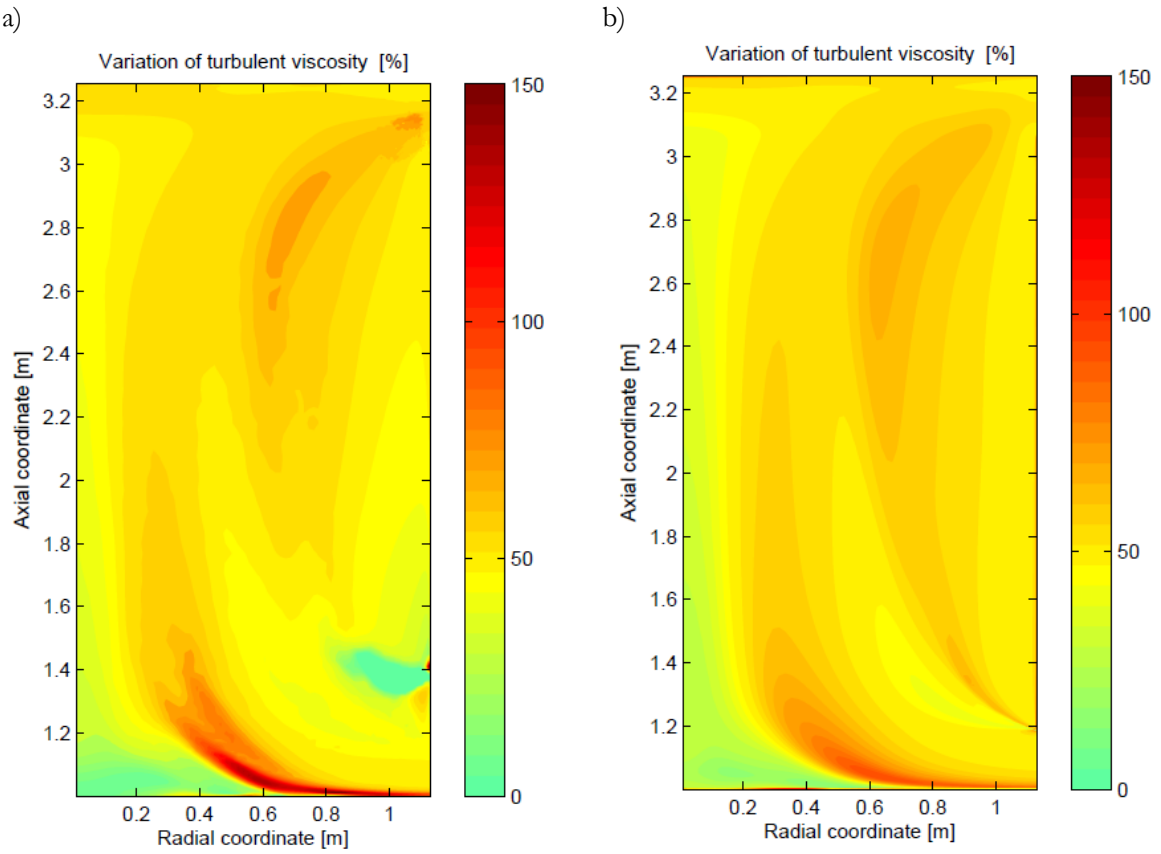

Figure 6.13: Asymptotic variation of turbulent dynamic viscosity (positive numbers mean increase) in case of a pump overspeed transient as predicted by a) Polimi and b) TUDelft models

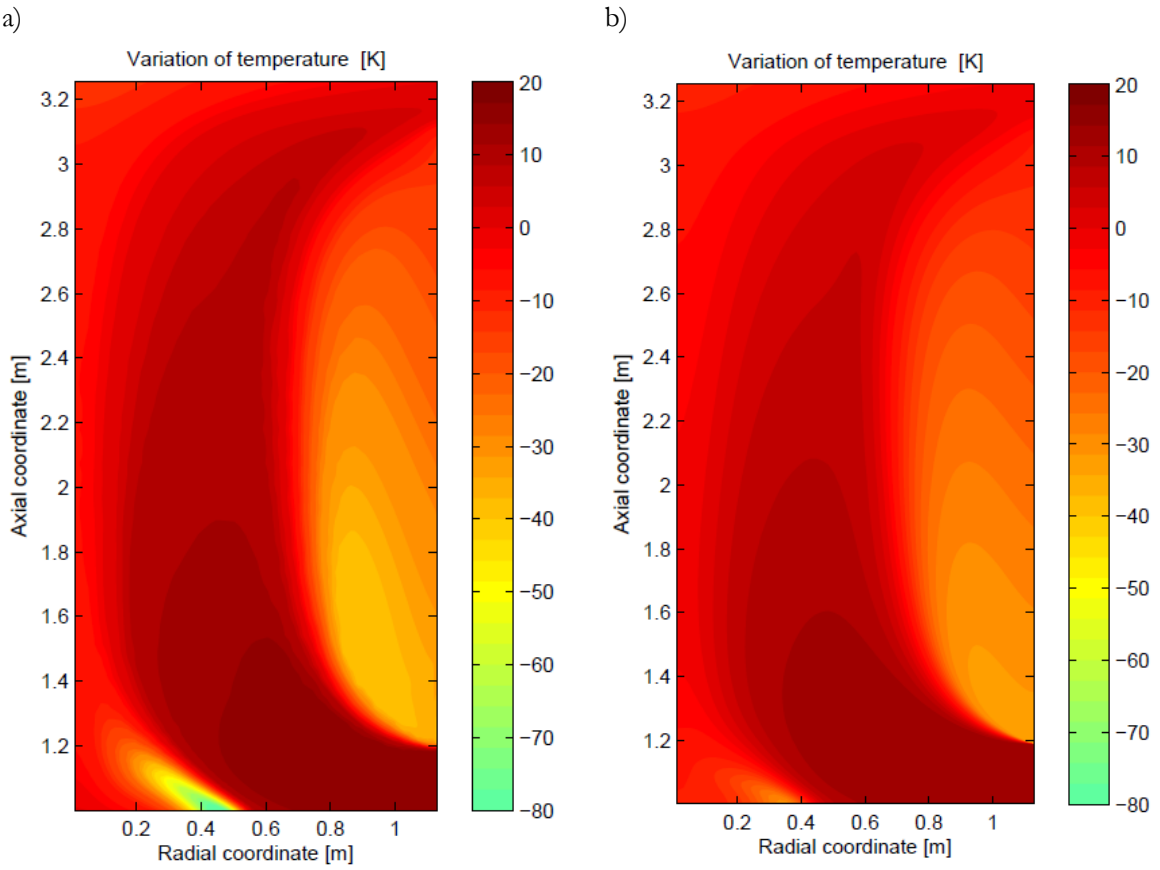

Figure 6.14: Asymptotic temperature variation (positive numbers mean increase) in case of a pump overspeed transient as predicted by a) Polimi and b) TUDelft models

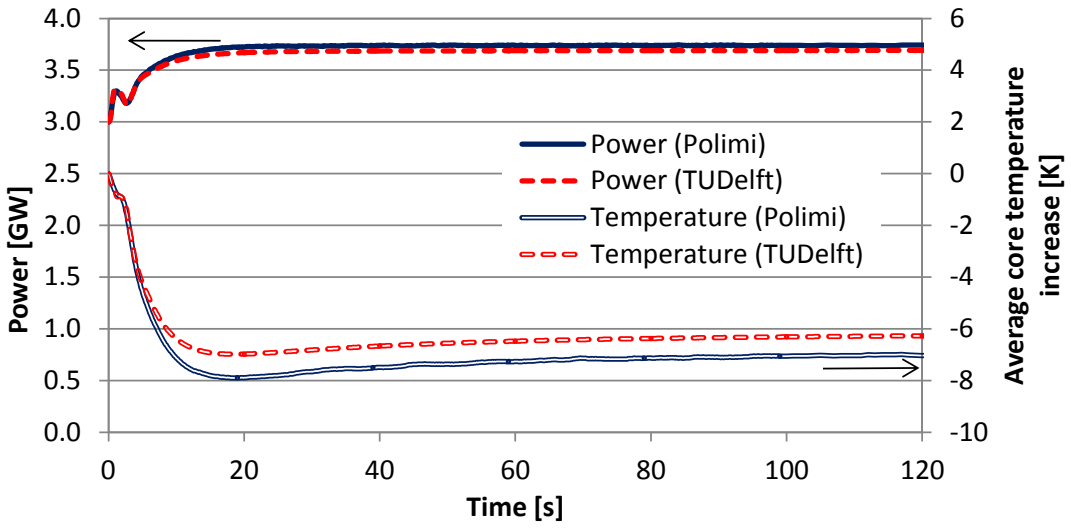

Figure 6.15: Evolution of power and average temperature in the core during a pump overspeed accident

6.5.4 ULOF

In subsection 4.4.2, it has been shown that an ULOF will generally result in an increment of the power-to-flow ratio, with unacceptable reduction of the inlet core temperature, and increment of the outlet core temperature. Impact on the average core temperature is instead mild thanks to the limited reactivity increment (due to less precursors decaying out of the core) and to the high fuel temperature coefficient.

The Polimi and TUDelft models have been employed to simulate an accidental transient where the pumps in the primary circuit coasts down exponentially with a time constant of 5 seconds. Fig. 6.16 shows that the flow rate reduces rapidly during the first 20 seconds, after which it stabilizes thanks to the set-up of a natural circulation regime.

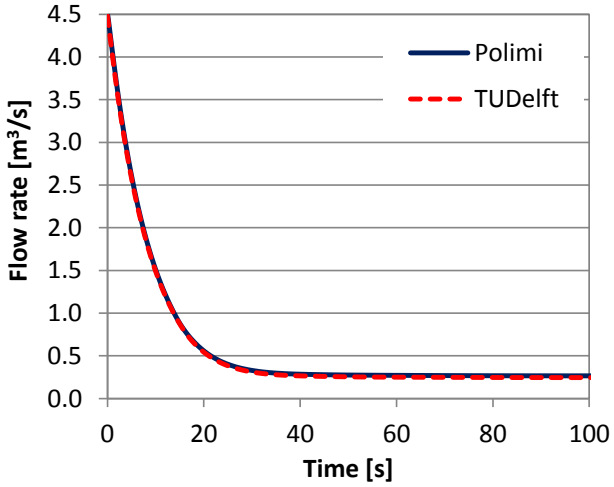

Figure 6.16: Evolution of flow rate during an ULOF

The MSFR response to this flow rate variation is shown in Fig. 6.17. The core average temperature initially grows as the precursor hold-back causes the power-to-flow ratio to increase. This is a well-known phenomenon in nuclear reactors and it is of great concern for traditional liquid-metal FRs. For the MSFR, it appears instead as a minor problem, causing a reassuring 15 K average core temperature increase. After about 15 seconds the flow pattern changes in the core and the recirculation zones start disappearing. At that point, the hot salt contained in these zones flows out of the core, causing a sudden reduction of the average core temperature. After about 40 seconds, the mass of the hot salt originating from the recirculation zone re-enters the core causing a small temperature increase, after which the core average temperature reduces till its asymptotic value. The power decreases monotonically and reaches in 40 seconds an asymptotic value equal to 500-600 MW. The power-to-flow ratio is at that point ~3-4 times higher compared to the reactor nominal conditions.

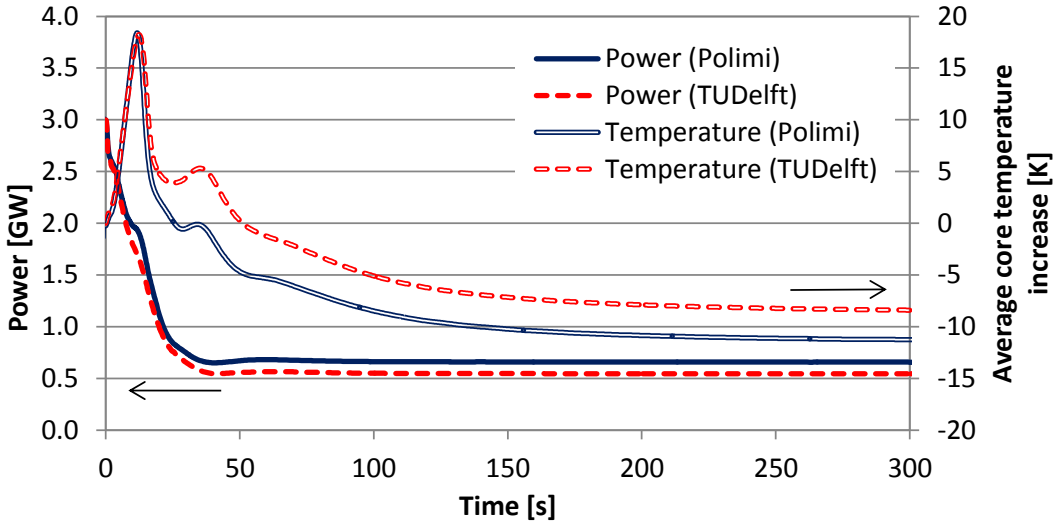

Figure 6.17: Evolution of power and average temperature in the core during an ULOF

The lower flow rate reduces the out-of-core precursor decay, leading to a ~90 pcm reactivity increment that should be offset by ~15 K temperature increase. In this sense, Fig. 6.17 singles out clearly that the core average temperature is not suitable to describe reactivity feedbacks in this case. In fact, the core average temperature reaches an asymptotic value below the initial one. By weighting the temperature distribution with direct and adjoint fluxes provided by Dalton, the resulting effective temperature results to be increased by 13-14 K, consistently with the 90 pcm reactivity increment and the 6-7 pcm/K reactivity feedback (Fig. 6.6).

Fig. 6.18 shows the velocity and temperature fields for the MSFR core at the end of an ULOF. As already pointed out, the reduced flow rate eliminates the recirculation zones and the temperature monotonically increases from the bottom to the top of the core. The difference between outlet and inlet temperatures is approximately 300-400 K, consistently with the increased power-to-flow ratio. Due to the initially high core temperature caused by recirculation zones, the increased power-to-flow ratio mainly affects the outlet temperature, as the average fuel temperature must be approximately maintained to preserve the reactivity balance.

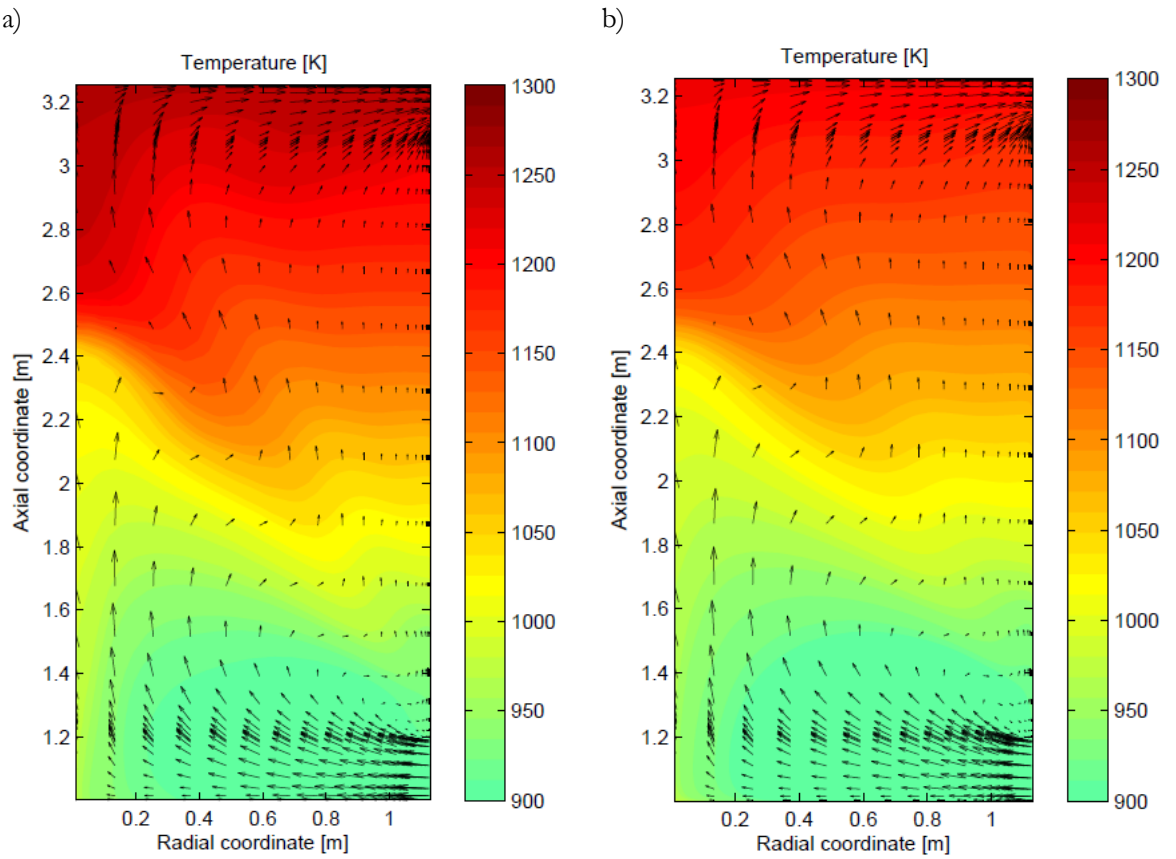

Figure 6.18: Velocity and temperature fields in the core at the end of an ULOF predicted by a) Polimi and b) TUDelft models

In spite of the similar predicted flow rate variation, Figs. 6.17 and 6.18 single out some notable discrepancies between the Polimi and TUDelft models. Most discrepancies can be ascribed to the different prediction for the initial temperatures (Fig. 6.7). In fact, when the initial flow patterns in the core disappear and the hot salt in the recirculation zones is expelled,

the Polimi model predicts a stronger average core temperature decrement (Fig. 6.17) due to the hotter recirculation zones. In addition, core temperature variations are set by neutronic constraints, as the temperature feedback has to compensate for the reduced delayed neutron loss. As a consequence, the higher initial core temperatures in the Polimi model must be accompanied by a higher average core temperature at the new steady-state, which can only be achieved through a higher core power.

The results provided by the Polimi and TUDelft models suggest that the new steady-state achieved by the MSFR at the end of the transient can be used to predict the reactor capabilities to withstand an ULOF, since the transition is relatively quick and the initial increase of the power-to-flow ratio limited. On the other hand, several differences exist between the results provided by the Polimi and TUDelft models, and those presented in subsection 4.4.2. This is first due to the simplifying assumptions made in the Polimi and TUDelft models concerning the flow dependency of pressure losses and heat transfer coefficient in the heat exchangers (see subsection 6.2.1). If the same (simpler) dependencies here considered were assumed in the approach employed in subsection 4.4.2, the predicted final power and flow rate would be 500 MW and 0.24 m^3/s, respectively, comparable to the results shown in Figs. 6.16 and 6.17. In addition, the model of subsection 4.4.2 does not consider the possible existence of recirculation regions in the core, whose main effect is to increase the average of inlet and outlet temperatures at the end of the transient. This determines a higher power, but also higher inlet and outlet core temperatures, which in turn reduces the problem of salt freezing but exacerbates the problem of an excessively high outlet temperature.

Summarizing, also for the ULOF transient the asymptotic state is the worst condition for the core integrity. In fact, the initial increment of the power-to-flow ratio due to the precursor hold-back is a lower concern. Different form the transients previously analyzed, the asymptotic state displays an excessive power-to-flow ratio, unless precautions are taken to improve its natural circulation capabilities (see subsection 4.4.2). Recirculation zones in the core are beneficial in terms of inlet temperature reduction but further increase the outlet temperature.

6.5.5 ULOHS

An ULOHS will generally occur following a loss of flow at the intermediate circuit. The loss of cooling capabilities of the heat exchangers has been assumed to follow an exponential trend with a time constant of 1 second. The system response to such perturbation is shown in Fig. 6.19 that also shows the decay heat level.

As soon as the cooling capabilities are lost, the temperature feedbacks quickly reduce the reactor power. The precursor hold-back time maintains the reactor power above the decay heat level for about 40 seconds. The decay heat starts contributing substantially to the overall power generation after 20-30 seconds and becomes dominant after 40-50 seconds.

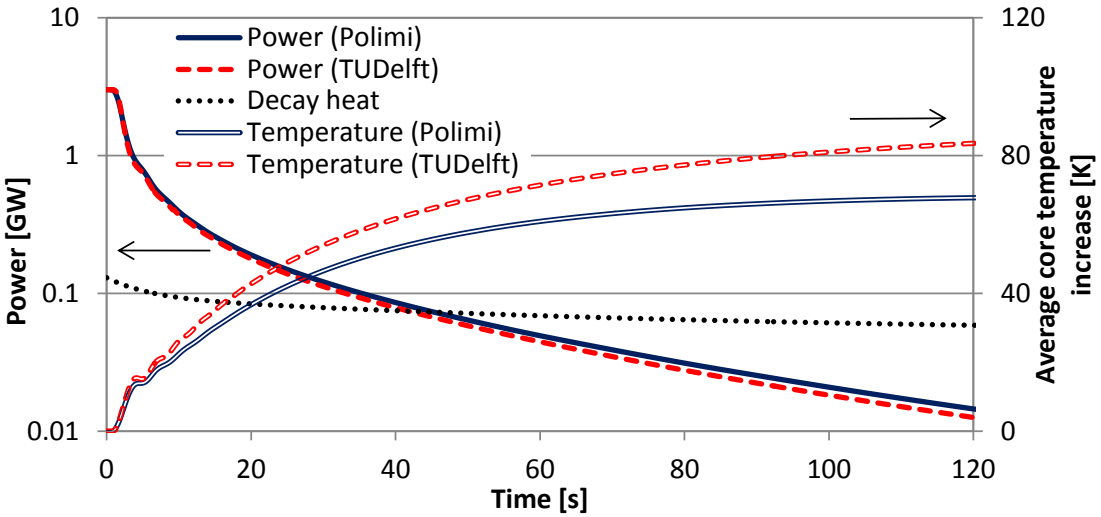

Figure 6.19: Evolution of power and average temperature in the core during an ULOHS

A small discrepancy is observed between Polimi and TUDelft models in terms of reactor power, which is caused by the different precursor groups considered. A more visible discrepancy is observed in the average core temperature. In fact, temperatures in the primary circuits are gradually homogenized by the disappearance of the heat source and sink. The average core temperature must converge to the average temperature in the primary loop, whose variation is set by energy conservation and is the same for the two models. Hence, the higher initial core average temperature in the Polimi model results in a lower increment of the core average temperature. Fig. 6.20 shows that the predicted increment of the loop-averaged temperature is the same in the two models. It also shows the estimated increment of the loop-averaged temperature when including the effect of decay heat, confirming its primary effect already in the first two minutes of an ULOHS. As expected, the decay heat causes a prolonged temperature increment and precludes the achievement of a steady-state.

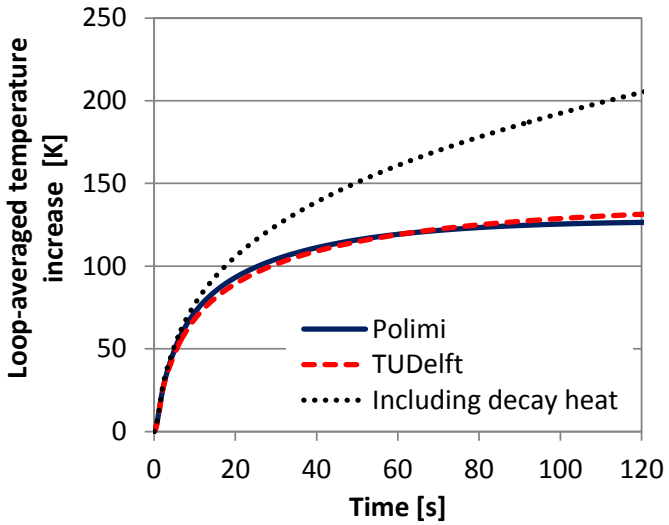

Figure 6.20: Evolution of the loop-averaged temperature during an ULOHS

For the MSFR, salt draining in passively cooled tanks is envisioned in case of severe accidents, with a freezing valve that is expected to open as soon as the electrical power is lost or the fuel salt heats up abnormally. Drain tanks are especially important in case of an

ULOHS, as they would represent the only decay heat removal system. However, Fig. 6.20 singles out a fuel temperature increase of 100 K in 20 seconds and casts doubts on the effectiveness of such system.

6.6 CONCLUDING REMARKS

An investigation has been carried out of the steady-state and transient behavior of the MSFR, based on the conceptual design currently available. To this purpose a dedicated multi-physics model of the MSFR primary circuit has been developed. It is capable of predicting and node-wise coupling velocity and temperature fields, neutron fluxes, and precursor concentrations. The model has been systematically assessed against a similar model developed at the Technical University of Delft, showing a good agreement. Discrepancies have been observed in the predicted temperature field, with ensuing mild impact on the transient behavior. However, both models are suitable to obtain first important information on the MSFR steady-state and transient behavior.

Steady-state analysis of the reactor has pointed out some points of enhancement needed in the current MSFR conceptual design. Specifically, 3 zones of salt recirculation have been identified in the core, causing excessive temperatures, as well as accumulation of precursors in low flux regions with detrimental effects on the β_{eff}. The reduction of this parameter compared to a condition with static fuel has been estimated to be close to 60%.

The reactor response to major accidental transient initiators has been also evaluated. Although the core design is not yet optimized, the results provide useful information on the general reactor behavior and on the critical issues to be addressed while designing or optimizing this reactor concept. It has been shown that the asymptotic state after an accidental transient can be considered as representative of the reactor worst conditions, thus generally confirming the promising inherent safety features of the MSFR pointed out in Chapter 4. In particular, the MSFR shows exceptional load-following characteristics and resistance to overpower accidents. Pump overspeed does not lead to increased core temperatures, while a chilled inlet transient may result in a notable increment of core temperatures only in case recirculation zones exist in the core. Recirculation zones also cause a particularly reduced inlet temperature after a chilled inlet, determining some additional concerns related to the possibility of salt freezing at the heat exchangers. A main problem is associated to the high specific power, which leads to a quick temperature increase in case of an ULOHS. In addition, natural circulation sets up in case of pump failure but the final power-to-flow ratio is increased, as predicted in Chapter 4. This poses concerns related to both excessive outlet temperature and the possible salt freezing at the heat exchangers. The problem of salt freezing is reduced by the existence of salt recirculation zones in the core, but the problem of the increased outlet temperature is exacerbated.

Core draining in passively cooled tanks seems necessary in case of an ULOHS or an ULOF, for the current conceptual design. To ensure the core integrity, the salt draining system must be proved capable of emptying the core in few tens of seconds, with a high degree of reliability. Use of freezing valves is envisioned for the MSFR, which should open as soon as the electrical power is lost, or in case of salt overheating. In this sense, it is worth noting that the temperature in the lower part of the core during an ULOF tends to decrease,

thus counteracting the melting of the valve. On the other hand, it has been shown in Chapter 4 that the possibility exists to improve the reactor safety during an ULOF through a proper design of the primary circuit. In general, a better assessment of the MSFR safety features would require a more detailed hydrodynamic design of both the core and the out-of-core components (especially pumps and heat exchangers), as well as of the intermediate and secondary circuits.

REFERENCES

Aufiero, M., Cammi, A., Fiorina, C., Luzzi, L. 2012. Modification of the SERPENT code to study the fuel isotopic evolution of molten salt reactors with online (continuous) reprocessing. Presentation for "2012 SERPENT International Users Group Meeting". September 19-21, Madrid, Spain.

Aufiero, M., Cammi, A., Fiorina, C., Leppänen, J., Luzzi, L., submitted. An extended version of the SERPENT-2 code to investigate fuel burn-up and core material evolution of the Molten Salt Fast Reactor. Submitted to Journal of Nuclear Materials. Presentation at NuMat 2012 conference, October 22-25, Osaka, Japan.

Boer, B., Lathouwers, D., Kloosterman, J.L., Van der Hagen, T.H.J.J., 2010. Validation of the DALTON-THERMIX code system with transient analyses of the HTR-10 and application to the PBMR. Nuclear Technology 170, 306-321.

Cammi, A., Di Marcello, V., Fiorina, C., Luzzi, L., 2009. Assessment of COMSOL capabilities to analyse the thermo-hydrodynamic behaviour of the MSR core. Proc. COMSOL Conference 2009, October 14-16, Milan, Italy.

Cammi, A., Di Marcello, V., Luzzi, L., Memoli, V., Ricotti, M.E., 2011. A multi-physics modelling approach to the dynamics of Molten Salt Reactors. Annals of Nuclear Energy 38, 1356-1372.

Cammi, A., Fiorina, C., Guerrieri, C., Luzzi, L., 2012. Dimensional Effects in the Modelling of MSR Dynamics: Moving on from Simplified Schemes of Analysis to a Multi-Physics Modelling Approach. Nuclear Engineering and Design 246, 12-26.

Cebeci, T., Shao, J.P., Kafyeke, F., Laurendeau, E., 2005. Computational Fluid Dynamics for Engineers. Springer. Horizons Publishing. Long Beach, California / Heidelberg, Germany.

Chadwick, M.B. et al., 2006. ENDF/B-VII.0: Next Generation Evaluated Nuclear Data Library for Nuclear Science and Technology. Nuclear Data Sheets 107, 2931–3060.

de Zwaan, S.J., Boer, B., Lathouwers, D., Kloosterman, J.L., 2007. Static design of a liquid-salt-cooled pebble bed reactor. Annals of Nuclear Energy 34, 83-92.

Dittus, F.W., Boelter, L.M.K., 1930. Heat transfer in automobile radiators of the tubular type. University of California publications in Engineering, 443-461.

Dulla, S., Ravetto, P., Rostagno, M.M., 2004. Neutron kinetics of fluid-fuel systems by the quasi-static method. Annals of Nuclear Energy 31, 1709–1733.

Dulla, S., Ravetto, P., 2007. Interactions between fluid-dynamics and neutronics phenomena in the physics of molten-salt systems. Nuclear Science and Engineering 155, 475–488.

EVOL Project 2012 - Evaluation and Viability of Liquid Fuel Fast Reactor Systems. Available at: http://www.li2c.upmc.fr/.

Fiorina, C., 2009. A generalized approach to assess the COMSOL® capabilities for the analysis of the MSR thermo-fluid dynamics. MSc thesis. Politecnico di Milano, Milan, Italy.

Fiorina, C., Aufiero, M., Cammi, A., Guerrieri, C., Krepel, J., Luzzi, L., Mikityuk, K., Ricotti, M. E., 2012. Analysis of the MSFR Core Neutronics Adopting Different Neutron-Transport Models. Proc. ICONE 2012 International Conference. July 30 – August 3, Anaheim, US.

Fiorina, C., Aufiero, A., Cammi, A., Franceschini, F., Krepel, J., Luzzi, L., Mikityuk, K., Ricotti, M. E., submitted (a). Investigation of the MSFR core physics and fuel cycle characteristics. Submitted to Progress in Nuclear Energy.

Fiorina, C., Aufiero, M., Cammi, A., Guerrieri, C., Kloosterman, J.L., Lathouwers, D., Luzzi, L., Ricotti, M.E., submitted (b). Modelling and analysis of the MSFR transient behavior. Submitted to the Special Issue "Progress in the development of Molten Salt Reactors and salt-cooled reactors" of Annals of Nuclear Energy.

Incropera, F.P., DeWitt, D.P., Bergman, T.L., Lavine, A., 2006. Fundamentals of Heat and Mass Transfer. John Wiley and Sons, Hoboken, US.

Jiang, L.-Y., Campbell, I., 2008. Reynolds analogy in combustor modeling. International Journal of Heat and Mass Transfer 51, 1251–1263.

Koning, A., Forrest, R., Kellett, M., Mills, R., Henriksson, H., Rugama, Y., 2006. The JEFF-3.1 Nuclear Data Library. Nuclear Energy Agency. JEFF Report 21.

Kophazi, J., Lathouwers, D., Kloosterman, J.L., 2009. Development of a three-dimensional time-dependent calculation scheme for molten salt reactors and validation of the measurement data of the molten salt reactor experiment. Nuclear Science and Engineering 163, 118-131.

Krepel, J., Grundmann, J., Rohde, U., Weiss, F.P., 2005. DYN1D-MSR dynamics code for molten salt reactors. Annals of Nuclear Energy 32, 1799–1824.

Krepel, J., Rohde, U., Grundmann, U., Weiss, F.P., 2007. DYN3D-MSR spatial dynamics code for molten salt reactors. Annals of Nuclear Energy 34, 449–462.

Lapenta, G., Mattioda, F., Ravetto, P., 2001. Point kinetic model for fluid fuel systems. Annals of Nuclear Energy 28, 1759–1772.

Lecarpentier, D., Carpentier, V., 2003. A neutronics program for critical and nonequilibrium study of mobile fuel reactors: the Cinsf1D code. Nuclear Science and Engineering 143, 33–46.

Leppänen, J., 2007. Development of a new Monte Carlo reactor physics code. PhD Thesis. Helsinki University of Technology.

Nicolino, C., Lapenta, G., Dulla, S., Ravetto, P., 2008. Coupled dynamics in the physics of molten salt reactors. Annals of Nuclear Energy 35, 314–322.

SCALE: A Modular Code System for Performing Standardized Computer Analyses for Licensing Evaluations, ORNL/TM-2005/39, Version 5.1, Vols. I–III, November 2006. Available from Radiation Safety Information Computational Center at Oak Ridge National Laboratory as CCC-732.

Singh, K.P., Modak, R.S., Degweker, S.B., Kanchhi Singh, 2009. Iterative schemes for obtaining dominant alpha-modes of the neutron diffusion equation. Annals of Nuclear Energy 36, 1086–1092.

Suzuki, N., Shimazu, Y., 2006. Preliminary Safety Analysis on Depressurization Accident without Scram of a Molten Salt Reactor. Journal of Nuclear Science and Technology 43, 720–730.

Suzuki, N., Shimazu, Y., 2008. Reactivity-Initiated-Accident Analysis without Scram of a Molten Salt Reactor. Journal of Nuclear Science and Technology 45, 575–581.

van der Linden, E., 2012. Coupled neutronics and computational fluid dynamics for the molten salt fast reactor. MSc Thesis. Technical University of Delft, Netherlands.

Wang, S., Rineiski, A., Maschek, W., 2006. Molten salt related extensions of the SIMMER-III code and its application for a burner reactor. Nuclear Engineering and Design 236, 1580–1588.

Wilcox, D.C., 1998. Turbulence Modeling for CFD. Dcw Industries, Inc., La Canada, US.

Yamamoto, T., Mitachi, K., Suzuki, T., 2005. Steady state analysis of small molten salt reactor. JSME International Journal Series B 48, 610–717.

Yamamoto, T., Mitachi, K., Ikeuchi, K., Suzuki, T., 2006. Transient characteristics of small molten salt reactor during blockage accident. Heat Transfer Asian Research 35, 434–450.

Zhang, D.L., Qiu, S.Z., Su, G.H., Liu, C.L., Qian, L.B., 2009a. Analysis on the neutron kinetics for a molten salt reactor. Progress in Nuclear Energy 51, 624–636.

Zhang, D.L., Qiu, S.Z., Su, G.H., 2009b. Development of a safety analysis code for molten salt reactors. Nuclear Engineering and Design 239, 2778–2785.

Zhang, D.L., Qiu, S.Z., Su, G.H., Liu, C.L., 2009c. Development of a steady state analysis code for a molten salt reactor. Annals of Nuclear Energy 36, 590–603.

CONCLUSIONS

Main results

The thesis work was aimed at evaluating the Th-based MSFR technology through a first-of-a-kind comparative analysis with U- and Th-based traditional Fast Reactors (FR), and through the investigation of specific and poorly-known MSFR features, i.e., the thermal-hydraulics of internally heated molten salts, and the reactor steady-state and transient behavior. The following main conclusions can be drawn:

- The ERANOS-based EQL3D procedure developed at the Paul Scherrer Institut (Switzerland) for equilibrium FR analysis has been extended to allow 1) investigation of both solid- and liquid-fuelled reactors; 2) simulation of U- and Th-based fuel cycle strategies; 3) use of fertile blankets; 4) computation of radiotoxicity and decay heat of wastes. The new features have been tested against dedicated codes, showing a very good agreement. The extended-EQL3D procedure proved itself a powerful tool for comparative analyses between different fast-spectrum concepts from the viewpoint of waste management, fuel cycle and safety aspects.
- The capability of the MSFR to operate as a flexible-Conversion-Ratio (CR) reactor has been demonstrated, showing the possibility of employing it as breeder, iso-breeder or burner reactor. Different CRs can be achieved by varying the reprocessing rate for soluble fission product, which in turn affects their content in the core and ultimately the neutron economy.
- Operation of the MSFR as breeder reactor allows to achieve an equilibrium doubling time of approximately 40 years by reprocessing less than 100 liters per day of salt. Higher reprocessing rates negligibly improve the neutron economy. Doubts exist about the real breeding capabilities of the MSFR due to major uncertainties on the U-233 capture cross-section in the energy range of interest for the MSFR. A doubling time equal to 40 years has been predicted using the JEFF3.1 nuclear data library, but a doubling time two/three times longer is predicted using e.g. the ENDF/B-VII.0 library.
- Iso-breeding can be achieved by reprocessing ~5-10 liters per day of salt, the exact rate depending on the adopted nuclear data library and on the modeling assumptions.
- As far as waste generation is concerned, use of Th in a closed cycle based on fast-spectrum systems has been found to foster notable advantages in terms of decay heat of actinide wastes, with the caveats of an increased Sr-90 generation of U-233 vs Pu-239. As a result, incremental costs are expected for interim fuel storage or initial forced cooling in a geological repository, but the number of geological repositories required might be reduced. Limited advantages are observed in terms of radiotoxicity, with a drastic reduction in the first few thousands of years, but an increment in the longer term due to the progenies of U-233 and U-234. Among various fast-spectrum concepts, the MSFR features higher specific fuel decay heat and radiotoxicity due to a relatively soft spectrum and ensuing build-up of hazardous isotopes, but waste generation is reduced or

comparable to the solid-fuelled concepts thanks to the high average burnups and lower reprocessing rates allowed by adoption of a liquid fuel.

- Transmutation of an initial loading of TRansUranic isotopes (TRU) through a subsequent prolonged operation in a fully closed cycle has been investigated. This strategy is ineffective in traditional U-based FRs, while some benefits can be achieved in a Th cycle, especially in terms of decay heat. The MSFR presents pros and cons compared to traditional FRs. On one hand, the softer spectrum partly frustrates the effectiveness of transmutation due to the higher specific radiotoxicity and decay heat at equilibrium. On the other hand, the high specific power combines with the lack of out-of-core cooling time for the fuel to yield a relatively short transmutation time for an initial TRU loading, of the order of 50 years. In this sense, the MSFR emerges as a unique reactor system for a quick transition from the current U-based cycle to a novel Th fuel cycle. This feature might be jeopardized by the necessity to mix the initial TRU loading with U enriched in U-235 for solubility issues, though the problem could be circumvented by: 1) operation of the reactor at higher temperature in the first few years, which would increase solubility of TRUs, or 2) use of U-233 instead of enriched U.
- Waste burning via a TRU feed in the MSFR closed cycle is limited by 1) solubility of TRUs in the salt fed to the core, and 2) solubility of trivalent isotopes (mainly TRUs and lanthanide fission products) inside the core at equilibrium. These two constraints are approximately equivalent and limit the TRU burning rate to ~150 kg/GWe-yr, much lower than the 500-600 kg/GWe-yr achievable with traditional low-CR FRs using TRUs from once-through Light Water Reactor (LWR) operation. However, the TRU composition is constrained in the solid-fuelled reactors here investigated by problems of fuel handling and safety deterioration. A traditional 5% limit on the content of Minor Actinides (MA - Np, Am, Cm, Cf) in the core leads to an upper limit to the MA burning rate of the order of 60-70 kg/GWe-yr. On the other hand, fuel management is not an issue for the MSFR while its safety margins appear relatively wide. As a consequence, the MSFR shows the potential of using a Th-MA feed (without Pu), leading to a MA burning rate of ~150 kg/GWe-yr, i.e., two times higher compared to traditional FRs. This may be of interest for fuel cycle options envisioning Pu recycle in advanced LWRs or other innovative reactors, with only the MA inventory to be disposed.
- Fuel handling is confirmed as a major problem for traditional FRs employed for TRU burning and/or for Th use, requiring remote fuel fabrication under thick shielding. The MSFR shows in this sense one of its most promising features, since reprocessing requirements would be reduced, fuel fabrication would be avoided and transportation strongly limited thanks to the online reprocessing. In addition, the in-core fissile inventory of the MSFR is smaller compared to a sodium-cooled FR and, particularly, a lead-cooled FR, while out-of-core inventories are virtually eliminated.
- Th use in fast-spectrum systems determines a lower reactivity insertion in case of spectrum hardening thanks to the lower cross-section and higher threshold for fission of Th-232 vs U-238, and to the steeper fission cross-section and flatter capture cross-section of U-233 vs Pu-239. In case of traditional FRs, Th use fosters significant advantages in terms of void reactivity and Doppler, with the caveats of reduced core and fuel expansion

coefficients, and of a possibly higher number of required control rods. If burner FRs are considered with a very high TRU burning rate, differences between Th and U tightens due to the lower fertile-to-fissile ratio.

- The MSFR safety parameters have been investigated in details for different fuel cycle strategies, also through the adoption of recently developed reactivity decomposition techniques, which helped highlighting their different phenomenology compared to traditional FRs. Doppler and fuel expansion represent the only significant feedbacks. Their combined effect yields a strongly negative feedback, one order of magnitude higher compared to a sodium-cooled FR. The strong Doppler has been ascribed to the use of Th and, particularly, to the relatively soft spectrum. The fuel expansion coefficient has instead different phenomenology compared to traditional FRs, since it originates mainly from a change in diffusion length and not from a variation of the fuel-to-coolant ratio. Core expansion has been singled out as a positive feedback, but its importance turned out to be negligible. β_{eff} has been found to be reduced by ~60% by fuel recirculation, but the lack of burnup reactivity swing and of positive feedbacks strongly limits its potentially negative impact. The overall safety features appear promising, especially in view of the lack of significant positive reactivity feedbacks generally observed in traditional FRs.
- Investigation of the inherent safety features of a traditional sodium-cooled FR has been carried out through a consolidated approach from the available literature. This analysis preliminarily confirmed the capability of traditional FRs to withstand typical double-fault accidents, setting reference performances for the MSFR. Thorium use has a small impact and presents both pros and cons from this perspective: the higher Doppler opposes a power decrement in the core while a reduced coolant coefficient reduces the reactivity insertion when core temperatures increase.
- A simple approach has been developed to investigate the inherent safety features of the MSFR through prediction of the new steady-state reached after an accidental transient, for different fuel cycle options. The MSFR response to unprotected transient overpower, chilled inlet or pump overspeed accidents appears acceptable in all cases, though for the chilled inlet accident some concerns originate from the possibility of salt freezing in the heat exchangers. In case of an unprotected loss of flow, the final steady-state shows instead unacceptable temperatures. However, the MSFR response to this kind of accident can be improved by a proper design and position of the heat exchangers, as well as by increased temperatures in the intermediate circuits. The possibility also exists of draining the fuel salt in the passively-cooled tanks envisioned for the MSFR. The same safety measure will be necessary in case of an unprotected loss of heat sink, since the decay heat will determine a quick temperature rise in the core, preventing the achievement of a steady-state. Provided the effectiveness of the draining system will be proved and its intervention fully passive, the inherent safety of the MSFR is promising and appears at least comparable to that of the traditional FRs investigated, both U- and Th-based.
- A theoretical investigation of the MSFR thermal-hydraulics has been carried out, resulting in the proposal of a general correlation form for the Nusselt number in case of forced convection of internally heated fluids flowing in turbulent regime in straight circular channels. A generalized approach to heat transfer in internally heated fluids has been used

to derive a specific correlation for the case of molten salts and for the range of Reynolds numbers of interest for the MSFR. Application to the MSFR out-of-core piping and components has allowed to exclude major impacts of decay heat on the heat transfer processes in the system, though attention should be paid to the design of components with low salt velocities and large diameters. A preliminary design has been proposed of a possible experimental facility that could be used to validate the proposed correlation.

- A detailed assessment has been performed of the MSFR steady-state and transient behavior. The liquid fuel and the lack of graphite in the core prevent the use both of traditional tools for the reactor transient analysis, and of recently developed codes for the analysis of graphite-moderated Molten Salt Reactors. For this reason, a dedicated tool has been developed in this and other 2 PhD thesis, envisioning the simultaneous solution, in the same computational environment, of all the partial differential equations governing thermo-fluid dynamics, neutron transport, and precursor diffusion and convection. A 2-D axial-symmetric geometry has been assumed to reduce the computational burden. The developed model has been assessed against a similar model developed in the same period at the Technical University of Delft (Netherlands). The Delft model presents similar modeling choices but different numerical implementation, which is based on the coupling of dedicated codes for thermo-fluid dynamics and neutronics. The agreement between the two models is satisfactory. Some discrepancies have been observed in the temperature field at steady-state, with ensuing mild impact on the predictions of the reactor transient behavior.
- Some points of enhancement have been individuated in the MSFR thermal-hydraulic design. In particular, three recirculation zones have been observed in the core, causing excessive temperatures and accumulation of delayed neutron precursors in low flux regions, with detrimental effects on the β_{eff}.
- Transient simulations demonstrated a generally benign response of the MSFR to major accidental transient initiators. It has been shown that the new asymptotic state reached by the reactor can be considered as representative of the reactor worst conditions during an accidental transient. This allowed to confirm the promising inherent safety features of the MSFR already pointed out in the thesis using simpler approaches, with a note of caution on possible recirculation zones in the core that may alter the predicted reactor response. As expected, the main concern comes from the high specific power, leading to a quick temperature increase in case of a loss of heat sink, and requiring the intervention of the salt draining system.

Future work to be considered

The thesis work has investigated the MSFR features in terms of fuel cycle, system design and safety aspects, showing potential benefits over traditional FRs. However, further investigation, possibly on an experimental ground, would be required to exclude uncertainties and possible show-stoppers for the deployment of this technology. The followings aspects have emerged as particularly relevant:

- Detailed fuel salt properties are needed, since the full exploitation of the MSFR fuel cycle flexibility implies the adoption of a wide variety of fuel salt compositions, which raises

concerns for the possible variations of the salt properties and for the solubility of selected components.

- Solubility limits for trivalent isotopes have emerged as a main constraint both for the reduction of the reprocessing rate, and for the composition of the initial actinide inventory. The possibility should be investigated of increasing the solubility limits through increased core temperatures, at least for short periods. In addition, in this thesis work it has been assumed that fresh fissile and fertile isotopes are inserted into the core at the lowest salt temperature in the system, which strongly limits the amount of TRUs in the feed. The possibility should be investigated of inserting the feed at higher temperatures, though this would clearly increase the overall complexity of the system.
- Detailed investigation of the efficiencies of the reprocessing system for different fuel cycle strategies would be important. It would allow a better evaluation of the MSFR radiotoxicity and decay heat generation, as well as a more accurate evaluation of its neutron economy. A known issue is the difficulty to extract Zr from the fuel salt.
- In this thesis work, radiotoxicity and decay heat have been employed as metrics to preliminary characterize the waste generation or consumption associated to a fuel cycle strategy. A better assessment would require a detailed investigation of the repository thermal performances, and of the actual probabilities of each isotope to reach the biosphere.
- Uncertainty analysis on the nuclear data libraries would be needed to point out the cross-sections requiring new experimentation. A known problem relates the scarce experimental data for the U-233 capture cross-section in the energy range of interest for the MSFR, leading to major uncertainties on its actual breeding capability and on the generation of Pu-238, a main responsible for radiotoxicity and decay heat in the first few centuries.
- Structural materials for the primary circuit would require extensive investigation and experimentation. Although preliminary studies are demonstrating the long-term resistance of advanced Ni-alloys to high-temperature molten salts, a limit would be needed for the maximum allowed temperature in the shorter time scales typical of an accident.
- Experimental investigation is suggested of the heat transfer phenomena involving internally heated fluids. In fact, the analyses performed in this thesis have singled out potentially excessive wall temperatures in channels with large diameters and/or low velocities, which might be the case e.g. of the salt reprocessing system.
- Thermal-hydraulic optimization is required for the MSFR core and primary circuit to eliminate salt recirculation regions, which cause unacceptable core temperatures and reduce the β_{eff}.
- To enhance the MSFR resistance to loss of flow accidents, the primary loops should be designed to promote natural circulation after a pump coast-down, e.g. through a proper design and position of the heat exchangers. In addition, the possibility should be considered to increase the temperatures in the intermediate circuit above the melting point of the primary salt, which would greatly reduce concerns related to salt freezing e.g. in chilled inlet or loss of flow accidents.

- A preliminary design is suggested of the emergency core draining system, since the quick temperature rise observed in case of a loss of heat sink casts doubts on the effectiveness of such safety measure.
- For a better safety assessment, a detailed design of the MSFR system would be needed, especially for the out-of-core components of the primary circuit, and for intermediate and secondary circuits.
- As regards the model employed for the analysis of the MSFR steady-state and transient behavior, further development is primarily recommended in the direction of improving the reliability of the thermo-fluid dynamic modeling, possibly through the use of turbulence models more suitable for simulating stagnation and recirculation regions. In addition, extension of the geometrical capability to generic 3-D configurations would be of great advantage to better characterize local effects, to optimize the core design, as well as to allow the simulation of asymmetric transients like the coast-down of a single pump.

APPENDIX A: Methodology employed for core physics and fuel cycle calculations: the extended-EQL3D procedure

ABSTRACT

The present Appendix focuses on tools and methodologies employed in the thesis for the core physics and fuel cycle analyses. In particular, the ERANOS-based EQL3D procedure is presented, including its extension to the investigation of the Molten Salt Reactors, as well as to the analysis of radiotoxicity and decay heat of actinide wastes. The extended-EQL3D procedure is assessed against dedicated codes, showing an excellent agreement. Finally, a reactivity decomposition technique frequently employed in the thesis work is briefly discussed. Some of the main results have been presented in (Fiorina et al., 2012a, 2012b, 2013, submitted; Aufiero et al., 2012, submitted).

A.1 INTRODUCTION

A primary objective of the thesis work is to characterize the MSFR from the viewpoints of core physics and fuel cycle, including a systematic comparison with traditional solid-fuelled Fast Reactors (FR). To ease the investigation while excluding major sources of biasing, a common tool has been employed to investigate the performances of the MSFR and of the traditional FRs. An existing ERANOS-based (Rimpault et al., 2002) procedure, developed at the Paul Scherrer Institut (Switzerland) for the analysis of solid-fuelled FRs (Krepel et al., 2009), has been employed and extended to allow the simulation of Th-containing cores, the possible use of fertile blankets and the online reprocessing system of the Molten Salt Reactors (MSR). In addition, dedicated sub-procedures have been set up for the calculation of radiotoxicity and decay heat of wastes.

Throughout the thesis, a particular attention is given to the equilibrium core state that is reached in a reactor after prolonged operation with constant feed and fuel management scheme. The equilibrium concentration for a given isotope is achieved when a net zero balance is established between its consumption, from neutron absorption and decay, and its generation from its precursors through two main pathways, neutron capture and decay. For a given reactor and fuel management scheme, the equilibrium compositions are mainly determined by the feed. The EQL3D procedure has been primarily developed for the purpose of predicting the equilibrium state of a FR operating in closed or open cycles, though it is also

able to predict with good accuracy the transition from the initial core loading to the equilibrium.

Section A.2 presents the ERANOS code and the original EQL3D procedure, including its extension to the Th cycle. Extension to the analysis of MSRs, to the use of blankets and to the calculation of radiotoxicity and decay heat is presented in Sections A.3 and A.4. Additional routines for reaction-wise, isotope-wise and group-wise decomposition of nominal reactivity and feedback coefficients are presented in Section A.5. Concluding remarks are drawn in Section A.6.

A.2 ERANOS AND THE EQL3D PROCEDURE FOR THE ANALYSIS OF TRADITIONAL SOLID-FUELLED FAST REACTORS

The main core physics and fuel depletion tool employed in the thesis work is ERANOS 2.2N (Rimpault, 2002). It is a deterministic code system purpose-made for FR analysis. In particular, the ERANOS-based EQL3D procedure developed at the Paul Scherrer Institut has been employed. Starting from an initial fuel composition, EQL3D simulates the cycle-by-cycle behavior of a reactor. The main assumptions are constant imposed reactor power, constant mass of actinides in the fabricated fuel and constant fuel management. Under these assumptions, the simulated reactor always reaches its final equilibrium state. The resulting equilibrium reactivity indicates the capability of the reactor to support a closed fuel cycle: for instance, breeder or iso-breeder reactors are expected to show a positive reactivity at equilibrium using only Th or natural U as feed. The core is represented in its full dimensionality, thus allowing a meaningful characterization in terms of core performance as well as safety-related parameters, both at equilibrium and during the transition toward it. Further details about the EQL3D procedure can be found in (Krepel et al., 2009, 2010).

A.2.1 Assumptions and specific methodological choices

Full recycle of actinides has been assumed for all cases presented in the thesis work, i.e. during reprocessing fission products are removed, all actinides are recycled and an actinide feed is added until the total inventory of the initial fresh fuel is restored. Due to the scoping nature of the calculations performed, a single-batch irradiation scheme has been assumed for convenience. Under the assumed scheme, the core is irradiated for a period of time corresponding to the batch irradiation time, unloaded (and ideally replaced with another one), cooled for an equally long period, reprocessed, and reloaded once again. The End Of Cycle (EOC) reactivity of a corresponding multi-batch scheme can be approximated by properly averaging the reactivity from the single-batch core. For instance, the EOC reactivity of a 3-batch core design, where each third of the assemblies is burned respectively for 1/3, 2/3 and the entire fuel irradiation time, can be obtained averaging reactivities at 1/3, 2/3 and at the end of the cycle of the single-batch core. Single-batch simulations using the above averaging technique to represent a typical multi-batch core have been employed throughout this study, including the evaluation of the core safety coefficients. This is a reasonable approximation as discussed e.g. by Artioli et al. (2009) and Krepel et al. (2010).

Full core flux and burnup calculations have been performed with ERANOS in the 33 energy-group structure optimized for FR calculations (Table A.1). The multigroup nodal

transport theory code VARIANT has been used for flux calculations (Ruggeri, 1999), employing a P3 approximation with simplified spherical harmonics. The 33-group cross-sections have been obtained from assembly-wise lattice calculations using the collision-probability code ECCO in 1968 energy groups based on the JEFF3.1 library available in ERANOS (Sublet et al., 2006). The ECCO lattice calculations have been performed with the consistent solution method (Rimpault, 1997).

Each fuel assembly has been discretized in 6 to 8 axial nodes for fuel depletion calculations. Evolution of masses is computed for each node according to the specific power derived through the full core flux calculations. During each cycle (corresponding to the entire irradiation time in a single-batch approximation), fluxes are recalculated 9 times. Between two flux recalculations, macroscopic cross-sections are computed 3 times, and the specific power of each node is accordingly renormalized to maintain a constant core power. The microscopic cross-sections are calculated every few cycles, the exact number depending on the rate of variation of the fuel composition. A set of microscopic cross-sections is calculated for each radial core zone (e.g., inner, middle and outer in the ELSY (Section B.2)).

Table A.1: Upper energy limits for the 33 energy groups adopted for the ERANOS calculations

Group	Boundary [eV]	Group	Boundary [eV]	Group	Boundary [eV]
1	$1.96\cdot10^{7}$	**12**	$6.74\cdot10^{4}$	**23**	$3.04\cdot10^{2}$
2	$1.00\cdot10^{7}$	**13**	$4.09\cdot10^{4}$	**24**	$1.49\cdot10^{2}$
3	$6.07\cdot10^{6}$	**14**	$2.48\cdot10^{4}$	**25**	$9.17\cdot10^{1}$
4	$3.68\cdot10^{6}$	**15**	$1.50\cdot10^{4}$	**26**	$6.79\cdot10^{1}$
5	$2.23\cdot10^{6}$	**16**	$9.12\cdot10^{3}$	**27**	$4.02\cdot10^{1}$
6	$1.35\cdot10^{6}$	**17**	$5.53\cdot10^{3}$	**28**	$2.26\cdot10^{1}$
7	$8.21\cdot10^{5}$	**18**	$3.35\cdot10^{3}$	**29**	$1.37\cdot10^{1}$
8	$4.98\cdot10^{5}$	**19**	$2.03\cdot10^{3}$	**30**	8.32
9	$3.02\cdot10^{5}$	**20**	$1.23\cdot10^{3}$	**31**	4.00
10	$1.83\cdot10^{5}$	**21**	$7.49\cdot10^{2}$	**32**	$5.40\cdot10^{-1}$
11	$1.11\cdot10^{5}$	**22**	$4.54\cdot10^{2}$	**33**	$1.00\cdot10^{-1}$

A.2.2 Isotope selection for Th cycle analysis

Consideration has been given to selecting the isotopes whose evolution had to be explicitly simulated when considering also Th-based fuel cycles. Calculations have been initially performed considering as many as 56 Heavy Nuclides (HN), and 179 fission products. In particular, all the actinides lighter than Cf-252 and available in ERANOS JEFF 3.1 libraries were used, except for Np-235, Cm-249, Cm-250, Bk-247 and Bk-250.

Due to the scoping nature of the present calculations, and to reduce the computational burden, it was eventually decided not to consider explicit fission products for the analysis of solid-fuelled FRs, but to limit the analysis adopting the 18 "global pseudo fission products" prepared for sodium-cooled FRs and available in the ERANOS libraries. Such fictitious isotopes were created to account for the main reactivity effects due to fission products in a FR (Tommasi, 2001). Use of pseudo-fission products was found to affect mildly the obtained results (e.g., an underestimation in the 300-500 pcm range was found for a typical equilibrium reactivity, for U and Th cycle in ELSY, respectively). On the other hand, this choice allowed a reduction of the computational time by a factor of three. A further assessment of the impact

of pseudo-fission products on the EQL3D procedure calculations is available in (Krepel et al., 2009).

The selection of the HN was performed based on their impact on reactivity, radiotoxicity and decay heat. As a result, it was decided to consider the following 41 isotopes: Ra-226; Ac-227; Th from 228 to 233, excluding Th-231; Pa from 231 to 233; U from 232 to 238; Np from 237 to 239; Pu from 238 to 242; Am from 241 to 243; Cm from 242 to 248; Bk-249; and Cf from 249 to 252. With respect to other actinide chains commonly adopted in literature for the analysis of the U-based cycle (e.g., by Krepel et al. (2009)), Ra-226, Ac-227, Th-228 and Th-229 were included to calculate the evolution of radiotoxicity and decay heat (see Section A.4). Th-233 has major effects on in-core decay heat. Pa-232 is parent of U-232 and was considered due to its importance in reprocessing and non-proliferation issues. U-237 represents the gateways for the production of TRansUranic isotopes (TRU) in the Th fuel cycle. Finally, Th-230 was considered because it is present in non-negligible amounts in an equilibrium Th cycle. The resulting chain is very similar to the one proposed by Coates and Parks (2010). In particular, with respect to Coates and Parks, the actinide chain is extended above Cm-244 and below Th-230, but it bypasses Th-231, U-231, U-239, Pu-243, Am-244. The isotopes Th-231, U-231 and U-239 are not available in the ERANOS JEFF 3.1 library, while Pu-243 and Am-244 are present in negligible amounts in the core (in the order of few mg in a 50 t inventory) even in a fully closed U-Pu equilibrium cycle. As concerns reactivity at equilibrium, use of the 41 HN (instead of 56) led to an overestimation in the order of few pcm in a typical equilibrium core (U or Th cycle), but allowed a further 10-15% reduction of the computational time.

A.3 EXTENSION TO THE MSR CASE AND APPLICATION TO THE MSFR

The EQL3D procedure has been developed to analyze traditional solid-fuelled FRs. In order to study the performance of MSRs, the procedure has been modified to simulate the online fuel reprocessing. This can be approximated by fission products removal in amounts proportional to their quantity and simulated in EQL3D by adding to the physical decay constant of each fission products a fictitious component. To simulate this reprocessing system, the same actinide chain employed for solid-fuelled FRs is employed (see previous Section) but pseudo-fission products had to be substituted with 126 explicit fission products (not reported here for brevity). Fission products that are removed online are batch-wise replaced with a fresh actinide feed and the time interval for replacement can be arbitrarily selected. A full recycle of actinides is considered in this thesis work. The refueling time is employed as basis for determining the time intervals for cross-section recalculation and flux renormalization, thus representing for the MSRs the equivalent of a cycle of the solid-fuelled FRs (see previous Section).

The overall concentration of actinides and fission products is preserved during irradiation, meaning that a build-up of fission products will reduce the actinide inventory and the density of the fuel. Other studies consider instead the actinide content as constant, with the fission products substituting Li atoms (see e.g. (Aufiero et al., 2012, submitted)). The reason why it has been here decided to maintain a constant concentration of actinides and fission products is that most of the soluble fission products are trivalent lanthanides, whose chemical behavior

is closer to that of the trivalent actinides like Pu, Am and Cm, than to that of LiF. A main consequence is that the actinide content will be reduced with increasing inventory of fission products. This implies that, for a given reprocessing rate, lower conversion ratios will generally be predicted in the present work (see Section 2.2) compared e.g. to (Aufiero et al., 2012, submitted).

Due to the presence of blankets in the MSFR, EQL3D has also been modified to allow for such possibility. In particular, the EQL3D procedure was able to treat blankets only by considering them as part of the fuel. This choice forced to reprocess the blankets together with the fuel (i.e., after the same irradiation time). The possibility of an asynchronous reprocessing of part of the fuel has thus been introduced. In other words, the fuel can be divided into a number of regions, each one featured by a different irradiation time. In this way, the blanket is still to be considered as part of the fuel, but the possibility exists to reprocess it after a different irradiation time.

As regards the calculations performed in the thesis work, the lattice data for the core calculations have been generated using the ECCO cell code with JEFF 3.1-based 1968-group neutronic library. The core calculations have been performed using the transport BISTRO calculation scheme (Gho and Palmiotti, 1984) with S-16 discretization and 33-group (Table A.1) energy collapsed lattice data from ECCO. For symmetry reasons (see Chapter 1), a 2-D r-z geometry is analyzed and only the bottom half of the core is simulated. A schematic view of the geometry implemented in the BISTRO code is reported in Fig. A.1.

The entire primary circuit is treated as a single fuel depletion node to take into account the continuous salt mixing. The addition of the actinide feed is performed every year, which has been proved to bring negligible errors compared to a core reloading performed on a daily basis. In the time interval between two actinide reloads, fluxes and macroscopic cross-sections are recalculated 9 times. The microscopic cross-sections are generally calculated at each actinide reloading (i.e., every year) at the beginning of the simulation, and every few reloadings afterwards.

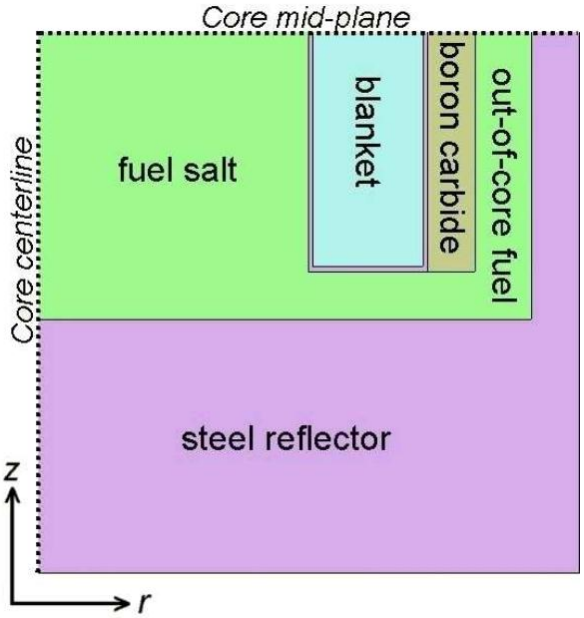

Figure A.1: Analyzed MSFR geometry

The extension of EQL3D procedure to the analysis of the MSFR has been assessed against a SERPENT-based (Leppänen, 2007) procedure subsequently developed at the Politecnico di Milano (Aufiero et al., 2012, submitted). Figs. A.2 and A.3 plot the neutron spectrum and the evolution of Pu and U isotopes, respectively, in a TRU started MSFR with a Th-feed (see Tables 1.3 and 1.7). Table A.2 compares the predictions of the two codes in terms of equilibrium safety parameters for three different feeds from those listed in Table 1.7. An excellent agreement is generally observed. Fig. A.2 shows that the 33-group representation in ERANOS is able to reproduce most spectrum features except for the complicate pattern between 10 keV and 100 keV. However, the impact on reactivity and safety parameters has been found to be minimal (Fiorina et al., 2012a). A slight discrepancy is observed in Fig. A.3 in the prediction of the equilibrium U-232 amount, though the approximation is acceptable for the scope of the work. Finally, discrepancies are observed in Table A.2 in the prediction of the generation time, but this is only due to the fact that SERPENT is not capable of adjoint flux calculations and the reported values are simply average neutron lifetimes.

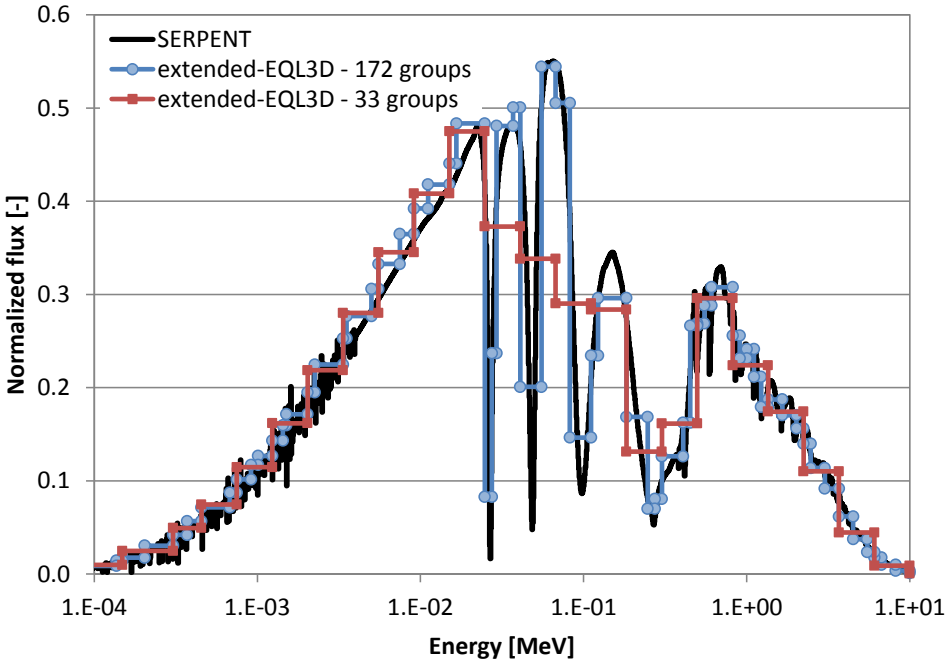

Figure A.2: Neutron spectrum as predicted by extended-EQL3D procedure and by SERPENT

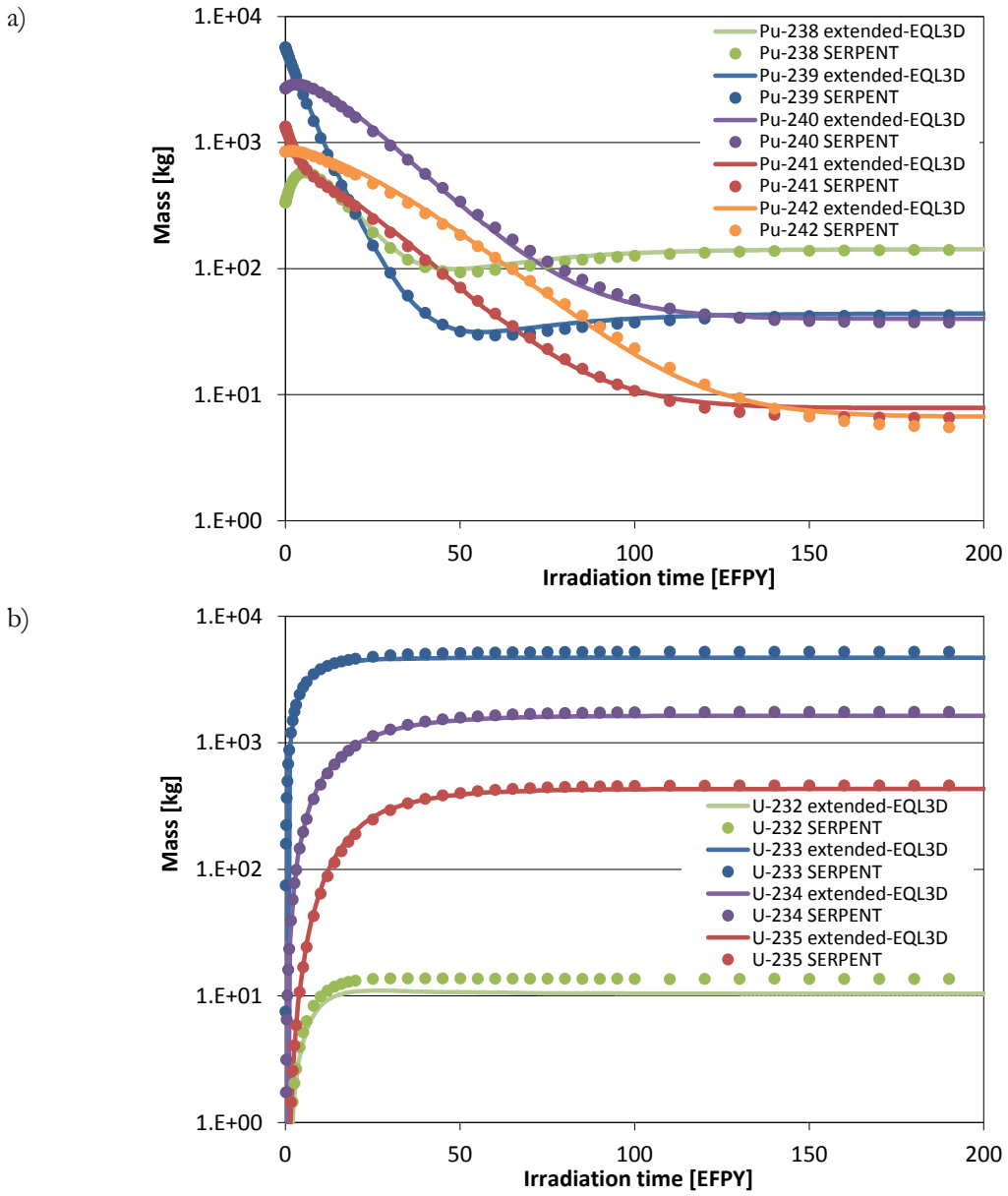

Figure A.3: Evolution of a) Pu and b) U isotopes in a TRU-started Th-feed MSFR as predicted by extended-EQL3D procedure and by SERPENT

Table A.2: Safety parameters as predicted by extended-EQL3D procedure and by SERPENT

		Doppler coeff. [pcm/K]	Expansion coeff. [pcm/K]	Generation time*[μs]	β_{eff} [pcm]
Equilibrium Th-feed	**Extended-EQL3D**	-3.25	-3.01	0.95	334.7
	SERPENT	-3.36±0.1	-3.25±0.1	1.25±0.001	322.2±1
Equilibrium ThU3-feed	**Extended-EQL3D**	-2.91	-3.23	1.01	332.3
	SERPENT	-3.04±0.1	-3.49±0.1	1.30±0.001	318.2±1
Equilibrium ThU3TRU-feed	**Extended-EQL3D**	-1.89	-3.25	0.96	321.6
	SERPENT	-1.95±0.1	-3.32±0.1	1.12±0.001	310.1±1

**Average neutron lifetime for the SERPENT calculations.*

A.4 DEVELOPMENT OF SUB-ROUTINES FOR RADIOTOXICITY AND DECAY HEAT CALCULATIONS

The original EQL3D procedure did not compute radiotoxicity and decay heat of the fuel. For this reason, it was decided to modify it and develop dedicated sub-routines. These new sub-routines use the isotopic composition from EQL3D to perform a simplified decay, keeping track of the most relevant isotopes, and applying the adult ingestion coefficients from the ICRP72 (ICRP, 1996) to calculate radiotoxicity. The decay heat is computed using the Q-value of the reactions. This is correct for alpha decay and represents a good approximation for gamma decay. The use of Q-value for beta decay leads to a systematic overestimation because the portion of the energy carried away by neutrinos is not subtracted. Beta decay is particularly important during reactor operation, but it becomes unimportant after few months of cooling (Salvatores, 2002). Accordingly, decay heat calculations are expected to be correct for long-term cooling, but will overestimate the in-core decay heat.

The main obstacle which was encountered while setting-up the new sub-routine is related to the limited number of isotopes available in the ERANOS JEFF3.1 library. This library was created for reactor calculations and only isotopes heavier than radium are available while, for radiotoxicity calculations, all the isotopes in the decay chains down to the stable isotopes need to be considered. There are four main actinide decay chains: the radium, actinium, thorium and neptunium chains, which end in the stable isotopes Pb-206, Pb-207, Pb-208, Bi-209, respectively (Krane, 1988). The decay time of the isotopes in the lower part of these chains (i.e., close to the stable isotopes) generally decreases with decreasing mass number, so that for each chain it was possible to select one parent isotope which: 1) is available in the adopted library, and 2) whose half-life is orders of magnitude longer than those in the progeny. Table A.3 reports the half-lives of these four isotopes, together with the longest-lived isotope in their progeny.

Table A.3: Isotopes selected for radiotoxicity and decay heat calculations for the lower part of the decay chains

Chain	Selected parent isotope	Parent isotope half-life	Longest-lived isotope in the progeny	Half-life of the longest-lived isotope in the progeny
Radium	^{226}Ra	1600 years	^{210}Pb	22.3 years
Actinium	^{227}Ac	21.8 years	^{227}Th	18.7 days
Thorium	^{228}Th	1.9 years	^{224}Ra	3.7 days
Neptunium	^{229}Th	7340 years	^{225}Ra	14.9 days

When the half-life of the progeny is orders of magnitude below that of the parent, and after a period of time equal to 6-7 times the half-life of the longest-lived isotope in the progeny, parent and progeny approximately reach a "secular equilibrium" state (Krane, 1988) where each isotope has the same activity. In the present thesis work, the 4 parents listed in Table A.3 are considered to be always in secular equilibrium with their progeny. The activity of the parents, that are all available in the JEFF3.1 ERANOS library, is then used for computing radiotoxicity and decay heat of the progeny, thus overcoming the incompleteness of the library. Secular equilibrium is also assumed for the other isotopes not directly simulated. In particular, Ra-228 and Ac-228 are considered to have the same activity as Th-232 and Th-

234, and Pa-234 the same as U-238. Cm-241, Th-231, Pu-243 and Pu-244 are instead considered to have the same activity as Am-241, U-235, Cm-247 and Cm-248, respectively.

As mentioned, secular equilibrium is approximately reached after a period equal to 6-7 times the half-life of the longest-lived isotope. This means that after ~100 days it is possible to correctly predict radiotoxicity and decay heat of the progeny of Ac-227, Th-228 and Th-229 by making use of the secular equilibrium assumption. Approximately 100 years are instead necessary for considering Ra-226 in equilibrium with the progeny. Assumption of secular equilibrium for shorter periods of time is then expected to lead to an overestimation of the activities and, consequently, of radiotoxicity and decay heat. In addition, the condition of secular equilibrium is applicable if an initial given amount of the parent nuclide is considered. In the present case, the chosen 4 parents are continuously fed by the decay of heavier nuclides. This leads to a systematic overestimation of the progeny activities when calculated assuming secular equilibrium.

The new sub-routines have been systematically assessed against ORIGEN-S (SCALE, 2006). In particular, ORIGEN-S is employed to calculate the radiotoxicity and decay heat starting from the masses calculated through the standard EQL3D procedure. A comparison between ERANOS and ORIGEN-S in terms of in-core fuel depletion calculations is instead beyond the scope of the work. As case study, the ELSY core (Section B.2) has been considered and three different core compositions have been selected, namely a Th-Pu BOL (Beginning Of Life) loading, with the Pu vector reported in column 2 of Table 1.3, and the equilibrium Th-U and U-Pu cases (Table 2.1).

Fig. A.4 plots the evolution with time of the radiotoxicity associated to the three mentioned fuel inventories in the ELSY, showing an excellent agreement between ORIGEN-S and the extended-EQL3D procedure. This indicates that the assumption of secular equilibrium adopted in the development of the EQL3D radiotoxicity sub-routine leads to negligible errors. Some problems could have been expected in the long-term radiotoxicity of the equilibrium Th-U core, which is dominated by Th-229 and Ra-226, two of the parent isotopes that are considered to be in secular equilibrium with their progeny. Nevertheless, discrepancies between ERANOS and ORIGEN-S in this period are on the order of few per cents (e.g., 1.2% at 10^5 years). This is explained by: 1) the time elapsed from the beginning of the decay, which is widely sufficient for the onset of secular equilibrium for Th-229, Ra-226 and their progenies; 2) the slow variation of the quantity of such isotopes, which does not strongly affect the equilibrium. In the first few years, where secular equilibrium is not established, the contribution of Ra-226, Ac-227, Th-228 and Th-229 to the total radiotoxicity is generally small, thus making the error introduced by assuming secular equilibrium negligible. Among these 4 isotopes, the only appreciable contributor is Th-228 in the Th-U equilibrium case. However, the longest-lived daughter of this isotope has a half-life of only 3.7 days (Table A.3), thus allowing a rapid establishment of the equilibrium.

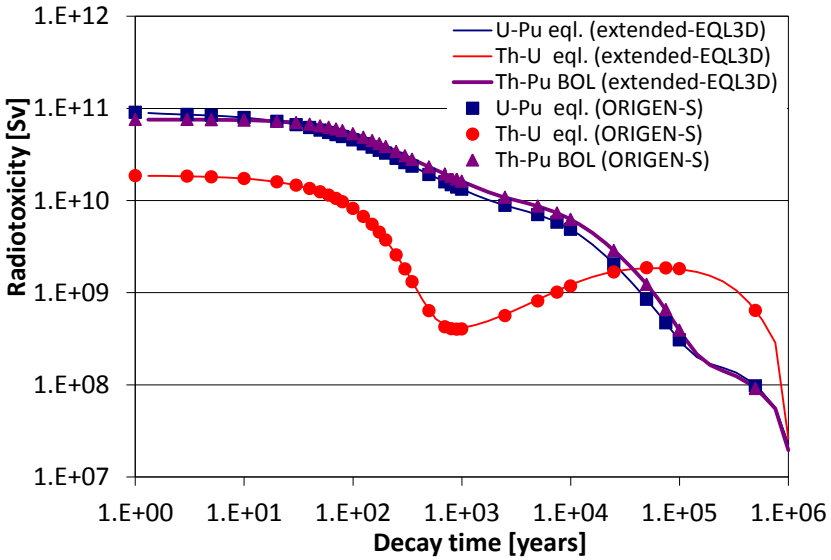

Figure A.4: Evolution of the radiotoxicity associated to the ELSY actinide inventory for a Th-Pu BOL core and the two U-Pu and Th-U equilibrium compositions. Comparison between the results provided by ORIGEN-S and by the extended-EQL3D procedure

Fig. A.5 plots the evolution with time of decay heat while Fig. A.6 shows the difference between the predictions of the extended-EQL3D procedure and ORIGEN-S. A systematic overestimation can be observed in Fig. A.6 for the results provided by the former, as a consequence of both: 1) secular equilibrium hypothesis; and 2) calculation of the heat released by beta decay by means of the reaction Q-value. However, the discrepancy between the two codes remains on the order of some percents (typically 3-4%) starting from one year, confirming that beta decay actually plays a minor role in decay heat of actinides (Salvatores, 2002). Use of Q-value for beta decay becomes instead unacceptable in calculating decay heat immediately after reactor shut-down. For U-Pu and Th-U equilibriums, this approximation leads to overestimations equal to 54% and 104%, respectively. In particular, immediately after shut-down decay heat from actinides is dominated by Np-239 for U-Pu equilibrium and by Th-233 and Pa-233 for Th-U equilibrium, which are all beta emitters. Np-239 accounts for 70% of the decay heat from actinides for U-Pu equilibrium, while Th-233 and Pa-233 accounts for 67% and 31% of it in the Th-U equilibrium. Problems are not encountered for Th-Pu BOL, which is free from beta emitters at the beginning of the decay. In view of the observed discrepancies, ORIGEN-S is used in the thesis to predict actinide decay heat in the short term.

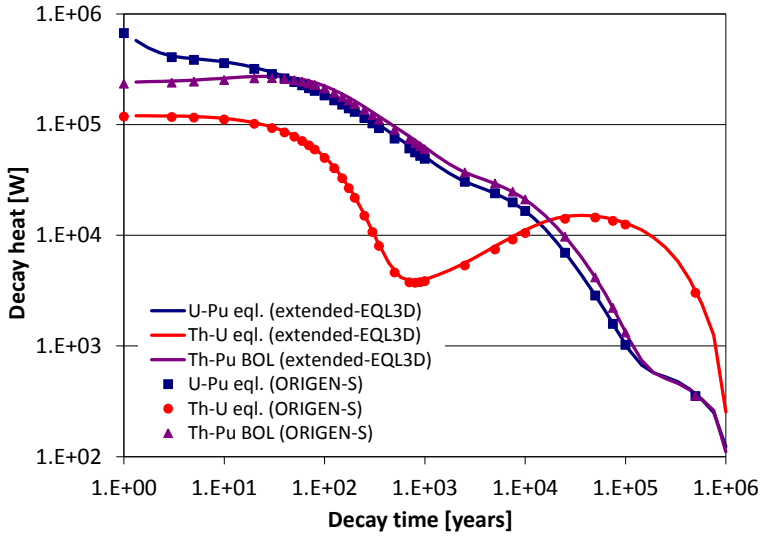

Figure A.5: Evolution of the decay heat associated to the ELSY actinide inventory for a Th-Pu BOL core and the two U-Pu and Th-U equilibrium compositions. Comparison between the results provided by ORIGEN-S and by the extended-EQL3D procedure

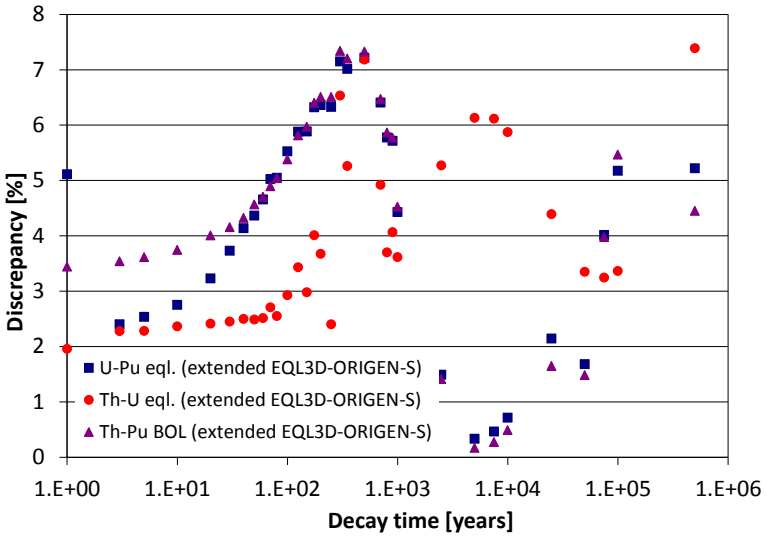

Figure A.6: Discrepancies in the decay heat as predicted by the extended-EQL3D procedure and by ORIGEN-S

A.5 REACTIVITY DECOMPOSION WITH ERANOS AND THE EQL3D PROCEDURE

Reactivity decomposition techniques are available based either on perturbation theory or on neutron balances. The latter technique has been adopted in the present thesis work. The starting point for this methodology is the well-known expression for reactivity:

$$\rho(x) = 1 - \frac{L(x)+C(x)+F(x)}{P(x)} \qquad (A.1)$$

where reaction rates are assumed to be a function of a parameter x (e.g., coolant density). Such methodology then focuses on the consequences of a perturbation, providing different results with respect to the more commonly adopted perturbation theory, which focuses on the causes of reactivity effects. By elaborating Eq. A.1, it is possible to decompose the reactivity variation associated to a variation of a parameter x from x_1 and x_2 as:

$$\delta\rho_L = -\frac{P(x_1)+P(x_2)}{2P(x_1)P(x_2)}\delta L \tag{A.2}$$

$$\delta\rho_C = -\frac{P(x_1)+P(x_2)}{2P(x_1)P(x_2)}\delta C \tag{A.3}$$

$$\delta\rho_F = -\frac{P(x_1)+P(x_2)}{2P(x_1)P(x_2)}\delta \mathrm{F} \tag{A.4}$$

$$\delta\rho_P = \frac{L(x_1)+L(x_2)+C(x_1)+C(x_2)+F(x_1)+F(x_2)}{2P(x_1)P(x_2)}\delta P \tag{A.5}$$

Reaction-wise components can be also subdivided into group-wise or isotope-wise subcomponents. In this case, the total difference of a reaction rate is broken-down into isotope and group-wise components.

An issue related to reactivity decomposition based on neutron balances is represented by normalization. In fact, reaction rates depend on the flux level, and a proper normalization is required to compare nominal and perturbed states. Typically, normalization is performed through production rates while, in the present thesis work, the average neutron flux in the active core is used as recently proposed by Krepel et al. (2011). In particular the following condition is applied:

$$\int_{core}\Sigma_g\ \phi_g(x_1)dVol\Big/_{Vol(x_1)} = \int_{core}\Sigma_g\ \phi_g(x_2)dVol\Big/_{Vol(x_2)} \tag{A.6}$$

This kind of normalization allows to preserve the effect of variation in effective one-group cross-sections. In fact, a core perturbation is always accompanied by a variation in cross-sections and, with a fixed flux, these variations will be reflected in the respective total reaction rates. In particular, a variation in one-group fission cross-section will determine a variation in fission rate, which is instead hidden by normalizations based on productions.

Safety parameters, reaction rates and fluxes in Eqs. A.1 to A.6 are obtained by means of the ERANOS 2.2N code (using VARIANT or BISTRO for solid-fuelled FRs and the MSFR, respectively) and calculations are always been performed using 33 energy groups, whose upper boundaries are those reported in Table A.1.

A.6 CONCLUDING REMARKS

This Appendix has focused on the main tools and methodologies employed in this thesis for core physics and fuel depletion calculations. The ERANOS-based EQL3D procedure for FR analysis has been presented, including all specific methodological choices made in the

frame of this thesis. Its extension to the analysis of MSRs (and the MSFR in particular) has then been presented and assessed against a SERPENT-based tool recently developed at the Politecnico di Milano. Additional sub-routines for calculating radiotoxicity and decay heat of the actinide inventory have been developed and assessed against the dedicated code ORIGEN-S. Finally, a reactivity decomposition technique frequently adopted in the thesis work has been presented.

REFERENCES

Artioli, C., Grasso, G., Sarotto, M., Krepel, J., 2009. ELSY neutronic analysis by deterministic and Monte Carlo methods: an innovative concept for the control rod systems. Proc. ICAPP 2009, May 10-14, Tokyo, Japan.

Aufiero, M., Cammi, A., Fiorina, C., Luzzi, L. 2012. Modification of the SERPENT code to study the fuel isotopic evolution of molten salt reactors with online (continuous) reprocessing. Presentation for "2012 SERPENT International Users Group Meeting". September 19-21, Madrid, Spain.

Aufiero, M., Cammi, A., Fiorina, C., Leppänen, J., Luzzi, L., submitted. An extended version of the SERPENT-2 code to investigate fuel burn-up and core material evolution of the Molten Salt Fast Reactor. Submitted to Journal of Nuclear Materials. Presentation at NuMat 2012 conference, October 22-25, Osaka, Japan.

Coates, D. J., Parks, G.Y., 2010. Actinide evolution and equilibrium in fast thorium reactors. Annals of Nuclear Energy 37, 1076-1088.

Fiorina, C., Aufiero, M., Cammi, A., Guerrieri, C., Krepel, J., Luzzi, L., Mikityuk, K., Ricotti, M. E., 2012a. Analysis of the MSFR Core Neutronics Adopting Different Neutron-Transport Models. Proc. ICONE 2012, July 30 – August 3, Anaheim, US.

Fiorina, C., Cammi, A., Krepel, J., Mikityuk, K., Ricotti, M. E., 2012b. Preliminary Analysis of the MSFR Fuel Cycle Using Modified-EQL3D Procedure. Proc. ICONE 2012, July 30 – August 3, Anaheim, US.

Fiorina, C., Cammi, A., Franceschini, F., Krepel, J., Mikityuk, K., Ricotti, M. E., 2013. Analysis of thorium and uranium fuel cycles in an iso-breeder Lead Fast Reactor using extended-EQL3D procedure. Annals of Nuclear Energy 53, 492-506.

Fiorina, C., Aufiero, A., Cammi, A., Franceschini, F., Krepel, J., Luzzi, L., Mikityuk, K., Ricotti, M. E., submitted. Investigation of the MSFR core physics and fuel cycle characteristics. Submitted to Progress in Nuclear Energy.

Gho, C.J., Palmiotti, G., 1984. BISTRO: bidimensionnel Sn transport optimise: un programme bidimensionnel de transport sn aux differences finies. Technical Report, NT - SPRC - LEPh - 84-270, CEA. France.

ICRP, International Commission on Radiological Protection, 1996. ICRP Publication 72: Age-dependent Doses to the Members of the Public from Intake of Radionuclides Part 5, Compilation of Ingestion and Inhalation Coefficients. Annals of the ICRP 26/1.

Krane, K. S., 1988. Introductory Nuclear Physics. John Wiley & Sons. New York, US.

Krepel, J., Pelloni, S., Mikityuk, K., Coddington, P., 2009. EQL3D: ERANOS based equilibrium fuel cycle procedure for fast reactors. Annals of Nuclear Energy 36, 550–561.

Krepel, J., Pelloni, S., Mikityuk, K., Coddington, P., 2010. GFR equilibrium cycle analysis with the EQL3D procedure. Nuclear Engineering and Design 240, 905–917.

Krepel, J., Saliba, J., Mikityuk, K., Chawla, R., 2011. Comparison of safety related parameters in the equilibrium closed cycle for Generation-IV fast reactors. Proc. GLOBAL 2011, December 11-16, Chiba, Japan.

Leppänen, J., 2007. Development of a new Monte Carlo reactor physics code. PhD Thesis. Helsinki University of Technology.

Rimpault, G., 1997. Physics documentation of eranos the ecco cell code. Technical Report. RT-SPRC-LEPh-97-001.

Rimpault, G., Plisson, D., Tommasi, J., Jacqmin, R., Rieunier, J., Verrier, D., Biron, D., 2002. The ERANOS code and data system for fast reactor neutronic analyses. Proc. PHYSOR 2002, October 7-10, Seoul, Korea.

Ruggeri, J.M., 1999. ERANOS : manuel des methodes : reconstruction fine d'un flux nodal. Technical Report. NT-SPRC-LEPH-99-217.

Salvatores, M., 2002. The physics of transmutation in critical or subcritical reactors. Comptes Rendus Physique 3, 999–1012.

SCALE: A Modular Code System for Performing Standardized Computer Analyses for Licensing Evaluations, ORNL/TM-2005/39, Version 5.1, Vols. I–III, November 2006. Available from Radiation Safety Information Computational Center at Oak Ridge National Laboratory as CCC-732.

Sublet, J.C., Dean., C., Plisson-Rieunier, D., 2006. ECCOLIB-JEFF-3.1 libraries. Technical Report. CEA-R-6100.

Tommasi, J., 2001. Creation de pseudo-produits de fission pour eranos (bibliotheques jeff-3.1). Technical Note. SPRC/LEPh 06-201.

APPENDIX B: Traditional solid-fuelled Fast Reactor designs

ABSTRACT

This Appendix presents two Fast Reactor designs employed throughout the thesis work to provide a comparison for the MSFR performances. In particular, a lead-cooled iso-breeder reactor and a sodium-cooled burner reactor have been selected. Both have been developed to operate in a close U-based cycle. Th-based versions have been here preliminary designed to allow for a better performance comparison with the MSFR. For the sodium-cooled reactor, also two iso-breeder core designs have been preliminarily set up. Some of the main results have been presented in (Fiorina et al., 2011, 2012, 2013).

B.1 INTRODUCTION

The present thesis work attempts a characterization of the MSFR performances primarily through a comparison with traditional Fast Reactors (FR). To this purpose, two representative FRs have been selected and analyzed in details, namely, the European Lead SYstem (ELSY) and the Toshiba-Westinghouse Advanced Recycling Reactor (ARR). The ELSY (Section B.2) is an iso-breeder (Conversion Ratio (CR) equal to 1) lead-cooled FR while the ARR (Section B.3) is a sodium-cooled FR designed for TRansUranic isotope (TRU) burning. Both reactors have been designed to use natural or depleted U as fertile material. Th-based versions have been here preliminary designed to allow a better performance comparison with the MSFR. For the ARR, also two Th- and U-based iso-breeder cores have been set up using a dense fuel (i.e., metal or nitride) an adding radial and axial fertile blankets.

B.2 EUROPEAN LEAD SYSTEM - ELSY

The ELSY (Alemberti et al., 2011) was designed during the EURATOM sixth framework program (2002-2006) and further developed in the LEADER (Lead-cooled European Advanced Demonstration Reactor) project of the seventh framework program (2007-2011). It is an iso-breeder lead-cooled FR for electricity production and capable of minor actinide burning. It was designed to work in a traditional U-Pu fuel cycle, with oxide fuel and a homogeneous core configuration (i.e., without blankets). The ELSY design presented by Alemberti et al. (2011) has been chosen as reference in this thesis. As mentioned, an additional modified version has also been designed to maintain the iso-breeder behavior in a Th cycle. In

this way, the new core can be operated with Th-232 as the only feed and maintain positive reactivity at equilibrium. In line with the nominal U-Pu core, Th oxides (Aronson et al., 1967; Benedict et al., 1981; Rodriguez and Sundaram, 1981) were selected as fuel form. Same pin and assembly designs as for the U-Pu counterpart have been adopted for the Th core. Characterizing parameters of the standard U-Pu ELSY core and of the preliminary designed Th-U version are summarized in Table B.1, while schematic representations of core and fuel assembly designs are reported in Fig. B.1.

Table B.1: Main design parameters for the ELSY core designs

	U-based	Th-based
CR	~1	
Thermal / electric power	1500 MW / 600 MW	
Coolant	Pb	
Coolant inlet / outlet temperatures	673 / 753 K	
Clad / duct material	T91	
Assembly type	Hexagonal with duct	
Assembly flat-to-flat distance: wrapper in /out	20.3 cm / 21.1 cm	
Assembly center-to-center distance	21.6 cm	
Pin lattice / pitch	Triangular / 15.5 mm	
Pins per assembly	169	
Active core height	1.2 m	1.7 m
Pellet diameter; clad diameter (inner / outer)	9.1; 9.4/10.6 mm (1.5 mm hole)	
Number of assemblies in inner / middle / outer zone	163 / 102 / 168	
Fuel form / smeared density	Oxides / 87 %TD*	
Fuel TD*	10.96 g/cm^3	
Number of control and safety rods	18	
Number of batches	3	
Refueling interval / time	2 years / 30 d	2.82 years / 30 d
Core HN inventory**	51 t	72 t

**Theoretical Density* ***Heavy Nuclides*

a) b)

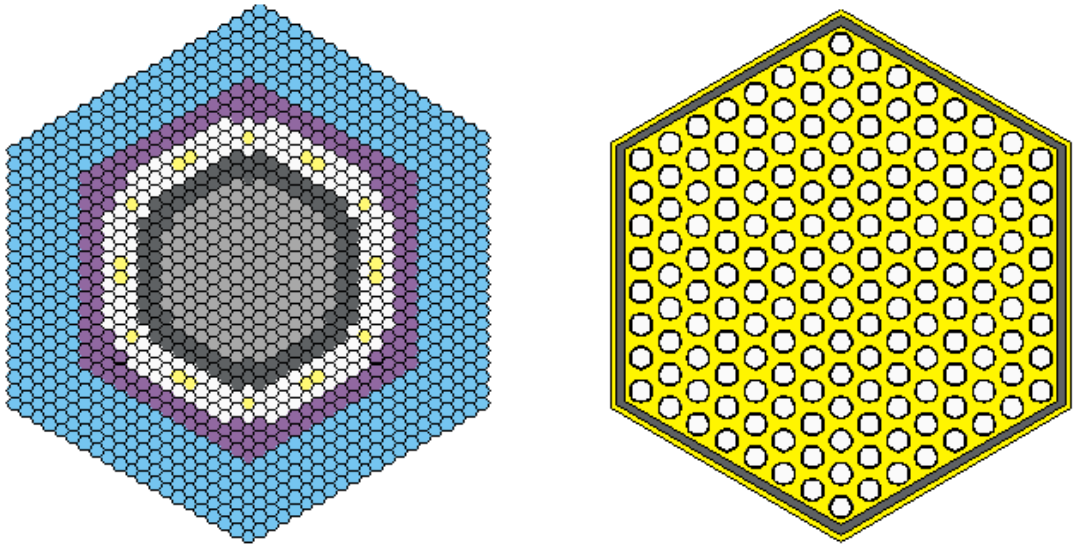

Figure B.1: a) ELSY core layout. Light grey=inner core; dark grey=middle core; white=outer core; yellow=control rods; violet=dummy assemblies; blue=lead. b) ELSY assembly layout

Replacing ThO_2 feed with UO_2 feed without any core modifications leads to a strongly negative equilibrium reactivity, as a consequence of the inferior breeding performance. In order to maintain an iso-breeding configuration, it was decided to increase the core height until the criticality at the end of the equilibrium cycle was reached. After some iteration, it was found that the core height needs to be increased from 1.2 m to 1.7 m. The choice of increasing the core height is not necessarily optimal from a design viewpoint. It minimizes leakages compared to other options, which in turn minimizes the actinide inventory necessary to achieve iso-breeding. Increasing the core height also allows to maintain lead velocities and lead axial temperature increase in the core, two of the main constraints in the ELSY design. This choice is convenient to illustrate the various effects at play without proceeding to a full core redesign, which is out of the scope of the present work. Some information about the impact of different design choices on the ELSY performance parameters can be found in (Fiorina et al., 2013).

The discharge burnup in the ELSY is limited by fuel cladding damage (<100 dpa (Sobolev et al., 2009)). The standard U-Pu core complies with this constraint. In order to maintain the cladding damage within acceptable limits, the average discharge burnup (64 GWth-d/t_{HN}) of the U-Pu core has been adopted for the Th-U core. This choice led to ~8.5-year fuel irradiation time, compared to the 6 years of the U-Pu option. Given the reduced specific power of the Th core design due to the taller core, the longer irradiation time still leads to a cladding fluence ~10 % below that of the U-Pu fuel. In view of the similar spectrum, cladding damage is also expected to remain smaller than, or comparable to, the U-Pu case.

The assumption of fixed mass of actinides in EQL3D (see Appendix A) implies that the density of the remanufactured fuel, from beginning of life to equilibrium, remains constant. In principle, the fuel theoretical densities will vary through the recycles due to the changing fuel actinide composition. In addition, the determination of the smeared density (i.e., the fuel mass divided by the volume inside the active part of the pins) depends on the fuel form and manufacturing technique, which is still speculative at this stage. Also the smeared density will likely change through the cycles of manufacturing as a result of challenging conditions from increasingly radioactive fuel and He release from alpha decay of higher actinides. Smeared densities are typically 80-90 %TD. For simplicity, a smeared density of 87%TD (Alemberti et al., 2011), and the UO_2 TD of 10.96 g/cm^3 (Orlov et al., 2001) were assumed for all cases considered. Uranium is the main component in a U-Pu core and the second in a Th-U core. The value adopted is between ThO_2 and PuO_2 densities, thus representing a reasonable value for an initial Th-Pu core. While the adopted value underestimates the U-Pu fuel density and overestimates that of Th-U, the impact on the core actinide content is expected to be marginal. In fact, in (Fiorina et al., 2011), the actinide content necessary for a Th-based iso-breeder reactor was found to be fairly independent of the actinide density of the adopted fuel. The assumed fuel density will impact core dimensions, leading to a slightly larger difference between the iso-breeder U-Pu and Th-U core height than that calculated here.

The fuel linear expansion coefficient depends on the fuel type, but differences are generally small for the fuels considered (Aronson et al., 1967; Orlov et al., 2001; Rodriguez and Sundaram, 1981). Therefore, the same linear expansion coefficient, equal to $12 \cdot 10^{-6}$ K^{-1}, has been considered for all fuels.

B.3 ADVANCED RECYCLING REACTOR - ARR

The second FR design employed is the sodium-cooled Toshiba-Westinghouse ARR (Dobson, 2008). Both metallic and oxide fuel options were foreseen in the original ARR, but only U was considered as the fertile material. The only blanket present was a lower axial blanket, which allowed to achieve a CR close to 1 for the metallic fuel option, and inferior to 1 for the oxide fuel option. Some modifications have been made to the original core design to lower the CR (burner designs) as well as to reach iso-breeder configurations. Both U and Th options have been considered. Table B.2 reports the main core parameters for the resulting 4 ARR versions while Figs. B.2 and B.3 show the radial core layouts and the assembly layout, respectively. Note that the core design is identical for the Th and U-based burner options, while the two iso-breeder cores have the same radial core map but different axial blankets.

Table B.2: Main design parameters for the ARR core designs

	U-based burner	**Th-based burner**	**U-based iso-breeder**	**Th-based iso-breeder**
CR	~0.4/0.5*	~0.3/0.4*	~1	~1
Thermal / electric power	1000 MW / 420 MW			
Coolant	Na			
Coolant inlet / outlet temperatures	668 / 823 K			
Clad / duct material	HT-9			
Assembly type	Hexagonal with duct			
Assembly flat-to-flat distance: wrapper in /out	12.4 cm / 13.0 cm			
Assembly center-to-center distance	13.3 cm			
Pin lattice / pitch	Triangular / 7.41 mm			
Pins per assembly	271			
Active core height	0.6 m			
Pellet diameter; clad diameter (inner / outer)	4.71; 5.44 / 6.50 mm			
Inner / outer fuel assemblies	192 / 132			
Fuel form / smeared density	Oxide / 85%TD		Metallic (10% Zr alloy) / 75%TD	Nitride (95% N-15 in N) / 85%TD
Fuel TD	10.51 g/cm³	11.14 g/cm³	16.01 g/cm³	12.33 g/cm³
Assemblies used as external radial blanket	-	-	90	90
Assemblies used as internal radial blanket	-	-	7	7
Number of control and safety rods	37	37	30	30
Upper axial blanket	-	-	10 cm	30 cm
Lower axial blanket	-	-	10 cm	36 cm
Number of batches	3			
Refueling interval / time	1 year / 30 d			
Core HN inventory	8.9 t	10.2 t	13.2 t	12.1 t
Blanket HN inventory	-	-	9.6 t	20.1 t

**Depending on the feed (see Table 3.4).*

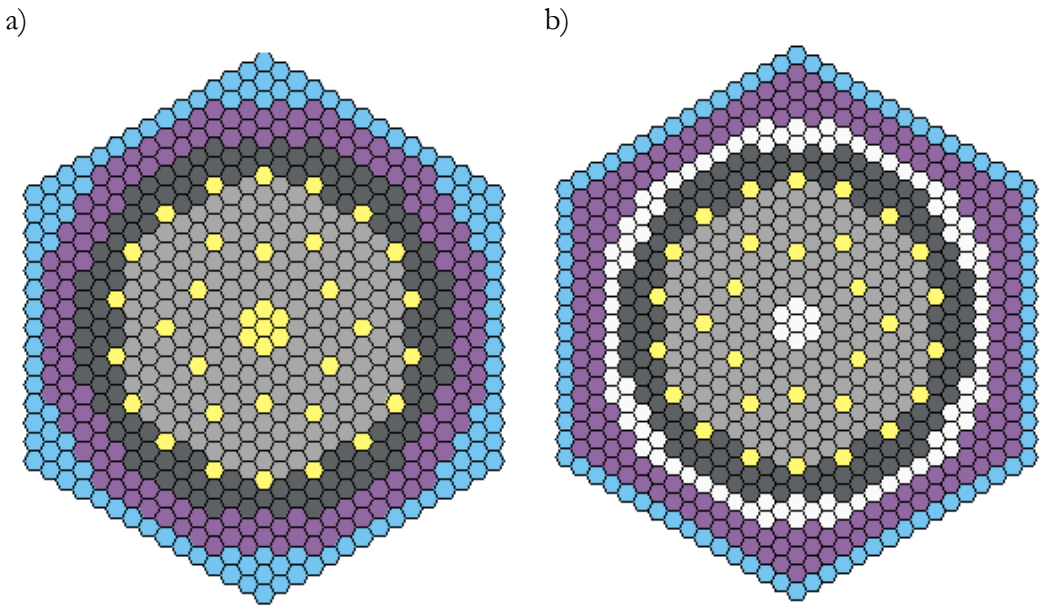

Figure B.2: ARR core layout: a) U- or Th-based burner, and b) U- or Th-based iso-breeder. Light grey=inner core; dark grey=outer core; yellow=control rods; violet=steel shield; blue=B4C shield; white=blanket

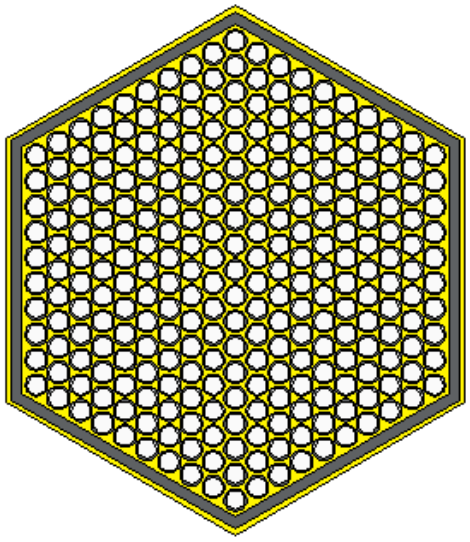

Figure B.3: ARR assembly layout

As shown in Table B.2, the oxide fuel option has been retained for the burner configuration developed for this study but the axial lower blanket has been removed to further decrease the CR. As concerns the iso-breeder cores, Zr-alloyed metallic fuel was chosen for the U iso-breeder configuration due to the superior breeding performance compared to U oxide fuel fostered by the higher HN density. Metallic Th features lower HN density (Rodriguez and Sundaram, 1981) than nitride Th fuel, further decreased if Zr-alloying is adopted. Therefore nitrides (95% enriched in N-15) have been selected for the iso-breeder Th configuration. Unlike the burner ARR design, the iso-breeder U and Th designs employ blankets of respectively ZrU with depleted U and ThN. The radial blankets consist of a peripheral blanket and one blanket region at the center of the core (Fig. B.2b). Axial blankets at the bottom and top of the active fuel are also employed. Compared to U, Th features same

radial blankets but a nearly 50 cm thicker axial blanket to compensate the deficit in breeding performance. Although not optimized, the two iso-breeder core designs adopted are suitable to compare the core physics performances of the two fuel options.

As noted, oxide fuel has been selected in this work for the burner ARR while Zr-alloyed metallic-fuel and nitrides enriched in N-15 have been chosen respectively for the U- and Th-based iso-breeder designs. The fuel density of each fuel mixture has been calculated through a volume-weighted average of the densities of the single components (e.g., ThO_2, UO_2, NpO_2, PuO_2, etc. for Th-U-TRU oxide fuel). Since the EQL3D neutronic procedure used assumes constant fuel density (see Appendix A), the fuel density of each option has been evaluated using the equilibrium compositions. Smeared densities have been assumed equal to 85%TD except for the metal fuel case, where 75%TD smeared density has been employed. The linear expansion coefficients assumed are $11.2 \cdot 10^{-6}$ K^{-1} and $12 \cdot 10^{-6}$ K^{-1} for the U-based and Th-based oxide fuels, $14 \cdot 10^{-6}$ K^{-1} and $8.2 \cdot 10^{-6}$ K^{-1} for the U-based metallic fuel and the Th-based nitride fuel, respectively (Aronson et al., 1967; Orlov et al., 2001).

While feasibility of the various options based on detailed power peak analysis has not been ascertained, the average fast fluence for the various cases in the single-batch model adopted is within 15% of the $1.6 \cdot 10^{23}$ n/cm^2 ARR design value. It is therefore reasonable to expect that optimized multi-batch refueling schemes can be found to convey similar peaking factors, and acceptable peak fast neutron fluences, for all cases investigated.

B.4 CONCLUDING REMARKS

This Appendix has focused on the traditional FR designs employed in the thesis work to provide comparative performances for the MSFR. The iso-breeder lead-cooled ELSY has first been presented, including a Th-based version that has been purposely set up to extend the comparison between MSFR and traditional solid-fuelled FRs to the case of Th use also in the latters. The burner sodium-cooled ARR has then been presented. Also in this case, Th-based versions have been included. In addition, two U- and Th-based iso-breeder designs have been preliminary proposed.

REFERENCES

Alemberti, A., Carlsson, J., Malambu, E., Orden, A., Struwe, D., Agostini, P., Monti, S., 2011. European lead fast reactor – ELSY. Nuclear Engineering and Design 241, 3470-3480.

Aronson, S., Cisney, E., Gingerich, K.A., 1967. Thermal expansion of some cubic refractory compounds of thorium. Journal of the American Ceramic Society 50, 248-252.

Benedict, M., Pigford, T.H., Levi, H. W, 1981. Nuclear Chemical Engineering (2nd Edition), McGraw Hill.

Dobson, A., 2008. GNEP Deployment Studies Preliminary Conceptual Design Studies. Technical Report. Volume IV - Advanced Recycling Reactor.

Fiorina, C., Franceschini, F., Krepel, J., Mikityuk, K., 2011. Comparative analysis of uranium and thorium fuel cycles in a Lead-cooled Fast Reactor from the perspective of safety and waste management. Proc. GLOBAL 2011, December 11-16, Chiba, Japan.

Fiorina, C., Cammi, A., Franceschini, F., Krepel, J., Luzzi, L., Ricotti, M. E. Thorium fuel cycle in Fast Reactors: potential benefits and challenges. Proc. NENE 2012, September 5-7, Ljubljana, Slovenia.

Fiorina, C., Cammi, A., Franceschini, F., Krepel, J., Mikityuk, K., Ricotti, M. E., 2013. Analysis of thorium and uranium fuel cycles in an iso-breeder Lead Fast Reactor using extended-EQL3D procedure. Annals of Nuclear Energy 53, 492-506.

Orlov, V.V., Filin, A.I., Smirnov, V.S., Sila-Novitsky, A.G., Tsykunov, V.S., Leonov, N., Smirnov, V.P., Lopatkin, A.V., Ganev, I.Kh., Bosin, S.N., Abramob, V.A., Emelyantseva, I., Khacharesov., G.A., Kogut, V.A., 2001. Naturally safe lead-cooled fast reactor for large-scale nuclear power. Final report ISTC, Moscow.

Rodriguez, P., Sundaram, C. V., 1981. Nuclear and materials aspects of the thorium fuel cycle. Journal of Nuclear Materials 100, 227-249.

Sobolev, V., Malambu, E., Aït Abderrahim, H., 2009. Design of a fuel element for a lead-cooled fast reactor. Journal of Nuclear Materials 385, 392-399.

APPENDIX C: Generalized approach to the heat transfer in channels with internally heated fluids

ABSTRACT

This Appendix presents an approach to the heat transfer in internally heated fluids flowing in forced convection and turbulent regime in a straight circular channel. The approach has been derived by Di Marcello et al. (2010), Di Marcello (2010) and by the author (Cammi et al., 2009; Fiorina, 2009; Luzzi et al., 2010) and is employed in Chapter 5 to derive a heat transfer correlation to be used for the MSFR out-of-core components.

C.1 INTRODUCTION

In view of the little information available in the open literature, a research activity has been undertaken at the Politecnico di Milano (Fiorina, 2009; Di Marcello et al., 2010; Di Marcello, 2010; Luzzi et al., 2010) regarding the heat transfer phenomena in the core of graphite-moderated Molten Salt Reactors (MSR). This activity allowed to obtain a general mathematical formulation to predict the temperature field in internally heated fluids flowing in turbulent regime in a straight circular channel. Such formulation is employed in Chapter 5 to derive a heat transfer correlation to be used for the MSFR out-of-core components, where heat is generated by the decay of actinides and fission products.

C.2 ANALYTIC SOLUTION TO THE HEAT TRANSFER PROBLEM

A fluid with internal heat generation, flowing in turbulent flow regime in a straight circular channel surrounded by a heat generating solid region is considered. The external part of the solid region is assumed to be adiabatic. Hydrodynamic development is assumed at the entrance of the heated section and buoyancy effects are neglected. Fig. C.1 illustrates schematically selected geometry, main assumptions, and the adopted coordinate system. This geometry is representative of the core channels of a graphite-moderated MSR, but also of a generic pipe or channel in the MSFR primary circuit. Application to the MSFR core is instead precluded and the computation of temperature and velocity fields requires in that case adoption of CFD codes.

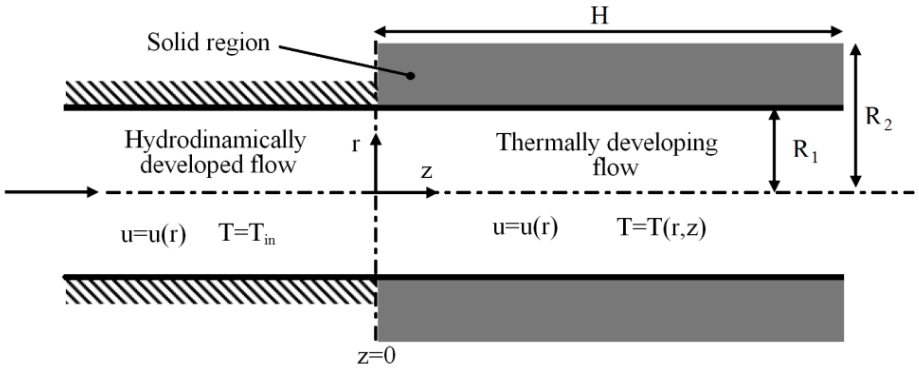

Figure C.1: Schematic view of the analyzed geometry and main assumptions

The overall analytic solution of the heat transfer problem, with reference to the geometry shown in Fig. C.1, is obtained by coupling two separate analytic solutions for the fluid and the solid region through an iterative procedure. The heat transfer problem of fluids inside circular channels, generally known as the Graetz problem (Graetz, 1883, 1885), is described by the following equation and boundary conditions:

$$u\frac{\partial T(r,z)}{\partial z} = \frac{1}{r}\frac{1}{\partial r}\left[r\left(\frac{k}{dc_p} + \varepsilon_H\right)\frac{\partial T(r,z)}{\partial r}\right] + \frac{Q}{dc_p} \tag{C.1a}$$

$$\left.\frac{\partial T(r,z)}{\partial r}\right|_{r=0} = 0 \tag{C.1b}$$

$$T(R_1,z) = T_w(z) \;\; or \;\; -k\left.\frac{\partial T(r,z)}{\partial r}\right|_{r=R_1} = j_w(z) \;\; or \;\; T(R_1,z) - \frac{k}{h_w}\left.\frac{\partial T(r,z)}{\partial r}\right|_{r=R_1} = T_E(z) \tag{C.1c}$$

$$T(r,0) = T_{in}(r) \tag{C.1d}$$

Eq. C.1a is valid under the following hypotheses: 1) axial-symmetric conditions are taken into account; 2) steady-state exists; 3) the fluid is incompressible with no phase change, and constant physical properties; 4) the hydrodynamic pattern is established; 5) natural convection effects are not considered; and 6) axial conduction of heat is negligible. The last assumption has been shown by Weigand et al. (2001) to introduce a negligible error for Peclet numbers larger than 10^2. This condition is satisfied in the case of MSRs (*Pr* on the order of 10) in all cases of turbulent flow. Eqs. C.1 were solved by Di Marcello et al. (2010), based on the non-dimensional form of Eqs. C.1 reported in Fig. C.2 and making use of a general mathematical formulation proposed by Mikhailov and Őzişik (1984).

Dimensionless form of the energy equation:

$$f(R)\frac{\partial\theta(R,Z)}{\partial Z} = \frac{1}{R}\frac{\partial}{\partial R}\left[R\cdot g(R)\frac{\partial\theta(R,Z)}{\partial R}\right] + S(R,Z) \qquad \text{in } 0 < R < 1$$

Dimensionless form of the boundary conditions:

$$\left.\frac{\partial\theta(R,Z)}{\partial R}\right|_{R=0} = 0 \qquad \theta(R,0) = \theta_{in}(R)$$

$$\alpha\theta(1,Z) - \beta\left.\frac{\partial\theta(R,Z)}{\partial R}\right|_{R=1} = \Phi(Z) \qquad \begin{cases} \text{(i)} & \alpha = 1,\ \beta = 0, & \Phi(Z) = \theta_w(Z) \text{ (first kind)} \\ \text{(ii)} & \alpha = 0,\ \beta = 1, & \Phi(Z) = J_w(Z) \text{ (second kind)} \\ \text{(iii)} & \alpha = 1,\ \beta = \frac{k}{h_w\cdot R_1}, & \Phi(Z) = \theta_E(Z) \text{ (third kind)} \end{cases}$$

Dimensionless variables:

$$R = \frac{r}{R_1} \qquad Z = \frac{2z}{Re\cdot Pr\cdot R_1} \qquad \theta(R,Z) = \frac{T(r,z) - T^*}{\Delta T}$$

$$\theta_w(Z) = \frac{T_w(z) - T^*}{\Delta T} \qquad \theta_E(Z) = \frac{T_E(z) - T^*}{\Delta T} \qquad \theta_{in}(Z) = \frac{T_{in}(z) - T^*}{\Delta T}$$

$$J_w(Z) = \frac{j_w(z)R_1}{k\cdot\Delta T} \qquad \theta_b(Z) = \frac{T_b(z) - T^*}{\Delta T} \qquad f(R) = \frac{u}{u_{avg}}$$

$$g(R) = \frac{\frac{\nu}{Pr} + \varepsilon_H}{\frac{\nu}{Pr}} \qquad S(R,Z) = \frac{Q(r,z)\cdot R_1^2}{k\cdot\Delta T} \qquad P(R,Z) = R\cdot S(R,Z)$$

Figure C.2: Non-dimensional form of the problem defined by Eqs. C.1

The results can be written as follows:

$$\theta(R,Z) = \sum_{j=0}^{q}\theta_j(R)Z^j + \sum_{i=1}^{\infty}C_i e^{-\mu_i^2 Z}\psi_i(R) \tag{C.2a}$$

$$C_i = \frac{\int_0^1 R[\theta_{in}(R) - \theta_0(R)]f(R)\psi_i(R)dR}{\int_0^1 Rf(R)\psi_i^2(R)dR} \tag{C.2b}$$

$$\begin{aligned}\theta_j(R) = \frac{1}{\alpha}\Bigg\{&\phi_j + \beta\int_0^1\left[P_j(R) - (j+1)Rf(R)\theta_{j+1}(R)\right]dR \\ &+ \alpha\int_0^1\frac{1}{Rg(R)}\int_0^R\left[P_j(R') - (j+1)R'f(R')\theta_{j+1}(R')\right]dR'dR\Bigg\} \\ &- \int_0^R\frac{1}{Rg(R'')}\int_0^{R'}\left[P_j(R') - (j+1)R'f(R')\theta_{j+1}(R')\right]dR'dR''\end{aligned} \tag{C.2c}$$

where the assumption is made that the non-homogeneous term $\Phi(Z)$ and the term $P(R,Z) = R\cdot S(R,Z)$ can be expressed in terms of q-order polynomials of the non-dimensional axial coordinate Z as follows:

$$\phi(Z) = \sum_{j=0}^{q}\phi_j Z^j \tag{C.2d}$$

$$P(R,Z) = \sum_{j=0}^{q} P_j(R) Z^j \tag{C.2e}$$

In Eqs. C.2a and C.2b $\psi_i(R)$ and μ_i are the eigenfunctions and the eigenvalues, respectively, of the Sturm-Liouville problem:

$$\frac{d}{dR}\left[Rg(R)\frac{d\psi_i(R)}{dR}\right] + \left[\mu_i^2 Rf(R)\right]\psi_i(R) = 0 \tag{C.2f}$$

$$\left.\frac{d\psi_i(R)}{dR}\right|_{R=0} = 0 \tag{C.2g}$$

$$\alpha\psi_i(1) - \beta g(1)\left.\frac{d\psi_i(R)}{dR}\right|_{R=1} = 0 \tag{C.2h}$$

The velocity profile required for the solution of Eqs. C.2 has still been obtained through a solution (not reported here for brevity) proposed by Di Marcello et al. (2010).

Once the temperature distribution $\vartheta(R,Z)$ is known, the Nusselt number can be evaluated as

$$Nu = \frac{2}{\theta(1,Z)-\theta_b(Z)}\left.\frac{\partial\theta(R,Z)}{\partial R}\right|_{R=1} \tag{C.3}$$

with

$$\theta_b(Z) = \frac{\int_0^1 Rf(R)\theta(R,Z)dR}{\int_0^1 Rf(R)dR} \tag{C.4}$$

The temperature distribution in the solid region surrounding the duct of Fig C.1 is governed by a classical heat diffusion equation. By assuming constant material properties and radially constant power production, this equation can be written for an axial-symmetric geometry as:

$$\frac{1}{r}\frac{\partial}{\partial r}\left[k_r r\frac{\partial T(r,z)}{\partial r}\right] + \frac{\partial}{\partial z}\left[k_z\frac{\partial T(r,z)}{\partial z}\right] = -Q(z) \tag{C.5a}$$

Consistently with the hypothesis taken at the beginning of the Appendix, thermal insulation is imposed on the outer radius ($r=R_2$) of the solid region. Thermal insulation has been assumed also in correspondence of the outlet section ($z=H$), while a uniform temperature is assigned on the inlet section ($z=0$). As far as the inner radius ($r=R_1$) is concerned, a temperature of arbitrary axial distribution is considered to allow for the coupling with the fluid domain. Boundary conditions for Eq. C.5a can then be written as:

$$\left.\frac{\partial T(r,z)}{\partial r}\right|_{r=R_2} = 0 \tag{C.5b}$$

$$\left.\frac{\partial T(r,z)}{\partial z}\right|_{z=H} = 0 \tag{C.5c}$$

$$T(r,0) = T_{in} \tag{C.5d}$$

$$T(R_1,z) = T_w(z) \tag{C.5e}$$

To solve the problem described by Eqs. C.5, the separation-of-variables method (Carlsaw and Jaeger, 1959) is adopted. Details about the solution procedure can be found in (Cammi et al., 2009; Fiorina, 2009; Luzzi et al., 2010), while here only the final result is reported (Eqs. C.6):

$$T(r,z) = T_{in} + \sum_{n=0}^{\infty} c_n \, sin(\gamma_n z) \, F_n(r) + \omega(z) \tag{C.6a}$$

$$c_n = \frac{1}{F_n(R_1)} \frac{\int_0^H (T_w(z) - T_{in} - \omega(z)) sin(\gamma_n z) dz}{\int_0^H (sin^2(\gamma_n z) dz} \tag{C.6b}$$

$$\gamma_n = \frac{\pi}{2H}(2n+1) \qquad n \, \epsilon \, N \tag{C.6c}$$

$$F_n(r) = I_0\left(\left(\frac{k_z}{k_r}\right)^{1/2} \gamma_n r\right) + \frac{I_1\left(\left(\frac{k_z}{k_r}\right)^{1/2} \gamma_n R_2\right)}{K_1\left(\left(\frac{k_z}{k_r}\right)^{1/2} \gamma_n R_2\right)} K_0\left(\left(\frac{k_z}{k_r}\right)^{1/2} \gamma_n r\right) \tag{C.6d}$$

$$\omega(z) = -\int_0^z dz' \int_0^{z'} \frac{Q(z'')}{k_z} dz'' + z \int_0^H \frac{Q(z')}{k_z} dz' \tag{C.6e}$$

The temperature fields of the fluid region (Eqs. C.2) and of the solid region (Eq. C.6) are coupled through the condition of continuity of the heat flux and temperature at their common boundary ($r = R_1$). This coupling is achieved by means of a numerical iterative MATLAB procedure, based on a trial and error method. A systematic sensitivity analysis has been carried out in order to get a good compromise between accuracy and computational time, by varying the number of terms of the series, as well as the discretization of the domains. As a result, 0.1% discrepancy (if normalized with the maximum temperature difference in the domain) with respect to the asymptotic solution has been achieved, which can be considered acceptable for the scope of the present work.

In (Di Marcello et al., 2010; Luzzi et al., 2010), the results obtained for velocity and temperature fields have been assessed for a large variety of fluids, showing that they are able to reproduce with a good agreement the experimental data concerning heat transfer evaluations for both fully developed and thermally developing flow conditions, in a wide range of Prandtl ($10^{-3}<Pr<10^{4}$) and Reynolds ($2\cdot10^{3}<Re<5\cdot10^{5}$) numbers, with and without internal heat generation. Solutions of the analytic model have also been widely tested against CFD codes (Cammi et al., 2009; Fiorina, 2009; Luzzi et al., 2010), showing a good agreement.

C.3 CONCLUDING REMARKS

In this Appendix, a general mathematical formulation has been presented for the analysis of the heat transfer phenomena in internally heated fluids flowing in turbulent regime in a straight circular channel. This formulation is employed in Chapter 5 to derive a heat transfer correlation capable of predicting the temperature field in the MSFR out-of-core components.

REFERENCES

Cammi, A., Di Marcello, V., Fiorina, C., Luzzi, L., 2009. Assessment of COMSOL Capabilities to Analyse the Thermo-Hydrodynamic Behaviour of the MSR Core. Proc. COMSOL Conference 2009, October 14-16, Milan, Italy.

Carslaw, H.S., Jaeger, J.C., 1959. Conduction of Heat in Solids, Oxford University Press, London.

Di Marcello, V., Cammi, A., Luzzi, L., 2010. A Generalized Approach to Heat Transfer in Pipe Flow with Internal Heat Generation. Chemical Engineering Science 65, 1301-1310.

Di Marcello, 2010. Development of a multiphysics approach to the modelling and analysis of Molten Salt Reactors. PhD thesis. Politecnico di Milano, Milan, Italy.

Fiorina, C., 2009. A generalized approach to assess the COMSOL® capabilities for the analysis of the MSR thermo-fluid dynamics. MSc thesis. Politecnico di Milano, Milan, Italy.

Graetz, L., 1883. Über die Wärmeleitungsfähigkeit von Flüssigkeiten, Part I. Annalen der Physik und Chemie 18, 79–94.

Graetz, L., 1885. Über die Wärmeleitungsfähigkeit von Flüssigkeiten, Part II. Annalen der Physik und Chemie 25, 337–357.

Luzzi, L.; Cammi, A.; Di Marcello, V., Fiorina, C., 2010. An Approach for the Modelling and the Analysis of the MSR Thermo-Hydrodynamic Behaviour. Chemical Engineering Science 65, 4873-4883.

Mikhailov, M.D., Őzişik, M.N., 1984. Unified Analysis and Solutions of Heat and Mass Diffusion, Dover Publications Inc., New York.

Weigand, B.; Kanzamar, M., Beer, H., 2001. The extended Graetz problem with piecewise constant wall heat flux for pipe and channel flows. International Journal of Heat and Mass Transfer 44, 3941-3952.

Acronyms and abbreviations

BOL	Beginning Of Life
CFD	Computational Fluid Dynamics
CR	Conversion Ratio
EFPY	Equivalent Full Power Years
ELSY	European Lead SYstem
EOC	End Of Cycle
EVOL	Evaluation and Viability Of Liquid fuel fast reactor system
FP	Fission Product
FR	Fast Reactor
GIF-IV	Generation IV International Forum
HN	Heavy Nuclides (corresponding to actinides and Ra isotopes)
IAEA	International Atomic Energy Agency
ICRP	International Commission on Radiological Protection
LEADER	Lead-cooled European Advanced Demonstration Reactor
LWR	Light Water Reactor
MA	Minor Actinides (Np, Am, Cm and Cf isotopes)
MSBR	Molten Salt Breeder Reactor
MSFR	Molten Salt Fast Reactor
MSR	Molten Salt Reactor
MSRE	Molten Salt Reactor Experiment
ORNL	Oak Ridge National Laboratory
pcm	per cent mille
RANS	Reynolds-Averaged Navier-Stokes
RL	Reference radiotoxicity Level
TD	Theoretical Density
TRU	TRansUranic isotope
ULOF	Unprotected Loss Of Flow
ULOHS	Unprotected Loss of Heat Sink
UTOP	Unprotected Transient OverPower

Nomenclature

Latin symbols

a_1, a_2, a_3	coefficients of Eq. 5.10
A	reactivity variation associated to the fuel temperature increase from the average coolant temperature to the average fuel temperature at nominal conditions, m$
B	reactivity variation associated to the increase in fuel and coolant temperatures from iso-thermal zero-power conditions, m$
B^2	buckling, m^{-2}
c_i	concentration of the i^{th} precursor group, m^{-3}
c_n	coefficients defined by Eq. C.6b, K
c_p	specific heat, $J \cdot kg^{-1} \cdot K^{-1}$
C	capture rate, s^{-1} *only in subsection 4.4.1:* reactivity coefficient associated to the core inlet coolant temperature, $m\$ \cdot K^{-1}$
C_i	coefficients defined by Eq. C.2b
CR	conversion ratio
CR_{AC}	conversion ratio for the active core (excluding blankets)
d	density, $kg \cdot m^{-3}$
d^*	reference density, $kg \cdot m^{-3}$
D	channel diameter, m
D_i	decay heat of the i^{th} group, $W \cdot m^{-3}$
D_T	total decay heat, $W \cdot m^{-3}$
$\overline{D}$	diffusion coefficient for neutrons, m
$\overline{D}_g$	diffusion coefficient for neutrons for the energy group g, m
f	Darcy friction factor
$f(R)$	function defined in Fig. C.2
f_i	fraction of power generation associated to the i^{th} decay heat group
ff	fraction of fissions in the fertile isotopes
f_z	volumetric force in the axial direction, $N \cdot m^{-3}$
$\boldsymbol{f}$	volumetric force, $N \cdot m^{-3}$
F	fission rate, s^{-1}
F_n	function defined in Eq. C.6d
$\overline{F}$	flow rate normalized to the nominal level
h	heat transfer coefficient, $W \cdot m^{-2} \cdot K^{-1}$
h_w	heat transfer coefficient from the channel wall to the environment, $W \cdot m^{-2} \cdot K^{-1}$
H	channel axial length, m
H_c	core height, m
g	gravitational acceleration, $m \cdot s^{-2}$
$g(R)$	function defined in Fig. C.2
I_i	modified Bessel function of first kind and i^{th} order
j_w	wall heat flux, $W \cdot m^{-2}$

$J_w(Z)$	dimensionless wall heat flux defined in Fig. C.2
k	thermal conductivity, $W \cdot m^{-1} \cdot K^{-1}$
k_{eff}	effective multiplication factor
k_r	thermal conductivity in the radial direction, $W \cdot m^{-1} \cdot K^{-1}$
k_T	turbulent thermal conductivity, $W \cdot m^{-1} \cdot K^{-1}$
k_z	thermal conductivity in the axial direction, $W \cdot m^{-1} \cdot K^{-1}$
k_∞	infinite multiplication factor
K_D	Doppler constant, pcm
K_i	modified Bessel function of second kind and i^{th} order
l	generic linear dimension, m
L	leakage rate, s^{-1}
L^2	diffusion area, m^2
N	natural numbers
Nu	Nusselt number
p	pressure, Pa
P	production rate, s^{-1}
$P(R,Z)$	function defined in Fig. C.2
$P_j(R)$	j^{th} coefficient of the polynomial expansion of P(R,Z) (Eq. C.2e)
Pow	core power, W
Pr	molecular Prandtl number
Pr_T	turbulent Prandtl number
$\bar{P}$	reactor power normalized to the nominal level
q	order of the polynomial expansion of P(R,Z) and Φ(Z) (Eqs. C.2d, C.2e)
Q	volumetric heat source, $W \cdot m^{-3}$
Q_{tot}	total heat source in a heated channel, W
r	radial coordinate, m
R	dimensionless radial coordinate defined in Fig. C.2
R_c	core radius, m
Re	Reynolds number
R_1	channel radius (Fig. C.1), m
R_2	outer radius of the solid region surrounding a channel (Fig. C.1), m
$S(R,Z)$	dimensionless internal heat source defined in Fig. C.2
t	time, s
T	temperature, K
T_{AV}	average core temperature, K
T_b	bulk temperature, K
T_E	temperature of the environment, K
T_{in}	inlet temperature (of a core or a channel), K
T_{out}	outlet temperature (of a core or a channel), K
T_{sec}	temperature at the secondary side of the heat exchangers, K
T_w	wall temperature, K
T^*	reference temperature, K
T^+	dimensionless temperature $\{= (T_w - T) \cdot d \cdot c_p \cdot (\tau_W / d)^{0.5} / j_w \}$
u	axial velocity, $m \cdot s^{-1}$

u_{avg}	average axial velocity in a channel, $m \cdot s^{-1}$
$\boldsymbol{u}$	velocity vector, $m \cdot s^{-1}$
U	overall heat transfer coefficient between primary and intermediate circuit, $W \cdot K^{-1}$
v_g	neutron velocity for the energy group g, $m \cdot s^{-1}$
V	effective phase voltage, V
Vol	volume, m^3
x	generic core parameter
x_1, x_2	generic core parameter in state 1 and 2
X_1, X_2, X_3, X_4	parameters defined in Eqs. 2.2 to 2.7
y	distance from the wall, m
y^+	dimensionless distance from the wall $\{= y \cdot (\tau_W \cdot d)^{0.5} / \mu\}$
z	axial coordinate, m
Z	dimensionless axial coordinate defined in Fig. C.2

Greek symbols

a, β	dimensionless coefficients defining the boundary condition at wall in Fig. C.2
a_d	fuel expansion reactivity feedback coefficient, $pcm \cdot K^{-1}$
a_D	Doppler reactivity feedback coefficient, $pcm \cdot K^{-1}$
β_e	volumetric expansion coefficient, K^{-1}
β_{eff}	effective delayed neutron fraction, pcm
β^i_{eff}	effective fraction of delayed neutrons associated to the i^{th} precursor group, pcm
γ_n	function defined in Eq. C.6c
Γ	flow rate, $kg \cdot s^{-1}$
Δp	pressure drop in the primary circuit, Pa
ΔT	reference temperature difference used in Fig. C.2, K
ΔT_c	temperature increase of the coolant across the core, K
$\Delta\Theta$	vertical distance between the centers of core and heat exchangers, m
ε	energy per fission, J
ε_H	turbulent diffusivity for heat, $m^2 \cdot s^{-1}$
ζ	correction factor to be applied to the Nusselt number in case of internal heat generation (Eq. 5.4)
$\theta(R,Z)$	dimensionless temperature defined in Fig. C.2
$\theta_b(Z)$	dimensionless bulk temperature defined in Fig. C.2
$\theta_E(Z)$	dimensionless environment temperature defined in Fig. C.2
$\theta_{in}(R)$	dimensionless inlet temperature defined in Fig. C.2
$\theta_j(R)$	j^{th} coefficient of the polynomial expansion of θ(R,Z) (Eqs. C.2a and C.2c)
$\theta_w(Z)$	dimensionless wall temperature defined in Fig. C.2
κ	von Karman constant
λ_i	decay constant associated to the i^{th} precursor or decay heat group, s^{-1}
μ	dynamic viscosity, Pa·s
μ_i	i^{th} eigenvalue of the Sturm-Liouville problem given by Eqs. C.2f, C.2g, C.2h
μ_T	turbulent dynamic viscosity, Pa·s
ν	kinematic viscosity, $m^2 \cdot s^{-1}$

ρ	reactivity, pcm
ρ_C	reactivity associated to captures, pcm
ρ_{ext}	reactivity inserted through control rods, pcm
ρ_F	reactivity associated to fissions, pcm
ρ_L	reactivity associated to leakages, pcm
ρ_P	reactivity associated to productions, pcm
ρ_0	reactivity loss due to out-of-core decay of delayed neutron precursors, pcm
ρ^*	reference reactivity, pcm
σ	function defined in Eq. 5.6
σ_e	electric conductivity, $S \cdot m^{-1}$
σ'	function defined in Eq. 5.7, m
Σ_a	absorption macroscopic cross-section, m^{-1}
$\Sigma_{a,g}$	absorption macroscopic cross-section for the energy group g, m^{-1}
Σ_c	capture macroscopic cross-section, m^{-1}
$\Sigma_{c,g}$	capture macroscopic cross-section for the energy group g, m^{-1}
Σ_f	fission macroscopic cross-section, m^{-1}
$\Sigma_{f,g}$	fission macroscopic cross-section for the energy group g, m^{-1}
$\Sigma_{g \to g'}$	group transfer cross-section from the energy group g to g', m^{-1}
τ_C	transit time in the core, s
τ_{EC}	transit time in the out-of-core part of the primary circuit, s
τ_W	wall shear stress, Pa
υ	neutrons emitted per fission
$\upsilon_{d,g}$	delayed neutrons emitted per fission in the energy group g
$\upsilon_{p,g}$	prompt neutrons emitted per fission in the energy group g
φ	function defined in Eq. 5.8
$\Phi(Z)$	function defining the boundary condition at wall in Fig. C.2
Φ_g	neutron flux in the energy group g, $m^{-2} \cdot s^{-1}$
Φ_j	j^{th} coefficient of the polynomial expansion of $\Phi(Z)$ (Eq. C.2d)
$\chi_{d,i}$	probability that a delayed neutron is emitted in the i^{th} precursor group
$\chi_{p,g}$	probability that a prompt neutron is emitted in the energy group g
$\psi_i(R)$	i^{th} eigenfunction of the Sturm-Liouville problem given by Eqs. C.2f, C.2g, C.2h
$\omega(\xi)$	function defined in Eq. C.6e, K

Subscripts

$()_{jw}$	related to a channel with a wall heat flux different than zero but without internal heat generation
$()_Q$	related to a channel with internal heat generation but with a wall heat flux equal to zero
$()_{Q+jw}$	related to a channel with both internal heat generation and a wall heat flux different than zero

δ indicates the difference between the values of a quantity before and after a perturbation

Acknowledgments

There are a lot of people I really wish to thank. They have all given, in some way, fundamental contributions to the development of this work.

Let's start from the Politecnico di Milano. I have spent there 8 years, but I'd better limit my acknowledgments to the last 3 or 4, before ending up writing a second thesis… There is only one exception, Prof. Daniela Lupo. She has been my Professor of Mathematical Analysis during the first year of my university courses. I owe her a good portion of my interest for Science and Engineering.

Let's now move to the years of my PhD. First of all, I wish to thank my tutor, Prof. Marco Ricotti. He has helped me with his wide expertise and he has supported me in all my ideas and initiatives, always conveying me the enthusiasm necessary to do a (hopefully) good job. I also thank him for putting me in contact with Westinghouse Electric Company as soon as I started my PhD studies, paving the way toward a fruitful and truly international research experience.

I would like to thank my supervisor Dr. Antonio Cammi. My desire to achieve his wide engineering expertise has been a source of motivation for starting my PhD, and for continuing improving my knowledge in a variety of scientific fields. He has steadily helped me in the development of the thesis work with his deep expertise in the field of System Dynamics and Control. I feel as invaluable his moral support in all these years.

I am really grateful to my supervisor Dr. Lelio Luzzi. He has the capability to teach nuclear engineering in an exceptionally clear and synthetic way while making lectures interesting, even entertaining. During my PhD, he has helped me with his wide research experience and he has offered an important organizational support. Last but not least, he has played a main role in organizing my unforgettable stay at TUDelft.

I am grateful to Prof. Carlo Lombardi and Prof. Hisashi Ninokata. I had few chances of interacting with them, but each time unforgettable lessons have come along.

I wish to thank all Professors of the Department of Energy at Polimi. Among them, I am particularly grateful to Prof. M. Mariani and P.M. Colombo for the kind support they have given me whenever they could.

Thanks to all PhD students of the Nuclear Reactor Group. Marco Colombo and Claudia Guerrieri have started the PhD with me. We have confronted together this adventure and shared the same office for three years, during which they have always offered an invaluable support. I wish them lots of achievements in their studies, researches and personal life. I am grateful to Dr. Davide Papini. He is a good guy and a good friend and he has always helped me whenever he could (he has also given me the template for this thesis work!). I wish to thank Dr. Vito Memoli, who helped me out when I was tackling for the first time a research activity on core physics. Thanks to Manuele Aufiero. He has been an irreplaceable colleague, both from a personal and a scientific viewpoint. He is a generous person with uncommon intelligence and each discussion with him has taught me a lot. Thanks to Roberto Ponciroli and Stefano Lorenzi for their pleasant company and some nice discussions on their beloved

LFRs. I am grateful for them bearing some unbearable monologue of mine on that subject… Thanks to Alberto Sartori for his kindness and his help. I have enjoyed the time spent together trying to learn ERANOS. To all the PhD students that I have mentioned and that have not yet finished their studies, I wish them all the best for their continuation. Thanks also to Jacopo De Amicis. He has shared for some months the office with Claudia, Marco and me, before leaving the PhD studies for new adventures. I wish him the best.

Let's cross the ocean and let's go to Westinghouse in Pittsburgh, US. There I would like to thank my supervisor Dr. Fausto Franceschini. I really owe him a lot. He has guided me throughout the PhD, offering me tremendous opportunities for my personal and scientific growth, motivating me but never putting pressure on me. He has organized my stay at the PSI and he has hosted me in Westinghouse for 4 weeks, during which he spent continuous efforts to help me in my studies, to make me meet knowledgeable people, and even to make me have fun. I have learnt from him almost everything I know about the nuclear fuel cycle. He has been an unparalleled mentor and has become a very good friend.

I also would like to personally thank Dr. Mario Carelli, who initiated the collaboration with the Politecnico di Milano that resulted in my PhD studies. Thanks to Dr. Mike Wenner for his fundamental and competent help with the ORIGEN-S code. Thanks to Ben Lindley, from Cambridge. We shared the apartment during my second stay in Westinghouse. I enjoyed the time spent together in Pittsburgh and I really appreciate his efforts in teaching me some British English.

Back to Europe, to the PSI (Switzerland), where I have spent 7 wonderful months. First of all, I wish to thank Dr. Jiri Krepel. He has helped organizing my stay at the PSI and he has immediately welcomed me as a friend. He has taught me all fundamental notions on fuel cycle and equilibrium methodologies, setting the basis for this thesis work. He has explained me how to use EQL3D (his most beloved creature, at least before he had a son). He has eventually become a very good friend.

Thanks to Dr. Konstantin Mikityuk for hosting me in the FAST group, and for his kind and extremely competent help throughout my PhD.

I wish to thank Dr. Sandro Pelloni for all the nice discussions I had with him every day at the PSI. He has given me fundamental hints for my studies, and taught me a lot about the Swiss culture and habits.

Thanks also to all other people in the FAST group and in the LRS laboratory for setting up such a friendly, welcoming, collaborative and interesting environment.

Let's now move to Delft (Netherlands). I am deeply grateful to Prof. Jan-Leen Kloosterman and Prof. Danny Lathouwers for hosting me at TUDelft for two months, for their kindness, and for helping me with their uncommon expertise. Thanks to all the people from the Physics of Nuclear Reactors research group, who welcomed me and made me spend two unforgettable months. Special thanks to Dr. Luca Gilli and his wife Shalini Kurapati. They managed to make me feel at home in a couple of days. I wish them a bright career and a happy married life.

I wish to acknowledge all the colleagues in the frame of the EURATOM EVOL Project, and of the IAEA CRP "Near term and promising long term options for deployment of thorium based nuclear energy".

Back to Italy, in Italian language this time.

Vorrei ringraziare innanzitutto i miei genitori, Ada e Giovanni. A loro è dedicata questa tesi. Mi hanno guidato fin da piccolo nella mia istruzione e a loro va il merito delle mie fortune scolastiche ed universitarie. Soprattutto, li ringrazio per avermi offerto, nel corso degli anni, un insostituibile supporto in ogni scelta importante e in ogni momento difficile. Li ringrazio per essermi stati vicini, offrendo sempre un aiuto gentile, dando tutto senza mai chiedere niente.

Ringrazio tutta la mia famiglia, ed in particolare mia sorella Silvia, suo marito Andrea, i miei cugini Roberto e Maria, e i miei Zii Paola e Adolfo. Ringrazio i miei nonni Carmen, Giuseppe e Maria. Vorrei ricordare in particolare mio nonno paterno Bruno, che tanto mi ha insegnato quando ero piccolo e che non mi ha potuto vedere dottore.

Grazie anche ai genitori della mia ragazza, Andreina e Valerio, a suo fratello Riccardo, ai suoi zii Anna e Patrizio, e a sua nonna Elena. Sono per me una seconda insostituibile famiglia.

Ringrazio i miei amici di sempre: Alex, Anto, Feli, Francy, Friz, Giorgio, Hanto e Pipi (l'ordine è alfabetico! prima che qualcuno si offenda...). Mi hanno insegnato il valore dell'amicizia e a loro sono legati molti dei miei ricordi più belli.

Un ringraziamento speciale alla mia ragazza Monica. La ringrazio per essermi sempre stata vicina, accettando il mio frequente stacanovismo (e relative intemperanze), non mostrando mai disappunto per le mie continue trasferte. Mi ha aiutato quando ne avevo bisogno, sempre e incondizionatamente, come nessun altro avrebbe potuto fare. Mi sento profondamente fortunato ad avere al mio fianco da ormai 10 anni un persona come lei.